DOC.20070807.0006

QA: QA

ANL-NBS-HS-000047 REV 01

August 2007

THC Sensitivity Study of Heterogeneous Permeability and Capillarity Effects

NOTICE OF OPEN CHANGE DOCUMENTS - THIS DOCUMENT IS IMPACTED BY THE LISTED CHANGE DOCUMENTS AND CANNOT BE USED WITHOUT THEM.

----

1) ACN-001, DATED 01/11/2008

Prepared for:
U.S. Department of Energy
Office of Civilian Radioactive Waste Management
Office of Repository Development
1551 Hillshire Drive
Las Vegas, Nevada 89134-6321

Prepared by:
Sandia National Laboratories
OCRWM Lead Laboratory for Repository Systems
1180 Town Center Drive
Las Vegas, Nevada 89144

Under Contract Number
DE-AC04-94AL85000

DISCLAIMER

This report was prepared as an account of work sponsored by an agency of the United States Government. Neither the United States Government nor any agency thereof, nor any of their employees, nor any of their contractors, subcontractors or their employees, makes any warranty, express or implied, or assumes any legal liability or responsibility for the accuracy, completeness, or any third party's use or the results of such use of any information, apparatus, product, or process disclosed, or represents that its use would not infringe privately owned rights. Reference herein to any specific commercial product, process, or service by trade name, trademark, manufacturer, or otherwise, does not necessarily constitute or imply its endorsement, recommendation, or favoring by the United States Government or any agency thereof or its contractors or subcontractors. The views and opinions of authors expressed herein do not necessarily state or reflect those of the United States Government or any agency thereof.

QA: QA

THC Sensitivity Study of Heterogeneous Permeability and Capillarity Effects

ANL-NBS-HS-000047 REV 01

August 2007

Sandia National Laboratories

Scientific Analysis/Calculation Signature Page/Change History

Complete only applicable items.

1. Total Pages: 214

2. Document Title

THC Sensitivity Study of Heterogeneous Permeability and Capillarity Effects

3. DI (including Rev. No.)

ANL-NBS-HS-000047 REV 01

	Printed Name	Signature	Date
4. Originator	Sumit Mukhopadhyay	Y. Tsang for Sumit Mukhopadhyay	08/02/2007
5. Checker	Clifford Ho	Clifford K. Ho	8/2/2007
6. QCS	Robert E. Spencer	Robert E Spencer	08/02/07
7. Responsible Manager/ Lead	Ernest Hardin	E Hardin	8/2/07
8. Responsible Manager	Geoff Freeze For Paul R. Dixon	Paul	8-3-07

9. Remarks

Change History

10. Revision No.	11. Description of Change
REV 00	Initial Issue.
REV 01	Revision 01 of this report implements multiple realizations of the spatially heterogeneous permeability field (previous work used only one). This report also applies TOGHREACT V3.1.1 software, which corrected errors in the previous code version that were documented in CR 8032. Importantly, this revision incorporates a physical process not considered in the previous revision, namely Leverett scaling, which accounts for changes in fracture capillarity associated with spatial and temporal variations in fracture permeability. The analysis in this revision is also based on more comprehensive evaluation of the sensitivity of the THC seepage model, addressing initial variability in fracture capillary-strength parameters, and enhanced infiltration fluxes. This revision addresses in part CR-7037, which notes that information provided in Revision 00 shows that predicted seepage is enhanced by THC effects not considered in *Abstraction of Drift Seepage*. This revision also addresses in part CR-7193, implementing several recommendations for improvement including integration of the THC and seepage models (PLI-042504-150205-94), and flow-focusing effects (PLI-042604-132118-89). This revision does not address chemical responses associated with local thermal conditions near the repository edge, which are covered in *Drift-Scale THC Seepage Model* (SNL 2007 [DIRS 177404]). Because the changes described above are so extensive, change bars are not used in this revision of the report.

CONTENTS

Page

CONTENTS (Continued)

Page

CONTENTS (Continued)

Page

INTENTIONALLY LEFT BLANK

FIGURES

Page

FIGURES (Continued)

Page

FIGURES (Continued)

Page

INTENTIONALLY LEFT BLANK

TABLES

Page

TABLES (Continued)

Page

ACRONYMS AND ABBREVIATIONS

2-D	two-dimensional
3-D	three-dimensional
CR	Condition Report
DIRS	Document Input Reference System
DOE	U.S. Department of Energy
DST	Drift Scale Test
DTN	data tracking number
ECRB	Enhanced Characterization of the Repository Block
FEPs	features, events, and processes
GFM	geologic framework model
LA	license application
LBNL	Lawrence Berkeley National Laboratory
SCM	seepage calibration model
SMPA	seepage model for performance assessment
TDMS	Technical Data Management System
TH	thermal-hydrologic
THC	thermal-hydrologic-chemical
Tptpll	Topopah Spring Tuff Lower Lithophysal Hydrogeologic Unit
TSPA	total system performance assessment
TWP	technical work plan
UZ	unsaturated zone
YMRP	*Yucca Mountain Review Plan, Final Report*

INTENTIONALLY LEFT BLANK

1. PURPOSE

1.1 OBJECTIVE

The purpose of this report is to document the sensitivity of the drift-scale thermal-hydrologic-chemical (THC) seepage model (SNL 2007 [DIRS 177404]) to heterogeneities in permeability and capillarity, which could affect predicted fluxes and chemistries of water and gases seeping into the emplacement drifts. This report has been developed following *Technical Work Plan for: Revision of Model Reports for Near-Field and In-Drift Water Chemistry* (SNL 2007 [DIRS 179287]). Furthermore, this report has been prepared in accordance with the latest version of SCI-PRO-005, *Scientific Analyses and Calculations*.

This is a revision of the analysis report *THC Sensitivity Study of Repository Edge and Heterogeneous Permeability Effects* (BSC 2006 [DIRS 174104]), hereafter referred to as the THC Sensitivity Study. In accordance with *Technical Work Plan for: Revision of Model Reports for Near-Field and In-Drift Water Chemistry* (SNL 2007 [DIRS 179287], Section 1.1), the present revision of the THC sensitivity study will be called *THC Sensitivity Study of Heterogeneous Permeability and Capillarity Effects*, as it no longer addresses the repository edge effects. Per the technical work plan (TWP) (SNL 2007 [DIRS 179287], Section 1.1), the analyses pertaining to repository edge effects have been moved to the model report *Drift-Scale THC Seepage Model* (SNL 2007 [DIRS 177404]).

The objective of this report is to address in part Condition Report (CR) 7037, which notes that information provided in Revision 00 of the THC sensitivity study (BSC 2006 [DIRS 174104]) shows that predicted seepage is enhanced by THC effects not considered in *Abstraction of Drift Seepage* (BSC 2004 [DIRS 169131]). The observations in the THC sensitivity study were based on limited analyses (such as relying only on one realization of the heterogeneous fracture permeability distribution) of the THC seepage model sensitivity to permeability heterogeneities. The THC sensitivity study also did not account for the corresponding changes in fracture capillarity associated with spatially/temporally variable fracture permeability distributions. The revised analysis in the present report is based on a more comprehensive evaluation of the sensitivity of the THC seepage model to heterogeneities, both in fracture permeability and capillarity. It also documents the sensitivity of the THC seepage model through implementation of multiple realizations of the heterogeneous fracture permeability distribution, multiple initial fracture capillary-strength parameters of the host rock, and enhanced infiltration fluxes. The ultimate goal of these sensitivity analyses is to evaluate the effects from THC processes on the predicted occurrence of seepage. The other goal of the present report is to provide sufficient technical bases regarding whether any change in abstraction of drift seepage is necessary.

1.2 OVERVIEW OF THE THC SEEPAGE MODEL

The drift-scale THC seepage model has been fully documented and validated in *Drift-Scale THC Seepage Model* (SNL 2007 [DIRS 177404]). The model provides an analysis of the effects of coupled thermal, hydrological, and chemical processes on infiltration water chemistry and gas-phase composition in the near-field host rock around waste emplacement drifts. The model includes a complete description of the pertinent mineral–water processes in the host rock and their effect on the near-field environment. It is used to evaluate the effects of mineral dissolution

and precipitation; the effects of CO_2 exsolution and transport in the region surrounding emplacement drifts; the potential for forming calcite, silica, or other mineral "precipitation caps"; and the resulting changes to porosity and permeability (SNL 2007 [DIRS 177404], Section 6.5.5]). Sensitivity studies with this model have documented the effect of varying rock properties, reaction rates, temporal discretization, CO_2 transport properties, geochemical systems, dryout mineral assemblage, infiltration rates, and input water compositions, as documented in *Drift-Scale THC Seepage Model* (SNL 2007 [DIRS 177404], Section 6.6).

1.3 OVERVIEW OF ANALYSES PRESENTED IN THIS REPORT

The sensitivity study documented in this report (Section 6) consists of the integration of the thermal-hydrologic (TH) and THC seepage models with the seepage model for performance assessment (SMPA) documented in *Seepage Model for PA Including Drift Collapse* (BSC 2004 [DIRS 167652]), and the TH seepage model documented in *Drift-Scale Coupled Processes (DST and TH Seepage) Models* (BSC 2005 [DIRS 172232]). The purpose is to show the impact of fracture permeability and capillarity heterogeneity on the occurrence of seepage, if any. The purpose is also to show the effects of fracture heterogeneity on THC seepage water composition. This analysis includes the following elements:

- Implementation into the THC seepage model of a heterogeneous permeability field consistent with the SMPA. Multiple realizations of the heterogeneous permeability field are used in the analyses.

- Incorporation of the impacts of heterogeneous porosity changes and permeability heterogeneities on capillarity in the THC seepage model.

- Simulations, including the heterogeneous permeability fields and variable infiltration fluxes with or without capillarity heterogeneities, as follows:

  – Ambient, TH, THC simulation with a "normal" infiltration rate
  – Ambient, TH, and THC simulation with ten times "normal" infiltration rate.

- Additional simulations for multiple realizations of the heterogeneous permeability field, and "normal" and enhanced infiltration fluxes with different values of the initial fracture capillary-strength parameter for the host rock.

- The use of W0 (DTN: MO0005PORWATER.000 [DIRS 150930], Sample ID: ESF-HD-PERM-3/34.8-35.1, frequently referred to as water HDPERM3 or water W0) as initial pore-water composition for these simulations. This is the same starting water that was used in the previous THC sensitivity study (BSC 2006 [DIRS 174104]). Use of this water, consistent with that of the previous model, allows evaluation of results from model evolution. In addition, this water is potentially of high importance with respect to performance assessment, because it is the starting water that most commonly results in the predicted occurrence of potentially corrosive, low pH (SNL 2007 [DIRS 177412], Figure 6.13-7), high chloride:nitrate ratio (SNL 2007 [DIRS 177412], Figure 6.13-11) conditions on the waste package surface.

Simulations developed in this revision of the THC sensitivity study will also be used, as they were in the previous revision, to support the selection of THC seepage model output from zones of high liquid saturation further from the drift opening than the boiling/wetting front, to represent potential seepage water compositions. An alternative selection criterion (e.g., high liquid flux) will also be justified. Selection of potential seepage water compositions from the top front (FRONT) waters, high-saturation (HISAT) crown waters, or high liquid flux (FLUX) waters, will include consideration of two factors. First, the FRONT waters occur at such low saturations that flow is unlikely. Second, analyses presented in the previous THC sensitivity study (BSC 2006 [DIRS 174104]) show that the predicted compositions of in-drift seepage are more similar to HISAT waters than to FRONT waters, and also that both tend to have similar compositions at later time. However, these simulations made use of widely spaced, pre-defined printout time intervals that may have missed transients in seepage composition. Therefore, simulations of in-drift seepage composition presented in this report are performed with more printout intervals than previously used.

1.4 LIMITATIONS

Analyses presented in this report are sensitivity analyses of simulations performed with the THC seepage model and presented in *Drift-Scale THC Seepage Model* (SNL 2007 [DIRS 177404], Section 1.3). The modeling approach, numerical model (TOUGHREACT V3.1.1; see Section 3.1), and thermal, chemical, hydrological, thermodynamic, and kinetic data for these sensitivity analyses are the same as for other simulations (SNL 2007 [DIRS 177404], Section 6.5.5), except for heterogeneous permeability distributions (Section 6.4.10), variations in infiltration rates (Sections 6.4.5, 6.5, 6.6, and 6.7), and range of initial fracture capillary-strength parameters of the host rock (Sections 6.4.11, 6.5, 6.6, and 6.7), which are the object of the sensitivity analyses presented in this report. Therefore, analyses presented in this report do not include limitations other than those already presented in *Drift-Scale THC Seepage Model* (SNL 2007 [DIRS 177404], Sections 1.3 and 6.7) for the THC seepage model. This model is limited by its mathematical formulations (SNL 2007 [DIRS 177404], Section 6.4) and associated assumptions and approximations (SNL 2007 [DIRS 177404], Sections 5, 6.4.6, and 6.5). For example, the THC seepage model was not designed for accurate computation of mineral precipitation from very saline waters (ionic strength >4 molal) resulting from evaporative concentration. This limitation and others affecting the uncertainty of model results are discussed in *Drift-Scale THC Seepage Model* (SNL 2007 [DIRS 177404], Section 6.7). Nevertheless, these limitations were for the most part overcome by evaluating the model sensitivity to key input parameters (SNL 2007 [DIRS 177404], Section 6.6), and by comparing model results against data from the Drift Scale Test (DST) and laboratory experiments (SNL 2007 [DIRS 177404], Section 7). Also, the model conceptualization and mathematical formulation (SNL 2007 [DIRS 177404], Sections 6.2 to 6.5) have been improved through successive revisions of the THC seepage model, such that a reasonably good agreement between calculated and measured data has been achieved (SNL 2007 [DIRS 177404], Section 7).

By definition, models are idealizations of the real world. Input data summarized in Section 4 characterize the average physical properties of the rock, but cannot include every detail of a natural system. In particular, the infiltration of water is laterally uniform over the model top boundary. Because the THC seepage model is a continuum model, with averaged properties or realizations of idealized permeability fields, the model results describe general, overall changes in space and time within the model domain.

2. QUALITY ASSURANCE

Development of this report and the supporting analyses activities have been determined to be subject to the Yucca Mountain Project's Quality Assurance Program as indicated in *Technical Work Plan for: Revision of Model Reports for Near-Field and In-Drift Water Chemistry* (SNL 2007 [DIRS 179287]). Approved quality assurance implementing procedures identified in the TWP (SNL 2007 [DIRS 179287], Section 4) have been used to conduct and document the activities described in this report. The main governing procedure for this document was SCI-PRO-005, *Scientific Analyses and Calculations*. An evaluation in accordance with IM-PRO-002, *Control of the Electronic Management of Information,* has been conducted, and this work is subject to requirements to manage and control electronic data. The evaluation was submitted to the Records Processing Center as part of the TWP records package.

This report is intended to complement results of the THC seepage model, presented in *Drift-Scale THC Seepage Model* (SNL 2007 [DIRS 177404]). This report investigates the effect of drift-scale THC processes on the following safety category barriers that are important to the demonstration of compliance with the postclosure performance objective prescribed in 10 CFR 63.113 [DIRS 173273]:

- Unsaturated zone above the repository
- Unsaturated zone below the repository.

The barriers are classified as "Safety Category" with regard to importance to waste isolation as defined in *Q-List* (BSC 2005 [DIRS 175539]). The report contributes to the analyses and modeling data used to support the total system performance assessment (TSPA), but is not directly used by TSPA. The conclusions from this report do not directly impact the engineered features important to preclosure safety as defined in LS-PRO-0203.

INTENTIONALLY LEFT BLANK

3. USE OF SOFTWARE

The following software was used in the preparation of this report:

3.1 QUALIFIED SOFTWARE

The qualified software used in this study is listed in Table 3-1. The software has been baselined in accordance with IM-PRO-003, *Software Management*, or previously approved procedures, is adequate and appropriate for the intended use, is used within the range of validation, and has been obtained from Software Configuration Management. The software performs the functions described in Table 3-1 in the qualified environment described. Input limitations are discussed in the table column "Range of Use." Unless specifically listed in Table 3-1, there are no limitations on the software output, provided that the appropriate input limitations are observed.

TOUGHREACT Version 3.1.1 (TOUGHREACT V3.1.1 [DIRS 180937], STN: 10396-3.1.1-00) was used for the sensitivity studies documented in this report because this software was the primary code used for the THC seepage model (SNL 2007 [DIRS 177404]). The software program iTOUGH2 Version 5.0 (iTOUGH2 V5.0 [DIRS 160106], STN: 10003-5.0-00) is used here for simulating synthetic liquid-release experiments and predicting seepage rates (see Section 6.4.11.3). Moreover, it is used to solve the inverse problem of estimating the capillary-strength parameter by automatically calibrating the model against synthetic seepage-rate data (see Section 6.4.11.3). The GSLIB software module SISIM V1.204 (GSLIB V. 1.0SISIMV1.204 [DIRS 175981], STN: 10397-1.0SISIMV1.204-00) generates three-dimensional (3-D) and two-dimensional (2-D) spatially correlated random fields by means of sequential indicator simulations. It is used in this report to generate spatially correlated fields of log-permeability modifiers (see Sections 6.4.10 and 6.4.11.3). CUTCHEM Version 2.0 (CUTCHEM V. 2.0 [DIRS 181352], STN: 10898-2.0-00) is used to automatically extract data from large output data files created by the reactive transport model TOUGHREACT V3.1.1. Other routines listed in Table 3-1 are used for various data pre- and post-processing tasks. Note that TOUGHREACT V3.1.1 and CUTCHEM V2.0 were used prior to qualification. The baselined executable files are identical to the versions used to conduct the modeling, as documented in Appendix G.

This report documents sensitivity analyses for the THC seepage model, as listed in Section 1. The input and output files for generating a heterogeneous fracture permeability field are given in Appendix A.1. The input and output files for the model runs presented in this report are listed in Appendices A.2 (for THC simulations), A.3 (TH simulations), and A.4 (ambient simulations).

3.2 EXEMPT SOFTWARE

The commercial, off-the-shelf software code Microsoft Excel 2000 (installed on a desktop PC running the Windows 2000 operating system) has been used in the preparation of this report in an exempt manner to tabulate data and to do basic calculations using built-in functions. TECPLOT V9.0 (installed on a PC platform running the Windows 2000 operating system) was used for plots in Sections 6. TECPLOT is commercial off-the-shelf software and is used solely for graphical representation of output data (i.e., plotting). This software is therefore exempt in accordance with Section 2 of IM-PRO-003.

Table 3-1. Qualified Software Used

Software Name and Version	Software Tracking Number	Platform	Operating System	Range of Use	Description
TOUGHREACT V3.1.1 [DIRS 180937]	10396-3.1.1-00	Linux System	CAOS	Porous and fractured media in a pressure-temperature-composition (P-T-X) range defined by the P-T-X range of the thermodynamic database. Ionic strength limit of ~4 molal (NaCl-dominant solutions).	Used to calculate coupled thermal-hydrological and chemical processes for kinetic and/or equilibrium mineral–water reactions and equilibrium gas–water reactions
CUTCHEM V2.0 [DIRS 181352]	10898-2.0-00	PC	Windows XP	Only for use with TOUGHREACT output files *TEC_nnn.dat*. Limit of 30 extracted points per general location per point in time.	Used to extract automatically data from large output data files created by the reactive transport model TOUGHREACT V2.1 and above
GSLIB V1.0SISIM V1.204 [DIRS 175981]	10397-1.0SISIMV1.204-00	Sun	SUN O.S. 5.5.1	Gridblocks are rectangular.	Used to generate heterogeneous fields of permeability modifiers from input statistical data
avgperm.f V1.0 [DIRS 175950]	10378-1.0-00	DEC	OSF1 V4.0	Total number of gridblocks may not exceed 400,000.	Used to average permeabilities over a number of specific model gridblocks
AddBound V 1.0 [DIRS 152823]	10357-1.0-00	Sun	SunOS 5.5.1	N/A	Adds boundary elements to a mesh file
CutDrift V 1.0 [DIRS 152816]	10375-1.0-00	Sun	SunOS 5.5.1	N/A	Cuts a cylindrical drift from a mesh file
Perm2Mesh V 1.0 [DIRS 152826]	10359-1.0-00	Sun	SunOS 5.5.1	N/A	Maps a field of log-permeability modifiers onto a mesh file
MoveMesh V1.0 [DIRS 152824]	10358-1.0-00	Sun	SunOS 5.5.1	N/A	Adds a constant to the coordinates of a mesh file, translating the coordinate system
AddBorehole V1.0 [DIRS 152822]	10373-1.0-00	Sun	SunOS 5.5.1	N/A	Inserts a borehole into a mesh file
iTOUGH2 V5.0 [DIRS 160106]	10003-5.0-00	Sun Linux System	SunOS 5.5.1 Linux, Red Hat V7.3	Within the range of validation	Provides forward and inverse modeling capabilities for unsaturated and multiphase flow in fractured porous media

4. INPUTS

4.1 DIRECT INPUTS

This section discusses input data used for the THC seepage model sensitivity analyses presented in this report (i.e., for the simulations presented in Sections 6). The qualified status of all direct inputs is shown in the Document Input Reference System (DIRS) database.

Because this report documents analyses of coupled phenomena, a wide variety of input data is required. However, for the sensitivity analyses presented here, input data consist mostly (except as noted in Section 4.1.1) of TOUGHREACT V3.1.1 input files that are unchanged from TOUGHREACT V3.1.1 input files used for THC seepage model simulations (SNL 2007 [DIRS 177404]). These TOUGHREACT V3.1.1 input files were submitted to the Technical Data Management System (TDMS) as qualified output from the THC seepage model (SNL 2007 [DIRS 177404], Appendix G). The same files are used as inputs here, as listed in Table 4.1-1. Only parameters with which sensitivity analyses have been performed in this report are changed from the original input files. These are discussed in more detail in Sections 4.1.1 and 6.4.

The sources of data contained in the original input files are listed in *Drift-Scale THC Seepage Model* (SNL 2007 [DIRS 177404], Section 4). Specific details of input and output file formats can be obtained by reference to the user's manual for TOUGHREACT V3.1.1.

This report is a sensitivity analysis of simulation results from *Drift-Scale THC Seepage Model* (SNL 2007 [DIRS 177404]) to changes in certain parameters, as discussed in Section 6.4. Therefore, use of simulation input files from *Drift-Scale THC Seepage Model* (SNL 2007 [DIRS 177404]) as inputs to this report is both appropriate and substantiated.

Input data other than existing TOUGHREACT V3.1.1 input files have also been used in this report and are listed in Table 4.1-1 as well. These include input files for GSLIB V1.0, which is qualified for use in *Seepage Model for Performance Assessment Including Drift Collapse* (BSC 2004 [DIRS 167652]) to generate heterogeneous fracture permeability fields (Section 6); and calibrated fracture capillary-strength parameter data consistent with *Seepage Calibration Model and Seepage Testing Data* (BSC 2004 [DIRS 171764]) and *Seepage Model for Performance Assessment Including Drift Collapse* (BSC 2004 [DIRS 167652]) (Section 6.2.2.1.5).

Table 4.1-1. Sources of Direct Input Data for the Sensitivity Studies Documented in This Report

Type of Property	Source DTN	File Name and Location
Numerical mesh for steady-state simulations	LB0704DSSSTFLW.002 [DIRS 180853]	File: "MESH" Folder: *\2dflow_81m*
Infiltration fluxes for steady-state simulations	LB0704DSSSTFLW.002 [DIRS 180853]	File: "GENER" Folder: *\2dflow_81m*
Rock thermal and hydrological properties, and simulation parameters pertaining to steady-state flow processes	LB0704DSSSTFLW.002 [DIRS 180853]	File: "flow.inp" Folder: *\2dflow_81m*
Top and bottom boundary conditions	LB0701UZMTHCAL.001 [DIRS 179286],	File: "Th_30%_gas_calibrated.out" (see also Section 6.4.3)
Numerical mesh for ambient, TH, and THC simulations	LB0705DSTHC001.002 [DIRS 180854]	File: "MESH" Folder: *\thc7_81_w0_*
Infiltration fluxes and thermal load for TH and THC simulations	LB0705DSTHC001.002 [DIRS 180854]	File: "GENER" Folder: *\thc7_81_w0_* (for 0 to 50 years)
		File: "GENER" Folder: *\thc7_81_w0_a* (for 50 to 600 years)
		File: "GENER" Folder: *\thc7_81_w0_b* (for 600 to 2,000 years)
		File: "GENER" Folder: *\thc7_81_w0_c* (for 2,000 to 10,000 years)
Rock thermal and hydrological properties, and simulation parameters pertaining to flow processes	LB0705DSTHC001.002 [DIRS 180854]	File: "flow.inp" Folder: *\thc7_81_w0_* (for 0 to 50 years)
		File: "flow.inp" Folder: *\thc7_81_w0_a* (for 50 to 600 years)
		File: "flow.inp" Folder: *\thc7_81_w0_b* (600 to 2,000 years)
		File: "flow.inp" Folder: *\thc7_81_w0_c* (for 2,000 to 10,000 years)
Geochemical input system including initial water composition, boundary water composition, initial mineral abundances, porosity and permeability relations, and initial gas zones (corresponding to water "w0")	LB0705DSTHC001.002 [DIRS 180854]	File: "chemical.inp" Folder: *\thc7_81_w0_*
Transport properties including simulation parameters	LB0705DSTHC001.002 [DIRS 180854]	File: "solute.inp" Folder: *\thc7_81_w0_*
Simulated water chemistry from THC seepage model with homogeneous fracture permeability (corresponding to water "W0")	LB0705DSTHC001.001 [DIRS 181217]	Files: *frac_81_162_dr_w0.xls* and *frac_81_162_w0.xls*

Table 4.1-1. Sources of Direct Input Data for the Sensitivity Studies Documented in This Report (Continued)

Type of Property	Source DTN	File Name and Location
Thermodynamic database	LB0705DSTHC001.002 [DIRS 180854]	File: "thc_ymp_1.1.dat" Folder: *\thc7_81_w0_*
Input files for GSLIB V1.0 (SISIM) simulations for generation of heterogeneous fracture permeability fields	LB0304SMDCREV2.001 [DIRS 173235]	File: "perm.par" Folder: *\20_k-realizations*
Mean and standard deviation of post-excavation log-permeabilities	LB0302SCMREV02.002 [DIRS 162273]	Table 3; SMPA model calibrated fracture capillary-strength parameter for Topopah Spring Lower Lithophysal (Tptpll) unit
Matrix porosity	LB0208UZDSCPMI.002 [DIRS 161243]	File: *drift-scale calibrated properties for mean infiltration2.xls*
Dry and wet thermal conductivities of repository units	MO0612MEANTHER.000 [DIRS 180552]	File: *Repository_ Unit_Mean_Kthermal.xls*
Dry and wet thermal conductivities of non-repository units	SN0303T0503102.008 [DIRS 162401]	File: *NonrespositoryThermal Conductivity Model_031403.xls*
Grain densities and grain-specific heat capacities	SN0307T0510902.003 [DIRS 164196]	File: *rock_grain_heat_capacity (edited).xls* (for grain specific heat capacity, values used are rounded to two significant figures when expressed in J/kg between 25°C and 325°C)

NOTE: DTN = data tracking number.

4.1.1 Modifications in Input Files Obtained from DTN: LB0704DSSSTFLW.002

The input files ("MESH," "GENER", and "flow.inp") obtained from DTN: LB0704DSSSTFLW.002 [DIRS 180853] were used mostly "as is" for steady-state simulations. Minor differences exist between the downloaded files and the files actually used for steady-state simulations in this report. These minor differences are listed below.

4.1.1.1 Modifications in File "GENER"

The downloaded "GENER" files were used without modifications, i.e., no difference exists between the downloaded "GENER" file and the one used in steady-state simulations.

4.1.1.2 Modifications in File "flow.inp"

The following minor modifications were made when appropriate:

- The dry thermal conductivity of model layer "pp1Fz" is provided as 1.10×10^{-4} W/m-K, instead of 1.11×10^{-4} W/m-K in the downloaded "flow.inp." This small difference happened inadvertently and does not affect model results in any significant way. (The pp1Fz fracture rock block is situated far away from the emplacement drift. Evolution of THC processes near the emplacement drift is not impacted by the minor difference in pp1fz thermal conductivity value.)

- For simulations with Leverett scaling, the simulation flag MOPR(6) was set to 1. For simulations without Leverett scaling, the same flag was set to 0. The downloaded "flow.inp" always has this parameter as "1" (Leverett scaling included).

- The convergence criterion used in the steady-state simulations is 1.0×10^{-4}. In the downloaded "flow.inp," it is 1.0×10^{-5}. The selected convergence criterion is small enough such that the difference between the two is not expected to affect model results (see discussion in Section 6.5).

- The maximum time step that the steady-state simulations could adopt is different. This is not an issue, because the steady-state simulations never took as big a time step as is allowed in the parameter file.

- Printouts are obtained at different times compared to the downloaded "flow.inp" file.

4.1.1.3 Modifications in File "MESH"

There is no difference between the downloaded "MESH" file and the one actually used in steady-state simulations in this report, except some minor formatting difference in elements F1388 through F1408. These elements do not enter the actual flow simulations (they are excluded in the connection list) and are retained in the "MESH" file mostly as a placeholder. Thus, this difference will not impact the model results.

4.1.2 Modifications in Input Files Obtained from DTN: LB0705DSTHC001.002

The input files ("MESH," "GENER," "flow.inp," "chemical.inp," "solute.inp," and "thc_ymp1.1.dat") obtained from DTN: LB0705DSTHC001.002 [DIRS 180854] were used mostly in "as is" condition. Minor modifications were made in some of the files to suit the specific need of a sensitivity simulation. These minor modifications and their purpose are described below.

4.1.2.1 Modifications in File "GENER"

For TH and THC simulations with present-day mean infiltration fluxes, the downloaded "GENER" files were used without modifications. For ambient simulations (i.e., simulations without applications of heat), the "GENER" files were edited with a text editor to delete the information pertaining to heat generation. The edited "GENER" files for ambient simulations thus contain only the water infiltration fluxes. For simulations (ambient, TH, or THC) with ten times the mean infiltration fluxes (see Section 6.4.5), the infiltration fluxes in the "GENER" files were obtained by multiplying the infiltration fluxes in the "GENER" files for mean infiltration fluxes by a factor of 10. This was accomplished by a text editor and hand calculations.

4.1.2.2 Modifications in File "flow.inp"

The following minor modifications were made when appropriate:

- For simulations with Leverett scaling, simulation flag MOPR(6) was set to 1. For simulations without Leverett scaling, the same flag was set to 0.

- For ambient and TH simulations, simulation flag MOPR(1) was set to 2. For THC simulations, the same flag was set to 0.

- For carrying out simulations with different values of the initial fracture capillary-strength parameter for the Tptpll (or tsw35) unit, the ICP(4) parameter for that rock unit was modified. The actual value used in a particular simulation is the subject of this sensitivity study, and further discussion on this matter can be found in Section 6.

- To obtain more spatial output in file "GASOBS.DAT," the number of gridblocks in which outputs were to be obtained was changed (see the list below the keyword "wdata" in file "flow.inp")

- The ε parameter for invert materials ("*invu*," "*invl*," "*wallu*," and "*walll*" in the "ROCKS" block of file "flow.inp") was changed from 0.01 to 0.031. This parameter is needed for linearizing the capillary pressure versus saturation curve beginning at liquid saturation $S_{lr}+\varepsilon$, where S_{lr} is the residual liquid saturation. The ε parameter is calculated such that the maximum capillary pressure at $S_l = 0$ does not exceed 1×10^8 Pa. Since the invert materials have different capillary properties compared to the host rock (matrix or fractures of Tptpll or tsw35), as can be seen in file "flow.inp," the parameter ε was recalculated for the invert materials. The recalculated value of ε for the invert materials is 0.0331, which is used in the ambient, TH, and THC simulations of this report. The value of $\varepsilon = 0.01$, which is used for the invert materials in *Drift-Scale THC Seepage Model* (SNL 2007 [DIRS 177404]), is a deviation from the actual value of 0.0331. However, this minor deviation is not expected to have any significant impact on the predictions from that report (SNL 2007 [DIRS 177404]).

- Residual saturations for "innr" and "outr" rock blocks were changed from 0.0 to 0.01 in simulations where enhanced infiltration fluxes (see Sections 6.4.5, 6.5, 6.6, and 6.7) were used. The rock blocks "innr" and "outr" are situated in the air space inside the emplacement drift. Consequently, these rock blocks do not have any real residual saturations (since they are not porous media). However, they have been conceptualized as porous media, since flow processes are simulated using the reactive transport software TOUGHREACT (see Section 3.1), which is formulated for porous media. In simulations with present-day mean infiltrations (see Sections 6.6 and 6.7), water does not actually enter the emplacement drift. As a result, the "innr" and "outr" rock blocks can be modeled using zero residual saturations. The same approach has been used in *Drift-Scale THC Seepage Model* (SNL 2007 [DIRS 177404]). However, with enhanced infiltration fluxes (see Section 6.4.5), water actually enters the emplacement drift, and if a zero residual saturation value is provided for "innr" and

"outr" rock blocks, numerical difficulties are encountered. To resolve these numerical difficulties, a small number (such as 0.01) is provided as the residual saturation of those two rock blocks. This is a conceptual choice and is not expected to affect the simulation results in any significant manner.

4.1.3 Modifications in File "perm.par"

- To obtain three different realizations of the heterogeneous Tptpll fracture permeability field with the same statistics, three different (random) seeds were used in file "perm.par" downloaded from DTN: LB0304SMDCREV2.001 [DIRS 173235]. The actual values of the random seeds used are of no consequence.

- The original "perm.par" file was used for generating 3-D permeability fields. This was modified to generate 2-D heterogeneous fracture permeability fields (see Section 6.4.10).

- The original "perm.par" had different spatial step sizes in horizontal and vertical directions. For generating the permeability fields for this study, this was modified. The permeability fields for this report were generated with a spatial step size of 0.2 m in both horizontal and vertical directions (see Section 6.4.10 for more details).

4.1.4 Thermal Properties of the UZ Model Layers

The thermal properties are a compilation of the data from matrix porosity in DTN: LB0208UZDSCPMI.002 [DIRS 161243], dry and wet thermal conductivities of the repository stratigraphic units in DTN: MO0612MEANTHER.000 [DIRS 180552], dry and wet thermal conductivities of the nonrepository stratigraphic units in DTN: SN0303T0503102.008 [DIRS 162401], and grain densities and grain specific heat capacities in DTN: SN0307T0510902.003 [DIRS 164196]. While those source DTNs provide the thermal properties for different stratigraphic units of the mountain, thermal properties are needed for the different model layers of the THC model grid. Since the THC model layers do not always match (for example, there is more than one model layer in certain stratigraphic units) the stratigraphic units of the geologic framework model (GFM), some averaging is needed. Appendix B describes how the thermal properties for the THC model layers are derived from those of the GFM stratigraphic units. Appendix B also provides the thermal properties for various unsaturated zone (UZ) model layers.

4.2 CRITERIA

This report is intended to complement results of the THC seepage model. Details on the specific regulatory requirements that apply to the THC seepage model are presented in *Drift-Scale THC Seepage Model* (SNL 2007 [DIRS 177404], Section 4.2). The applicable federal regulations and technical requirements related to the work activities associated with the DST seepage model report and the THC sensitivity study have been identified in *Technical Work Plan for: Revision of Model Reports for Near-Field and In-Drift Water Chemistry* (SNL 2007 [DIRS 179287], Section 3.2). There are no

U.S. Department of Energy (DOE) orders applicable to the scope of this report identified in the TWP (SNL 2007 [DIRS 179287]).

The acceptance criteria that will be used by the U.S. Nuclear Regulatory Commission to determine whether the technical requirements have been met are identified in *Yucca Mountain Review Plan, Final Report* (YMRP) (NRC 2003 [DIRS 163274]). The pertinent requirements and acceptance criteria for the THC sensitivity study are summarized in Table 4.2-1. These acceptance criteria are identified in Section 2.2.1.3.3.3 of the YMRP (NRC 2003 [DIRS 163274]), and their applicability to the THC seepage model is summarized in *Drift-Scale THC Seepage Model* (SNL 2007 [DIRS 177404], Section 4.2).

Table 4.2-1. Applicable Project Requirements and YMRP Acceptance Criteria for the THC Seepage Model

Requirement	YMRP Acceptance Criteria [a]
10 CFR 63.114(a)-(c) and (e)-(g)	Criteria 1 to 5 for *Quantity and Chemistry of Water Contacting Waste Packages and Waste Forms*

[a] From NRC 2003 [DIRS 163274], Section 2.2.1.3.3.3.

The acceptance criteria identified in Section 2.2.1.3.3.3 of the YMRP (NRC 2003 [DIRS 163274]) are given below, followed by a short description of their applicability to this report:

- **Acceptance Criterion 1—***System Description and Model Integration Are Adequate*

  The applicable subcriteria are:

  (1) Total System Performance Assessment (TSPA) adequately incorporates important design features, physical phenomena, and couplings, and uses consistent and appropriate assumptions throughout the quantity and chemistry of water contacting engineered barriers and waste-forms abstraction processes.

  (2) The abstraction of the quantity and chemistry of water contacting engineered barriers and waste forms uses assumptions, technical bases, data, and models that are appropriate and consistent with other related U.S. Department of Energy abstractions.

  (3) Important design features, such as waste package design and material selection, backfill, drip shield, ground support, thermal loading strategy, and degradation processes, are adequate to determine the initial and boundary conditions for calculations of the quantity and chemistry of water contacting engineered barriers and waste forms.

  (5) Sufficient technical bases and justification are provided for TSPA assumptions and approximations for modeling coupled thermal-hydrologic-mechanical-chemical effects on seepage and flow, the waste package chemical environment, and the chemical environment for radionuclide release. The

effects of distribution of flow on the amount of water contacting the engineered barriers and waste forms are consistently addressed, in all relevant abstractions.

(8) Adequate technical bases are provided, including activities such as independent modeling, laboratory or field data, or sensitivity studies, for inclusion of any thermal-hydrologic-mechanical-chemical couplings and features, events, and processes.

(9) Performance-affecting processes that have been observed in thermal-hydrologic tests and experiments are included into the TSPA.

(10) Likely modes for container corrosion (Section 2.2.1.3.1 of the YMRP) are identified and considered in determining the quantity and chemistry of water entering the engineered barriers and contacting waste forms. For example, the model abstractions consistently address the role of parameters, such as pH, carbonate concentration, and the effect of corrosion on the quantity and chemistry of water contacting engineered barriers and waste forms.

(12) Guidance in NUREG–1297 (Altman et al. 1988 [DIRS 103597]) and NUREG-1298 (Altman et al. 1988 [DIRS 103750]), or other acceptable approaches, is followed.

- **Acceptance Criterion 2—***Data Are Sufficient for Model Justification*

  The applicable subcriteria are:

  (1) Geological, hydrological, and geochemical values used in the license application are adequately justified. Adequate description of how the data were used, interpreted, and appropriately synthesized into the parameters is provided.

  (2) Sufficient data were collected on the characteristics of the natural system and engineered materials to establish initial and boundary conditions for conceptual models of thermal-hydrological-mechanical-chemical coupled processes that affect seepage and flow and the engineered barrier chemical environment.

  (3) Thermal-hydrologic tests were designed and conducted with the explicit objectives of observing thermal-hydrologic processes for the temperature ranges expected for repository conditions and making measurements for mathematical models. Data are sufficient to verify that thermal-hydrologic conceptual models address important thermal-hydrologic phenomena.

  (4) Sufficient information to formulate the conceptual approach(es) for analyzing water contact with the drip shield, engineered barriers, and waste forms is provided.

- **Acceptance Criterion 3—***Data Uncertainty Is Characterized and Propagated Through the Model Abstraction*

  The applicable subcriteria are:

  (1) Models use parameter values, assumed ranges, probability distributions, and bounding assumptions that are technically defensible, reasonably account for uncertainties and variabilities, and do not result in an under-representation of the risk estimate.

  (2) Parameter values, assumed ranges, probability distributions, and bounding assumptions used in the TSPA calculations of the quantity and chemistry of water contacting engineered barriers and waste forms are technically defensible and reasonable, based on data from the Yucca Mountain region (e.g., results from large block and drift-scale heater and niche tests), and a combination of techniques that may include laboratory experiments, field measurements, natural analog research, and process-level modeling studies.

  (3) Input values used in the TSPA calculations of the quantity and chemistry of water contacting engineered barriers (e.g., drip shield and waste package) are consistent with the initial and boundary conditions and the assumptions of the conceptual models and design concepts for the Yucca Mountain site. Correlations between input values are appropriately established in the U.S. Department of Energy TSPA. Parameters used to define initial conditions, boundary conditions, and computational domain in sensitivity analyses involving coupled thermal-hydrologic-mechanical-chemical effects on seepage and flow, the waste package chemical environment, and the chemical environment for radionuclide release, are consistent with available data. Reasonable or conservative ranges of parameters or functional relations are established.

  (4) Adequate representation of uncertainties in the characteristics of the natural system and engineered materials is provided in parameter development for conceptual models, process-level models, and alternative conceptual models. The U.S. Department of Energy may constrain these uncertainties using sensitivity analyses or conservative limits. For example, the U.S. Department of Energy demonstrates how parameters used to describe flow through the engineered barrier system bound the effects of backfill and excavation-induced changes.

- **Acceptance Criterion 4—***Model Uncertainty Is Characterized and Propagated Through the Model Abstraction*

  The applicable subcriteria are:

  (1) Alternative modeling approaches of features, events, and processes are considered and are consistent with available data and current scientific

understanding, and the results and limitations are appropriately considered in the abstraction.

(2) Alternative modeling approaches are considered and the selected modeling approach is consistent with available data and current scientific understanding. A description that includes a discussion of alternative modeling approaches not considered in the final analysis, and the limitations and uncertainties of the chosen model, is provided.

(3) Consideration of conceptual-model uncertainty is consistent with available site characterization data, laboratory experiments, field measurements, natural analog information and process-level modeling studies; and the treatment of conceptual-model uncertainty does not result in an under-representation of the risk estimate.

(4) Adequate consideration is given to effects of thermal-hydrologic-mechanical-chemical coupled processes in the assessment of alternative conceptual models.

(5) If the U.S. Department of Energy uses an equivalent continuum model for the TSPA abstraction, the models produce conservative estimates of the effects of coupled thermal-hydrologic-mechanical-chemical processes on calculated compliance with the postclosure public health and environmental standards.

- **Acceptance Criterion 5—***Model Abstraction Output Is Supported by Objective Comparisons*

  The applicable subcriterion is:

  (3) Accepted and well-documented procedures are used to construct and test the numerical models that simulate coupled thermal-hydrologic-mechanical-chemical effects on seepage and flow, engineered barrier chemical environment, and the chemical environment for radionuclide release. Analytical and numerical models are appropriately supported. Abstracted model results are compared with different mathematical models, to judge robustness of results.

Additional completion criteria are identified in the TWP (SNL 2007 [DIRS 179287]). This work will satisfy the requirements of AP-16.1Q, *Condition Reporting and Resolution*, to enable closure of CRs related to this report. This revision of the THC sensitivity study is associated with CR-7037 and CR-7193.

CR-7037

The governing TWP (SNL 2007 [DIRS 179287]) specifies the action items on CR-7037 as follows.

(i) TOUGHREACT simulations at repository center and edge conditions were shown to have different bin histories in the THC sensitivity study (BSC 2006

[DIRS 174104]). A sensitivity analysis will be run to evaluate differences in composition of potential seepage waters at the repository edge. In addition, potential seepage water compositions will be selected from zones of higher liquid saturation, further away than the boiling/wetting front (e.g., from waters designated "HISAT" instead of those designated "FRONT," as defined in BSC 2004 [DIRS 169858], Section 6.2.1.3). This change in approach is based on the comparison of in-drift seepage composition with HISAT compositions.

According to the governing TWP (SNL 2007 [DIRS 179287], Section 1.2.1), this portion of CR-7037 is addressed in *Drift-Scale THC Seepage Model* (SNL 2007 [DIRS 177404]). Consequently, this portion of CR-7037 is not addressed in this report.

(ii) According to the governing TWP (SNL 2007 [DIRS 179287], Section 1.2.4), the THC sensitivity study (BSC 2006 [DIRS 174104]) will be revised to address CR 7037, which notes that information provided in Revision 00 of the THC sensitivity study (BSC 2006 [DIRS 174104]) shows that predicted seepage is enhanced by THC effects not considered in *Abstraction of Drift Seepage* (BSC 2004 [DIRS 169131]). The revised analysis will further evaluate effects from THC processes on the predicted occurrence of seepage, while eliminating the sensitivity study on repository edge effects, which will be addressed in the THC seepage report (SNL 2007 [DIRS 177404]).

The sensitivity analysis in this report addresses the above portion of CR-7037. Section 7.3 provides a summary of how this has been accomplished in this report.

CR-7193

Improve integration of the THC and seepage models. Section 7.3 provides a summary of how this has been accomplished in this report.

Two other CRs (CR-6691 and CR-8009) have some relevance to this sensitivity study. CR-6691 reports concerns regarding "failure to maintain mass balance in THC normative salt precipitation calculations." Per the TWP (SNL 2007 [DIRS 179287], Section 1.2.1), CR-6691 is addressed in *Drift-Scale THC Seepage Model* (SNL 2007 [DIRS 177404]), and is therefore not addressed here. CR-8009 reports concerns about proper implementation of "capillary pressure function flag of 10 and Leverett scaling function in TOUGHREACT." The CR found these deficiencies in a previous version (V3.0) of the TOUGHREACT software. Since the CR was generated, the TOUGHREACT software has been updated and qualified to address these concerns. The qualified software TOUGHREACT V3.1.1 (see Section 3.1) has been used in performing the simulations in this report, and the previous version (V3.0) has not been used at all. Thus, it can be concluded that CR-8009 has no adverse impact on this sensitivity report. No other discussion on CR-8009 will be provided in this report.

4.3 CODES, STANDARDS, AND REGULATIONS

No specific, formally established codes, standards, or regulations, other than those discussed in Section 4.2, have been identified as applying to this analysis.

5. ASSUMPTIONS

There are no assumptions specific to the sensitivity analyses documented in this report. Assumptions, approximations, and simplifications related to the development and implementation of the THC seepage model are presented in *Drift-Scale THC Seepage Model* (SNL 2007 [DIRS 177404], Sections 5, 6.2.3, and 6.4.6). The development of the methodology used for the numerical modeling of heat and fluid flow in unsaturated fractured porous media, calculation of mineral–water reactions, and transport of aqueous and gaseous species are discussed in *Drift-Scale THC Seepage Model* (SNL 2007 [DIRS 177404], Sections 6.2, 6.4, and 6.5).

INTENTIONALLY LEFT BLANK

6. SCIENTIFIC ANALYSIS DISCUSSION

This section documents sensitivity studies carried out with the THC seepage model. The scientific approach and technical methods followed to conduct these analyses, the results, and the sources and impacts of uncertainties are detailed in Sections 6.1 through 6.11. Conclusions are discussed in Section 7. Outputs were submitted to the TDMS under DTNs listed in Section 7.4.

The results from this analysis report are part of the basis for the treatment of features, events, and processes (FEPs) as discussed in *Technical Work Plan for: Revision of Model Reports for Near-Field and In-Drift Water Chemistry* (BSC 2007 [DIRS 179287], Section 2.1.3). FEPs that are relevant to the subject matter of this report are summarized in Table 6-1. These FEPs have been taken from the current license application (LA) FEPs list (DTN: MO0706FEPLA.001 [DIRS 181613]). Each FEP is cross-referenced to the relevant section (or sections) in this report in Table 6-1. The discussions provided in this and other model and abstraction reports form the technical basis for evaluating these FEPs for TSPA-LA.

Table 6-1. Features, Events, and Processes Associated with This Report

FEP No.	FEP Name	FEP Description	Sections Discussing FEPs-Related Items
2.1.09.12.0A	Rind (Chemically Altered Zone) Forms in the Near-Field	Thermal-chemical processes involving precipitation, condensation, and re-dissolution could alter the properties of the adjacent rock. These alterations may form a rind, or altered zone, in the rock, with hydrological, thermal, and mineralogical properties different from the initial conditions.	6.1.1, 6.1.2, 6.3, 6.4.7, 6.4.9, 6.6.2, 6.7.1, 6.7.2, 6.8, 6.9, 6.10, 7.1, and 7.2.
2.2.07.02.0A	Unsaturated Groundwater Flow in the Geosphere	Groundwater flow occurs in unsaturated rocks in most locations above the water table at Yucca Mountain, including at the location of the repository. See related FEPs for discussions of specific issues related to unsaturated flow.	6.1.1, 6.1.2, 6.3, 6.4.10, 6.4.11, 6.5, 6.6.1, 6.6.2, 6.7.1, 6.7.2, 6.8, 6.9, 6.10, 7.1, and 7.2
2.2.07.08.0A	Fracture Flow in the UZ	Fractures or other analogous channels may act as conduits for fluids to move into the subsurface to interact with the repository and as conduits for fluids to leave the vicinity of the repository and be conducted to the saturated zone. Water may flow through only a portion of the fracture network, including flow through a restricted portion of a given fracture plane.	6.1.1, 6.1.2, 6.3, 6.4.10, 6.4.11, 6.5, 6.6.1, 6.6.2, 6.7.1, 6.7.2, 6.8, 6.9, 6.10, 7.1, and 7.2
2.2.08.03.0B	Geochemical Interaction and Evolution	Groundwater chemistry and other characteristics, including temperature, pH, Eh, ionic strength, and major ionic concentrations, may change through time, as a result of the evolution of the disposal system or from mixing with other waters. Geochemical interactions may lead to dissolution and precipitation of minerals along the groundwater flow path, affecting groundwater flow, rock properties, and sorption of radionuclides. Effects on hydrologic flow properties of the rock, radionuclide solubilities, sorption processes, and colloidal transport are relevant. Kinetics of chemical reactions should be considered in the context of the time scale of concern.	6.1.1, 6.1.2, 6.3, 6.4, 6.6.2, 6.6.3, 6.8, 6.8, 6.10, and 7.1

Table 6-1. Features, Events, and Processes Associated with This Report (Continued)

FEP No.	FEP Name	FEP Description	Sections Discussing FEPs-Related Items
2.210.01.0A	Repository-Induced Thermal Effects on Flow in the UZ	Thermal effects in the geosphere could affect the long-term performance of the disposal system, including effects on groundwater flow (e.g., density-driven flow), mechanical properties, and chemical effects in the UZ.	6.1.1, 6.1.2, 6.3, 6.4.4, 6.6.1, 6.6.2, 6.6.3, 6.7.1, 6.7.2, 6.8, 6.9, 6.10, 7.1, and 7.2

6.1 OVERVIEW

6.1.1 TH and THC Processes

Emplacement of hot waste packages in underground tunnels is expected to cause various coupled thermal-hydrological-chemical (THC) processes in the unsaturated, fractured host rock. Focusing first on coupled thermal-hydrological (TH) processes (Figure 6.1-1), it is expected that the heat will cause vaporization and boiling of the matrix pore water, with subsequent migration of vapor out of the matrix into the embedded fractures. Once in the fracture, water vapor will move away from the tunnel through the permeable fracture network by buoyancy, by the increased vapor pressure resulting from heating and boiling, and by local convection. In cooler regions, vapor will condense on fracture walls, where it will flow through the fracture network under gravity drainage or be absorbed back into the matrix (because of the stronger capillarity of the matrix pores). Slow imbibition of water from fractures into the matrix gradually leads to increases in the liquid saturation of the rock matrix. Under conditions of continuous thermal loading, a dryout zone will eventually develop closest to the heat source, separated from the condensation zone by a nearly isothermal zone maintained at about the boiling temperature of water. This nearly isothermal zone is characterized by a continuous process of boiling, vapor transport, condensation, and migration of water back to the heat source (either by capillary forces or gravity drainage), often called a heat pipe (Pruess et al. 1990 [DIRS 100819]). TH processes in the unsaturated fractured rocks of Yucca Mountain have been extensively examined since the early 1980s (Pruess et al. 1984 [DIRS 144801]; Pruess et al. 1990 [DIRS 100819]; Buscheck and Nitao 1993 [DIRS 100617]; Pruess 1997 [DIRS 144794]; Kneafsey and Pruess 1998 [DIRS 139133]; Haukwa et al 1999 [DIRS 137562]; Buscheck et al. 2002 [DIRS 160749]; Haukwa et al. 2003 [DIRS 165165]; Birkholzer et al. 2004 [DIRS 172262]; BSC 2005 [DIRS 172232]; BSC 2005 [DIRS 174101]; Wu et al. 2006 [DIRS 180274]). The methods used in these predictive studies have also been validated against the TH response of heater tests conducted at the repository site (Tsang and Birkholzer 1999 [DIRS 137577]; Birkholzer and Tsang 2000 [DIRS 154608]; Mukhopadhyay and Tsang 2002 [DIRS 160788]; Mukhopadhyay and Tsang 2003 [DIRS 160790]; BSC 2005 [DIRS 172232]).

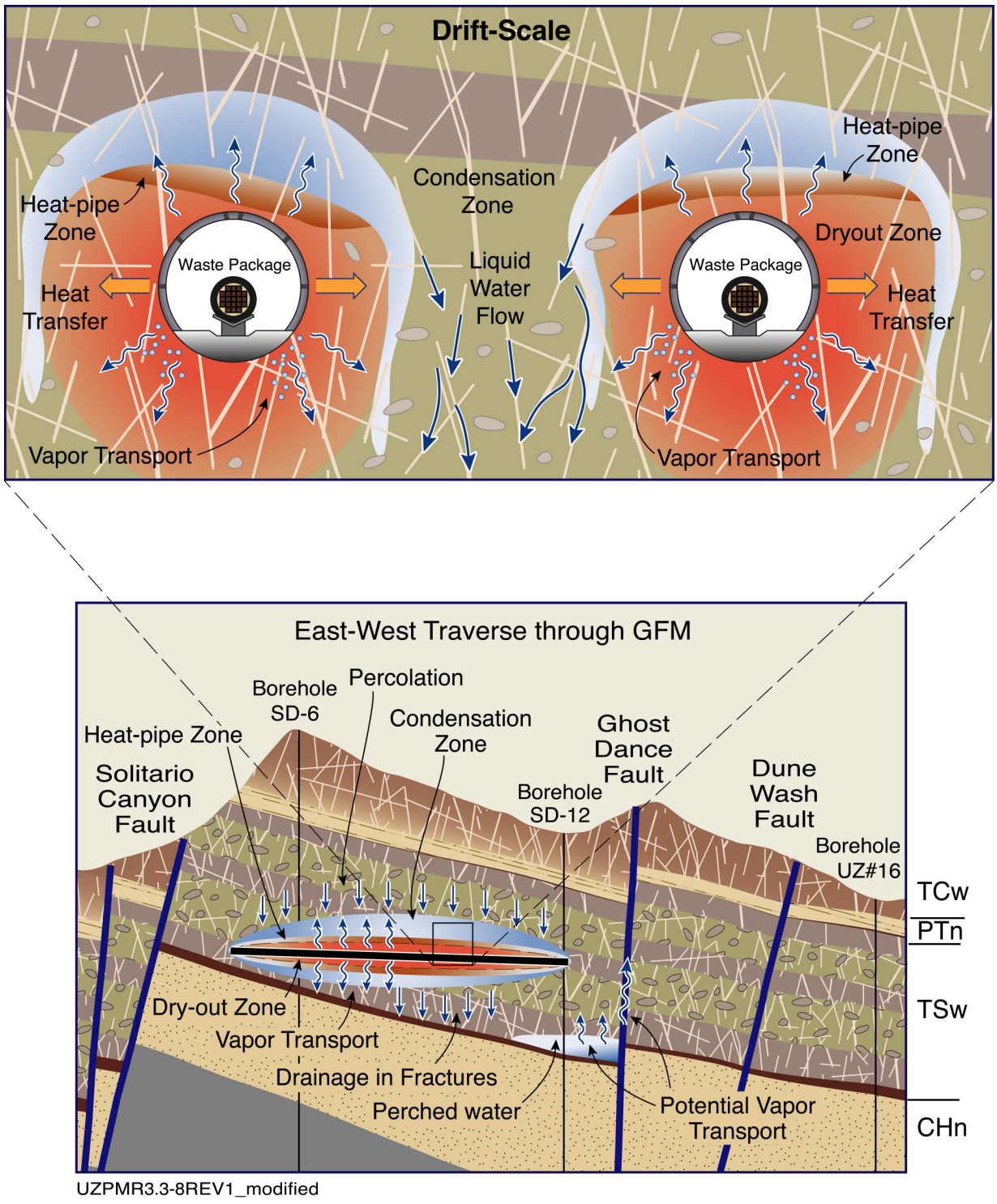

Figure 6.1-1. Schematic of TH Processes at the Drift Scale and the Mountain Scale

Simultaneous to the TH processes, the unsaturated fractured rock also undergoes substantial chemical changes. The chemical evolution of waters, gases, and minerals is intimately coupled to the TH processes (boiling, condensation, and drainage) discussed above. Distribution of

condensate in the fracture system determines where mineral dissolution and precipitation can occur in the fractures and where there can be direct interaction (via diffusion) between matrix pore waters and fracture waters. Figure 6.1-2 schematically shows the relationships between TH and chemical processes in the zones of boiling, condensation, and drainage, in the rock mass at the fracture–matrix interface surrounding an emplacement tunnel.

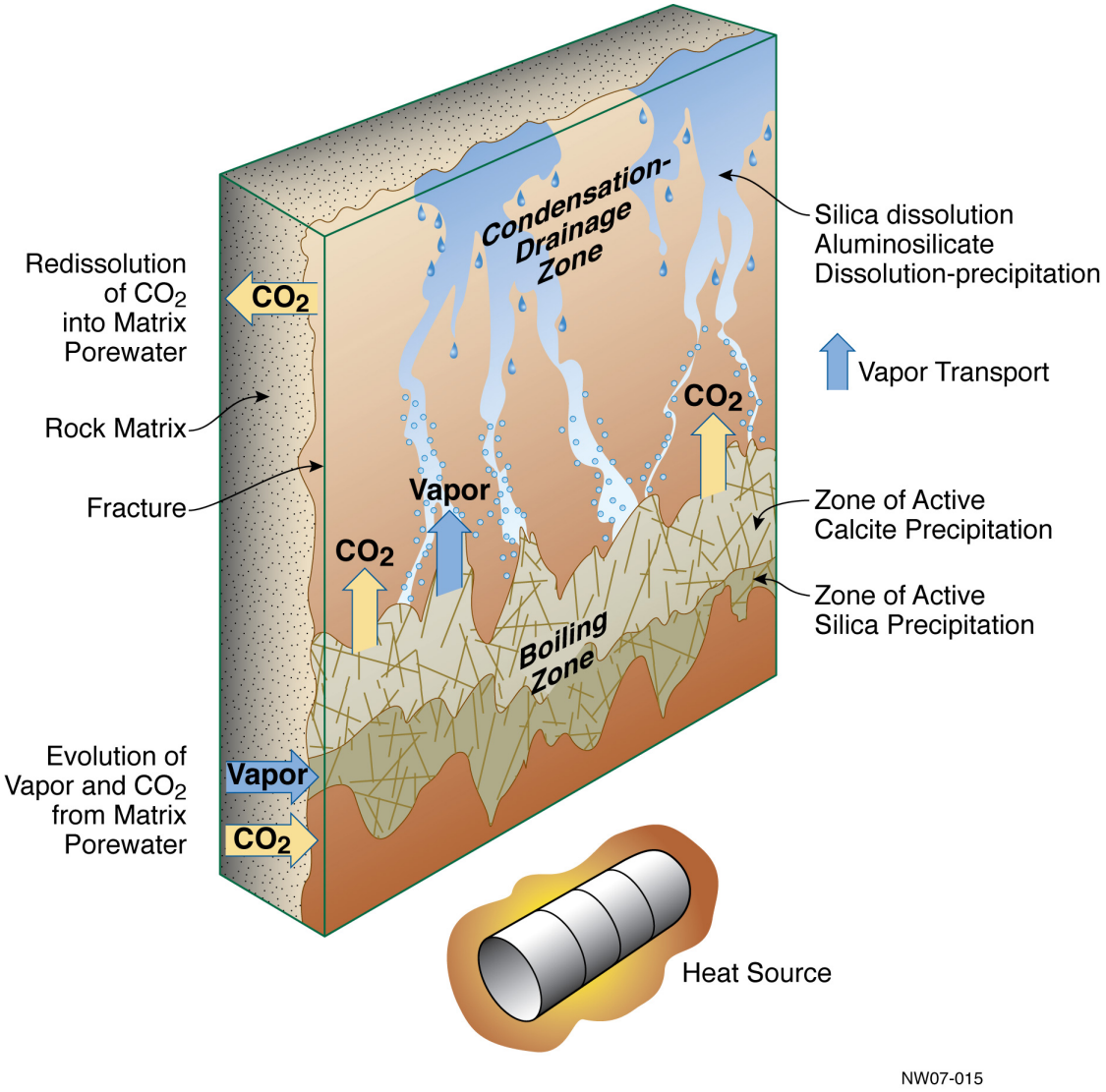

Figure 6.1-2. Schematic Diagram of Fracture–Matrix Interface Showing the Relationship between TH Processes and Geochemical Processes

In short, redistribution of mineral phases will occur as a result of differences in mineral solubility as a function of temperature. The inverse relation between temperature and calcite solubility (as opposed to the silica phases, which are more soluble at higher temperatures) will also cause zonation in the distribution of calcite and silica phases in both the condensation and boiling zones (Figure 6.1-2). Precipitation of amorphous silica or another silica phase is likely to be confined to a narrower zone, where the evaporative concentration from boiling exceeds its solubility. In contrast, calcite could precipitate in fractures over a broad zone of elevated

temperature and where CO_2 has exsolved because of temperature increases or boiling. Alteration of feldspars to clays and zeolites is likely to be most rapid in the boiling zone because of their increased solubility (as well as higher dissolution and precipitation fluxes) at higher temperatures (Lasaga 1998 [DIRS 117091]). Coupled THC processes in the unsaturated fractured rock of Yucca Mountain have been under investigation for some time now (Spycher et al. 2003 [DIRS 162121]; Sonnenthal et al. 2005 [DIRS 176005]; BSC 2006 [DIRS 174104]; Mukhopadhyay et al. 2006 [DIRS 180822]; SNL 2007 [DIRS 177404]). These THC modeling studies investigate the coupling among heat, water, and vapor flow, aqueous and gaseous species transport, kinetic and equilibrium mineral–water reactions, and feedback of mineral precipitation/dissolution on porosity, permeability, and capillary pressure. Such studies developed the underlying conceptual and mathematical models, which provide the basis for modeling the TH effects of the relevant mineral-water-gas reactions and transport processes in the host rock.

While the overall impact of THC processes in unsaturated fractured rock has been dealt with in those previous investigations, this report focuses on one particular aspect—the changes in the hydrologic properties of the unsaturated fractured rock, caused by the THC processes. THC processes of mineral precipitation and dissolution dynamically change the hydraulic properties of the rock (such as porosity, permeability, and capillary characteristics). These changes, in turn, cause perturbations in the flow fields around an emplacement tunnel, which may lead to local flow channeling. In this report, it is shown that simulations may predict seepage (i.e., dripping of liquid water from the unsaturated rock into the emplacement tunnels) because of such local flow channeling, depending on how changes in capillary response are represented.

6.1.2 Seepage

Seepage refers to dripping of liquid water into the emplacement tunnels from the rock above. Understanding the processes affecting seepage is important, because seepage (or its absence) is directly connected to the overall performance of a repository in successfully isolating nuclear waste from the geosphere. For example, if seepage occurs, it may promote corrosion of the waste packages, which may lead to release of radioactive materials from the emplacement tunnels into the surrounding rock. Both experimental and modeling analyses (Wang et al. 1999 [DIRS 106146]; Trautz and Wang 2002 [DIRS 160335]; Finsterle et al. 2003 [DIRS 163214]; BSC 2004 [DIRS 171764]) have been performed to determine the processes affecting seepage under ambient conditions, i.e., in the absence of any thermal effects. Predictive modeling studies, based on a stochastic continuum model, have also been carried out to predict the probability and magnitude of seepage under ambient conditions at Yucca Mountain (Li and Tsang [DIRS 163714]; BSC 2004 [DIRS 167652]).

These previous ambient seepage studies have generally concluded that seepage under ambient conditions is reduced or prevented by the “capillary-barrier” effect (i.e., the difference in capillary pressure between the rock formation and a large underground opening such as the emplacement tunnel). This capillary-barrier effect causes water to be mostly diverted around the tunnels rather than seeping into them. However, according to those earlier investigations, seepage under ambient conditions can still occur when local flow channeling, caused by heterogeneities in the host rock, results in local saturation buildup. If saturation buildup exceeds a certain threshold saturation (see below for further discussion), the capillary barrier

is overcome, and seepage commences. Thus, heterogeneity plays a crucial role in controlling seepage.

Since spent fuel waste can impose considerable thermal load on the surrounding rock, seepage under thermal conditions has also been investigated at Yucca Mountain through development of TH seepage models (Birkholzer et al. 2004 [DIRS 172262]; BSC 2005 [DIRS 172232]). While the capillary-barrier effect and heterogeneity of the host rock were found to control seepage even under thermal conditions (similar to ambient seepage), some significant differences in the mechanism of seepage between the two were also observed. The superheated dryout zone outside the emplacement tunnel under thermal conditions subjected incoming water to vigorous boiling, preventing liquid water from reaching the tunnel (i.e., liquid water could reach the tunnel wall only after the dryout zone had disappeared). In other words, the dryout zone provides an additional barrier to seepage, effectively creating what has been termed a "vaporization barrier" (Birkholzer et al. 2004 [DIRS 172262]; BSC 2005 [DIRS 172232]). While the analyses in the study by Birkholzer et al. (2004 [DIRS 172262]) and in *Drift-Scale Coupled Processes (DST and TH Seepage) Models* (BSC 2005 [DIRS 172232]) provide an important framework for investigating seepage including TH effects, the THC changes in the host rock are not included in their conceptual model. It has only recently been shown (BSC 2006 [DIRS 174104]; Mukhopadhyay et al. 2006 [DIRS 180822]) that the THC conditions in the rock are pertinent for seepage, not only for the chemistry of the seepage water but also for the amount and duration of seepage. As stated earlier, heterogeneity in the host rock plays a key role in controlling seepage. By changing the hydrologic properties of the rock, the THC processes introduce dynamic (i.e., time-dependent) heterogeneities in the rock. Thus, the transient pattern of seepage under THC processes is different from that when only ambient or TH processes are considered.

The feedback of the THC processes on the hydrologic properties of the rock has been shown (BSC 2006 [DIRS 174104]; Mukhopadhyay et al. 2006 [DIRS 180822]) to cause alteration of the flow pattern near the emplacement tunnels, resulting in seepage under some circumstances. However, the analyses in *THC Sensitivity Study of Repository Edge and Heterogeneous Permeability Effects* (BSC 2006 [DIRS 174104]) and in the study by Mukhopadhyay et al. (2006 [DIRS 180822]) were performed assuming dynamic changes in permeability and porosity only, i.e., the feedback of THC processes was restricted to only those two hydrologic properties. However, mineral precipitation and dissolution also alter the capillary characteristics of the rock, which have a direct impact on flow channeling and seepage (see Figure 6.1-3 for a schematic representation of THC processes, local flow channeling, and seepage). In this report, simulations are performed to analyze the feedback of THC processes on the hydrologic properties (porosity, permeability, and capillarity) of the rock and ultimately on seepage. Ambient and TH simulations are also performed to illustrate the difference between these processes in the context of seepage (or its absence).

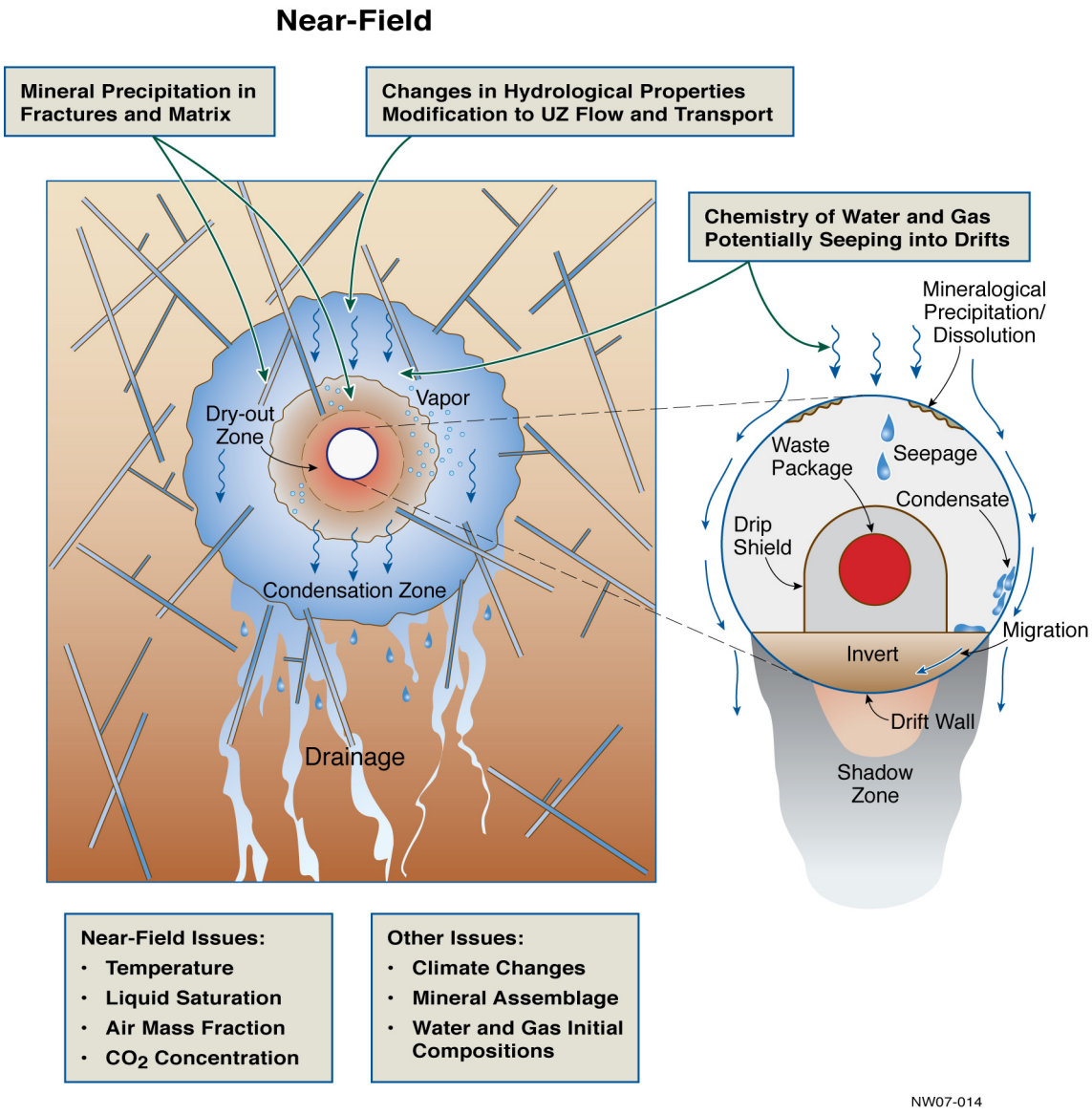

Figure 6.1-3. Schematic Representation of Interplay of THC Processes, Local Flow Channeling, and Seepage

6.2 OBJECTIVE

The primary objective of this work is to perform sensitivity analyses through integration of certain aspects of the seepage model for performance assessment (SMPA) (BSC 2004 [DIRS 167652]) with the drift-scale THC seepage model (SNL 2007 [DIRS 177404]). More specifically, the purpose of this report is to investigate the effects of heterogeneity in fracture permeability and fracture capillary-strength parameter (1/α) on seepage fluxes, seepage water and gas chemistry, near-field hydrological properties, near-field flow patterns, and effects on infiltration fluxes owing to THC processes.

Seepage under ambient conditions has been extensively investigated in *Seepage Model for PA Including Drift Collapse* (BSC 2004 [DIRS 167652]). Seepage has also been found to occur under thermal conditions in *Drift-Scale Coupled Process (DST and TH Seepage) Models* (BSC 2005 [DIRS 172232]). This latter report analyzed the TH conditions in the near-field rock and provided estimates of seepage into drifts. However, in estimating duration and amount of seepage into the drifts, the report did not include the impact of THC changes in the near-field rock, which might impact seepage into drifts. Alongside ambient and TH seepage models, drift-scale THC seepage models (SNL 2007 [DIRS 177404]) have also been developed. Investigations with the homogeneous drift-scale THC seepage model (SNL 2007 [DIRS 177404]) provided estimates of THC changes in the near-field rock and chemistry of likely seepage water. However, they did not report any seepage into the drifts because of the absence of heterogeneities in fracture permeability and capillarity (which are key parameters controlling seepage; see Sections 6.1.2) in the homogeneous drift-scale THC seepage model (SNL 2007 [DIRS 177404]). Thus, for the sake of consistency, there is a need to integrate some aspects of the seepage calibration model (SCM) and the SMPA model into the drift-scale THC seepage model. This is what is accomplished in the present report.

6.3 IMPACT OF THC PROCESSES ON SEEPAGE

When liquid water, having flowed through the unsaturated rock, reaches the immediate vicinity of an emplacement tunnel, a layer of increased saturation is expected to develop as a result of the capillary-barrier effect from the tunnel opening (Philip et al. 1989 [DIRS 105743]; Jackson et al. 2000 [DIRS 141523]; Finsterle 2000 [DIRS 151875]; Finsterle et al. 2003 [DIRS 163214]). Water is prevented from seeping into the tunnel because of capillary suction, which retains the wetting fluid in the pore space of the rock. This barrier effect leads to a local saturation buildup in the rock next to the interface between the geologic formation and the tunnel. If the permeability (as well as the capillarity) of the fracture network within this layer is sufficiently high, all or a portion of the water is diverted around the tunnel under partially saturated conditions. Locally, however, the water potential in the formation may be higher than that in the tunnel, and then water exits the formation and enters the tunnels, resulting in seepage.

In the unsaturated fractured rock of Yucca Mountain, the fractures form a well-connected network. As a result, flow is mostly carried in the fractures. Moreover, because the permeability of the rock matrix is a few orders of magnitude smaller than that of the fracture network, flow in the rock matrix is considerably slower. In addition, the smaller pores of the rock matrix ensured a stronger capillary suction compared to the fractures. Thus, the matrix mainly provides storage, while flow takes place through the fractures. The potential for seepage from the matrix is thus significantly smaller than from the fractures. The formulation that follows is therefore focused on the flow in fractures.

Earlier studies (Jackson et al. 2000 [DIRS 141523]; Or and Ghezzehei 2000 [DIRS 144773]; Finsterle 2000 [DIRS 151875]; Finsterle et al. 2003 [DIRS 163214]; BSC 2004 [DIRS 171764]) have shown that a heterogeneous porous continuum representation can be consistently used to analyze flow in unsaturated fractured rock, particularly if the fractures are rough-walled or are partially filled. For analyzing the impact of THC processes on seepage, the same fundamental approach is adopted in this report. As an example, the mechanism of seepage into an emplacement tunnel is schematically shown in Figure 6.3-1. In that figure, flow is shown to be

channeled onto a small block of rock situated above a large underground cavity. Assuming single-phase, incompressible, isothermal flow conditions, the conservation of mass in the fracture element of a discrete rock block *i* can be written as

$$V_i \frac{\partial}{\partial t}\left(\varphi_i S_i^l\right) = \sum A_{ij} q_{ij} \qquad \text{(Eq. 6.3-1)}$$

where $\sum A_{ij} q_{ij}$ represents the net flow of water into block *i*. When this quantity is larger than zero, the liquid saturation in that particular block (S_i^l) increases, and the capillary suction of the rock formation decreases. This process continues until a threshold liquid saturation, S_i^{lt}, is reached, when the capillary suction of the rock formation is so weak that it cannot hold the water any more, and liquid water is allowed to seep into the drift. Once seepage begins to occur, the mass-balance equation needs to be rewritten as

$$V_i \frac{\partial}{\partial t}\left(\varphi_i S_i^l\right) = \sum A_{ij} q_{ij} - A_s q_s, \qquad \text{(Eq. 6.3-2)}$$

where q_s is the rate of seepage and A_s is the area of contact between the rock block and the cavity. The rate of seepage can be further written as

$$q_s = -\frac{k_s}{\mu h}(P_C - \rho g h) \qquad \text{(Eq. 6.3-3)}$$

where k_s is the permeability (including both the absolute permeability and relative permeability of water) of the vertical connection between the rock block and cavity underneath it, and *h* is the vertical distance between the center of the rock block and the surface of the cavity. Implicit in the above equation is the fact that seepage can occur only when (Finsterle et al. 2003 [DIRS 163214], Birkholzer et al. 2004 [DIRS 172262])

$$P_C \le \rho g h, \qquad \text{(Eq. 6.3-4)}$$

i.e., when the capillary forces of the rock are smaller than the gravity forces pulling the water into the cavity. Note that once seepage begins to occur, it will continue as long as the net flow of water into the rock block *i* is greater than or equal to the seepage flux out of it (Equation 6.3-2), i.e.,

$$\sum A_{ij} q_{ij} \ge \frac{k_s}{\mu h}\left|P_C - \rho g h\right|, P_C \le \rho g h. \qquad \text{(Eq. 6.3-5)}$$

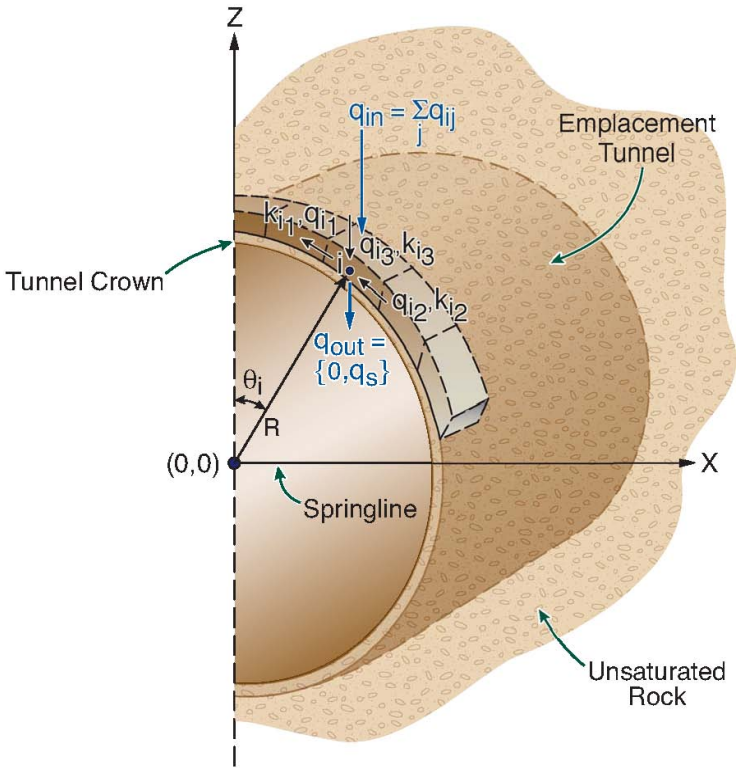

Figure 6.3-1. Schematic Representation of Seepage into an Emplacement Tunnel Situated in Unsaturated Fractured Rock

On the other hand, if the above condition is not satisfied (i.e., if the net flow of water into the block is less than the seepage flux), the saturation in rock block *i* will decrease (and fall below the threshold saturation over time), the capillary suction of the rock will increase, and seepage will stop.

It has already been shown (Equation 6.3-4) that seepage can take place only when the capillary suction of the fractures is smaller than the gravitational forces. Since the capillary pressure is a function of liquid saturation, Equation 6.3-4 can be rewritten as

$$\frac{1}{\alpha_i} F\left(S_i^l\right) \leq \rho g h \qquad \text{(Eq. 6.3-6)}$$

where $(1/\alpha_i)$ is the fracture capillary-strength parameter of block *i* and $(1/\alpha_i)F(S_i^l)$ represents the dependence of fracture capillary pressure on liquid saturation (S_i^l). It is also known that the fracture $(1/\alpha_i)$ parameter changes with fracture porosity (φ_i) and permeability (k_i) of block *i* through Leverett scaling (Leverett 1941 [DIRS 100588]) as

$$\frac{1}{\alpha_i} = \frac{1}{\alpha_0}\sqrt{\frac{k_0}{k_i}\frac{\varphi_i}{\varphi_0}} \qquad \text{(Eq. 6.3-7)}$$

where $(1/\alpha_0)$ is the ambient (or pre-heating) value of the fracture $(1/\alpha)$ parameter, assumed homogeneous, and φ_0 and k_0 are the mean fracture porosity and permeability, respectively (see also Section 6.4.9 for a discussion on permeability changes resulting from porosity changes).[1] Thus, a seepage threshold saturation, S_i^{lt}, can be defined such that

$$F\left(S_i^{lt}\right)=\left[\alpha_0 \rho g h \sqrt{\frac{k_i}{k_0}\frac{\varphi_0}{\varphi_i}}\right] \qquad \text{(Eq. 6.3-8)}$$

In other words, seepage will happen only when the fracture saturation is larger than or equal to S_i^{lt}. According to the van Genuchten (van Genuchten 1980 [DIRS 100610]) relations and the formulations of the active fracture model (Liu et al. 1998 [DIRS 105729]), $F(S_i^l)$ can be written as

$$F(S_i^l)=\left[\left(S_i^{l,e}\right)^{-1/m}-1\right]^{1-m}, S_i^{l,e}=\left[\frac{S_i^l-S_i^{lr}}{1-S_i^{lr}}\right]^{1-\gamma} \qquad \text{(Eq. 6.3-9)}$$

where m and γ are the van Genuchten exponent (van Genuchten 1980 [DIRS 100610]) and active fracture coefficient (Liu et al. 1998 [DIRS 105729]), respectively, and S_i^{lr} is the irreducible fracture saturation. Combining Equations 6.3-8 and 6.3-9,

$$S_i^{lt}=S_i^{lr}+\left(1-S_i^{lr}\right)\left[1+\left\{\alpha_0 \rho g h \sqrt{\frac{k_i}{k_0}\frac{\varphi_0}{\varphi_i}}\right\}^{\frac{1}{1-m}}\right]^{-\frac{m}{1-\gamma}} \qquad \text{(Eq. 6.3-10)}$$

It is now easy to understand the impact of THC processes (specifically mineral precipitation and dissolution) on seepage. Observe that the seepage threshold saturations (Equation 6.3-10) when THC processes are accounted for are different from when they are not. To understand this more clearly, one can assume that all the fractures have the same capillarity, i.e., one can ignore Leverett scaling (Leverett 1941 [DIRS 100588]) as depicted in Equation 6.3-7. In this instance, fractures with a relatively large deposition of minerals will have smaller porosities and permeabilities, and will tend to carry less flow (because of the relatively large reduction in permeabilities within these fractures). As a result, flow is diverted into fractures with relatively larger permeabilities (i.e., with less deposition), causing local flow channeling. Because of this local flow channeling, saturation in fractures with relatively larger permeabilities builds up quickly compared to other neighboring fractures and may even exceed the threshold saturation

[1] From Equation 6.3-7, it may appear that fracture $(1/\alpha)$ decreases (i.e., capillary suction will decrease) with a decrease in porosity. Intuitively, though, the converse should be true (i.e., decrease in porosity results in an increase of capillary suction). The way to resolve this apparent anomaly is to remember that a decrease in porosity also decreases the permeability (see Section 6.4.9.2 for more details). In fact, reduction in permeability occurs at a faster rate (for example, through a cubic law dependence) than the reduction in porosity. Overall, in the event of mineral precipitation, the permeability-porosity ratio of block *i,* (k_i/φ_i), becomes smaller than the permeability-porosity ratio of the reference state, (k_0/φ_0), and subsequently the fracture capillary suction increases.

(Equation 6.3-10). This buildup of saturation in certain fractures caused by flow channeling leads to conditions favorable for seepage. Compare this situation with ambient or TH-only models. In ambient and TH-only models, where the dynamic changes in hydrologic properties (because of chemical changes) are not accounted for, local flow channeling is expected to be less compared to THC models.

At this stage, the impact of dynamic changes in capillarity arising from changes in fracture porosity and permeability can be addressed. When Leverett scaling is included (i.e., changes in fracture permeability and porosity result in corresponding changes in fracture capillarity), the effect is to enhance flow channeling if the same initial fracture capillary-strength parameter is used. This is because a fracture with smaller porosity and permeability (because of mineral precipitation) should also have stronger capillary suction. Thus, the presence of capillarity heterogeneity owing to THC processes may increase the local flow channeling seen in simulations without consideration for such effects, provided the same initial fracture capillary-strength is used. However, it will shortly be shown (Section 6.4.11.3) that, to make a direct comparison between simulations with and without Leverett-scaling effects, the same initial fracture capillary-strength parameter may not be used (the overall capillary-barrier effects imposed with or without Leverett-scaling effects are different), and additional facts need to be taken into consideration (see Section 6.4.11). Thus, seepage prediction (BSC 2006 [DIRS 174104]; Mukhopadhyay et al. 2006 [DIRS 180822]) based on dynamic changes in porosity and permeability may be different from seepage prediction based on dynamic changes in all three hydrologic properties (porosity, permeability, and capillarity). This will be discussed in greater detail in Sections 6.4.11 and 6.7.2.

6.4 APPROACH

From the discussion in Section 6.3, it can be seen that THC processes of mineral precipitation and dissolution can alter the flow pattern around the emplacement drifts. To determine whether such alterations in flow paths around the emplacement drift will lead to increased seepage, a number of numerical simulation experiments with the 2-D THC seepage model (SNL 2007 [DIRS 177404]) are performed. Two key parameters in controlling seepage are the heterogeneities in the fracture permeabilities of the host rock and the heterogeneities in local capillarity characteristics. The numerical simulation experiments are designed in such a way as to demonstrate the impact of these two parameters on seepage. Using the 2-D THC seepage model (SNL 2007 [DIRS 177404]), the seepage flux into an emplacement drift, if any, is determined under the present-day mean infiltration conditions with various combinations of permeability and capillarity distributions. For one selected case, which predicts seepage (i.e., water is predicted to actually enter the emplacement drift), the composition of the seepage water is provided. As part of the sensitivity analyses, the 2-D THC seepage model (SNL 2007 [DIRS 177404]) is also used to determine the seepage flux when enhanced infiltration fluxes are provided as input into the model.

The 2-D THC seepage model is based on the TOUGHREACT V3.1.1 reactive transport software (see Section 3.1 and Table 3-1 for information about applicability of this software). TOUGHREACT simultaneously solves a set of chemical mass-action, kinetic-rate expressions for mineral dissolution/precipitation, and mass-balance equations. This provides the extent of reaction and mass transfer between a set of given aqueous species, minerals, and gases

at each gridblock of the flow model. Equations for heat, liquid and gas flow, aqueous and gaseous species transport, and chemical reactions are provided in the user's manual for TOUGHREACT V3.1.1.

The numerical mesh, boundary conditions, and modeling procedure for the model presented in this report are obtained from *Drift-Scale THC Seepage Model* (SNL 2007 [DIRS 177404]); a brief summary of these is given below for the sake of completeness. Additional model setup information described in this section relates to the heterogeneous fracture permeability realizations (BSC 2004 [DIRS 167652]) used in the simulations and other seepage-specific data (BSC 2004 [DIRS 171764]).

6.4.1 Justification for Using a 2-D Model

The THC behavior of near-field Yucca Mountain fractured rock is simulated in 2-D vertical domains perpendicular to the drift axis (SNL 2007 [DIRS 177404]). A fully 3-D simulation of drift-scale THC processes is difficult, on account of computational limitations. The THC simulation requires a large vertical model domain because the thermally disturbed zone extends far into the overlying and underlying geological units. Also, with this report's focus on the near-drift conditions, it is important to represent the drift vicinity with refined spatial discretization. As a result, a 3-D simulation model would be too time-consuming to allow for large numbers of simulation runs, which are needed in this sensitivity study to cover a wide range of parameters and conditions relevant for seepage. The consequences of using a 2-D representation of a 3-D problem (in the context of thermal seepage) have been analyzed previously (BSC 2005 [DIRS 172232]) and are equally applicable to THC seepage. The consequences are:

1. A 2-D representation of the TH and THC processes ignores the effects from cooler rock temperatures at the end of each emplacement drift and at the edges of the repository than those at center locations. It has been shown (BSC 2006 [DIRS 174104]) that these edge effects are not expected to have any significant impact on the model outcome (as far as prediction of seepage is concerned).

2. In the 2-D representation, the thermal output of individual waste canisters placed into drifts is represented by an average linear thermal power per drift length. Using an average value ignores the thermal power differences between adjacent waste packages. To account for such effects, several sensitivity cases for the thermal load, covering a wide range of thermal conditions representative of local TH conditions close to individual waste packages, were considered in *Drift-Scale Coupled Processes (DST and TH Seepage) Models* (BSC 2005 [DIRS 172232]). It should be noted that the differences between individual waste packages have rather limited impact on the near-field rock temperatures, because radiative heat exchange within the drift equilibrates most of the differences with respect to heat transmitted to the drift wall. While the observation in *Drift-Scale Coupled Processes (DST and TH Seepage) Models* (BSC 2005 [DIRS 172232]) is made with respect to TH models only, it is valid for the THC seepage model as well, particularly in the context of seepage.

3. A 2-D representation of THC processes does not account for the axial transport of vapor and air along the open drifts, a result of natural convection processes and gas pressure differences along the drifts. As demonstrated in *In-Drift Natural Convection and Condensation* (BSC 2004 [DIRS 164327]), such processes can effectively move water vapor from the heated emplacement sections of the drifts to the cooler rock surfaces at the drift ends outside of the emplacement sections (turn-out sections). Principles of thermodynamics suggest that the maximum amount of vapor that can be present in an air–vapor mixture decreases with declining temperature. Thus, the warm moist gas moving from hot waste packages into the comparably cool turnouts will be depleted of most of its vapor content by condensation on cooler rock surfaces. At the same time, relatively dry gas circulates back towards the emplacement sections of the drifts, thereby reducing the vapor mass and the relative humidities in these heated areas. Thus, a 2-D representation—that does not account for axial vapor transport along drifts—is likely to overestimate the amount of vapor in the near-field rock mass in all heated drift sections, i.e., in those drift sections that are most relevant for thermal seepage and the related abstraction model. Overestimating the humidity in the drift leads to underestimation of evaporation, and thus overestimation of seepage. Thus, a 2-D representation without accounting for in-drift vapor flux is an upper-bounding case for seepage.

4. A 2-D representation does not capture the three-dimensional behavior of small-scale flow channeling in the fractured rock, as caused by heterogeneity in the rock properties. However, with respect to the effectiveness of the capillary-barrier for seepage into drifts, a 2-D representation is more critical in most cases of heterogeneous fracture permeability fields, because the potential diversion of flow in the third dimension is neglected (Hardin et al. 1998 [DIRS 100350], Section 3.6).

It can be concluded from the itemized list that the 2-D representation used in this report is adequate for the intended application of predicting seepage.

6.4.2 2-D Model Domain

Simulations were performed in a 2-D vertical cross section through the unsaturated fractured rock at Yucca Mountain, using the numerical grid shown in Figure 6.4-1. The source of this model domain is DTN: LB0705DSTHC001.002 [DIRS 180854] (folder: *\thc7_81_w0_*, file: "MESH"), which is included in Table 4.1-1 as a direct input. Since thermal perturbation from repository heating is expected to occur over tens of meters above and below an emplacement drift (see Section 6.6.1), the vertical model domain comprises the entire unsaturated zone at Yucca Mountain (the model domain extends approximately 364 m above and approximately 353 m below an emplacement drift). Such an approach ensures proper implementation of boundary conditions (see Sections 6.4.3 and 6.6.1). The model domain extends 40.5 m laterally (or in the horizontal direction), extending from the center of one emplacement drift to the mid-point between two drifts. Both vertical boundaries are treated as no-flow boundaries. Symmetry is assumed with the symmetry plane parallel to the drift axis. The grid is radial (owing to the cylindrical geometry of the emplacement tunnel) and refined (with gridblocks as small as 0.2 m) in the vicinity of the drift, but coarser farther away from the drifts, gradually transforming into a rectangular grid. Drift radius is 2.75 m, and the model domain has a thickness of 1 m.

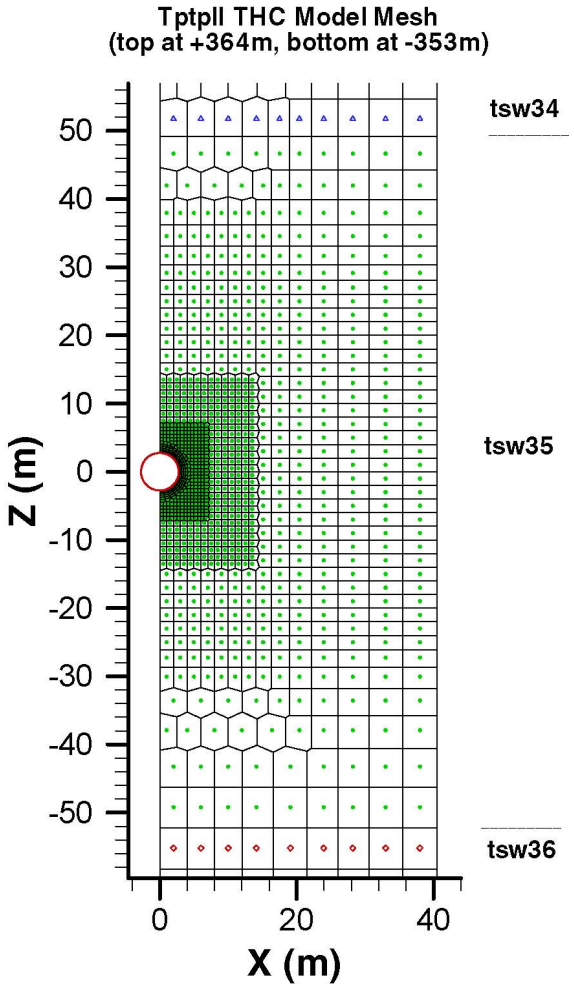

Source: DTN: LB0705DSTHC001.002 [DIRS 180854], folder: *thc7_81_w0_*, file: "MESH."

NOTE: The drift is located in the center of tsw35 (Tptpll). The units above and below are tsw34 (Tptpmn) and tsw36 (Tptpln), respectively.

Figure 6.4-1. 2-D Numerical Grid Used in Ambient, TH, and THC Simulations with the Drift-Scale THC Seepage Model (SNL 2007 [DIRS 177404])

6.4.3 Boundary and Initial Conditions

The top boundary of the model is situated at the ground surface, whereas the bottom boundary coincides with the groundwater table. Both the top and bottom boundaries of the model are situated far away from the source of heat, the emplacement drift, and thermal perturbation is not expected to reach these boundaries. (See discussion in Section 6.6.1. There it is shown that thermal perturbation does not extend beyond approximately 80 m above and below the emplacement drift at the peak of repository thermal loading, whereas the boundaries are situated at 364 m above and 353 m below the emplacement drift; see Section 6.4.2 for a description of the THC seepage model domain.) These boundaries are assigned Dirichlet-type conditions with fixed temperature, pressure, and liquid saturation values. The top boundary is treated as an open atmosphere with constant CO_2 partial pressure and fixed composition of the percolating water. The groundwater table at the bottom of the model is represented as a flat, stable surface saturated

with water and CO_2 partial pressure at equilibrium. The lateral vertical boundaries are no-flow boundaries for flow, heat, and chemical fluxes. To provide initial thermal and hydrological conditions, a simulation was performed without reactive transport, heat load, or a drift (i.e., with rock at the location of the drift), until steady-state conditions were achieved.

The THC model grid extends from the land surface at the top to the water table at the bottom. The grid is located at approximately Nevada State Plane coordinates E170604.2 m, N233255.7 m. The location closest to the THC model grid location is Column "c82" in the updated UZ model grid in DTN: LB0701UZMTHCAL.001 [DIRS 179286] (file: "MESH_THN.V1"). This DTN also contains the input and output files for the 3-D ambient thermal model and calibration results for the present-day climate of 10th, 30th, 50th, and 90th percentile infiltration maps. For obtaining the top and bottom boundary conditions for the THC model grid, conditions (pressure, temperature, and gas saturation) at the top and bottom, respectively, of Column "c82" were extracted. The calibration results for the 30th percentile infiltration map can be found in file "Th_30%_gas_calibrated.out" of DTN: LB0701UZMTHCAL.001 [DIRS 179286]. The top and bottom boundary conditions of the THC model grid are thus those of gridblocks "TP TPc82" (top of Column "c82") and "BT BTc82" (bottom of Column "c82"), respectively. The top and bottom boundary conditions so obtained are listed in Table 6.4-1.

Table 6.4-1. Top and Bottom Boundary Conditions for the THC Model

Boundary	Boundary Condition
Top Boundary for THC model (ground surface)	T = 16.02°C Sg = 1.000 P = 84610 Pa
Bottom Boundary for THC model (water table)	T = 32.°C Sg = 0.000 P = 91762 Pa

Source: DTNs: LB0701UZMTHCAL.001 [DIRS 179286], file: "Th_30%_gas_calibrated.out."

NOTE: Note that the gas saturation (s_g) of element "TP TPc82" in "Th_30%_gas_calibrated.out" is 0.98791. A gas saturation value of 1.0 (representing air) has been used instead. Further, though the gas saturation in element "BT BTc82" is 0.01, a value of 0.000 (representing water) has been used. These minor differences are not expected to affect the outcome from the THC model.

6.4.4 Thermal Load

As indicated in Table 4.1-1, the thermal load for the 2-D TH and THC simulations is obtained from DTN: LB0705DSTHC001.002 [DIRS 180854]. The thermal output of individual waste canisters placed into drifts is represented by an average thermal line load of 1.45 kW/m, according to the current design. The thermal line load of 1.45 kW/m is defined in *Total System Performance Assessment Data Input Package for Requirements Analysis for Subsurface Facilities* (SNL 2007 [DIRS 179466]). Note that the value of 1.45 kW/m refers to the initial thermal line load at emplacement time. This value decreases with time as a result of radioactive decay, as shown in Figure 6.4-2. The time-dependent thermal-line-load values are also adopted from the same source (SNL 2007 [DIRS 179466]).

Ventilation efficiency denotes the fraction of heat removed from the repository as a result of ventilation during the 50-year preclosure period. The integrated ventilation efficiency

provided in *Ventilation Model and Analysis Report* (BSC 2004 [DIRS 169862]) is 87.97% when the emplacement drift is 600 m in length (DTN: MO0406MWDAC8VD.001 [DIRS 170541], worksheet: "Ventilation Efficiency"). On the other hand, when the emplacement drift is 800 m long, integrated ventilation efficiency is calculated to be 85.96% (DTN: MO0406MWDAC8VD.001 [DIRS 170541], worksheet: "Ventilation Efficiency"). For the TH and THC simulations, a ventilation efficiency of 88% (rounded up from 87.97% for a 600-m-long emplacement drift) is therefore used, which is also shown in Figure 6.4-2. In short, the blue line in Figure 6.4-2 is the actual input thermal load for subsequent simulations. This adopted value of ventilation efficiency is also consistent with previously used values (BSC 2004 [DIRS 169862], Table 8-2).

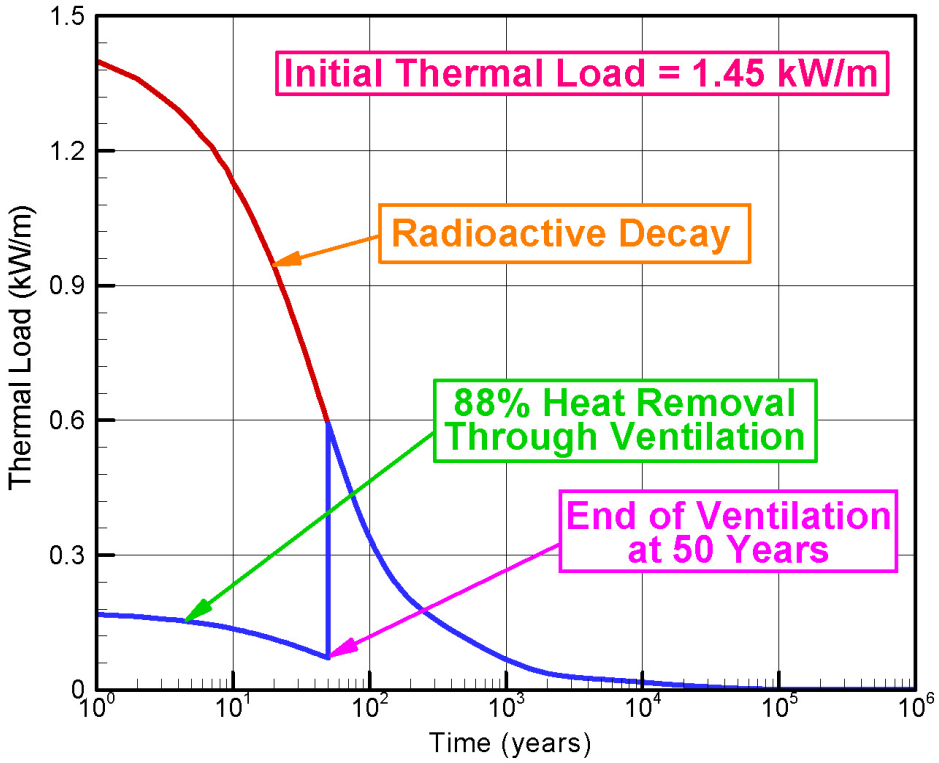

Source: DTN: LB0705DSTHC001.002 [DIRS 180854], folder: *thc7_81_w0*, file: "GENER."

NOTE: 88% of the generated heat is expected to be removed by ventilation during the first 50 years after emplacement. The blue line represents the actual heat input into the simulations.

Figure 6.4-2. Transient Thermal Loading History of the Emplaced Wastes at Yucca Mountain

6.4.5 Infiltration Fluxes

The infiltration fluxes for the THC seepage model are from DTN: LB0705DSTHC001.002 [DIRS 180854] (see Table 4.1-1 for more details). The ambient, TH, and THC simulations with the THC seepage model consider three long-term climate periods with constant net infiltration rate at the top of the model domain. These infiltration fluxes are 7.96, 12.89, and 20.45 mm/yr, respectively, during 0 to 600, 600 to 2,000, and beyond 2,000 years (SNL 2007 [DIRS 177404], Table 4.1-5). Simulations performed with these infiltration fluxes will be denoted as IMF1 (representing **i**nfiltration **m**ultiplication **f**actor of **1**). Additional infiltration scenarios have been

investigated with the THC seepage model to cover the range of variability in the infiltration fluxes within the repository horizon. These include applying ten times the IMF1 fluxes. These simulations will be referred to as IMF10.

6.4.6 Rock Hydrological and Thermal Properties

Rock hydrological and thermal properties are obtained from DTN: LB0705DSTHC001.002 [DIRS 180854]; Table 4.1-1 provides information about where the rock hydrological and thermal properties can be found in that DTN. Except for the fracture $1/\alpha$ parameter of the Tptpll unit (which is considered a sensitivity parameter), the calibrated matrix and fracture hydrological properties used in this report correspond to the 30th percentile parameter set as given in *Calibrated Unsaturated Zone Properties* (SNL 2007 [DIRS 179545], Table 6-7). More details about the thermal and hydrological properties can be found in *Drift-Scale THC Seepage Model* (SNL 2007 [DIRS 177404], Sections 4.1.1 and 6.4.7). Most of the layer-averaged hydrologic properties are based on calibration against borehole measurements such as saturation data, water-potential data, pneumatic pressure data, and ambient temperature data. For convenience, a summary of the key thermal and hydrological properties for the repository units (the host rock for the emplacement tunnels) is provided in Table 6.4-2, which is reproduced from *Drift-Scale THC Seepage Model* (SNL 2007 [DIRS 177404], Table 6.4-2).

Table 6.4-2. Summary of Hydrological and Thermal Properties of Repository Units

		30th Percentile Parameter Set		
Geological Unit>		*Tptpul (tsw33)*	*Tptpmn (tsw34)*	*Tptpll (tsw35)*
MATRIX DATA				
Permeability	k_m (m^2)	1.86E-17	3.16E-18	1.11E-17
Porosity	f_m (-)	0.155	0.111	0.131
van Genuchten α	α_m (1/Pa)	6.56E-6	1.71E-6	3.38E-6
van Genuchten m (or λ)	m_m (-)	0.283	0.317	0.216
Residual saturation	S_{lrm} (-)	0.12	0.19	0.12
Rock grain density	ρ (kg/m^3)	2,520	2,520	2,540
Rock grain specific heat capacity	C_p (J/kg K)	930	930	930
Dry thermal conductivity	λ_{dry} (W/m/K)	1.22	1.39	1.24
Wet thermal conductivity	λ_{wet} (W/m/K)	1.78	2.06	1.87
Tortuosity	τ (-)	0.20	0.20	0.20
FRACTURE DATA				
Permeability	k_f (m^2)	7.8E-13	3.3E-13	9.1E-13
Porosity	f_f (-)	5.8E-3	8.5E-3	9.6E-3
van Genuchten α	α_f (1/Pa)	1.58E-3	3.16E-4	5.75E-4
van Genuchten m (or λ)	m_f (-)	0.633	0.633	0.633
Residual saturation	S_{lrf} (-)	0.01	0.01	0.01

Table 6.4-2. Summary of Hydrological and Thermal Properties of Repository Units (Continued)

		30th Percentile Parameter Set		
	Geological Unit>	*Tptpul (tsw33)*	*Tptpmn (tsw34)*	*Tptpll (tsw35)*
Effective tortuosity	τ (-)	0.0041	0.0060	0.0067
Active fracture model coefficient	γ (-)	0.400	0.400	0.400

Source: DTN: LB0705DSTHC001.002 [DIRS 180854], folder: *\thc7_81_w0_*, file: "flow.inp"; see also SNL 2007 [DIRS 177404], Section 6.4.7 and Table 6.4-2.

NOTE: Fracture volumes in file "MESH" are calculated using the formula 2.0**f*f**(gridblock volume), where f_f is the fracture porosity provided above. Since twice the actual fracture volume is included in file "MESH," the fracture porosity is provided as 0.5 in file "flow.inp." This ensures that the true fracture volume has been used in flow simulations.

6.4.7 Initial and Boundary Water Composition

Initial and boundary water compositions for simulations presented in this report are shown in Table 6.4-3. The source of these data is DTN: LB0705DSTHC001.002 [DIRS 180854] (folder: *\thc7_81_w0_*, file: "chemical.inp") (see Table 4.1-1). The selected initial and boundary water composition corresponds to water "W0" as discussed in *Drift-Scale THC Seepage Model* (SNL 2007 [DIRS 177404], Section 6.2.2.1). Although water W0 represents one of the smallest of the four water groups (Group 1 = 21 waters; Group 2 = 7 waters; Groups 3 and 4 = 3 waters) discussed in *Engineered Barrier System: Physical and Chemical Environment* (SNL 2007 [DIRS 177412]), this water is potentially of high importance with respect to TSPA, because it is the starting water that most commonly results in the predicted occurrence of potentially corrosive, low pH (SNL 2007 [DIRS 177412], Figure 6.13-7), high chloride:nitrate ratio (SNL 2007 [DIRS 177412], Figure 6.13-11) conditions on the waste package surface. The pore-water composition input into the model was taken from analyses of pore water extracted by ultracentrifugation of core samples. The selection criteria for pore water compositions include reliability of analytical data (mainly on the basis of charge balance), potential end-brine compositions upon evaporation, span of natural variability, and other factors (SNL 2007 [DIRS 177412]; SNL 2007 [DIRS 177404], Section 6.2.2.1). The initial water was assumed to have the same chemical composition in the rock matrix and fractures; however, a distinction is made between the fracture and matrix water, and the infiltration water (i.e., boundary water). Iron, aluminum, and total aqueous carbonate concentrations (hereafter listed as HCO_3^-) were not measured and were calculated. Selected initial and boundary water compositions are summarized in Table 6.4-3.

Table 6.4-3. Input Pore-Water Compositions for the THC Seepage Model

Water Input Type:		**Fract/Matrix**	**Boundary**
	Units		
Temperature	°C	20	16
pH (measured)	pH	8.31	—
pH (calc)	pH	7.86	7.87
Na^+	mg/L	62	62
K^+	mg/L	9	9
Ca^{2+} (measured)	mg/L	97	—

Table 6.4-3. Input Pore-Water Compositions for the THC Seepage Model (Continued)

Water Input Type:		Fract/Matrix	Boundary
	Units		
Ca^{2+} (calc)	mg/L	64.1	66.3
Mg^{2+}	mg/L	17.4	17.4
SiO_2 (measured)	mg/L	75	—
SiO_2 (calc)	mg/L	49.3	42
Cl^-	mg/L	123	123
SO_4^{-2}	mg/L	120	120
HCO_3^- (measured)	mg/L	—	—
HCO_3^- (calc)	mg/L	85.8	93
NO_3^-	mg/L	10	10
F^-	mg/L	0.76	0.76
Al^{+3} (calc)	molal	2.30×10^{-9}	1.75×10^{-9}
Fe^{+3} (calc)	molal	2.06×10^{-12}	1.35×10^{-12}
log(PCO_2)	bar	–3.0	–3.0
CO_2 (approx)	ppmv	1,136	1,136

Source: DTN: LB0705DSTHC001.002 [DIRS 180854], folder: *thc7_81_w0_*, file: "chemical.inp"; see also SNL 2007 [DIRS 177404], Section 6.2.2.1 and Table 6.2-1.

6.4.8 Geochemical System

Minerals and chemical-aqueous components considered in this sensitivity study are shown in Table 6.4-4. The source of these data is DTN: LB0705DSTHC001.002 [DIRS 180854] (folder: *thc7_81_w0_*, file: "chemical.inp") (see also Table 4.1-1). Primary mineral types and abundances are derived from X-ray diffraction measurements on cores reported in the Yucca Mountain mineralogical model (DTN: LA9908JC831321.001 [DIRS 113495]) and analyses of fracture surfaces (Carlos et al. 1993 [DIRS 105210], p. 47; DTN: LA9912SL831151.001 [DIRS 146447]; DTN: LA9912SL831151.002 [DIRS 146449]), as well as literature data (Peterman and Cloke 2002 [DIRS 162576]). Amounts of minerals observed, but present in quantities below the detection limit (typically around a percent for X-ray diffraction), have been estimated. Potential secondary minerals (i.e., those allowed to precipitate but which may not necessarily form) have been determined from field observation of thermal alteration (e.g., Vaniman et al. 2001 [DIRS 157427]).

As described for the THC seepage model (SNL 2007 [DIRS 177404]), the bases for selection of aqueous species included in this study include: (1) use the major components of pore water, (2) use all components in major rock-forming minerals considered in the model, and (3) use additional components specifically requested by downstream users (nitrate, iron, and fluoride). Thus, the modeled geochemical system (Table 6.4-4) includes the major solid phases (minerals and glass) encountered in geologic units at Yucca Mountain, together with a range of possible reaction product minerals and CO_2 gas, as well as the aqueous species necessary to describe this system. A more detailed discussion can be found in *Drift-Scale THC Seepage Model* (SNL 2007 [DIRS 177404], Section 6.2.2.2 and Table 6.2-2). The initial mineral abundances and reactive surface areas in fractures and matrix can be found in *Drift-Scale THC Seepage Model* (SNL 2007 [DIRS 177404], Appendices A and B).

Table 6.4-4. Mineral, Aqueous, and Gaseous Species Used in the THC Seepage Model

Aqueous Basis Species	Minerals	Mineral Type[a]
H_2O	Cristobalite–α	P
H^+	Biotite	P
Na^+	Clinoptilolite (solid sol.)	P
K^+	Hematite	P
Ca^{2+}	Plagioclase	P
Mg^{2+}	Quartz	P
SiO_2	Rhyolitic Glass	P
AlO_2^-	Sanidine	P
$HFeO_2^{2-}$	Tridymite	P
HCO_3^-	Beidellite-Ca	P, S
Cl^-	Beidellite-Mg	P, S
SO_4^{2-}	Beidellite-Na	P, S
F^-	Calcite	P, S
NO_3^-	Fluorite	P, S
	Illite	P, S
Gases	Mordenite	P, S
CO_2	Opal-CT	P, S
H_2O	Stellerite	P, S
Air	Amorphous Antigorite	S
	Amorphous Silica	S
	Anhydrite	S
	Clinoptilolite-Ca	S
	Clinoptilolite-K	S
	Clinoptilolite-Na	S
	Goethite	S
	Kaolinite	S

Source: DTN: LB0705DSTHC001.002 [DIRS 180854], folder: *thc7_81_w0*, file: "chemical.inp"; see also SNL 2007 [DIRS 177404], Section 6.2.2.2 and Table 6.2-2

[a] Primary (P) and secondary (S) minerals.

6.4.9 Porosity and Permeability Changes

The modeled changes in capillary pressure (see Equation 6.3-7) because of porosity changes (through THC processes of mineral precipitation and dissolution) and permeability heterogeneities (either because of ambient geological heterogeneities or through THC processes) depend on the correlation used between porosity changes and corresponding permeability changes. The porosity-permeability relationship implemented in the THC seepage model (SNL 2007 [DIRS 177404]) is summarized below (see also Section 6.4.4 of SNL 2007 [DIRS 177404]).

6.4.9.1 Porosity Changes

Changes in porosity and permeability resulting from mineral dissolution and precipitation have the potential to modify percolation fluxes and seepage fluxes at the drift wall (see Section 6.3). In this analysis, porosity changes in matrix and fractures are directly tied to the volume changes

that result from mineral precipitation and dissolution. The molar volumes of hydrous minerals, such as zeolites and clays, created by hydrolysis reactions with anhydrous phases, such as feldspars, are commonly larger than those of the primary reactant minerals. Therefore, constant molar dissolution-precipitation reactions can lead to porosity reductions. These changes are taken into account in this analysis. The porosity of the medium (fracture or matrix) is given by

$$\phi = 1 - \sum_{m=1}^{nm} fr_m - fr_u \qquad \text{(Eq. 6.4-1)}$$

where nm is the number of minerals, fr_m is the volume fraction of mineral m in the rock ($V_{mineral}/V_{medium}$, including porosity), and fr_u is the volume fraction of nonreactive rock. As the fr_m of each mineral changes, the porosity is recalculated at each time step. The porosity is not allowed to go below zero.

6.4.9.2 Fracture Permeability Changes Resulting from Porosity Changes

Fracture permeability changes can be approximated using the porosity change and considering plane parallel fractures of uniform aperture (cubic law) (Steefel and Lasaga 1994 [DIRS 101480], p. 556). If the fracture spacing and density remain constant, the updated permeability, k, is given by

$$k = k_i \left(\frac{\phi}{\phi_i} \right)^3 \qquad \text{(Eq. 6.4-2)}$$

where k_i and ϕ_i are the initial permeability and porosity, respectively. This law yields zero permeability only under the condition of zero fracture porosity.

In most experimental and natural systems, permeability reductions to values near zero occur at porosities that are significantly greater than zero. This generally is the result of mineral precipitation preferentially closing the narrower interconnecting apertures. The hydraulic aperture, as calculated from the fracture spacing and permeability (as determined through air-permeability measurements) using a cubic law relation, is a closer measure of the smaller apertures in the flow system. Using the hydraulic aperture, a much stronger relationship between permeability and porosity can be developed. This relationship can be approximated as follows:

The initial hydraulic aperture $b_{0,h}$ (m) is calculated using the following cubic law relation:

$$b_{0,h} = \left[12 k_0 s \right]^{1/3} \qquad \text{(Eq. 6.4-3)}$$

where k_0 is the initial fracture permeability (m^2) and s is the fracture spacing (m) for a single fracture set. The permeability (k') resulting from a change in the hydraulic aperture is given by

$$k' = \frac{\left(b_{0,h} + \Delta b \right)^3}{12 s} \qquad \text{(Eq. 6.4-4)}$$

where Δb is the aperture change resulting from mineral precipitation/dissolution. The aperture change resulting from a calculated volume change can be approximated by assuming precipitation of a uniform layer over the entire geometric surface area of the fracture, assuming also that this area (as well as the fracture spacing) remains constant. In geologic systems, the actual distribution of mineral alteration is much more heterogeneous and depends on many factors that are active at scales much smaller than the resolution of the model. The combined effect of the initial heterogeneities and localized precipitation processes can only be treated through model sensitivity studies and experiments. The initial aperture available for precipitation (b_g, the geometric, rather than the hydraulic, aperture) can be calculated from the ratio of the initial fracture porosity ($\phi_{f,0}$) to the fracture surface area (A_f), as follows:

$$b_g = \phi_{f,0} \Big/ A_f \qquad \text{(Eq. 6.4-5)}$$

For a dual-permeability model, changes in the fracture porosity are calculated based on the porosity of the fracture medium, so that Δb can be approximated by:

$$\Delta b = \frac{\left(\phi'_{fm} - \phi_{fm,0}\right)}{\phi_{fm,0}} b_g \qquad \text{(Eq. 6.4-6)}$$

Equations 6.4-3, 6.4-4, and 6.4-6 were implemented in TOUGHREACT.

6.4.9.3 Matrix Permeability Changes Resulting From Porosity Changes

Matrix permeability changes are calculated from changes in porosity using ratios of permeabilities calculated from the Carman-Kozeny relation (Bear 1988 [DIRS 101379], p. 166, Equation 5.10.18, symbolically replacing n by ϕ), and neglecting changes in grain size, tortuosity, and specific surface area as follows:

$$k = k_i \frac{(1-\phi_i)^2}{(1-\phi)^2} \left(\frac{\phi}{\phi_i}\right)^3 \qquad \text{(Eq. 6.4-7)}$$

6.4.10 Heterogeneous Fracture-Permeability Distribution

Mean permeability of the fracture field is equal to the calibrated fracture permeability of the calibrated drift-scale property set (e.g., 0.91×10^{-12} m^2 for the Tptpll unit) obtained from DTN: LB0705DSTHC001.001 [DIRS 180854] (the file "flow.inp" in any of the subdirectories of this DTN contains these data; look for model layer "tswF5" representing the fractures of Tptpll unit). Geostatistical information on the variability of fracture permeability in the Tptpll is available from air-injection measurements in borehole SYBT-ECRB-LA#2 in the Enhanced Characterization of the Repository Block (ECRB) and Niche 1620. Measured permeability data in borehole SYBT-ECRB-LA#2 (DTN: LB0302SCMREV02.002 [DIRS 162273], Table 3) have a standard deviation of 0.21 in log10 space, which is partly a result of the injection intervals (approximately 6 ft) being six times longer than those in Niche 1620. The standard deviation for a six-times-shorter (i.e., on the order of 1 ft) measurement interval in the borehole can be

estimated to be on the order of $0.21 \times 6½ = 0.51$.[2] For measured data in Niche 1620 with a measurement interval of 1 ft, the standard deviation in small-scale fracture permeability is 1.31 in log10 space. The arithmetic average of 0.51 and 1.31 is 0.91 in log10 space. Consistent with these measured data, the heterogeneous fracture permeability distribution used in this section is developed with a standard deviation of 1.0 in log10 space. This same standard deviation is used in the base case simulations of the SMPA (BSC 2004 [DIRS 167652], Sections 6.3.3 and 6.3.7, Table 6-3). Note that the heterogeneous Tptpll fracture permeability field in *Drift-Scale Coupled Processes (DST and TH Seepage) Models* (BSC 2005 [DIRS 172232], Section 6.2.3.2.1) was generated with a mean of 0.91×10^{-12} m^2 (identical to the mean Tptpll fracture permeability in this report) and standard deviation of 0.84 in log10 space (compared to 1.0 in the ambient/TH/THC simulations in this report). Also, the heterogeneous fracture permeability field in the TH seepage model was drawn from a random distribution without any spatial correlation; the spatial correlation length in the THC seepage model is discussed below.

Using the specified mean and standard deviation, a log-normal fracture permeability field is generated. The choice of a log-normal permeability field is consistent with the ambient SMPA (BSC 2004 [DIRS 167652], Section 6.3.3). The spatial correlation length is set to 0.3 m, consistent with the SMPA (BSC 2004 [DIRS 167652], Section 6.3.5). Note that in contrast to the THC seepage model (SNL 2007 [DIRS 177404]), the SMPA has a regular grid with uniform element size and orientation. In the drift vicinity, the grid size designed for the THC seepage model is 0.2 m in the radial direction, compared to 0.1 m for the SMPA (BSC 2004 [DIRS 167652], Section 6.3.1). The issue of grid-resolution effects was analyzed in a previous version of the SMPA report (CRWMS M&O 2000 [DIRS 153314], Section 6.7). It was concluded that the grid-size dependence is rather small, similar to or less than the variability from different realizations of the heterogeneous permeability field. Also note that the model grid size used in the drift vicinity is comparable to the 1 ft interval length of the air-injection tests conducted in the niches, assuring that the scale of measurement is consistent with the scale of heterogeneity described in the model. While no sensitivity study has been carried out with the THC seepage model using different numerical grids, the following points need to be remembered:

- While no chemical processes were included, the thermal seepage studies in *Drift-Scale Coupled Processes (DST and TH Seepage) Models* (BSC 2005 [DIRS 172232]) (see Sections 6.2.1.2, 6.2.3, and 6.2.4) and in the report by Birkholzer et al. (2004 [DIRS 172262]) used a numerical grid (BSC 2005 [DIRS 172232], Section 6.2.1.2) different from the one used in the THC seepage model (SNL 2007 [DIRS 177404]). However, the qualitative nature of thermal seepage in *Drift-Scale Coupled Processes*

[2] Assume that the problem is to find mean fracture permeability and standard deviation of measured fracture permeability over a certain spatial domain. If each and every fracture in that domain could be mapped, having included an infinitely large number of fractures, the estimated standard deviation will be the true standard deviation (σ) of the measured fracture permeabilities. However, when a measurement interval of L_a is used, the sample standard deviation is of the order of $\sigma_a \sim \sigma / \sqrt{L_a}$ (Grinstead and Snell 1997 [DIRS 181353], p. 260). If a different measurement interval of L_b is now used, the sample standard deviation is similarly expected to be of the order of $\sigma_b \sim \sigma / \sqrt{L_b}$. It can now be seen that $\sigma_a \sim \sigma_b \sqrt{L_b / L_a}$. Since L_b = 6 ft, L_a = 1 ft, σ_b = 0.21, σ_a $\sim 0.21 \times 6^{1/2} \sim 0.51$.

(DST and TH Seepage) Models (BSC 2005 [DIRS 172232], Section 6.2.4) and the TH seepage results from this report (see Sections 6.6 and 6.7) are similar. (A direct quantitative comparison cannot be made because the rock hydrological properties are different and also the infiltration fluxes are different.)

- While the model sensitivity to spatial discretization (gridding) was not specifically evaluated with the THC seepage model, the model sensitivity to time discretization (for a given numerical grid) was evaluated (SNL 2007 [DIRS 177404], Section 6.6.1), such that confidence was gained about the appropriateness of the time/space discretization for simulations done with the THC seepage model.

Three realizations (Realization #1, Realization #2, and Realization #3) of the 2-D heterogeneous fracture permeability field were generated using the GSLIB V1.0 module SISIM V1.204 (see Section 3.1 and Table 3-1). The distribution was generated based on a cumulative distribution function obtained through analysis of air-permeability testing, as found in DTN: LB0304SMDCREV2.001 [DIRS 173235] (look for file "perm.par" in directory *\20_k_realizations*). This same cumulative distribution function for heterogeneous fracture permeability fields was used in the SMPA (BSC 2004 [DIRS 167652]). Because the THC seepage model grid has gridblocks varying from about 0.2 m across near the drift wall to several meters across in areas away from the drift, the fine resolution field had to be mapped onto the numerical mesh using an appropriate averaging scheme. A circular area was defined around the nodal point within each gridblock, corresponding to the average distance of the nodal point to the gridblock edges. Geometric means of the permeability multipliers within this area were calculated and used to modify the mean permeability assigned to the numerical mesh gridblocks. The net result of this averaging is that the permeabilities near the drift wall have the same or similar spatial variability, whereas areas away from the drift reflect a smoother averaged field appropriate to the resolution of the mesh in these areas. The averaging was performed using the software routine avgperm.f V1.0 (see Table 3-1). The averaged fracture permeability field for Realization #1 is shown in Figure 6.4-3. Appendix C provides more detail about the procedures adopted to generate the heterogeneous fracture permeability fields.

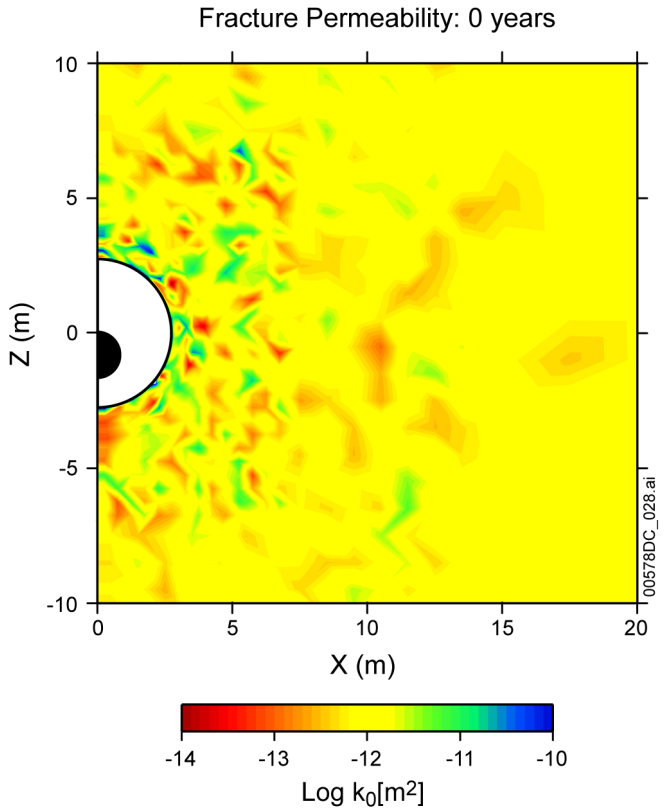

Source: Output DTN: LB0705THCSENR1.001.

NOTE: Only the area around the drift is shown.

Figure 6.4-3. Heterogeneous Fracture Permeability Distribution for Realization #1 at the Start of Ambient/TH/THC Simulations

6.4.11 Fracture Capillary-strength Parameter

In addition to heterogeneities in fracture permeabilities (which control local flow channeling), the other key parameter, which has a strong influence on whether seepage will occur, is the fracture capillary-strength parameter of the near-field rock. For the sensitivity studies in this report with focus on seepage (during and after the thermal periods), careful evaluation is required before selecting an appropriate fracture capillary-strength parameter for the host rock.

6.4.11.1 Recapitulation of Seepage Calibration Model

The SCM (BSC 2004 [DIRS 171764]) conducts calibration to niche and ECRB liquid-release data to derive specific $1/\alpha$ values that match the niche test results. A summary of all calibrated capillary-strength values is provided in Table 6.4-5 (DTN: LB0302SCMREV02.002 [DIRS 162273], Table 3; also given in BSC 2004 [DIRS 171764], Section 6.6.4, Table 6-8). Data from six test intervals are available in the lower lithophysal (Tptpll) zone: four intervals in boreholes located above the ECRB Cross Drift, and two intervals in boreholes above Niche 1620. Four intervals in the middle nonlithophysal zone have been analyzed, one interval in a borehole above Niche 3107 and three intervals in boreholes above Niche 4788. Based on these data, the spatial variability of the capillary-strength parameter over the repository is

described in *Abstraction of Drift Seepage* (BSC 2004 [DIRS 169131], Section 6.6.2). The abstraction report indicates uniform probability distributions to cover the variability of this parameter (DTN: LB0407AMRU0120.001 [DIRS 173280]; also given in BSC 2004 [DIRS 169131], Table 6.6-2). Four different methods to develop these statistics are discussed in the abstraction, all of which lead to similar overall seepage results (BSC 2004 [DIRS 169131], Section 6.8.2). The range of values defined by the above spatial variability statistics is shown in Table 6.4-6. Using Method A from *Abstraction of Drift Seepage* (BSC 2004 [DIRS 169131], Table 6.6-2), the mean of the calibrated values over all Tptpmn and Tptpll sample locations is 591 Pa; the standard deviation is 109 Pa. On the other hand, when samples from Tptpll only are considered, the mean is 582 Pa with a standard deviation of 105 Pa, which is quite similar to the overall statistics. All other methods in Table 6.6-2 of *Abstraction of Drift Seepage* (BSC 2004 [DIRS 169131], Methods B through D) give larger capillary-strength values; using these larger values will reduce the potential for seepage.

Table 6.4-5. Summary Statistics of Estimated Capillary-Strength Parameter for Lower Lithophysal Zone and Middle Nonlithophysal Zone from Seepage Calibration Model

Lower Lithophysal Zone (Tptpll)							
Location	**Interval**	**Number of Inversions[a]**	**Estimate 1/α [Pa]**				
			Mean	**Std. Dev.[b]**	**Std. Error[c]**	**Min.**	**Max.**
SYBT-ECRB-LA#1	zone 2	17	534.3	56.8	13.8	447.7	674.1
SYBT-ECRB-LA#2	zone 2	21	557.1	56.4	12.3	457.1	676.1
SYBT-ECRB-LA#2	zone 3	19	534.8	57.8	13.3	443.1	645.7
SYBT-ECRB-LA#3	zone 1	23	452.0	54.7	11.4	382.8	616.6
Niche 1620	BH #4	30	671.2	223.2	40.8	356.0	1197.0
Niche 1620	BH #5	24	740.5	339.0	69.2	231.1	1840.7
			Mean[d] =	**581.6**			
			Std. Dev.[e] =	**105.0**			
Middle Nonlithophysal Zone (Tptpmn)							
Niche 3107	UM	1	741	—	—	—	—
Niche 4788	UL	1	646	—	—	—	—
Niche 4788	UM	1	603	—	—	—	—
Niche 4788	UR	1	427	—	—	—	—
			Mean[d] =	**604.3**			
			Std. Dev.[e] =	**131.5**			

Source: DTN: LB0302SCMREV02.002 [DIRS 162273], file: "DTN_U0080_TPO.002," Table 3.

[a] Each inversion is based on a different realization of the heterogeneous permeability field.
[b] Represents estimation uncertainty on account of small-scale heterogeneity (not available for estimates for the middle nonlithophysal zone).
[c] Standard error of mean.
[d] Represents average for given hydrogeologic unit.
[e] Represents spatial variability.

NOTE: BH = borehole; UL = upper left; UM = upper middle; UR = upper right.

Table 6.4-6. Intermediate-Scale Variability Statistics of Estimated Capillary-Strength Parameter over Repository Rock Block, Using Different Calculation Methods

Method	Number of Samples	Mean μ (Pa)	Std. Dev. σ (Pa)	Std. Error (Std. Dev. of Mean) (Pa)
A: All Samples, Both Units	10	591	109	35
B: All Locations, Both Units	4	631	109	54
C: All Samples in Tptpmn	4	604	131	66
All Samples in Tptpll	6	582	105	43
D: All Locations in Tptpmn	2	650	129	91
All Locations in Tptpll	2	613	132	93

Source: DTN: LB0407AMRU0120.001 [DIRS 173280]; also given in BSC 2004 [DIRS 169131], Table 6.6-2. Inside the DTN, go to folder *capillary_strength_analysis* and locate the file *capillary_strength_summary_tables.doc* for the values reported in this table.

6.4.11.2 Dimensionality and Scale

The fracture capillary-strength parameters in *Seepage Calibration Model and Seepage Testing Data* (BSC 2004 [DIRS 171764], Section 6) were obtained by calibrating to liquid-release test data based on the following conceptualizations:

- 3-D flow fields
- Applicable to only small-scale fracture flow close to the emplacement tunnels
- Heterogeneities in fracture permeability have no impact on calibrated fracture capillary-strength parameters.

In previous thermal seepage studies (BSC 2005 [DIRS 172262]; BSC 2006 [DIRS 174104]), even though the conceptual model was 2-D, the calibrated fracture capillary-strength parameter (which was obtained through 3-D calibration) from *Seepage Calibration Model and Seepage Testing Data* (BSC 2004 [DIRS 171764]) was used. In addition, even though the calibrated fracture capillary-strength parameter was representative of a small zone close to the emplacement tunnel, it was adopted for the fracture continuum of the entire Tptpll (or tsw35) unit. Because the objective in the two earlier reports (BSC 2005 [DIRS 172262]; BSC 2006 [DIRS 174104]) was to use a conservative approach with respect to seepage (i.e., simulate conditions that were most favorable for seepage), it was appropriate to adopt the calibrated fracture capillary-strength parameter on the following grounds:

- If a 2-D conceptual model were to be used in calibrating the liquid-release test data, it would have resulted in a larger estimated fracture capillary-strength parameter for the host rock Tptpll (see Section 6.4.11.3). A larger fracture capillary-strength parameter for Tptpll would have resulted in prediction of less seepage. Therefore, using a smaller fracture capillary-strength parameter was justified, since it was conservative.

- The SCM calibrated fracture capillary-strength parameter value represents conditions close to an emplacement tunnel. However, the SCM calibrated fracture-capillary strength parameter value was used for the entire host rock, Tptpll. Applying the SCM calibrated fracture capillary-strength parameter value for the entire fracture continuum of Tptpll implied that the fractures in general had smaller water retention ability (because the SCM calibrated fracture capillary-strength parameter value was much smaller than the Tptpll value). This, again, created situations favorable for water entering an emplacement drift rather than staying in the rock. In other words, this approach provided conservative results with respect to seepage.

6.4.11.3 Leverett-Scaling Effects

While the approach adopted in earlier seepage studies (BSC 2005 [DIRS 172262]; BSC 2006 [DIRS 174104]) was justified on the basis of dimensionality and scale as discussed above, one issue that was not addressed in those reports was the impact of permeability heterogeneity on fracture capillarity. Further evaluation of the calibration process is needed to account for the Leverett-scaling effects.

The prediction of seepage under ambient conditions is based on an approach that uses a suite of consistent models: (1) seepage-relevant, model-related parameters are estimated by calibrating a numerical model to seepage data from liquid-release tests conducted in various niches and the ECRB (BSC 2004 [DIRS 171764]); (2) a conceptually consistent prediction model is used to examine seepage into waste emplacement drifts for many seepage-relevant parameter combinations (BSC 2004 [DIRS 167652]); and (3) a seepage abstraction model is developed that determines probability distributions for these seepage-relevant parameters, accounting for spatial variability and uncertainty, and incorporating other effects (BSC 2004 [DIRS 169131]). Since the calibration process yields parameters that can be considered optimal for the given process, scale, and model structure, it is essential that the prediction model be conceptually consistent with the calibration model to minimize the risk of introducing a potential bias. Thus, since the calibration (BSC 2004 [DIRS 171764]) was performed with homogeneous capillarity (i.e., Leverett scaling was excluded), the SMPA (BSC 2004 [DIRS 167652) and the seepage abstraction model (BSC 2004 [DIRS 169131]) also did not include the Leverett-scaling effects for the sake of consistency.

However, if the conceptual model (which includes governing equations, treatment of heterogeneity, model dimensionality, and discretization) is changed, the model parameters will need to be adjusted accordingly. Specifically, it is expected that the reference van Genuchten capillary-strength parameter $1/\alpha$ (determined using the three-dimensional calibration model with a heterogeneous permeability field but with homogeneous capillary-strength) needs to be changed if used in a predictive model in which the small-scale capillary-strength is correlated to the heterogeneous permeability field using the Leverett-scaling rule (Equation 6.3-7).

A synthetic inversion study is performed to examine the potential adjustment that needs to be made to the capillary-strength parameter when changing the conceptual model for SCM (i.e., by adding Leverett-scaling effects). Synthetic seepage data are generated by simulating a liquid-release test using a conceptual model similar to that used for the calibration of actual liquid-release test data, i.e., a three-dimensional, heterogeneous model with a uniform

capillary-strength parameter. The synthetic liquid-release test is similar to those conducted in Zone 2 of Borehole SYBT-ECRB-LA#2, which is located in the lower lithophysal zone. The synthetic data are then used to calibrate 2-D and 3-D models, with (in both 2-D and 3-D inversion models) and without (in 2-D inversion models only) including Leverett-scaling effects. For the 3-D inversion model, 15 random realizations of the small-scale permeability (and—related through the Leverett scaling rule—the small-scale capillary-strength field) are generated, and 15 inversions are performed. For the 2-D inversion model, 20 random realizations are generated, and 20 inversions are performed. Additionally, the width of the 2-D inversion model is taken to be equal to the length of the injection interval (1.83 m). Table 6.4-7 summarizes the input parameters and other information about both the 3-D model used for the generation of synthetic seepage data, and the 2-D and 3-D models used for the estimation of the fracture capillary-strength parameter. Figure 6.4-4 shows the log-permeability and liquid saturation fields after 30 days of liquid release as calculated with the 3-D model used for the generation of synthetic seepage data. Figure 6.4-5 shows the log-permeability and saturation fields for one realization of the 2-D model used for the estimation of an effective capillary-strength parameter by data inversion, including Leverett scaling.

In the 2-D inversion model, water arriving at the drift ceiling is partly diverted around the opening. However, heterogeneity is restricted to the X-Z plane, which means that features represented by this heterogeneity are all aligned with the drift axis. This configuration promotes seepage. Moreover, water cannot flow around an obstacle in the Y direction, as it can in the 3-D model. As a result, a 2-D model tends to result in higher seepage rates than a 3-D model. Promoting seepage is compensated during the calibration process by an increase in the capillary-strength parameter in the 2-D inversion model. While all 20 realizations of the calibration model are capable of matching the long-term seepage rate (see Figure 6.4-6), changes in the details of the small-scale permeability field have a relatively strong impact on calculated seepage rates. Consequently, the estimates for the 20 realizations vary considerably. This is illustrated in Figure 6.4-7, which shows the histogram of the estimated capillary-strength parameter.

The inclusion of Leverett scaling further promotes the onset of seepage, mainly because water is drawn into the lower-permeability regions due to stronger capillarity, more readily yielding full saturations, which leads to seepage. Moreover, capillary-strength is reduced in high-permeability regions, generally reducing the water retention potential. These effects are partly countered by the stronger retention potential in the low-permeability regions, and the lower saturation in the high-permeability regions. The former effects seem to dominate the overall system behavior. The smaller estimated fracture capillary-strength parameter from the 3-D inversion model also confirms that, if the predictive model is 2-D, a larger fracture capillary-strength parameter must be used in order to have an equivalent capillary-barrier effect.

The input and output files for this analysis have been submitted to the TDMS with DTN: LB0706THCSENFC.001. The results are also summarized in Table 6.4-8. This synthetic study illustrates that:

(1) The seepage-relevant capillary-strength parameter is model-related and needs to be adjusted when changing the model structure.

(2) A 2-D seepage model generally yields higher seepage rates, and consequently, a higher capillary-strength parameter should be used compared to that used in a 3-D model.

(3) Applying the Leverett scaling rule to correlate the small-scale capillary-strength to small-scale permeability field generally yields larger seepage rates. Consequently, a larger capillary-strength parameter should be used compared to that employed in a model that does not apply Leverett scaling.

(4) Based on this limited analysis, it can also be said that, if the calibrated fracture capillary strength parameter is based on a 3-D conceptual model excluding Leverett-scaling effects (such as in the SCM), and this parameter is to be used in a 2-D predictive model (such as the THC seepage model), two corrections are necessary. The first correction is for inclusion of Leverett-scaling effects (in this example analysis, it changes from 591 Pa to 920 Pa, or by a factor of approximately 1.6), and the second correction is for changing the conceptual model from 3-D to 2-D (in this example, it changes from 920 to 3,274, or by a factor of approximately 3.6). Overall, changing the conceptual model from 3-D excluding Leverett-scaling effects (as in SCM) to 2-D including Leverett-scaling effects may amount to an increase in the calibrated fracture capillary-strength parameter by a factor of as large as a half order of magnitude.

(5) Uncertainty in heterogeneity yields considerable uncertainty in the capillary-strength parameter.

Table 6.4-7. Synthetic Data Generation and Calibration Model Information

Parameter	Data-Generation Model	Calibration Model	Comment, Reference
Model dimensionality	3-D	2-D or 3-D	Effect to be tested
Porosity	0.0096	0.0096	LB0205REVUZPRP.001 [DIRS 159525][a]
van Genuchten m	0.611	0.611	LB997141233129.001 [DIRS 104055][b]
Residual liquid saturation, S_{lr}	0.01	0.01	LB997141233129.001 [DIRS 104055][c]
Satiated liquid saturation	1.0	1.0	LB997141233129.001 [DIRS 104055][d]
Reference permeability log(k_{ref} [m^2])	−12.11	−12.11	LB0610UZDSCP30.001 [DIRS 179180][e]
Geostatistical parameters for small-scale distribution of fracture permeability			BSC 2004 [DIRS 171764], Section 6.6.2.1
Variogram type:	Spherical	Spherical	
Standard deviation log(k [m^2])	1.0	1.0	
Correlation length [m]	0.2	0.2	
Reference capillary-strength parameter, $1/\alpha_{ref}$ [Pa]	591.0	To be estimated	LB0407AMRU0120.001 [DIRS 173280][f]

Table 6.4-7. Synthetic Data Generation and Calibration Model Information (Continued)

Parameter	Data-Generation Model	Calibration Model	Comment, Reference
Leverett scaling	No	Yes and no for 2-D Yes and no for 3-D	Effect to be tested
Liquid release rate, *q* [mL/min]	36.0	36.0	Similar to testing in SYBT-ECRB-LA#2
Duration of liquid release, [day]	30.0	30.0	Similar to testing in SYBT-ECRB-LA#2
Number of Heterogeneous Permeability Realizations	1	20 for 2-D 15 for 3-D	N/A

[a] Open the spreadsheet "Fracture Properties." Locate the Column "Porosity" (second from right). Then locate the value of porosity (9.6×10^{-3} or 0.0096) for tsw35 (which is Tptpll or the host rock).
[b] Open the spreadsheet *1dbase-caseR1wodis.xls* and then look into the workbook "Flow Parameters." Locate the column "van Genuchten *m* (λ)." Then read the value (=0.611) for tsw35.
[c] Same as above, except look into column "residual saturation."
[d] Same as above, except look into column "satiated saturation."
[e] Locate Column "$\mathbf{K_F}$," and then read value of 9.1×10^{-13} m^2 (which is also 0.91×10^{-12} m^2) for tsw35 (which is Tptpll). The logarithm of 9.1×10^{-13} is –12.04, which is slightly different from the actual value used (–12.11). This small difference is not expected to have any significant impact on the synthetic data analyses presented in this subsection.
[f] Look into folder *capillary_strength_analysis* and locate file *capillary_strength_summary_tables.doc*. Then read the value of 591 Pa from Method A. See also Table 6.4-6.

Table 6.4-8. Estimated Fracture Capillary-Strength Parameter

Model	Model Dimension	Leverett Scaling	$1/\alpha_{ref}$ [Pa] Mean	$1/\alpha_{ref}$ [Pa] Standard Deviation
Data-Generation Model	3-D	No	591	N/A
Calibration Model	3-D	Yes	920[a]	50[a]
Calibration Model	2-D	No	2,144[b]	473[b]
	2-D	Yes	3,274[c]	713[c]

Source: Output DTN: LB0706THCSENFC.001.
[a] DTN: LB0706THCSENFC.001, folder: *Inversion3D*. The mean and standard deviation was calculated using a hand-held calculator from the estimated parameters (last lines of files "Lsi.out#," where "#" is 1 to 15.
[b] DTN: LB0706THCSENFC.001, folder: *Inversion2D*. Results are summarized in the Excel spreadsheet *LeverettScaling.xls*.

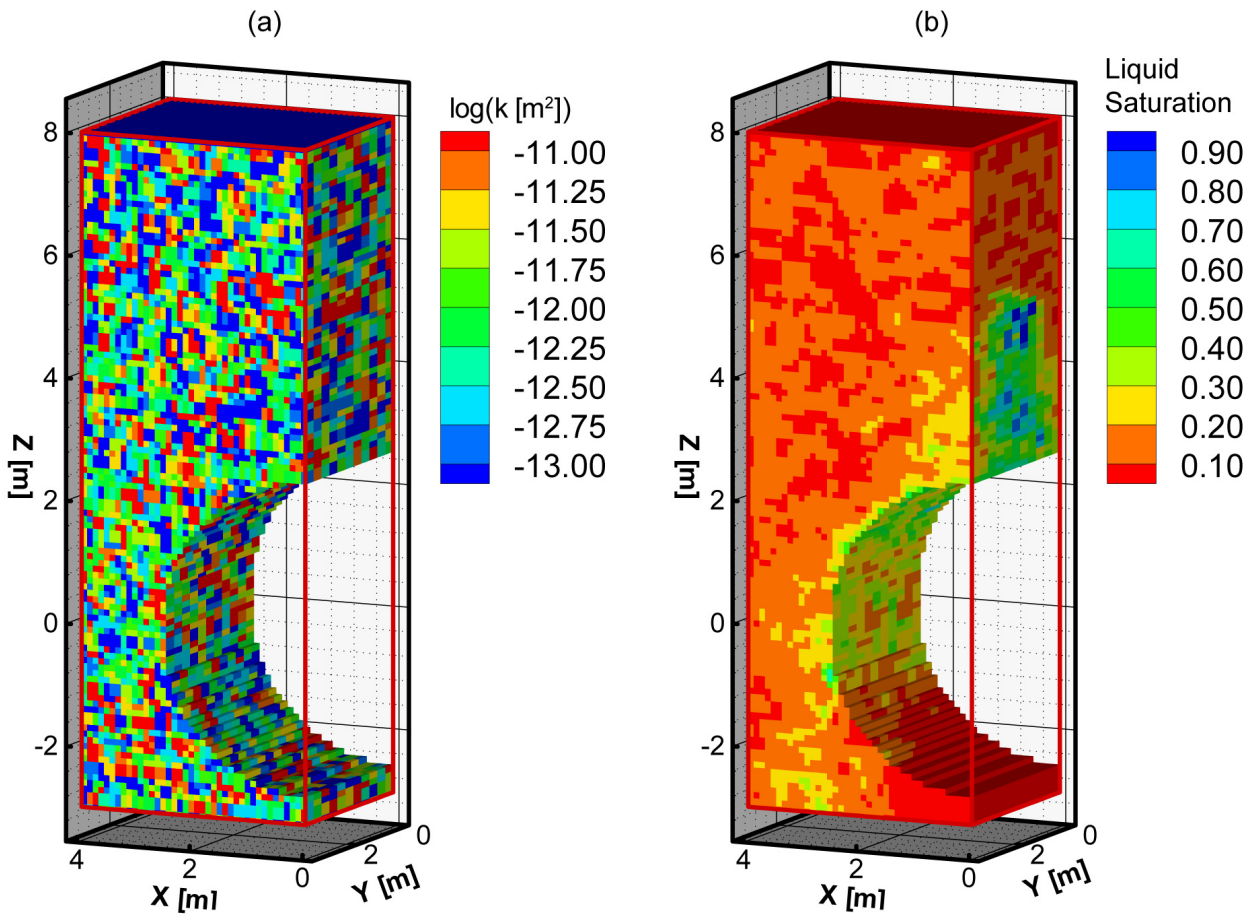

Source: Output DTN: LB0706THCSENFC.001.

NOTE: The 3-D log permeability field can be found in *Inversion2D/Figures/logk3D.wmf*. The 3-D liquid saturation plot can be found in *Inversion2D/Figures/sat3D.wmf*.

Figure 6.4-4. Three-Dimensional Data-Generation Model: (a) Log-Permeability Field, (b) Liquid Saturation after 30 Days of Liquid Release

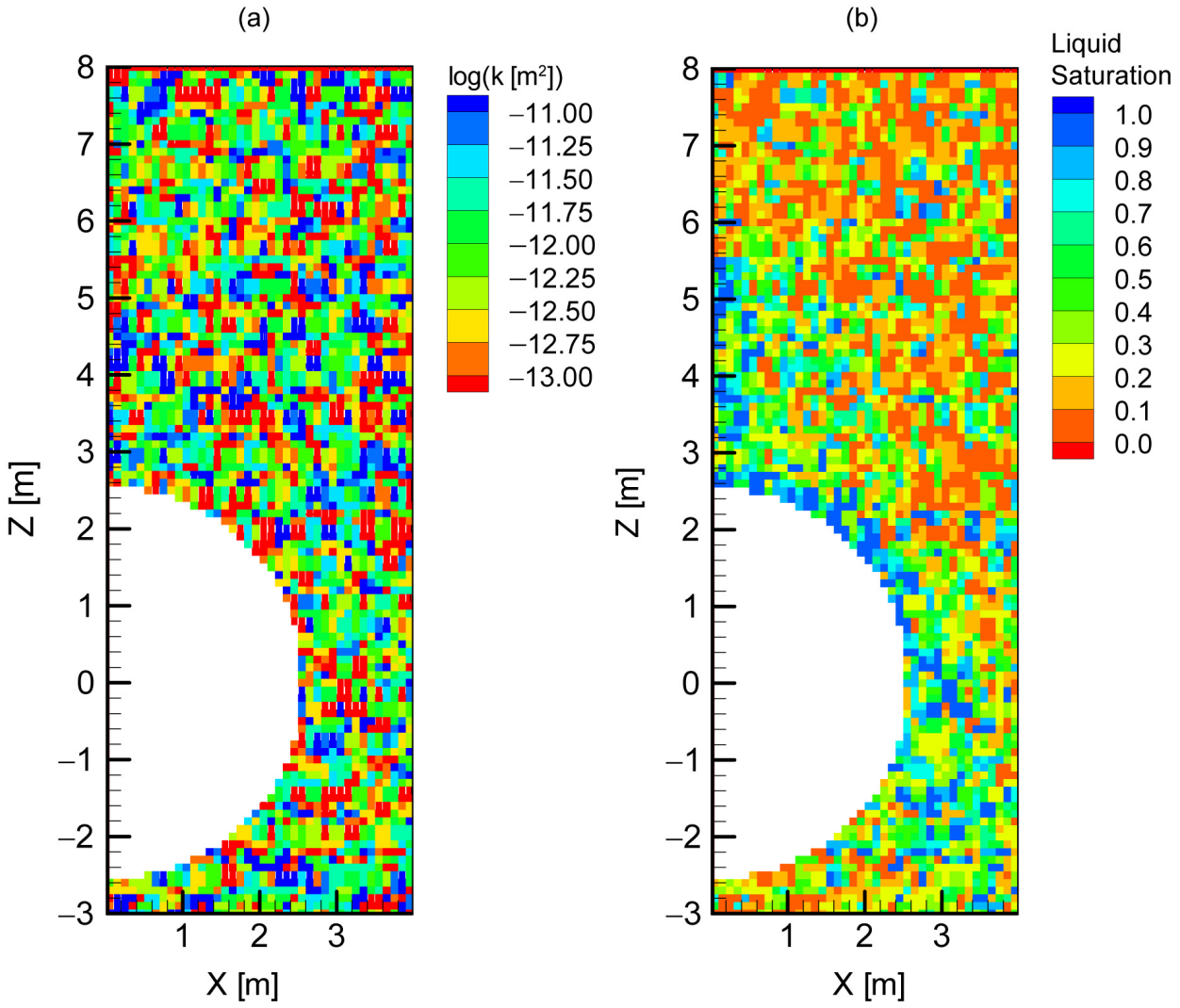

Source: Output DTN: LB0706THCSENFC.001.

NOTE: The 2-D log permeability field can be found in *Inversion2D/Figures/logk2D.wmf*. The liquid saturation plot can be found in *Inversion2D/Figures/Sat2D.wmf*.

Figure 6.4-5. Two-Dimensional Calibration Model: (a) One Realization of Log-Permeability Field, (b) Liquid Saturation after 30 Days of Liquid Release.

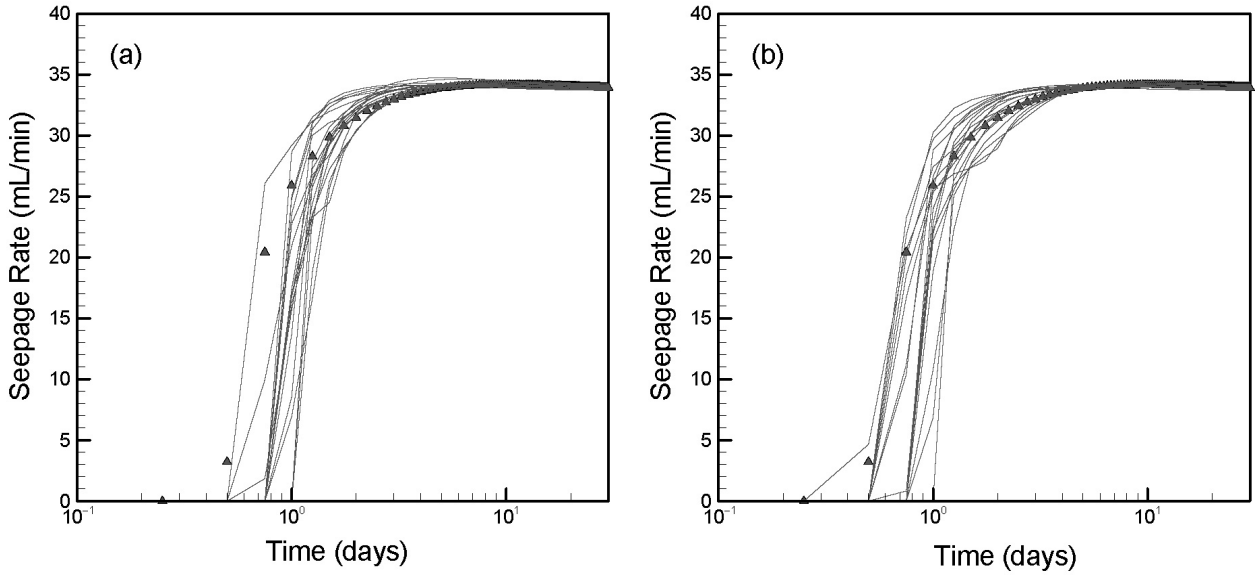

Source: Output DTN: LB0706THCSENFC.001.

Figure 6.4-6. Synthetic Seepage-Rate Data (symbols) and Matches Obtained by Two-Dimensional Calibration Models Using 20 Realizations of the Small-Scale Permeability Field: (a) without Leverett Scaling, (b) with Leverett Scaling

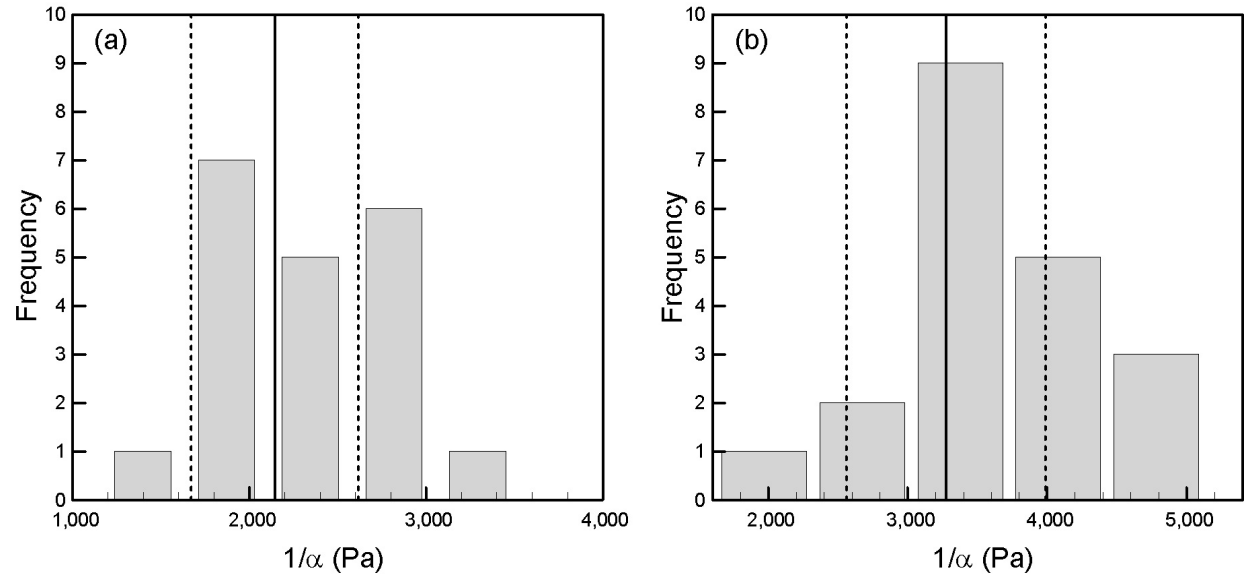

Source: Output DTN: LB0706THCSENFC.001.

NOTE: The solid, vertical line indicates the mean; dashed lines indicate the estimation uncertainty (one standard deviation).

Figure 6.4-7. Histogram of Estimated Capillary-Strength Parameter Obtained with 20 Different Calibration Models: (a) without Leverett Scaling, (b) with Leverett Scaling

6.4.11.4 Summary

The analyses in Section 6.4.11.3 illustrate the impact of Leverett-scaling effects and dimensionality on the estimated fracture capillary-strength parameter. For a 2-D conceptual model for seepage including Leverett-scaling effects, the synthetic liquid-release test data in Tptpll were best fitted with a mean fracture capillary-strength parameter of 3,274 Pa and a standard deviation of 713 Pa (providing a range of 2,561 to 3,987 Pa). If Leverett-scaling effects are not included, the estimated parameter range is 1,671 to 2,617 Pa (with a mean of 2,144 Pa). The range in the estimated fracture capillary-strength parameter is probably a function of the underlying heterogeneity.

On the other hand, the 30th percentile property set (DTN: LB0610UZDSCP30.001 [DIRS 179180]) provides the fracture capillary-strength parameter for Tptpll as 1,739 Pa. This value, although on the lower side of the range, is not very different from those estimated from the synthetic analyses in Section 6.4.11.3. Because a conservative approach is desired, the fracture capillary-strength parameter of 1,739 Pa is selected as the initial fracture capillary-strength parameter for the Tptpll unit. Additional sensitivity studies are performed in this report by changing the fracture capillary-strength parameter to cover the range of uncertainty in this parameter (see Section 6.7).

6.5 OVERVIEW OF SIMULATIONS

A number of simulations have been performed with the THC seepage model to determine its sensitivity to various parameters such as:

- Heterogeneity in fracture permeability, by using three realizations of the heterogeneous fracture permeability field (see Section 6.4.10): Realization #1, Realization #2, and Realization #3.
- Infiltration fluxes, using two sets of infiltration fluxes: IMF1 and IMF10 (see Section 6.4.5)
- Impact of Leverett scaling, by performing simulations with or without this effect
- Fracture capillary-strength parameter; most of the simulations are performed with an initial fracture capillary-strength parameter of 1,739 Pa (see Section 6.4.11) for Tptpll. Remember that fracture capillary-strength parameter changes with permeability and porosity (thus introducing heterogeneity in capillarity).

The simulations that have an initial fracture capillary-strength parameter of 1,739 are considered as “base-case” simulations and are identified as “base-case” hereafter. Results from these base-case simulations are presented in terms of extent of thermal perturbation (Section 6.6.1), seepage rate versus time plots (Section 6.6.2), and analysis of seepage water chemistry (Section 6.6.3). The procedure for extracting seepage rates from TOUGHREACT output files (“flow.out” files) is described in Appendix D. Before starting the ambient, TH, and THC simulations, simulations were carried out for obtaining steady-state flow conditions. These steady-state simulations were performed without the emplacement drifts (or heat) and are

summarized in Table 6.5-1. (The first six steady-state simulations in Table 6.5-1 are identified as base-case steady-state simulations.) As indicated in Section 4.1.1.2, these steady-state simulations were performed with a convergence criterion of 1×10^{-4}. However, the steady-state simulations in the original THC seepage model (SNL 2007 [DIRS 177404]) were performed with a convergence criterion of 1×10^{-5}. To determine whether this increase in convergence criterion (by an order of magnitude) has any impact on the final steady-state condition (which was eventually used as the initial condition in the various ambient, TH, and THC simulations), an additional steady-state simulation was performed. This additional steady-state simulation was performed with Realization #1 of the heterogeneous fracture permeability distribution and was inclusive of Leverett-scaling effects. It was performed with a convergence criterion of 1×10^{-5} (instead of 1×10^{-4}), and is identified in Table 6.5-1 as "addl_r1_lev_std." In Appendix E, the simulation results (i.e., physical conditions after 5×10^{6} years of simulation as given in file "SAVE") from simulation "addl_r1_lev_std" are compared with those from simulation "base_r1_lev_std." It is shown (Appendix E) that increasing the convergence criterion from 1×10^{-5} to 1×10^{-4} did not impact the final steady-state condition for this example in any significant way. While this exercise was not repeated for the other realizations of the heterogeneous permeability distribution and excluding Leverett-scaling effects, similar results (i.e., no significant impact of increasing the convergence criterion from 1×10^{-5} to 1×10^{-4} on eventual steady-state conditions) would logically be expected because the original convergence criterion of 1×10^{-4} was sufficiently small.

The primary objective of the base-case simulations was to analyze the impact of local fracture permeability heterogeneity (by using three different realizations of the heterogeneous fracture permeability distribution) on seepage rate and seepage water chemistry. However, the initial fracture capillary-strength parameter of the host rock, Tptpll, was maintained at the same value of 1,739 Pa for all these base-case simulations. The selection of this initial fracture capillary-strength parameter has been justified in Section 6.4.11.4. Identifying these as base-case simulations had another advantage. The homogeneous THC simulations in *Drift-Scale THC Seepage Model* (SNL 2007 [DIRS 177404], Section 6.5) were performed with the same Tptpll fracture capillary-strength parameter. As a result, results from the base-case simulations in this report could be directly compared with the results from *Drift-Scale THC Seepage Model* (SNL 2007 [DIRS 177404]) to illustrate the difference between heterogeneous and homogeneous simulations. This is also useful because it provides an opportunity for directly comparing seepage water chemistries from homogeneous and heterogeneous THC simulations (see Section 6.6.3), which is a requirement for the present report.

Some of the base-case simulations were performed with Leverett-scaling effects, while the rest did not include those effects (see Table 6.5-2). The capillary-barrier effects imposed by the base-case simulations inclusive of Leverett-scaling effects, however, are not equivalent to the capillary-barrier effects in the base-case simulations excluding Leverett-scaling effects. This is because the initial fracture capillary-strength parameter is the same in all base-case simulations irrespective of whether Leverett scaling is included or excluded. (See Section 6.4.11.3, where it is demonstrated that, when the same synthetic liquid-release test data were calibrated with and without Leverett-scaling effects, different fracture capillary-strength parameters were obtained. In other words, to achieve equivalent capillary-barrier effects with and without Leverett-scaling effects, different initial fracture capillary-strength parameters need to be used. Because the same

initial fracture capillary-strength parameter is used in all base-case simulations irrespective of whether Leverett scaling is included, the capillary-barrier effects imposed by a base-case simulation including Leverett scaling is different from a base-case simulation excluding Leverett scaling.) Additional sensitivity simulations (by changing the initial fracture capillary-strength parameters) were thereafter performed with the THC seepage model (SNL 2007 [DIRS 177404]) by changing the initial fracture capillary-strength parameter.

The choice of the initial fracture capillary-strength parameters for these additional sensitivity simulations depended on whether Leverett-scaling effects were excluded. When Leverett-scaling effects were excluded, the initial fracture capillary-strength parameter was adopted from the SCM (BSC 2004 [DIRS 171764]), since this presented a conservative approach for seepage. (The calibrated fracture capillary-strength parameter was obtained using a 3-D conceptual model but was used in a 2-D predictive model, lowering the capillary-barrier effects and increasing the potential for seepage.) These simulations are discussed in Section 6.7.1.

When Leverett-scaling effects are included, the choice of the initial fracture capillary-strength parameter is somewhat more complicated. Section 6.4.11.3 provides some guidelines; however, no direct calibrated fracture capillary-strength parameters are available for these simulations (the SCM cannot be used because it does not include Leverett scaling). An iterative scheme is therefore used to determine the initial fracture capillary-strength parameter, which will provide approximately the maximum potential for seepage (by adopting a fracture capillary-strength parameter that approximately provides a minimum of the capillary-barrier effects). These iterative simulations are described in Section 6.7.2.1, and seepage results from them can be found in Section 6.7.2.2.

6.5.1 Non-Convergent Simulations

One of the THC simulations (Simulation ID "base_r1_10x_lev_thc" in Table 6.5-2) was not completed. This simulation did not continue beyond 2,000 years because of numerical difficulties and was abandoned. Since results from a large number of simulations are available (see also Sections 6.6 and 6.7) satisfying the requirements of this THC sensitivity report, completion of this particular simulation is not considered essential. Also, because the simulation was not completed after 2,000 years, results from this simulation up to 2,000 years have not been submitted to the TDMS and have not been used in reaching any conclusion.

Table 6.5-1. Steady-State Simulation Runs

Serial No.	Infiltration Flux [a]	Fracture (1/α) Value (Pa)[b]	Permeability Heterogeneity[c]	Leverett Scaling[d]	Simulation Type	Run ID	Output DTN
1.	IMF1	1,739	Realization #1	Yes	STEADY	base_r1_1x_lev_std	LB0705THCSENR1.001
2.	IMF1	1,739	Realization #1	No	STEADY	base_r1_1x_nlev_std	LB0705THCSENR1.001
3.	IMF1	1,739	Realization #2	Yes	STEADY	base_r2_1x_lev_std	LB0705THCSENR2.001
4.	IMF1	1,739	Realization #2	No	STEADY	base_r2_1x_nlev_std	LB0705THCSENR2.001
5.	IMF1	1,739	Realization #3	Yes	STEADY	base_r2_1x_lev_std	LB0705THCSENR3.001
6.	IMF1	1,739	Realization #3	No	STEADY	base_r3_1x_nlev_std	LB0705THCSENR3.001
7.	IMF1	1,739	Realization #1	Yes	STEADY	addl_r1_1x_lev_std[e]	LB0706THCSENPP.001

[a] See Section 6.4.5 for definition of infiltration fluxes.
[b] See Section 6.4.11 for choice of fracture capillary-strength parameters.
[c] See Section 6.4.10 for definition of heterogeneous fracture permeability fields.
[d] See Sections 6.4.11.3 and 6.4.11.4.
[e] The difference between Serial No. 1 and Serial No. 7 is that the former has a convergence criterion of 1.0×10^{-4}, while the latter has a convergence criterion of 1×10^{-5} (see Appendix E for more discussion).

Table 6.5-2. Base-Case Simulation Runs

Serial No.	Infiltration Flux [a]	Fracture (1/α) Value (Pa)[b]	Permeability Heterogeneity[c]	Leverett Scaling[d]	Simulation Type[e]	Simulation ID	Output DTN
1.	IMF1	1,739	Realization #1	Yes	THC	base_r1_1x_lev_thc	LB0705THCSENR1.001
2.	IMF1	1,739	Realization #1	No	THC	base_r1_1x_nlev_thc	LB0705THCSENR1.001
3.	IMF10	1,739	Realization #1	Yes	THC	base_r1_10x_lev_thc	Not Available[f]
4.	IMF10	1,739	Realization #1	No	THC	base_r1_10x_lev_thc	LB0705THCSENR1.001
5.	IMF1	1,739	Realization #1	Yes	TH	base_r1_1x_lev_th	LB0705THCSENR1.002
6.	IMF1	1,739	Realization #1	No	TH	base_r1_1x_nlev_th	LB0705THCSENR1.002

Table 6.5-2. Base-Case Simulation Runs (Continued)

Serial No.	Infiltration Flux [a]	Fracture (1/α) Value (Pa)[b]	Permeability Heterogeneity[c]	Leverett Scaling[d]	Simulation Type[e]	Simulation ID	Output DTN
7.	IMF10	1,739	Realization #1	Yes	TH	base_r1_10x_lev_th	LB0705THCSENR1.002
8.	IMF10	1,739	Realization #1	No	TH	base_r1_10x_lev_th	LB0705THCSENR1.002
9.	IMF1	1,739	Realization #1	Yes	Ambient	base_r1_1x_lev_amb	LB0705THCSENR1.003
10.	IMF1	1,739	Realization #1	No	Ambient	base_r1_1x_nlev_amb	LB0705THCSENR1.003
11.	IMF10	1,739	Realization #1	Yes	Ambient	base_r1_10x_lev_amb	LB0705THCSENR1.003
12.	IMF10	1,739	Realization #1	No	Ambient	base_r1_10x_lev_amb	LB0705THCSENR1.003
13.	IMF1	1,739	Realization #2	Yes	THC	base_r2_1x_lev_thc	LB0705THCSENR2.001
14.	IMF1	1,739	Realization #2	No	THC	base_r2_1x_nlev_thc	LB0705THCSENR2.001
15.	IMF10	1,739	Realization #2	Yes	THC	base_r2_10x_lev_thc	LB0705THCSENR2.001
16.	IMF10	1,739	Realization #2	No	THC	base_r2_10x_lev_thc	LB0705THCSENR2.001
17.	IMF1	1,739	Realization #2	Yes	TH	base_r2_1x_lev_th	LB0705THCSENR2.002
18.	IMF1	1,739	Realization #2	No	TH	base_r2_1x_nlev_th	LB0705THCSENR2.002
19.	IMF10	1,739	Realization #2	Yes	TH	base_r2_10x_lev_th	LB0705THCSENR2.002
20.	IMF10	1,739	Realization #2	No	TH	base_r2_10x_lev_th	LB0705THCSENR2.002
21.	IMF1	1,739	Realization #2	Yes	Ambient	base_r2_1x_lev_amb	LB0705THCSENR2.003
22.	IMF1	1,739	Realization #2	No	Ambient	base_r2_1x_nlev_amb	LB0705THCSENR2.003
23.	IMF10	1,739	Realization #2	Yes	Ambient	base_r2_10x_lev_amb	LB0705THCSENR2.003
24.	IMF10	1,739	Realization #2	No	Ambient	base_r2_10x_lev_amb	LB0705THCSENR2.003
25.	IMF1	1,739	Realization #3	Yes	THC	base_r3_1x_lev_thc	LB0705THCSENR3.001
26.	IMF1	1,739	Realization #3	No	THC	base_r3_1x_nlev_thc	LB0705THCSENR3.001
27.	IMF10	1,739	Realization #3	Yes	THC	base_r3_10x_lev_thc	LB0705THCSENR3.001
28.	IMF10	1,739	Realization #3	No	THC	base_r3_10x_lev_thc	LB0705THCSENR3.001

Table 6.5-2. Base-Case Simulation Runs (Continued)

Serial No.	Infiltration Flux [a]	Fracture (1/α) Value (Pa)[b]	Permeability Heterogeneity[c]	Leverett Scaling[d]	Simulation Type[e]	Simulation ID	Output DTN
29.	IMF1	1,739	Realization #3	Yes	TH	base_r3_1x_lev_th	LB0705THCSENR3.002
30.	IMF1	1,739	Realization#3	No	TH	base_r3_1x_nlev_th	LB0705THCSENR3.002
31.	IMF10	1,739	Realization #3	Yes	TH	base_r3_10x_lev_th	LB0705THCSENR3.002
32.	IMF10	1,739	Realization #3	No	TH	base_r3_10x_lev_th	LB0705THCSENR3.002
33.	IMF1	1,739	Realization #3	Yes	Ambient	base_r3_1x_lev_amb	LB0705THCSENR3.003
34.	IMF1	1,739	Realization #3	No	Ambient	base_r3_1x_nlev_amb	LB0705THCSENR3.003
35.	IMF10	1,739	Realization #3	Yes	Ambient	base_r3_10x_lev_amb	LB0705THCSENR3.003
36.	IMF10	1,739	Realization #3	No	Ambient	base_r3_10x_lev_amb	LB0705THCSENR3.003

[a] See Section 6.4.5 for definition of infiltration fluxes.
[b] See Section 6.4.11 for choice of fracture capillary-strength parameters.
[c] See Section 6.4.10 for definition of heterogeneous fracture permeability fields.
[d] See Sections 6.4.11.3 and 6.4.11.4.
[e] THC = simulations with emplacement drifts, heat and chemistry; TH = simulations with emplacement drifts and heat (no chemistry); Ambient = simulations with emplacement drifts (no heat or chemistry).
[f] See Section 6.5.1.

6.6 BASE-CASE SIMULATION RESULTS

6.6.1 Thermal Perturbation

It was mentioned in Section 6.4.2 that the top and bottom boundaries of the THC seepage model domain are located at approximately 364 m above and approximately 353 m below the emplacement drift, respectively (Figure 6.4-1). It was also mentioned that fixed temperature boundaries (Section 6.4.3) have been imposed at the top and bottom of the THC seepage model domain (Figure 6.4-1). It has been indicated (Sections 6.4.2 and 6.4.3) that this is an acceptable approach, because thermal perturbation is not expected to extend beyond tens of meters above and below the emplacement drift. To determine the actual extent of thermal perturbation, the base-case simulation "base_r1_1x_lev_thc" can be taken as an example. Figure 6.6-1 shows the contours of temperature above and below the emplacement drift at 100 years (a time when temperatures are supposed to be near their peak adjacent to the emplacement drifts). The procedures required to obtain the temperature contours from file "flow.out" can be found in Appendix F.

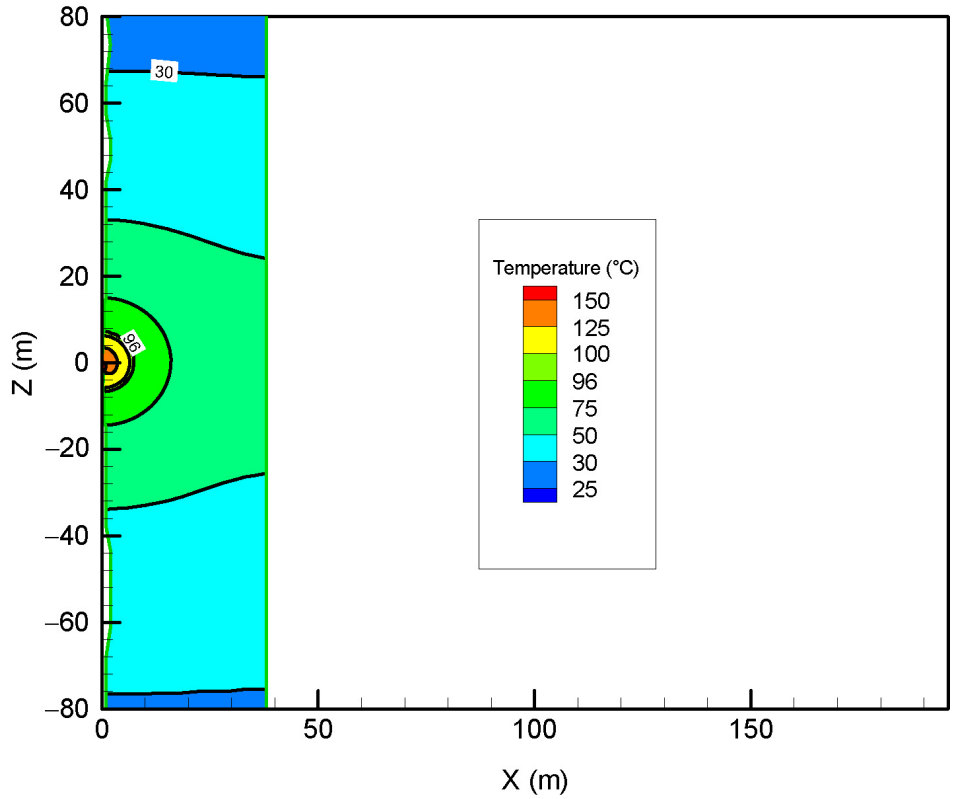

Output DTN: LB0706THCSENPP.001 (see file *Appendix_F/Contour_R1F1L_100y_Fdr.txt*).

Source DTN: LB0705THCSENR1.001, folder: *\THC\focus_1\leverett\alpha_fy07_30pc.dir\thc_50_600*.

NOTE: The contours demonstrate that thermal perturbation does not extend beyond about 80 m above and below the emplacement drift. The top and bottom boundaries of the THC seepage model are located at 364 m and 353 m above and below the emplacement drift, respectively (see Section 6.4.2 and Figure 6.4-1).

Figure 6.6-1. Sample Contours of Temperature above and below the Emplacement Drift

From Figure 6.6-1, it can be seen that temperatures are well above boiling near the emplacement drift. On the other hand, temperatures are close to ambient conditions beyond approximately 80 m above and below the emplacement tunnel. In other words, the thermal perturbation does not extend beyond 80 m above and below the emplacement drift for this particular simulation. Since temperatures are near maximum at 100 years after emplacement of waste packages (recall also that ventilation is turned off 50 years after emplacement of wastes), this possibly represents the maximum limits of the spatial extent of thermal perturbation. Though not shown here, temperature contours from the other base-case simulations are similar. In short, since the top and bottom boundaries are located at 364 m above and 353 m below the emplacement drift, respectively, it is reasonable to conclude that thermal perturbations do not reach the top and bottom boundaries of the THC seepage model domain. Thus, the constant temperature boundaries at the top and bottom of the THC seepage model domain have no significant impact on the evolution of temperatures in the host rock.

6.6.2 Seepage Rates

From Table 6.5-2, it can be seen that 36 base-case simulations were performed with the THC seepage model (though one of them could not be completed, see Section 6.5.1). These include simulations with three realizations of the heterogeneous fracture permeability distribution and two infiltration fluxes (IMF1 and IMF10). The simulations were performed with and without Leverett-scaling effects. All these combinations were repeated for ambient, TH, and THC simulations. The purpose of the base-case simulations was to analyze the sensitivity of the THC seepage model to permeability heterogeneity and infiltration fluxes, while keeping the initial fracture capillary-strength parameter for the Tptpll unit constant. Impact of capillarity heterogeneity can be observed by comparing the results from simulations with Leverett-scaling effects (capillarity is heterogeneous through Equation 6.3-7) and without those effects (capillarity is homogeneous). Thus, the base-case simulations cover a range of permeability and capillarity heterogeneity for a given initial fracture capillary-strength parameter (see Section 6.4.11).

Seepage results (whether seepage happens or not) from the base-case simulations are tabulated in Table 6.6-1. These results have been submitted to the TDMS; the output DTN for each of the 36 base-case simulations is also included in Table 6.6-1 (see also Table 6.5-2). The seepage results can be extracted from files “flow.out” in the output DTNs. Appendix D describes the procedures for how to extract the seepage results from the “flow.out” files.

Table 6.6-1. Summary of Seepage Results from Base-Case Simulations

Serial No.	Infiltration Flux [a]	Fracture (1/α) Value (Pa)[b]	Permeability Heterogeneity[c]	Leverett Scaling[d]	Simulation Type[e]	Simulation ID	Seepage?	Output DTN
1.	IMF1	1,739	Realization #1	Yes	THC	base_r1_1x_lev_thc	No	LB0705THCSENR1.001
2.	IMF1	1,739	Realization #1	No	THC	base_r1_1x_nlev_thc	No	LB0705THCSENR1.001
3.	IMF10	1,739	Realization #1	Yes	THC	base_r1_10x_lev_thc	Not Available[f]	—
4.	IMF10	1,739	Realization #1	No	THC	base_r1_10x_lev_thc	No	LB0705THCSENR1.001
5.	IMF1	1,739	Realization #1	Yes	TH	base_r1_1x_lev_th	No	LB0705THCSENR1.002
6.	IMF1	1,739	Realization #1	No	TH	base_r1_1x_nlev_th	No	LB0705THCSENR1.002
7.	IMF10	1,739	Realization #1	Yes	TH	base_r1_10x_lev_th	**Yes**	LB0705THCSENR1.002
8.	IMF10	1,739	Realization #1	No	TH	base_r1_10x_lev_th	No	LB0705THCSENR1.002
9.	IMF1	1,739	Realization #1	Yes	Ambient	base_r1_1x_lev_amb	No	LB0705THCSENR1.003
10.	IMF1	1,739	Realization #1	No	Ambient	base_r1_1x_nlev_amb	No	LB0705THCSENR1.003
11.	IMF10	1,739	Realization #1	Yes	Ambient	base_r1_10x_lev_amb	**Yes**	LB0705THCSENR1.003
12.	IMF10	1,739	Realization #1	No	Ambient	base_r1_10x_lev_amb	No	LB0705THCSENR1.003
13.	IMF1	1,739	Realization #2	Yes	THC	base_r2_1x_lev_thc	No	LB0705THCSENR2.001
14.	IMF1	1,739	Realization #2	No	THC	base_r2_1x_nlev_thc	No	LB0705THCSENR2.001
15.	IMF10	1,739	Realization #2	Yes	THC	base_r2_10x_lev_thc	**Yes**	LB0705THCSENR2.001
16.	IMF10	1,739	Realization #2	No	THC	base_r2_10x_lev_thc	No	LB0705THCSENR2.001
17.	IMF1	1,739	Realization #2	Yes	TH	base_r2_1x_lev_th	No	LB0705THCSENR2.002
18.	IMF1	1,739	Realization #2	No	TH	base_r2_1x_nlev_th	No	LB0705THCSENR2.002
19.	IMF10	1,739	Realization #2	Yes	TH	base_r2_10x_lev_th	**Yes**	LB0705THCSENR2.002
20.	IMF10	1,739	Realization #2	No	TH	base_r2_10x_lev_th	No	LB0705THCSENR2.002

Table 6.6-1. Summary of Seepage Results From Base-Case Simulation (Continued)

Serial No.	Infiltration Flux [a]	Fracture ($1/\alpha$) Value (Pa)[b]	Permeability Heterogeneity[c]	Leverett Scaling[d]	Simulation Type[e]	Simulation ID	Seepage?	Output DTN
21.	IMF1	1,739	Realization #2	Yes	Ambient	base_r2_1x_lev_amb	**Yes**	LB0705THCSENR2.003
22.	IMF1	1,739	Realization #2	No	Ambient	base_r2_1x_nlev_amb	No	LB0705THCSENR2.003
23.	IMF10	1,739	Realization #2	Yes	Ambient	base_r2_10x_lev_amb	**Yes**	LB0705THCSENR2.003
24.	IMF10	1,739	Realization #2	No	Ambient	base_r2_10x_lev_amb	No	LB0705THCSENR2.003
25.	IMF1	1,739	Realization #3	Yes	THC	base_r3_1x_lev_thc	No	LB0705THCSENR3.001
26.	IMF1	1,739	Realization #3	No	THC	base_r3_1x_nlev_thc	No	LB0705THCSENR3.001
27.	IMF10	1,739	Realization #3	Yes	THC	base_r3_10x_lev_thc	No	LB0705THCSENR3.001
28.	IMF10	1,739	Realization #3	No	THC	base_r3_10x_lev_thc	No	LB0705THCSENR3.001
29.	IMF1	1,739	Realization #3	Yes	TH	base_r3_1x_lev_th	No	LB0705THCSENR3.002
30.	IMF1	1,739	Realization#3	No	TH	base_r3_1x_nlev_th	No	LB0705THCSENR3.002
31.	IMF10	1,739	Realization #3	Yes	TH	base_r3_10x_lev_th	No	LB0705THCSENR3.002
32.	IMF10	1,739	Realization #3	No	TH	base_r3_10x_lev_th	No	LB0705THCSENR3.002
33.	IMF1	1,739	Realization #3	Yes	Ambient	base_r3_1x_lev_amb	No	LB0705THCSENR3.003
34.	IMF1	1,739	Realization #3	No	Ambient	base_r3_1x_nlev_amb	No	LB0705THCSENR3.003
35.	IMF10	1,739	Realization #3	Yes	Ambient	base_r3_10x_lev_amb	No	LB0705THCSENR3.003
36.	IMF10	1,739	Realization #3	No	Ambient	base_r3_10x_lev_amb	No	LB0705THCSENR3.003

[a] See Section 6.4.5 for definition of infiltration fluxes.
[b] See Section 6.4.11 for choice of fracture capillary-strength parameters.
[c] See Section 6.4.10 for definition of heterogeneous fracture permeability fields.
[d] See Sections 6.4.11.3 and 6.4.11.4.
[e] THC = simulations with emplacement drifts, heat and chemistry; TH = simulations with emplacement drifts and heat (no chemistry); Ambient = simulations with emplacement drifts (no heat or chemistry).
[f] See Section 6.5.1.

A few observations can be made from the results summarized in Table 6.6-1.

- No seepage is observed for any of the three realizations of the heterogeneous fracture permeability distribution with IMF1 infiltration fluxes (see Section 6.4.5), if *Leverett-scaling effects are ignored*. This is true even with IMF10 (ten times the IMF1 fluxes; see Section 6.4.5) infiltration fluxes. This is also true whether ambient, TH, or THC simulations are considered.

  The initial fracture capillary-strength parameter ($1/\alpha_0$) for the Tptpll unit in these base-case simulations is 1,739 Pa. If capillarity is assumed spatially uniform and independent of permeability (i.e., Leverett scaling is ignored), for the Tptpll fracture properties provided in Table 6.4-2, the seepage threshold saturation (Equation 6.3-10) is quite large (~0.8196). In other words, a fracture element just outside the emplacement drift must have a saturation of 0.8196 or larger for seepage to occur. The results show that this condition was not satisfied in any of the simulations, and consequently, seepage is not predicted from these simulations. This implies that the capillary-barrier effect is too strong and excludes flow from entering the drift in these simulations.

- When fracture capillarity is correlated to fracture permeability/porosity heterogeneity (i.e., *Leverett-scaling effects are included*), using the IMF1 fluxes, no seepage is predicted in TH or THC simulations with any of the realizations of the heterogeneous permeability distributions. Ambient simulations also predict no seepage for two of the realizations of the permeability distribution (Realization #1 and Realization #3). However, minor seepage (approximately 1.66 mm/yr or approximately 8.12% of the infiltration fluxes) is predicted in ambient simulation with Realization #2 (Simulation ID: "base_r2_1x_lev_amb"; see Tables 6.5-2 and 6.6-1). This particular simulation predicts seepage to occur after 2,000 years.

- When IMF10 (see Section 6.4.5) infiltration fluxes are used and Leverett-scaling effects are included, seepage is predicted to occur from both ambient and TH simulations with Realization #1 (Simulation IDs: "base_r1_10x_lev_amb" and "base_r1_10x_lev_th"; see Table 6.5-2). Note that results from the corresponding THC simulation (Simulation ID: "base_r1_10x_lev_thc") are not available (see Tables 6.5-2 and 6.6-1). Figure 6.6-2 compares the seepage fluxes from simulations "base_r1_10x_lev_amb" and "base_r1_10x_lev_th." Note that the ambient seepage fluxes are larger than seepage from TH simulations. Figure 6.6-2 also shows the infiltration fluxes for IMF10 scenario (see Section 6.4.5) and the different climate periods (present-day, monsoon, and glacial transition; see Section 6.4.5). Maximum seepage flux from these simulations is predicted to be less than 21% (ambient simulations) and 13% (TH simulations). Predicted TH seepage fluxes are less than ambient seepage fluxes because of the vaporization barrier effect created by the repository thermal load (see Sections 6.1.1 and 6.1.2). Note that the seepage percentages are calculated based on the maximum infiltration fluxes (i.e., infiltration fluxes of the glacial transition period).

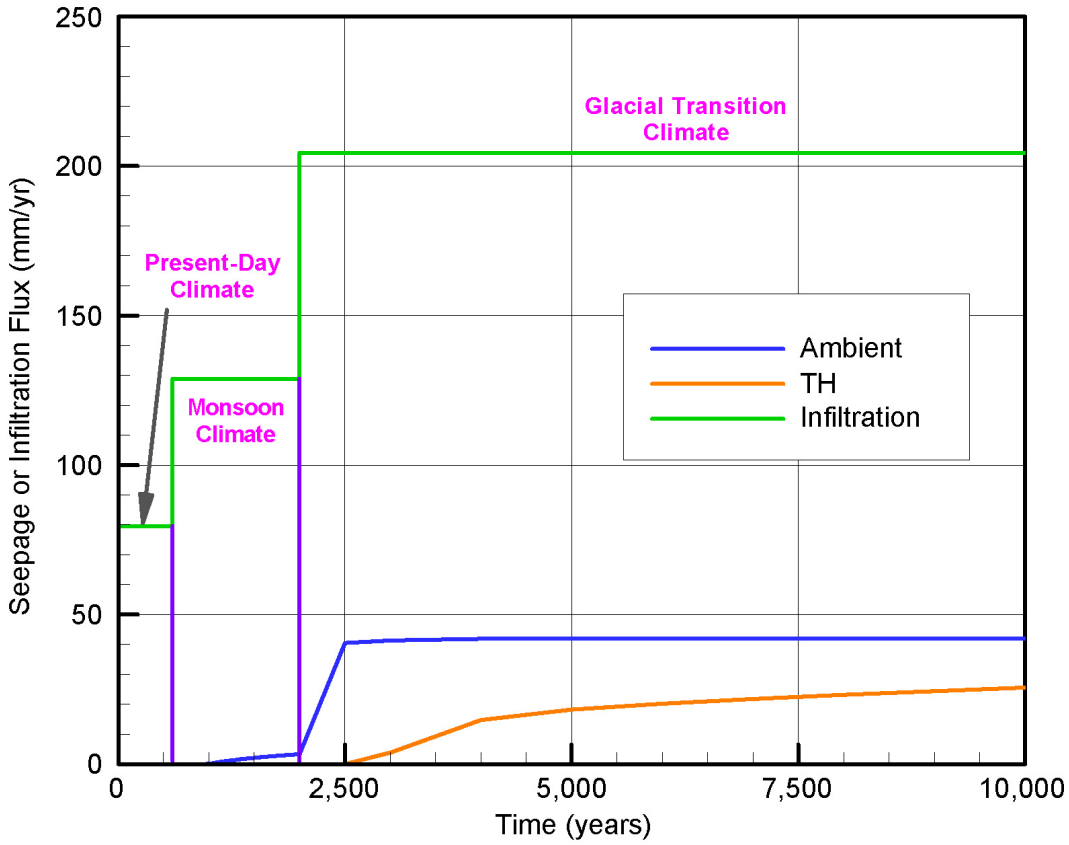

Source: Output DTNs: LB0705THCSENR1.002 and LB0705THCSENR1.003.

NOTE: See Table 6.5-2 for explanation of simulation IDs. The vertical violet lines are used to distinguish the different climatic periods and they do not represent any seepage data. The corresponding THC simulation (Simulation ID: "base_r1_10x_lev_thc") could not be completed (see Table 6.6-1).

Figure 6.6-2. Comparison of Seepage Fluxes from Ambient (Simulation ID: "base_r1_10x_lev_amb" and TH (Simulation ID: "base_r1_10x_lev_th") Simulations

For corresponding ambient, TH, and THC simulations with Realization #2 (Simulation IDs: "base_r2_10x_lev_amb," "base_r2_10x_lev_th," and "base_r2_10x_lev_thc"), seepage is predicted by all of them. Figure 6.6-3 compares the seepage fluxes from these three simulations for Realization #2. Ambient seepage fluxes are again predicted to be larger than both TH and THC seepage. The predicted pattern of seepage from these three simulations illustrates the dynamic nature of the underlying processes. For this realization of the heterogeneous permeability distribution (in combination with the initial fracture capillary-strength parameter of 1,739 Pa), ambient simulations predict seepage at all times (as confirmed by even the ambient simulation with IMF1 infiltration fluxes; see Simulation ID "base_r2_1x_lev_amb" in Tables 6.5-2 and 6.6-1). TH and THC simulations also predict small amounts of seepage at the beginning (between 0 and 50 years) and no seepage immediately after ventilation stops (as the host rock heats through the boiling temperatures). In TH and THC simulations, seepage returns after the boiling period is over and temperatures have dropped below boiling. Overall, the predicted patterns of seepage from TH and THC simulations are similar (with ambient seepage being marginally larger than the other two). Maximum seepage flux is approximately 32% of the infiltration fluxes.

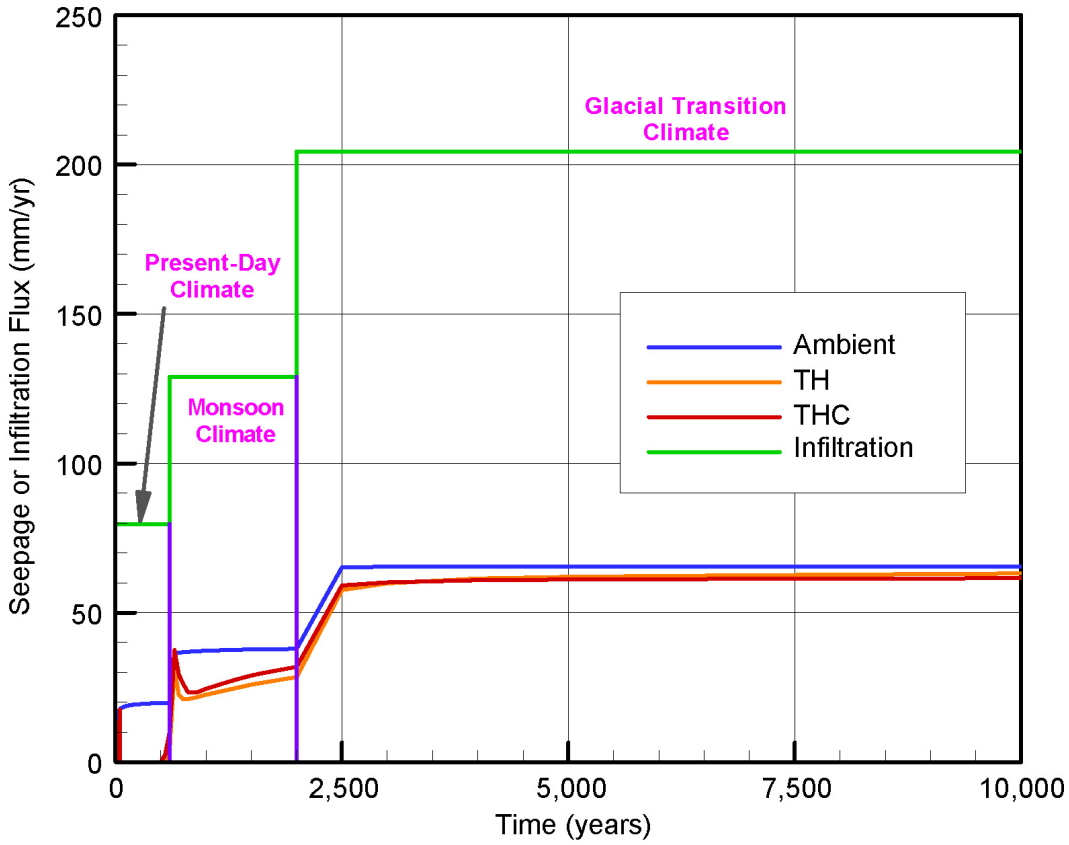

Source: Output DTNs: LB0705THCSENR2.001, LB0705THCSENR2.002, and LB0705THCSENR2.003.

NOTE: See Table 6.5-2 for explanation of simulation IDs. The vertical violet lines are used to distinguish the different climatic periods and they do not represent any seepage data.

Figure 6.6-3. Comparison of Seepage Fluxes from Ambient (Simulation ID: "base_r2_10x_lev_amb"), TH (Simulation ID "base_r2_10x_lev_th."), and THC (Simulation ID: "base-r2_10x_ lev_thc") Simulations

Thus, the combination of Realization #2 of the heterogeneous permeability distribution and an initial fracture capillary-strength parameter of 1,739 Pa did not provide a strong enough capillary-barrier to prevent even ambient seepage. Since fracture capillarity (and consequently, capillary-barrier) is in this case a local phenomenon because of the formulation of Leverett scaling (Equation 6.3-7), these results highlight the local nature of the process.

This result is further confirmed by the corresponding simulation results with Realization #3 of the heterogeneous fracture permeability distribution. In this case, none of the ambient (Simulation ID: "base_r3_10x_lev_amb"), TH (Simulation ID: "base_r3_10x_lev_th"), and THC (Simulation ID: "base_r3_10x_lev_thc") simulations shows any seepage. This implies that, for this realization of the fracture permeability distribution in combination with an initial fracture capillary-strength parameter, the local capillary-barrier effect is too strong.

- The base-case simulations demonstrate the impact of fracture permeability and capillarity heterogeneity on seepage. When fracture permeability heterogeneity is included in the conceptual model and capillarity is assumed homogeneous (i.e., Leverett scaling is not

included), the selected fracture capillary-strength parameter (1,739 Pa) resulted in a large seepage threshold saturation (~0.8196), which did not allow seepage to occur with either the IMF1 infiltration fluxes or the IMF10 infiltration fluxes. However, with inclusion of both permeability and capillarity heterogeneity in the conceptual model through Leverett scaling, local situations are created in which the seepage threshold saturations are considerably smaller (i.e., locations with considerably larger permeability than the mean fracture permeability). This is demonstrated in Table 6.6-2 where the impact of permeability heterogeneity (keeping porosity constant) on seepage threshold saturation is demonstrated for the fracture properties provided in Table 6.4-2. Observe that, if the permeability is two orders of magnitude larger than the mean fracture permeability, seepage threshold saturation decreases to approximately 0.017 (it is ~0.8196 when capillarity is uniform). Such a local decrease in seepage-threshold saturation makes seepage possible when capillarity heterogeneities are included in model conceptualization, particularly when enhanced infiltration fluxes are imposed.

Table 6.6-2. Example Calculations Showing Impact of Permeability Heterogeneity on Seepage Threshold Saturation through Leverett Scaling (Equations 6.3-7 and 6.3-10)

Item Number	Mean Fracture Permeability (m^2)	Local Gridblock Fracture Permeability (m^2)	Leverett Factor[a] (Equation 6.3-7) (−)	Seepage Threshold Saturation[b] (Equation 6.3-10) (−)
1.	0.91×10^{-12}	0.91×10^{-14}	0.1000	0.9996
2.	0.91×10^{-12}	0.91×10^{-13}	0.3162	0.9906
3.	0.91×10^{-12}	0.91×10^{-12}	1.0000	0.8196
4.	0.91×10^{-12}	0.91×10^{-11}	3.1622	0.1638
5.	0.91×10^{-12}	0.91×10^{-10}	10.0000	0.0168

[a] Porosity is assumed to be equal to mean fracture porosity. Leverett factor is calculated as the square root of the ratio of local gridblock fracture permeability and mean fracture permeability.

[b] For these seepage threshold calculations using Equation 6.3-10, water density ρ is 1,000 kg/m^3; h is 0.1 m (the distance of the center of the gridblock from the drift wall); and g (acceleration due to gravity) is 9.81 m2/s; α_0 is 1,739 Pa; m is 0.6330; γ is 0.4000; and S_{lr} is 0.01. For the source of the parameters α_0, m, γ, and S_{lr}, see Table 6.4-2.

- For the base-case simulations in which seepage happens, Table 6.6-3 provides the maximum seepage percentage (as a percentage of the imposed infiltration fluxes). Table 6.6-3 also identifies the simulation type (ambient, TH, or THC) from which maximum seepage happens. Observe that, when seepage happens (particularly for greater imposed infiltration fluxes), ambient seepage is always larger than TH or THC simulations. This is important because it implies that seepage abstraction can continue to be based on ambient seepage rates (i.e., THC processes provide no enhancement in seepage).

- The other important conclusion is that, even though the initial fracture capillary-strength parameter was the same between simulations excluding and including Leverett-scaling effects, the capillary-barrier effects by them were not the same. As the discussion in

Section 6.4.11.3 demonstrates, a larger initial fracture capillary-strength parameter needs to be used in a simulation that includes Leverett-scaling effects compared to one that does not, if there are to be equivalent capillary-barrier effects (this is also demonstrated by the calculated seepage saturation threshold values in Table 6.6-2). This will be discussed further in Section 6.7.2.

Table 6.6-3. Maximum Seepage Percentage and Base-Case Simulation Type from Which Maximum Seepage Happens

Serial No.	Simulation ID[a]	Permeability Realization[b]	Infiltration Flux[c]	Maximum Seepage Percentage	Simulation Type from Which Maximum Seepage Happens
1.	base_r2_1x_lev_amb	#2	IMF1	8.12	Ambient
2.	base_r1_10x_lev_amb	#1	IMF10	20.55	Ambient
3.	base_r2_10x_lev_amb	#2	IMF10	31.78	Ambient

[a] See Table 6.5-2. See also Table 6.6-1.
[b] See Section 6.4.10.
[c] See Section 6.4.5. For IMF1, the infiltration fluxes are 7.96 mm/yr (0 to 600 years); 12.89 mm/yr (600 to 2,000 years); and 20.45 mm/yr (2,000 years and beyond). For IMF10, the infiltration fluxes are 79.6 mm/yr (0 to 600 years); 128.9 mm/yr (600 to 2,000 years); and 204.5 mm/yr (2,000 years and beyond).

NOTE: Maximum seepage percentage is calculated by dividing the actual seepage rate by the largest infiltration flux (i.e., infiltration flux beyond 2,000 years) for a given infiltration scenario. Thus, for IMF1, the denominator is 20.45 mm/yr. On the other hand, for IMF10, the denominator is 204.5 mm/yr.

6.6.3 Seepage Water Chemistry

As indicated in Section 6.2, one of the objectives of this report is to provide an analysis of the seepage water chemistry. More specifically, the objective is to illustrate the impact, if any, of permeability and capillarity heterogeneity on seepage water chemistry. This can be accomplished by comparing seepage water chemistries from representative heterogeneous THC simulations (for example, any of the base-case simulations in Section 6.6.1) with seepage water chemistry from a homogeneous THC simulation (for example, considering the simulation run "thc7_81_w0" in Table 6.5-4 of SNL 2007 [DIRS 177404]). For this comparison, it is appropriate to select a heterogeneous THC simulation in which seepage actually occurs (so that actual simulated seepage water can be sampled). From Table 6.6-1, it can be seen that simulation "base-case_r2_10x_lev_thc" satisfies this condition. For completeness of the comparison process, seepage water from the corresponding IMF1 simulation ("base-case_r2_1x_lev_thc") is also included in the analysis. Since the simulation "base-case_r1_10x_lev_thc" with Realization #1 of the heterogeneous fracture permeability distribution could not be completed (because of numerical difficulties; see Section 6.5.1), it was decided that the analysis of seepage water be done with THC simulations corresponding to Realization #2 of the heterogeneous fracture permeability distribution. Also, no simulation without Leverett-scaling effects is selected, because the homogeneous THC simulation (SNL 2007 [DIRS 177404], Table 6.5-4) includes Leverett-scaling effects (recollect that, even though the homogeneous THC simulation has uniform fracture permeability and capillarity initially, THC processes of mineral precipitation and dissolution can introduce dynamic heterogeneity). In the following, the selection criteria for seepage water are provided, together

with a comparison of extracted seepage waters from homogeneous and selected heterogeneous THC simulations.

The THC seepage model provides, for each gridblock at each printout time interval, parameter values for variables such as temperature, pressure, gas, and liquid saturation; concentrations of aqueous species; mineral volume fractions; and the CO_2 volume fractions in matrix and fractures. Predicted pore-water chemistries for seven simulations, as shown in Table 6.6-4, were extracted from model output files following the same methodology as described in *Drift-Scale THC Seepage Model* (SNL 2007 [DIRS 177404], Section 6.4.8). This methodology involves selecting fracture gridblocks above the drift with non-zero liquid saturations on the basis of fluid mobility (these waters are referred to as "FLUX" water hereafter), where mobility is assessed as the vector sum of Darcy liquid fluxes over all connections of any particular gridblock to its adjacent gridblocks. Above the drift, in fractures, the location of FLUX waters closely coincides with zones of highest liquid saturations (HISAT), except that water compositions from gridblocks in which high liquid saturations result from enhanced capillarity (from the Leverett-scaling effect introduced by mineral precipitation; see Section 6.3) are mostly excluded from FLUX waters. Therefore, when the Leverett-scaling formulation is implemented, potential in-drift seepage is considered better represented by FLUX waters than simply by waters from zones of highest liquid saturation.

As explained in *Drift-Scale THC Seepage Model* (SNL 2007 [DIRS 177404], Section 6.4.8), model results are extracted for six gridblocks within a 45-degree quadrant from the drift crown (with given attribute "TOP") for each point in time, and each simulation, thus capturing the spatial variability above the drift. In addition, predicted concentrations were extracted for all model gridblocks showing non-zero liquid saturations inside the modeled drift within 20 cm of the drift wall and above the drift center. Predicted concentrations were also extracted for one model gridblock in rock (fractures) directly at the crown of the emplacement drift.

Data extracted in this manner, together with FLUX water chemistries predicted by the THC seepage model assuming homogenous rock properties (from DTN: LB0705DSTHC001.001 [DIRS 181217]; SNL 2007 [DIRS 177404], Section 6.5.5.4), are presented below as time profiles of predicted concentrations. The focus is on the comparison of FLUX waters with actual seepage (in-drift) waters, as well as the comparison of predicted water chemistries between the homogeneous and heterogeneous cases, and less on the spatial variability of model results around the drift (the latter is examined in SNL 2007 [DIRS 177404], Section 6.5.5.4). For this reason, for the case of FLUX waters, data are presented only for the gridblock (at each model result printout interval) with the highest liquid mobility (with given attribute INDX=1).

These data are also tabulated into file *frac_het_ff.xls* accompanying this report and submitted to the TDMS as Output DTN: LB0706THCSENSC.001. Note that this file contains plots for more aqueous species than presented below, and for six gridblocks (at each printout time interval) with highest fluid mobility ranked with attribute INDX=1 (highest) through 6.

Table 6.6-4. Water Chemistry Comparison Cases

Plot Legend	Simulation ID	Location	Fracture Permeability	Infiltration	Source and Output DTNs
Homgnes TF 1x	thc7_81_w0[a]	Fractures, TOP quadrant, highest liquid mobility	Homogeneous	IMF1	Source DTN: LB0705DSTHC001.001[b] [DIRS 181217] Output DTN: LB0706THCSENSC.001[c]
Hetgnes TF 1x	base_r2_1x_lev_thc[d]	Fractures, TOP quadrant, highest liquid mobility	Heterogeneous, Realization #2	IMF1	Output DTN: LB0706THCSENSC.001[c]
Hetgnes TF 10x	base_r2_10x_lev_thc[d]	Fractures, TOP quadrant, highest liquid mobility	Heterogeneous, Realization #2	IMF10	Output DTN: LB0706THCSENSC.001[c]
Hetgnes InDr 1x	base_r2_1x_lev_thc[d]	Drift, all wet in-drift gridblocks above the waste package within 20 cm from the drift wall	Heterogeneous, Realization #2	IMF1	Output DTN: LB0706THCSENSC.001[c]
Hetgnes InDr 10x	base_r2_10x_lev_thc[d]	Drift, all wet in-drift gridblocks above the waste package within 20 cm from the drift wall	Heterogeneous, Realization #2	IMF10	Output DTN: LB0706THCSENSC.001[c]
Hetgnes DW 1x	base_r2_1x_lev_thc[d]	Fractures at the drift crown (one gridblock)	Heterogeneous, Realization #2	IMF1	Output DTN: LB0706THCSENSC.001[c]
Hetgnes DW 10x	base_r2_10x_lev_thc[d]	Fractures at the drift crown (one gridblock)	Heterogeneous, Realization #2	IMF10	Output DTN: LB0706THCSENSC.001[c]

[a] See Section 6.5-4 and Table 6.5-4 of SNL 2007 [DIRS 177404] for description of this simulation ID.
[b] See files *frac_81_162_dr_w0.xls* and *frac_81_162_w0.xls*.
[c] See file *frac_het_ff.xls*.
[d] See Section 6.5 and Table 6.5-2 for description of these simulation IDs.

The time-profiles of distance from drift center, temperature, and liquid saturation for model gridblocks representing TOP FLUX waters are shown in Figures 6.6-4 to 6.6-6. These profiles provide a context for the chemistry profiles discussed afterwards. For simulated times up to 50 years, TOP FLUX waters represent gridblocks directly above, and adjacent to, the drift crown (i.e., at a distance ~2.8 m from drift center) (Figure 6.6-4). From the onset of boiling at approximately 50 years, the TOP FLUX waters correspond to the condensation/reflux zone in fractures directly above the boiling front, and thus their distance from drift center corresponds approximately to the extent of dryout zone in fractures (Figures 6.6-4 and 6.6-5). For the IMF1 infiltration scenario, these distances drop down to ~2.8 m at the same time drift-wall temperature drops down below ~96°C (Figure 6.6-5), the boiling point for the modeled elevation. This behavior indicates that the rewetting front in fractures around the drift more or less coincides with the collapse of the boiling front, with rewetting of the drift wall occurring at about 1,300 years. For the IMF10 infiltration scenario, the boiling front collapses earlier (at about 400 years), and boiling continues at the drift wall for several hundred years (Figures 6.6-4 and 6.6-5).

The spatial variability in liquid saturation for gridblocks located in the condensation/reflux zone typically translates directly to the variability of predicted concentrations of dissolved species in that zone. This is because variations in liquid saturation caused by dilution and evaporation directly affect concentrations. For each model run, predicted liquid saturations at TOP FLUX locations with highest liquid mobility (INDX=1) show trends of higher saturation with higher infiltration, as well as higher saturations in the heterogeneous (versus homogeneous) case (Figure 6.6-6).

Predicted profiles of concentration versus time for CO_2 gas and aqueous species of interest are shown in Figures 6.6-7 through 6.6-17. Details on processes affecting these concentration trends (evaporation, dilution, water–rock interactions) are discussed in *Drift-Scale THC Seepage Model* (SNL 2007 [DIRS 177404], Section 6.5.5.4) and not repeated here.

Several important observations can be made from these figures. The main observation is that for the IMF1 infiltration scenario, predicted concentration profiles of aqueous species with heterogeneous and homogeneous permeability fields do not differ significantly. In fact, when the full spread in results is taken into account (i.e., when considering data for gridblocks with attribute INDX = 1 though 6, instead of only 1, as shown in Figures 6.6-7 through 6.6-17), the profiles for both cases essentially overlap. This is consistent with conclusions from earlier work (BSC 2004 [DIRS 168848], Section 6.6) asserting that fracture permeability heterogeneity would not significantly affect predicted water compositions. This is because the host-rock mineralogical composition around drifts is fairly homogeneous, even though the permeability of these rocks is not. Since the predicted seepage chemistries from heterogeneous simulations are expected to be similar to those from homogeneous simulations (as evidenced by the results and discussion in this section), analyses of seepage water from other heterogeneous simulations are not included in this report.

Another observation from Figures 6.6-7 through 6.6-17 is that the character of in-drift water evolves, with time, from dilute, mildly acidic compositions representing in-drift condensation, to compositions representative of waters in rocks near the drift wall (e.g., Figures 6.6-7 and 6.6-9). Discarding initial effects of condensation, these results are consistent with earlier assertions that

the composition of in-drift seepage waters could be approximated by the predicted composition of waters percolating in rocks around the drift (SNL 2007 [DIRS 177404], Section 6.4.8).

The change in infiltration flux from IMF1 to IMF10 introduces noticeable changes in predicted concentration profiles, but does not affect the similarity between in-drift seepage and pore-water compositions near the drift. The increase in infiltration flux yields predicted CO_2 gas and aqueous species concentrations returning to near ambient conditions at ~5,000 years instead of ~30,000 years (e.g., Figure 6.6-6). As a result, the concentration profiles appear somewhat "compressed" in time, but with trends and fluctuations generally similar to those shown in profiles predicted for the IMF1 infiltration case. The profiles of sodium concentrations and sodium to chloride ratios (Figures 6.6-13 and 6.6-14) show somewhat lower long-term sodium concentrations for the IMF10 infiltration case, compared to the IMF1 infiltration case, because of decreased dissolution of feldspars (i.e., less reaction relative to transport) at higher infiltration rates. The concentrations of chloride (Figure 6.6-7) and other conservative species like nitrate and sulfate (Figures 6.6-16 and 6.6-17) at the drift crown (i.e., at a fixed location directly at the drift-wall crown; see lower right-hand corner of these figures) appear higher at the time of drift crown rewetting for the IMF10 infiltration case. This may be the result of increased mass flux and the fact that water spends a longer time boiling directly at the drift wall in the IMF10 case (more evaporative concentration at this location) than at lower infiltration rates (IMF1), even though the overall boiling period lasts longer in the latter case. The same is observed with calcium concentrations, which are much higher at the rewetting time of the drift crown for the IMF10 infiltration case (Figure 6.6-13). In this case, the effect may be primarily caused by increased CO_2 volatilization at the boiling front and subsequent stronger pH decrease (Figure 6.6-8) and calcite dissolution in the condensation/reflux zone. Higher calcium concentrations could also be suggested by lower temperatures (i.e., higher calcite solubility). Note, however, that the effect of increased infiltration rates on the composition of infiltration water (here given the composition of water W0; see Table 6.4-3) is neglected. It is likely that the modeled ten-times increase in infiltration rates would result in significant dilution of the infiltration water, and more so for conservative species such as chloride and sulfate. In this respect, predicted concentrations for the IMF10 infiltration case are likely to be biased on the higher side.

Plots of nitrate to chloride concentrations show essentially flat trends (Figure 6.6-18) in all cases because these species are essentially conservative (conservative here means that these species remain in the aqueous phase, and do not transform into the gas or solid phases). This is expected because redox processes are not considered in these simulations, and solid nitrate and chloride phases are formed only upon complete dryout (SNL 2007 [DIRS 177404], Sections 6.4.5 and 6.6.4). The dissolution of nitrate and chloride salts formed during dryout has some effect on the variability of these ratios during and shortly after the boiling period (Figure 6.6-18) but this variability is much less than the natural variability (SNL 2007 [DIRS 177404], Sections 6.6.4 and 6.7.2). Therefore, for all practical purposes, these ratios should be considered as remaining constant.

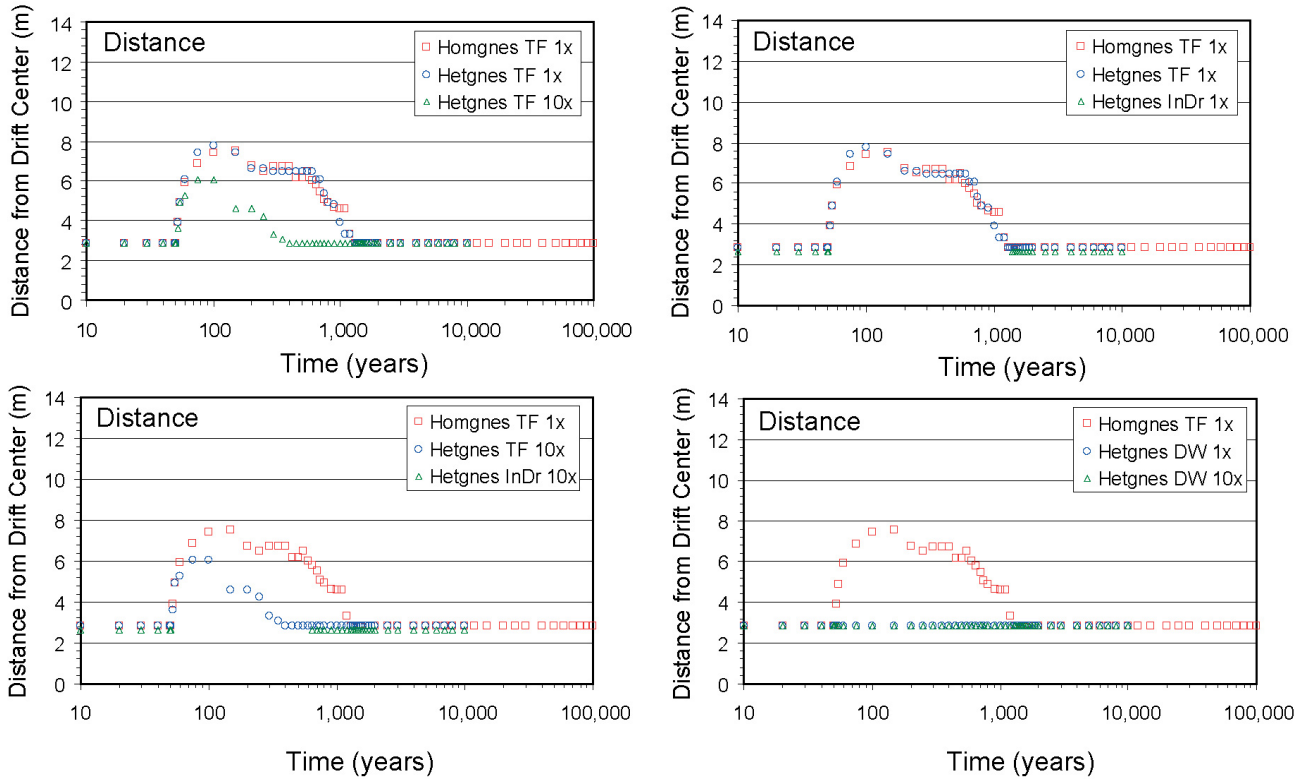

Source DTNs: LB0705DSTHC001.001 [DIRS 181217], file: *thc7_81_162_dr_w0.xls*; LB0705THCSENR2.001.

Output DTN: LB0706THCSENSC.001.

NOTE: See Table 6.6-4 for the definition of each case displayed. Away from the drift wall, data are from gridblocks exhibiting the highest liquid mobility in fractures above the modeled drift (waters with attribute TOP FLUX INDX=1 as defined in Section 6.4.8 of SNL 2007 [DIRS 177404]). The distance shown is the actual distance from the gridblock node to drift center.

Figure 6.6-4. Location of Model Gridblocks for Data Shown on Figures 6.6-5 through 6.6-17

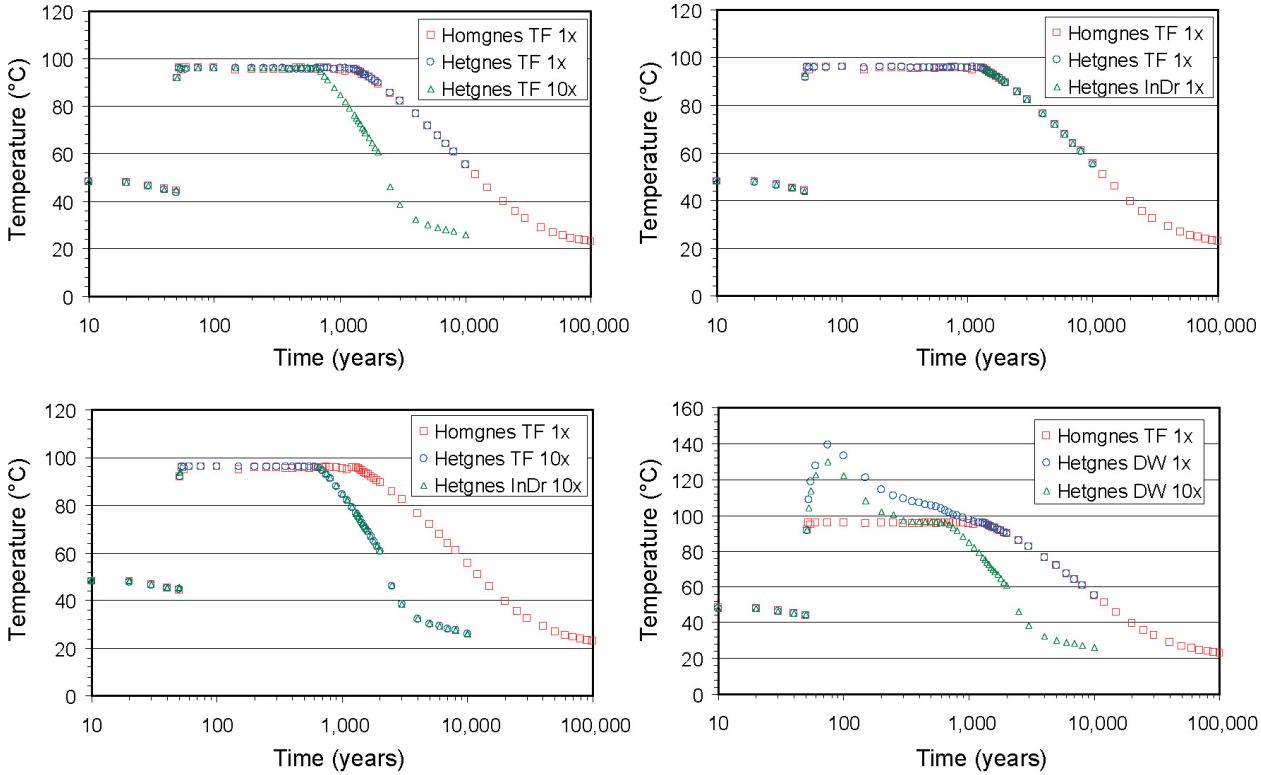

Source DTNs: LB0705DSTHC001.001 [DIRS 181217], file: *thc7_81_162_dr_w0.xls*; LB0705THCSENR2.001.

Output DTN: LB0706THCSENSC.001.

NOTE: See Table 6.6-4 for the definition of each case displayed. Away from the drift wall, data are from gridblocks exhibiting the highest liquid mobility in fractures above the modeled drift (waters with attribute TOP FLUX INDX=1 as defined in Section 6.4.8 of SNL 2007 [DIRS 177404]). The distance shown is the actual distance from the gridblock node to drift center.

Figure 6.6-5. Time Profiles of Modeled Temperatures in Water above the Drift in Fractures and inside the Drift

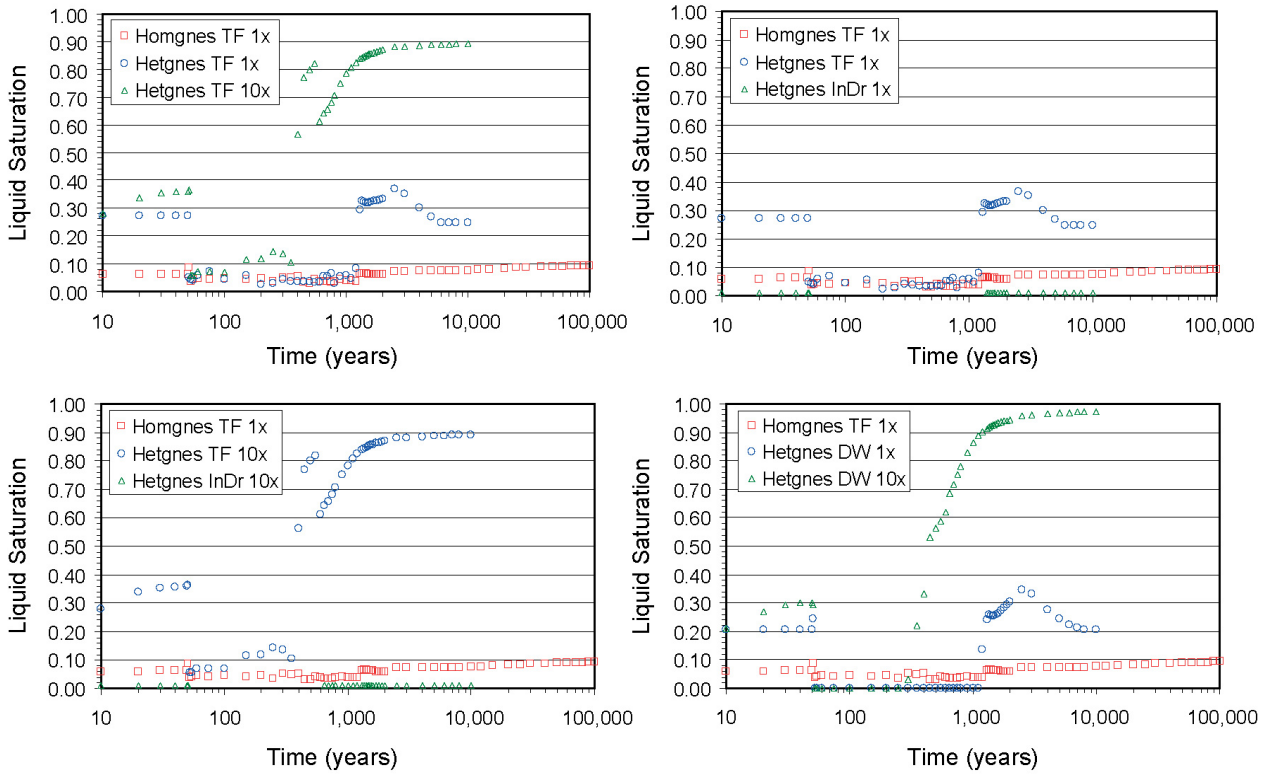

Source DTNs: LB0705DSTHC001.001 [DIRS 181217], file: *thc7_81_162_dr_w0.xls*; LB0705THCSENR2.001.

Output DTN: LB0706THCSENSC.001.

NOTE: See Table 6.6-4 for the definition of each case displayed. Away from the drift wall, data are from gridblocks exhibiting the highest liquid mobility in fractures above the modeled drift (waters with attribute TOP FLUX INDX=1 as defined in Section 6.4.8 of SNL 2007 [DIRS 177404]). The distance shown is the actual distance from the gridblock node to drift center.

Figure 6.6-6. Time Profiles of Modeled Liquid Saturations in Water above the Drift in Fractures and inside the Drift

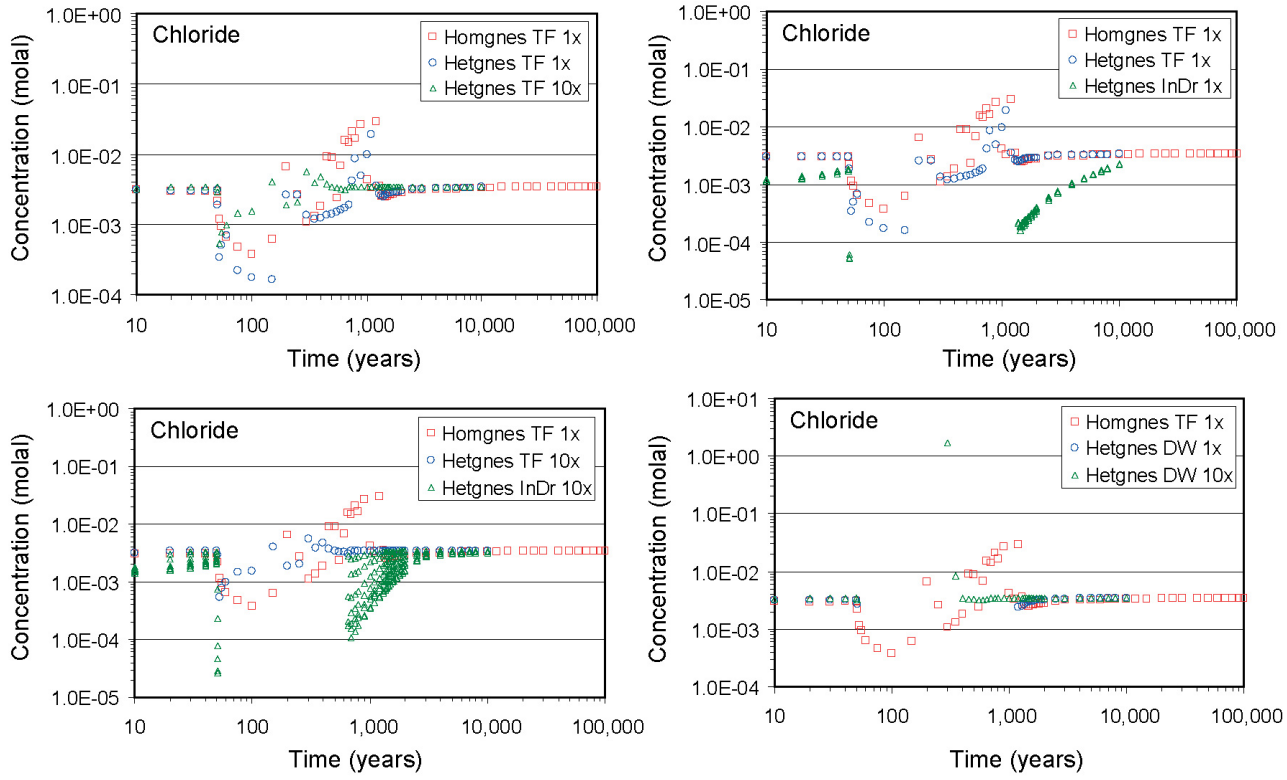

Source DTNs: LB0705DSTHC001.001 [DIRS 181217], file: *thc7_81_162_dr_w0.xls*; LB0705THCSENR2.00.

Output DTN: LB0706THCSENSC.001.

NOTE: See Table 6.6-4 for the definition of each case displayed. Away from the drift wall, data are from gridblocks exhibiting the highest liquid mobility in fractures above the modeled drift (waters with attribute TOP FLUX INDX=1 as defined in Section 6.4.8 of SNL 2007 [DIRS 177404]). The distance shown is the actual distance from the gridblock node to drift center.

Figure 6.6-7. Time Profiles of Modeled Total Aqueous Chloride Concentrations in Water above the Drift in Fractures and inside the Drift

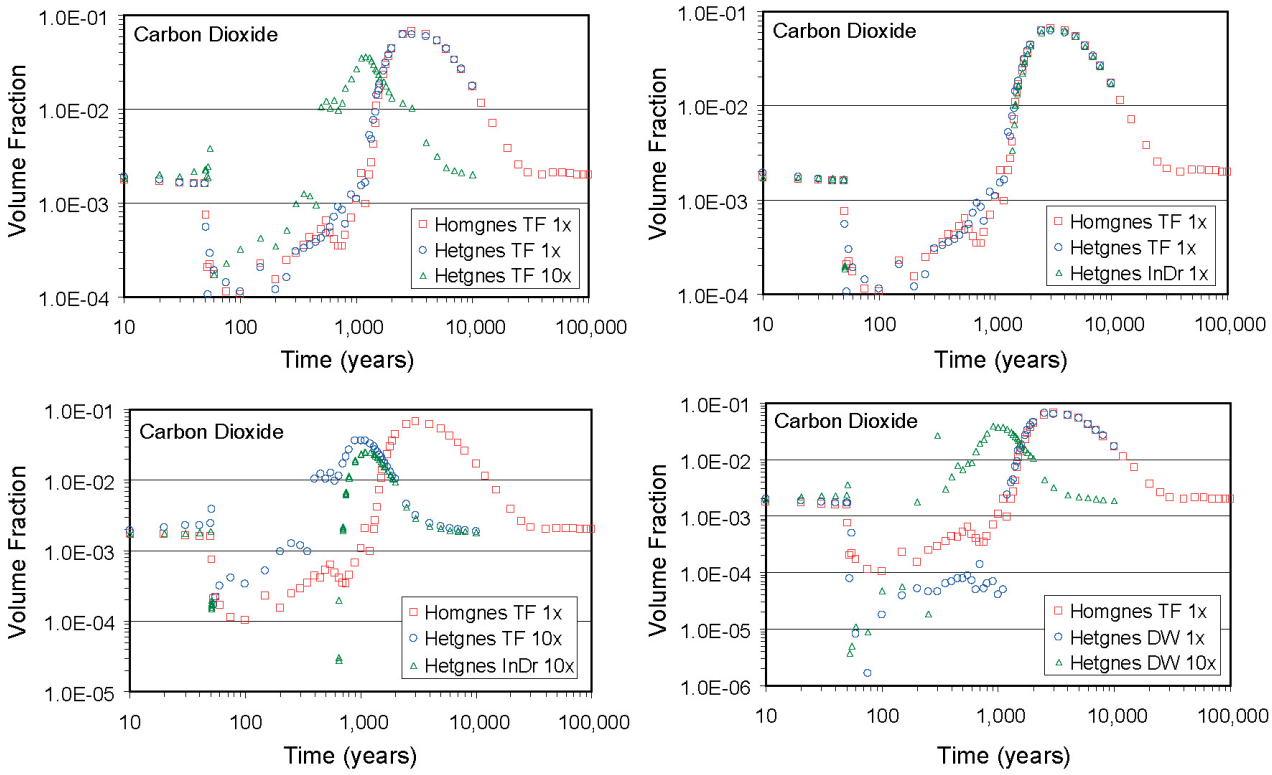

Source DTNs: LB0705DSTHC001.001 [DIRS 181217], file: *thc7_81_162_dr_w0.xls*; LB0705THCSENR2.001.

Output DTN: LB0706THCSENSC.001.

NOTE: See Table 6.6-4 for the definition of each case displayed. Away from the drift wall, data are from gridblocks exhibiting the highest liquid mobility in fractures above the modeled drift (waters with attribute TOP FLUX INDX=1 as defined in Section 6.4.8 of SNL 2007 [DIRS 177404]). The distance shown is the actual distance from the gridblock node to drift center.

Figure 6.6-8. Time Profiles of Modeled CO_2 Gas Concentrations above and inside the Drift

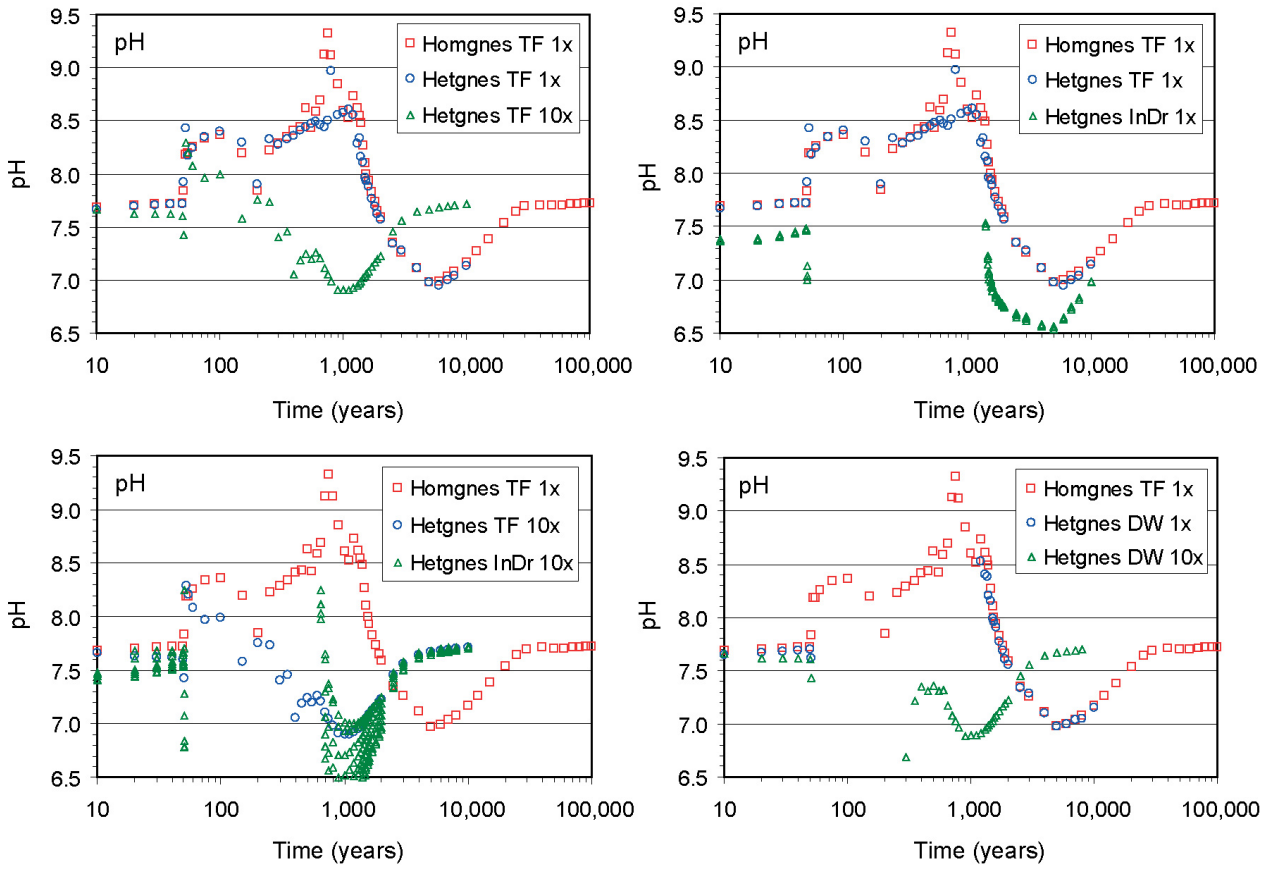

Source DTNs: LB0705DSTHC001.001 [DIRS 181217], file: *thc7_81_162_dr_w0.xls*; LB0705THCSENR2.001.

Output DTN: LB0706THCSENSC.001.

NOTE: See Table 6.6-4 for the definition of each case displayed. Away from the drift wall, data are from gridblocks exhibiting the highest liquid mobility in fractures above the modeled drift (waters with attribute TOP FLUX INDX=1 as defined in Section 6.4.8 of SNL 2007 [DIRS 177404]). The distance shown is the actual distance from the gridblock node to drift center.

Figure 6.6-9. Time Profiles of Modeled pH in Water above the Drift in Fractures and inside the Drift

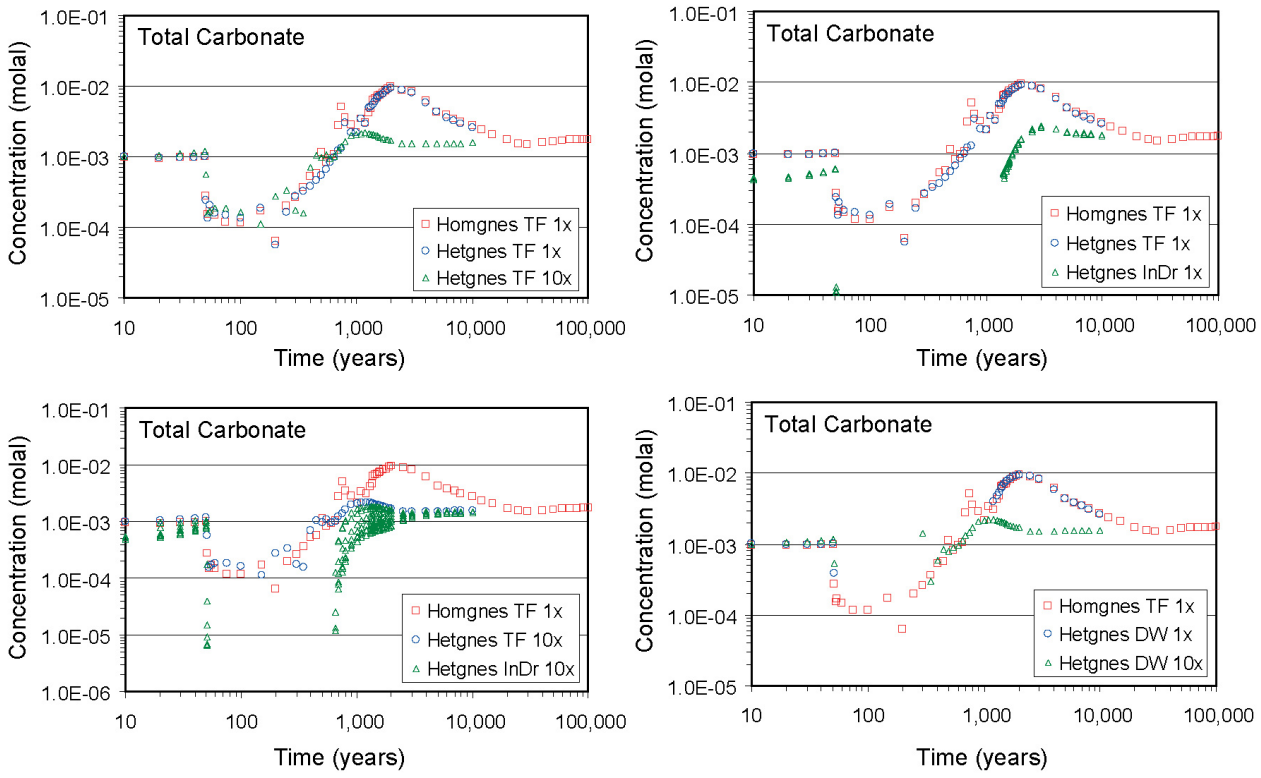

Source DTNs: LB0705DSTHC001.001 [DIRS 181217], file: *thc7_81_162_dr_w0.xls*; LB0705THCSENR2.001.

Output DTN: LB0706THCSENSC.001.

NOTE: See Table 6.6-4 for the definition of each case displayed. Away from the drift wall, data are from gridblocks exhibiting the highest liquid mobility in fractures above the modeled drift (waters with attribute TOP FLUX INDX=1 as defined in Section 6.4.8 of SNL 2007 [DIRS 177404]). The distance shown is the actual distance from the gridblock node to drift center.

Figure 6.6-10. Time Profiles of Modeled Total Aqueous Carbonate Concentrations in Water above the Drift in Fractures and inside the Drift

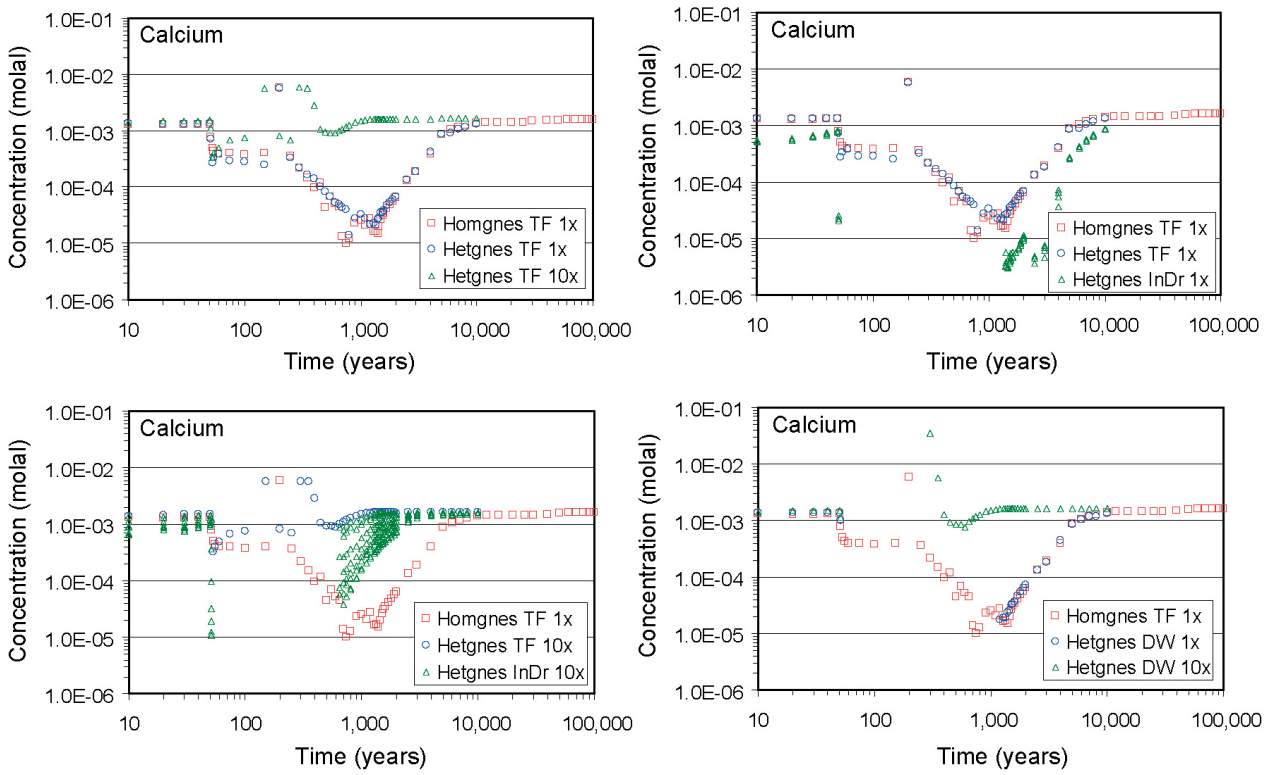

Source DTNs: LB0705DSTHC001.001 [DIRS 181217], file: *thc7_81_162_dr_w0.xls*; LB0705THCSENR2.001.

Output DTN: LB0706THCSENSC.001.

NOTE: See Table 6.6-4 for the definition of each case displayed. Away from the drift wall, data are from gridblocks exhibiting the highest liquid mobility in fractures above the modeled drift (waters with attribute TOP FLUX INDX=1 as defined in Section 6.4.8 of SNL 2007 [DIRS 177404]). The distance shown is the actual distance from the gridblock node to drift center.

Figure 6.6-11. Time Profiles of Modeled Total Aqueous Calcium Concentrations in Water above the Drift in Fractures and inside the Drift

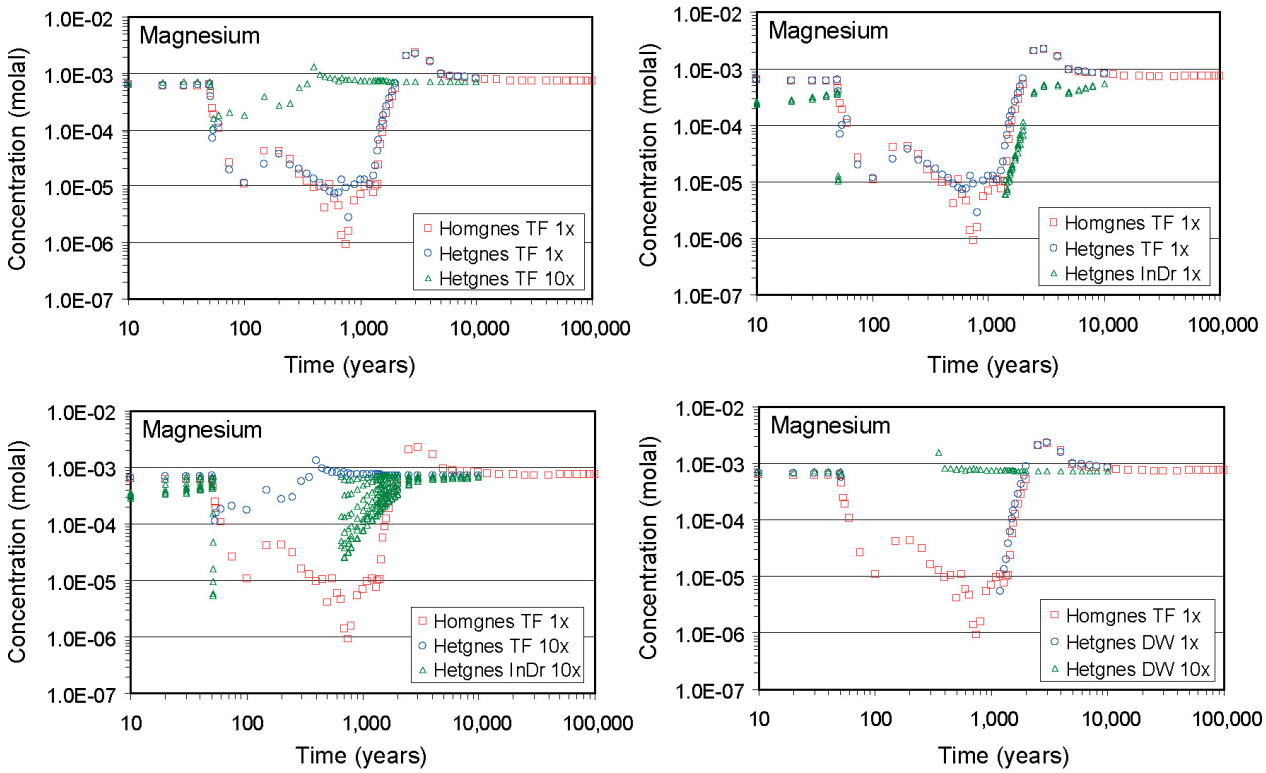

Source DTNs: LB0705DSTHC001.001 [DIRS 181217], file: *thc7_81_162_dr_w0.xls*; LB0705THCSENR2.001.

Output DTN: LB0706THCSENSC.001.

NOTE: See Table 6.6-4 for the definition of each case displayed. Away from the drift wall, data are from gridblocks exhibiting the highest liquid mobility in fractures above the modeled drift (waters with attribute TOP FLUX INDX=1 as defined in Section 6.4.8 of SNL 2007 [DIRS 177404]). The distance shown is the actual distance from the gridblock node to drift center.

Figure 6.6-12. Time Profiles of Modeled Total Aqueous Magnesium Concentrations in Water above the Drift in Fractures and inside the Drift

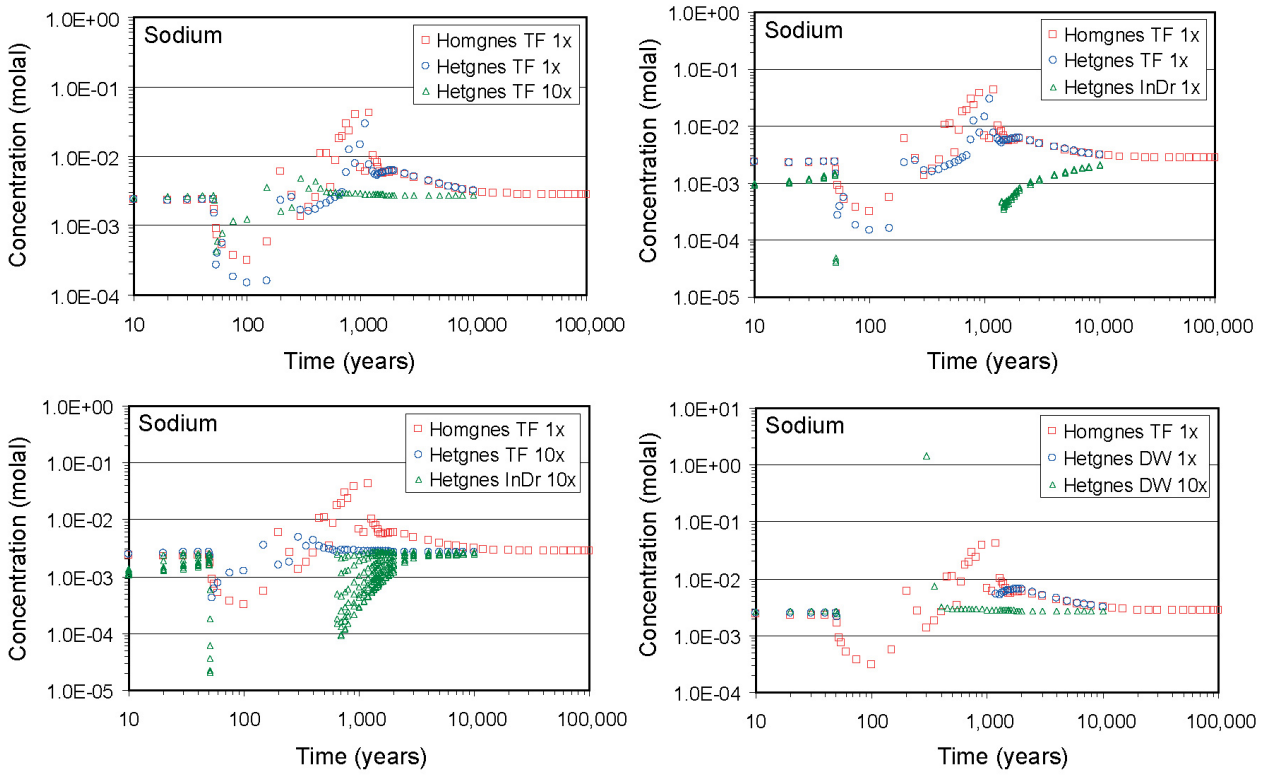

Source DTNs: LB0705DSTHC001.001 [DIRS 181217], file: *thc7_81_162_dr_w0.xls*; LB0705THCSENR2.001.

Output DTN: LB0706THCSENSC.001.

NOTE: See Table 6.6-4 for the definition of each case displayed. Away from the drift wall, data are from gridblocks exhibiting the highest liquid mobility in fractures above the modeled drift (waters with attribute TOP FLUX INDX=1 as defined in Section 6.4.8 of SNL 2007 [DIRS 177404]). The distance shown is the actual distance from the gridblock node to drift center.

Figure 6.6-13. Time Profiles of Modeled Total Aqueous Sodium Concentrations in Water above the Drift in Fractures and inside the Drift

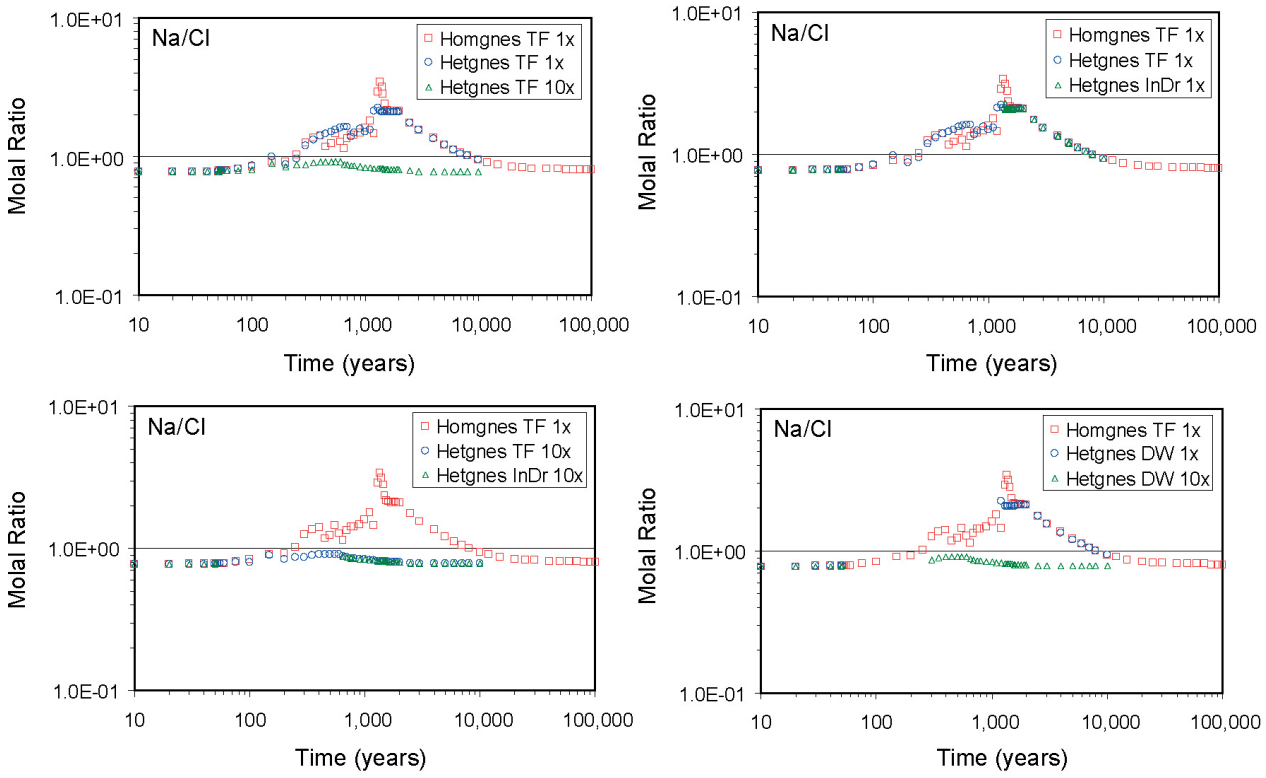

Source DTNs: LB0705DSTHC001.001 [DIRS 181217], file: *thc7_81_162_dr_w0.xls*; LB0705THCSENR2.001.

Output DTN: LB0706THCSENSC.001.

NOTE: See Table 6.6-4 for the definition of each case displayed. Away from the drift wall, data are from gridblocks exhibiting the highest liquid mobility in fractures above the modeled drift (waters with attribute TOP FLUX INDX=1 as defined in Section 6.4.8 of SNL 2007 [DIRS 177404]). The distance shown is the actual distance from the gridblock node to drift center.

Figure 6.6-14. Time Profiles of Modeled Total Aqueous Sodium to Chloride Concentration Ratios in Water above the Drift in Fractures and inside the Drift

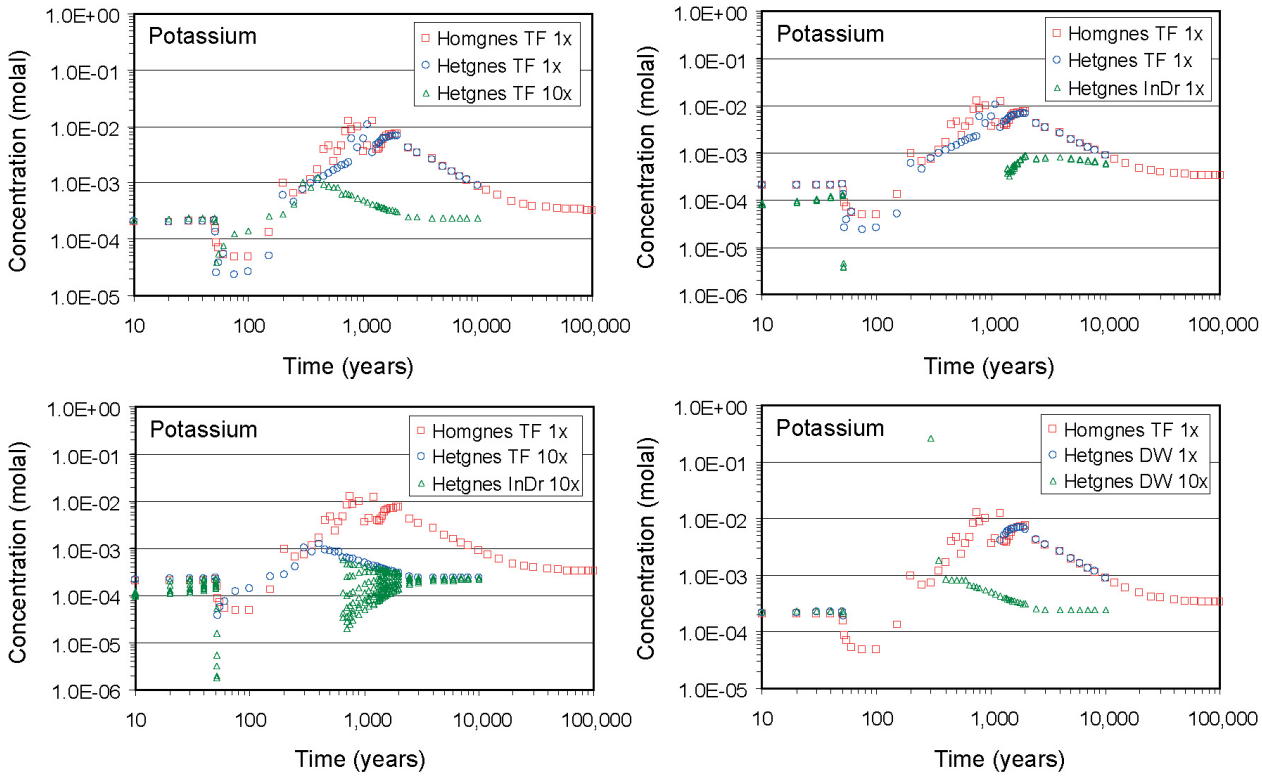

Source DTNs: LB0705DSTHC001.001 [DIRS 181217], file: *thc7_81_162_dr_w0.xls*; LB0705THCSENR2.001.

Output DTN: LB0706THCSENSC.001.

NOTE: See Table 6.6-4 for the definition of each case displayed. Away from the drift wall, data are from gridblocks exhibiting the highest liquid mobility in fractures above the modeled drift (waters with attribute TOP FLUX INDX=1 as defined in Section 6.4.8 of SNL 2007 [DIRS 177404]). The distance shown is the actual distance from the gridblock node to drift center.

Figure 6.6-15. Time Profiles of Modeled Total Aqueous Potassium Concentrations in Water above the Drift in Fractures and inside the Drift

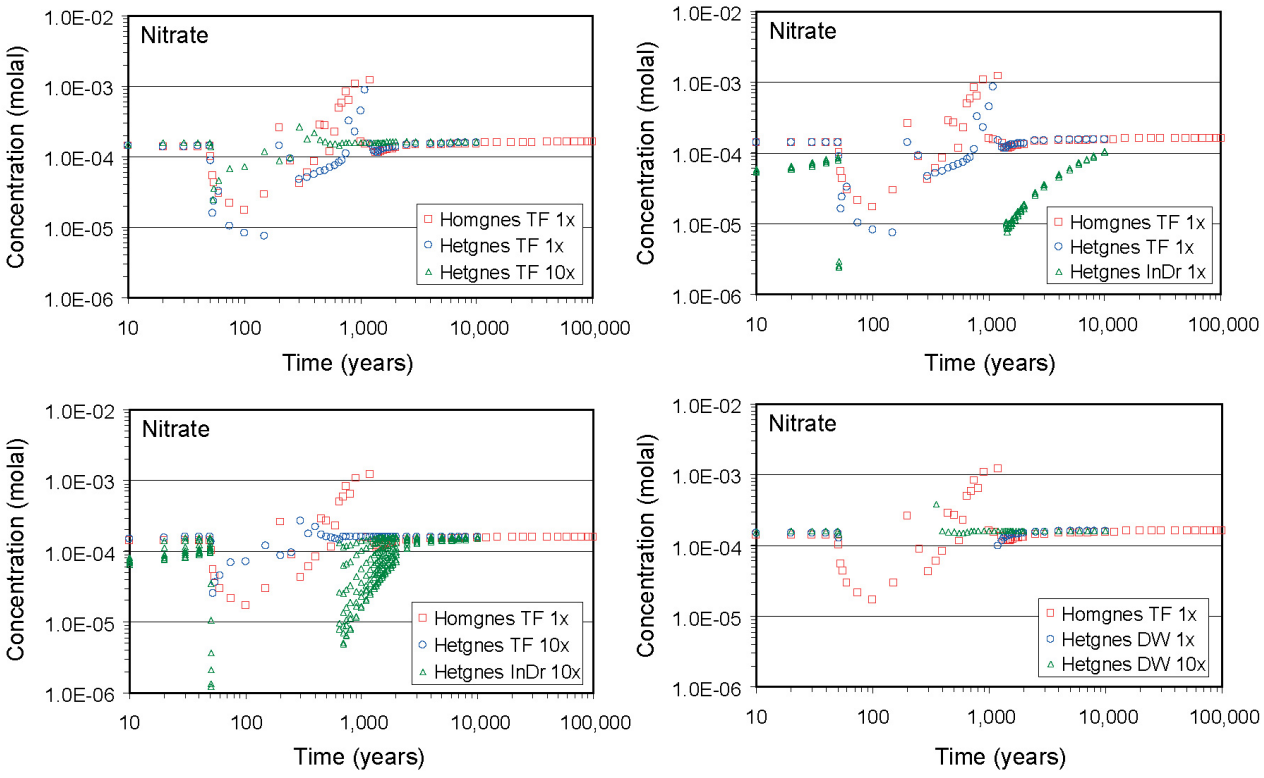

Source DTNs: LB0705DSTHC001.001 [DIRS 181217], file: *thc7_81_162_dr_w0.xls*; LB0705THCSENR2.001.

Output DTN: LB0706THCSENSC.001.

NOTE: See Table 6.6-4 for the definition of each case displayed. Away from the drift wall, data are from gridblocks exhibiting the highest liquid mobility in fractures above the modeled drift (waters with attribute TOP FLUX INDX=1 as defined in Section 6.4.8 of SNL 2007 [DIRS 177404]). The distance shown is the actual distance from the gridblock node to drift center.

Figure 6.6-16. Time Profiles of Modeled Total Aqueous Nitrate Concentrations in Water above the Drift in Fractures and inside the Drift

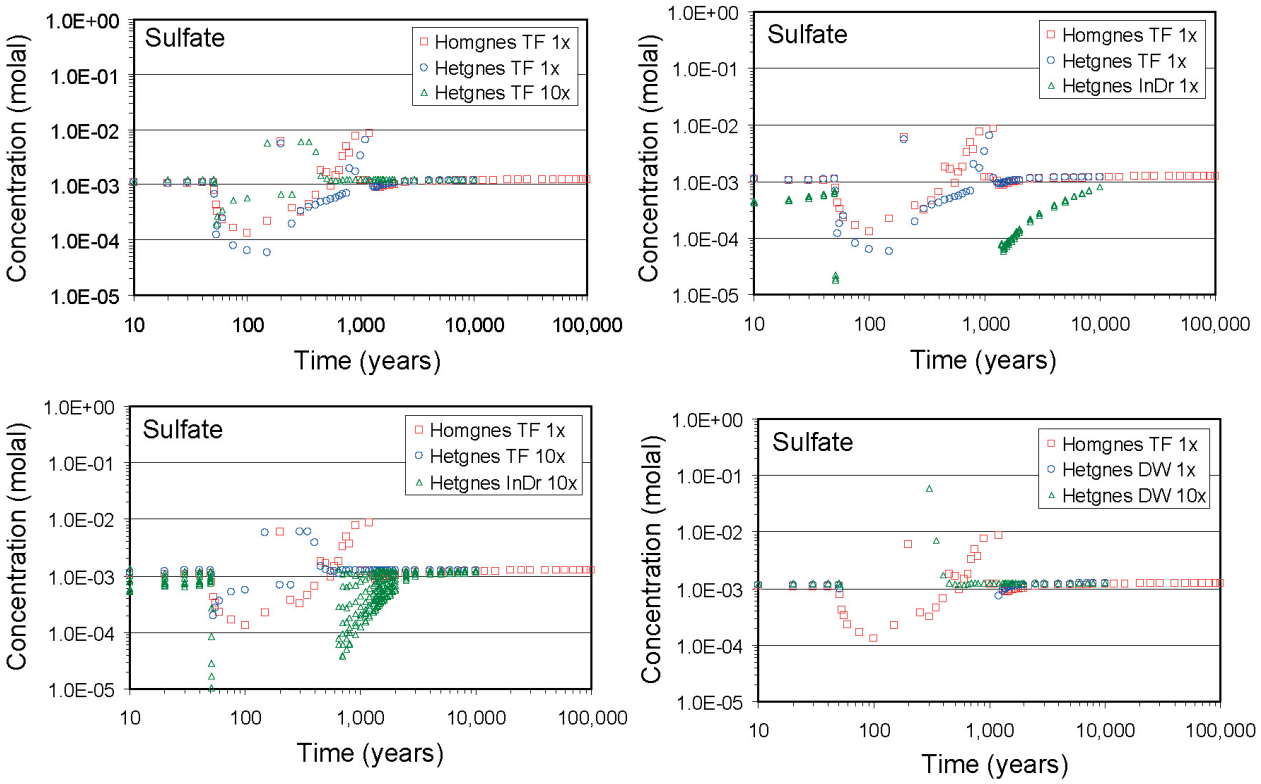

Source DTNs: LB0705DSTHC001.001 [DIRS 181217], file: *thc7_81_162_dr_w0.xls*; LB0705THCSENR2.001.

Output DTN: LB0706THCSENSC.001.

NOTE: See Table 6.6-4 for the definition of each case displayed. Away from the drift wall, data are from gridblocks exhibiting the highest liquid mobility in fractures above the modeled drift (waters with attribute TOP FLUX INDX=1 as defined in Section 6.4.8 of SNL 2007 [DIRS 177404]). The distance shown is the actual distance from the gridblock node to drift center.

Figure 6.6-17. Time Profiles of Modeled Total Aqueous Sulfate Concentrations in Water above the Drift in Fractures and inside the Drift

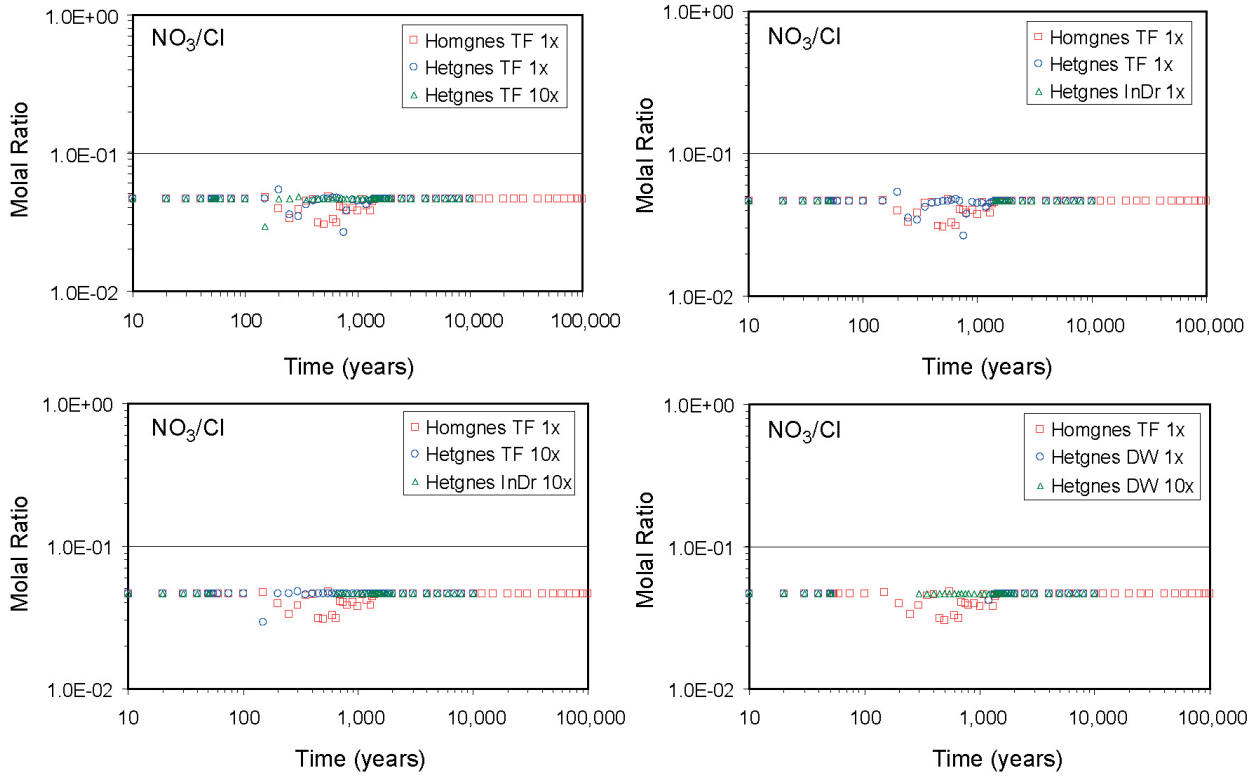

Source DTNs: LB0705DSTHC001.001 [DIRS 181217], file: *thc7_81_162_dr_w0.xls*; LB0705THCSENR2.001.

Output DTN: LB0706THCSENSC.001.

NOTE: See Table 6.6-4 for the definition of each case displayed. Away from the drift wall, data are from gridblocks exhibiting the highest liquid mobility in fractures above the modeled drift (waters with attribute TOP FLUX INDX=1 as defined in Section 6.4.8 of SNL 2007 [DIRS 177404]). The distance shown is the actual distance from the gridblock node to drift center.

Figure 6.6-18. Time Profiles of Modeled Total Aqueous Nitrate to Chloride Concentrations in Water above the Drift in Fractures and inside the Drift

6.7 SENSITIVITY TO INITIAL FRACTURE CAPILLARY-STRENGTH PARAMETER

The base-case simulations in Section 6.6 were performed with an initial fracture capillary-strength parameter of 1,739 Pa. This parameter was obtained from *Calibrated Unsaturated Zone Properties* (SNL 2007 [DIRS 179545]), and possibly is representative of the large-scale behavior of the Tptpll fracture continuum. Seepage, on the other hand, is a local phenomenon (as demonstrated in Section 6.6) and is controlled by the capillarity of a small zone close to the emplacement drift. The only capillarity data available at that scale that are relevant for seepage are those obtained from calibration to ambient liquid-release tests (BSC 2004 [DIRS 171764]). However, as discussed in Section 6.4.11, the calibration in *Seepage Testing Data and Seepage Calibration Model* (BSC 2004 [DIRS 171764]) was done without consideration of capillarity heterogeneity (while recognizing small-scale fracture permeability heterogeneities). Thus, the calibrated fracture capillary-strength parameters (see Section 6.4.11) obtained from *Seepage Testing Data and Seepage Calibration Model* (BSC 2004

[DIRS 171764]) are not directly applicable to situations where both fracture permeability and capillarity heterogeneities are considered (as demonstrated in Section 6.4.11.3).

However, the calibrated parameters from the SCM (BSC 2004 [DIRS 171764) are important in the sense that they were obtained from calibration to actual seepage testing data (even though they were estimated under the assumption of capillarity homogeneity) and provide a good starting point for any sensitivity study with regard to the fracture capillary-strength parameters of the near-field fractured rock. Since these parameters (i.e., the calibrated capillary-strength parameters) were obtained under the assumption of capillarity homogeneity, a set of sensitivity simulations with these parameters and without Leverett-scaling effects (i.e., under assumption of capillarity homogeneity) will first be performed. This will also permit a direct comparison with earlier results (BSC 2006 [DIRS 174104]; Mukhopadhyay et al. 2006 [DIRS 180822]).

In a second set of sensitivity simulations, an initial fracture capillary-strength parameter that is conservative for seepage is estimated, considering both permeability and capillarity heterogeneities (i.e., through inclusion of Leverett-scaling effects in the simulations). Ambient, TH, and THC simulations are then performed with that initial fracture capillary-strength parameter and with different infiltration fluxes. This produces seepage results over a range of initial fracture capillary-strength parameters and demonstrates the sensitivity of the THC seepage model to permeability and capillarity heterogeneities.

6.7.1 Homogeneous Fracture Capillarity Sensitivity to $1/\alpha_0$

6.7.1.1 Overview of Simulations

These simulations are performed considering heterogeneities in fracture permeability and porosity only, i.e., the fracture capillary-strength parameter of Tptpll is assumed constant. The source of the fracture capillary-strength parameter is the calibrated fracture capillary-strength parameter from the SCM (BSC 2004 [DIRS 171764]). This choice is justified because the SCM was based on an assumption of capillarity homogeneity and represented conditions in a small zone around the emplacement drifts. However, since a conservative approach to seepage is desired (i.e., the simulation of conditions most favorable for seepage), the small-scale SCM fracture capillary-strength parameter is applied for the entire Tptpll model layer. Since the source of the fracture capillary-strength parameter is the SCM, these simulations are identified with a leading "scm" in their IDs. Simulation IDs for these sensitivity simulations are provided in Table 6.7-1. Table 6.7-1 also provides the output DTNs for these sensitivity simulations. Similar to the base-case simulations, these sensitivity simulations are performed with three realizations of the heterogeneous fracture permeability distribution and two sets of infiltration fluxes (IMF1 and IMF10; see Section 6.4.5). As before, ambient, TH, and THC simulations are performed for all the combinations of permeability realization and infiltration fluxes, resulting in 18 sensitivity simulations. Since capillarity homogeneity is desired, it is implied that the simulations in this section (Section 6.7.1) are carried out without consideration to Leverett-scaling effects.

Table 6.7-1. Additional Sensitivity Simulations with Homogeneous Capillarity

Serial No.	Infiltration Flux [a]	Fracture (1/α) Value (Pa)[b]	Permeability Heterogeneity[c]	Leverett[d]	Simulation Type[e]	Simulation ID	Output DTN
1.	IMF1	591	Realization #1	No	THC	scm_r1_1x_nlev_thc	LB0705THCSENR1.004
2.	IMF10	591	Realization #1	No	THC	scm_r1_10x_nlev_thc	LB0705THCSENR1.004
3.	IMF1	591	Realization #1	No	TH	scm_r1_1x_nlev_th	LB0705THCSENR1.005
4.	IMF10	591	Realization #1	No	TH	scm_r1_10x_nlev_th	LB0705THCSENR1.005
5.	IMF1	591	Realization #1	No	Ambient	scm_r1_1x_nlev_amb	LB0705THCSENR1.006
6.	IMF10	591	Realization #1	No	Ambient	scm_r1_10x_nlev_amb	LB0705THCSENR1.006
7.	IMF1	591	Realization #2	No	THC	scm_r2_1x_nlev_thc	LB0705THCSENR2.004
8.	IMF10	591	Realization #2	No	THC	scm_r2_10x_nlev_thc	LB0705THCSENR2.004
9.	IMF1	591	Realization #2	No	TH	scm_r2_1x_nlev_th	LB0705THCSENR2.005
10.	IMF10	591	Realization #2	No	TH	scm_r2_10x_nlev_th	LB0705THCSENR2.005
11.	IMF1	591	Realization #2	No	Ambient	scm_r2_1x_nlev_amb	LB0705THCSENR2.006
12.	IMF10	591	Realization #2	No	Ambient	scm_r2_10x_nlev_amb	LB0705THCSENR2.006
13.	IMF1	591	Realization #3	No	THC	scm_r3_1x_nlev_thc	LB0705THCSENR3.004
14.	IMF10	591	Realization #3	No	THC	scm_r3_10x_nlev_thc	LB0705THCSENR3.004
15.	IMF1	591	Realization #3	No	TH	scm_r3_1x_nlev_th	LB0705THCSENR3.005
16.	IMF10	591	Realization #3	No	TH	scm_r3_10x_nlev_th	LB0705THCSENR3.005
17.	IMF1	591	Realization #3	No	Ambient	scm_r3_1x_nlev_amb	LB0705THCSENR3.006
18.	IMF10	591	Realization #3	No	Ambient	scm_r3_10x_nlev_amb	LB0705THCSENR3.006

[a] See Section 6.4.5 for definition of infiltration fluxes.
[b] See Sections 6.4.11 and 6.7.1 for choice of fracture capillary-strength parameters.
[c] See Section 6.4.10 for definition of heterogeneous fracture permeability fields.
[d] See Sections 6.4.11.3 and 6.4.11.4.
[e] THC = simulations with emplacement drifts, heat and chemistry; TH = simulations with emplacement drifts and heat (no chemistry); Ambient = simulations with emplacement drifts (no heat or chemistry).

As mentioned previously, the fracture capillary-strength parameter (of Tptpll) selected for these sensitivity simulations represents the calibrated fracture capillary-strength parameter from the SCM (BSC 2004 [DIRS 171764]). The mean fracture capillary-strength parameter calibrated to all measurements is 591 Pa (see Table 6.4-5), the value used for all the sensitivity simulations in this section (Section 6.7.1). This value (of 591 Pa) is slightly larger than the mean Tptpll fracture capillary-strength parameter of 582 Pa (see Table 6.4-5). However, this small difference (of less than 1.6%) in the fracture capillary-strength parameter is not expected to alter the model outcome significantly. The selected fracture capillary-strength parameter of 591 Pa is also almost identical to the fracture capillary-strength parameter (of 589) used in earlier thermal seepage studies (Birkholzer et al. 2004 [DIRS 172262]; BSC 2005 [DIRS 172262]; BSC 2006 [DIRS 174104]; Mukhopadhyay et al. 2006 [DIRS 180822]). This will allow for a direct comparison with results from those earlier studies.

6.7.1.2 Seepage Rates

Seepage results (whether seepage occurs) from the sensitivity simulations in this section (Section 6.7.1) are summarized in Table 6.7-2. These results have been submitted to the TDMS; the output DTNs for each of the 18 sensitivity simulations are also included in Table 6.7-2 (see the note below Table 6.7-2). The seepage results can be extracted from files "flow.out" in the output DTNs. Appendix D describes the procedures for extracting the seepage results from the "flow.out" files.

Table 6.7-2. Summary of Seepage Results from Sensitivity Simulations with Homogeneous Capillarity (Leverett-Scaling Effects Not Included)

Serial No.	Infiltration Flux [a]	Fracture (1/α) Value (Pa)[b]	Permeability Heterogeneity[c]	Leverett[d]	Simulation Type[e]	Simulation ID	Seepage	Output DTN
1.	IMF1	591	Realization #1	No	THC	scm_r1_1x_nlev_thc	No	LB0705THCSENR1.004
2.	IMF10	591	Realization #1	No	THC	scm_r1_10x_nlev_thc	Yes	LB0705THCSENR1.004
3.	IMF1	591	Realization #1	No	TH	scm_r1_1x_nlev_th	No	LB0705THCSENR1.005
4.	IMF10	591	Realization #1	No	TH	scm_r1_10x_nlev_th	Yes	LB0705THCSENR1.005
5.	IMF1	591	Realization #1	No	Ambient	scm_r1_1x_nlev_amb	No	LB0705THCSENR1.006
6.	IMF10	591	Realization #1	No	Ambient	scm_r1_10x_nlev_amb	Yes	LB0705THCSENR1.006
7.	IMF1	591	Realization #2	No	THC	scm_r2_1x_nlev_thc	No	LB0705THCSENR2.004
8.	IMF10	591	Realization #2	No	THC	scm_r2_10x_nlev_thc	Yes	LB0705THCSENR2.004
9.	IMF1	591	Realization #2	No	TH	scm_r2_1x_nlev_th	No	LB0705THCSENR2.005
10.	IMF10	591	Realization #2	No	TH	scm_r2_10x_nlev_th	Yes	LB0705THCSENR2.005
11.	IMF1	591	Realization #2	No	Ambient	scm_r2_1x_nlev_amb	No	LB0705THCSENR2.006
12.	IMF10	591	Realization #2	No	Ambient	scm_r2_10x_nlev_amb	Yes	LB0705THCSENR2.006
13.	IMF1	591	Realization #3	No	THC	scm_r3_1x_nlev_thc	No	LB0705THCSENR3.004
14.	IMF10	591	Realization #3	No	THC	scm_r3_10x_nlev_thc	Yes	LB0705THCSENR3.004
15.	IMF1	591	Realization #3	No	TH	scm_r3_1x_nlev_th	No	LB0705THCSENR3.005
16.	IMF10	591	Realization #3	No	TH	scm_r3_10x_nlev_th	No	LB0705THCSENR3.005
17.	IMF1	591	Realization #3	No	Ambient	scm_r3_1x_nlev_amb	No	LB0705THCSENR3.006
18.	IMF10	591	Realization #3	No	Ambient	scm_r3_10x_nlev_amb	No	LB0705THCSENR3.006

[a] See Section 6.4.5 for definition of infiltration fluxes.
[b] See Sections 6.4.11 and 6.7.1 for choice of fracture capillary-strength parameters.
[c] See Section 6.4.10 for definition of heterogeneous fracture permeability fields.
[d] See Sections 6.4.11.3 and 6.4.11.4.
[e] THC = simulations with emplacement drifts, heat and chemistry; TH = simulations with emplacement drifts and heat (no chemistry); Ambient = simulations with emplacement drifts (no heat or chemistry).

From Table 6.7-2, it can be seen that seepage is not predicted to occur for any of the three realizations of heterogeneous fracture permeability distribution, if IMF1 infiltration fluxes are imposed. This is true for THC simulations as well as ambient and TH simulations. In other words, for the IMF1 infiltration fluxes (7.96 mm/yr for 0 to 600 years, 12.45 mm/yr for 600 to 2,000 years, and 20.45 mm/yr for 2,000 years and beyond), the saturation buildup near the emplacement drift is not sufficient to overcome the capillary-barrier effect created by a fracture capillary-strength parameter of 591 Pa (the seepage threshold saturation, ignoring Leverett-scaling effects, when the initial fracture capillary-strength parameter 591 Pa, is approximately 0.1921).

When IMF10 infiltration fluxes (79.6 mm/yr for 0 to 600 years, 128.9 mm/yr for 600 to 2,000 years, and 204.5 mm/yr for 2,000 years and beyond) are imposed on the THC seepage model (SNL 2007 [DIRS 177404]), the saturation buildup at certain locations on the drift wall does exceed the seepage saturation threshold of approximately 0.1921, leading to occurrence of seepage. Figures 6.7-1, 6.7-2, and 6.7-3 show the seepage flux (in mm/yr) from Realizations #1, #2, and #3, respectively.

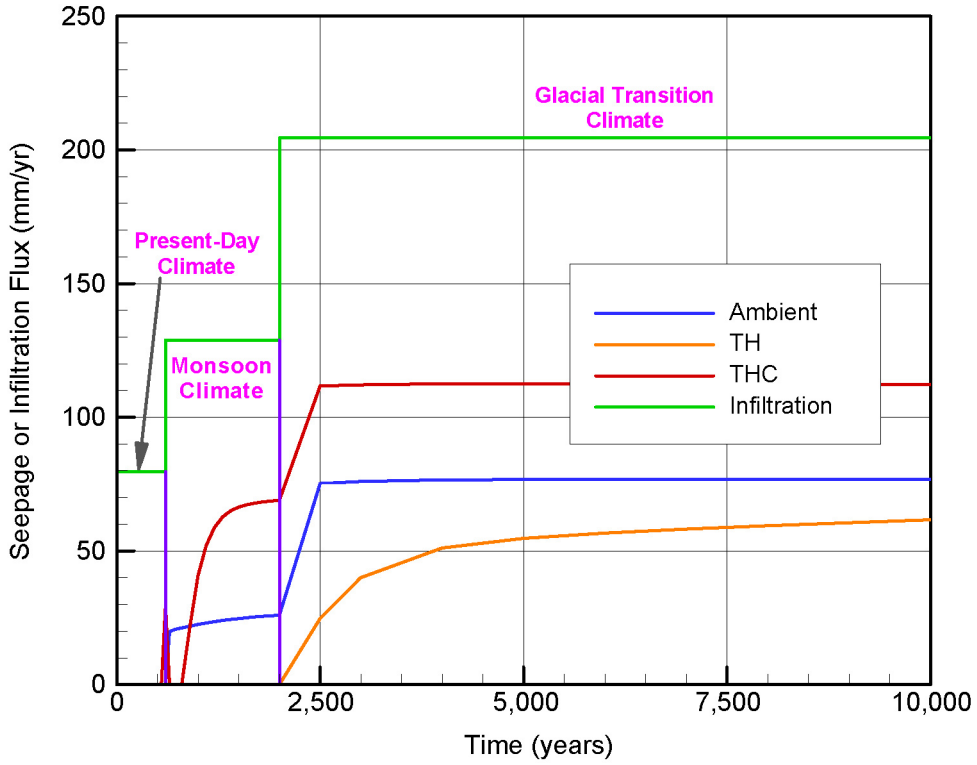

Source: Output DTNs: LB0705THCSENR1.004, LB0705THCSENR1.005, and LB0705THCSENR1.006.

NOTE: See Table 6.7-1 for explanation of simulation IDs. The vertical violet lines are used to distinguish the different climatic periods and they do not represent any seepage data.

Figure 6.7-1. Comparison of Seepage Fluxes from Ambient (Simulation ID: "scm_r1_10x_nlev_amb"), TH (Simulation ID: "scm_r1_10x_nlev_th."), and THC (Simulation ID: "scm_r1_10x_nlev_thc") Simulations with Realization #1 of the Heterogeneous Fracture Permeability Distribution

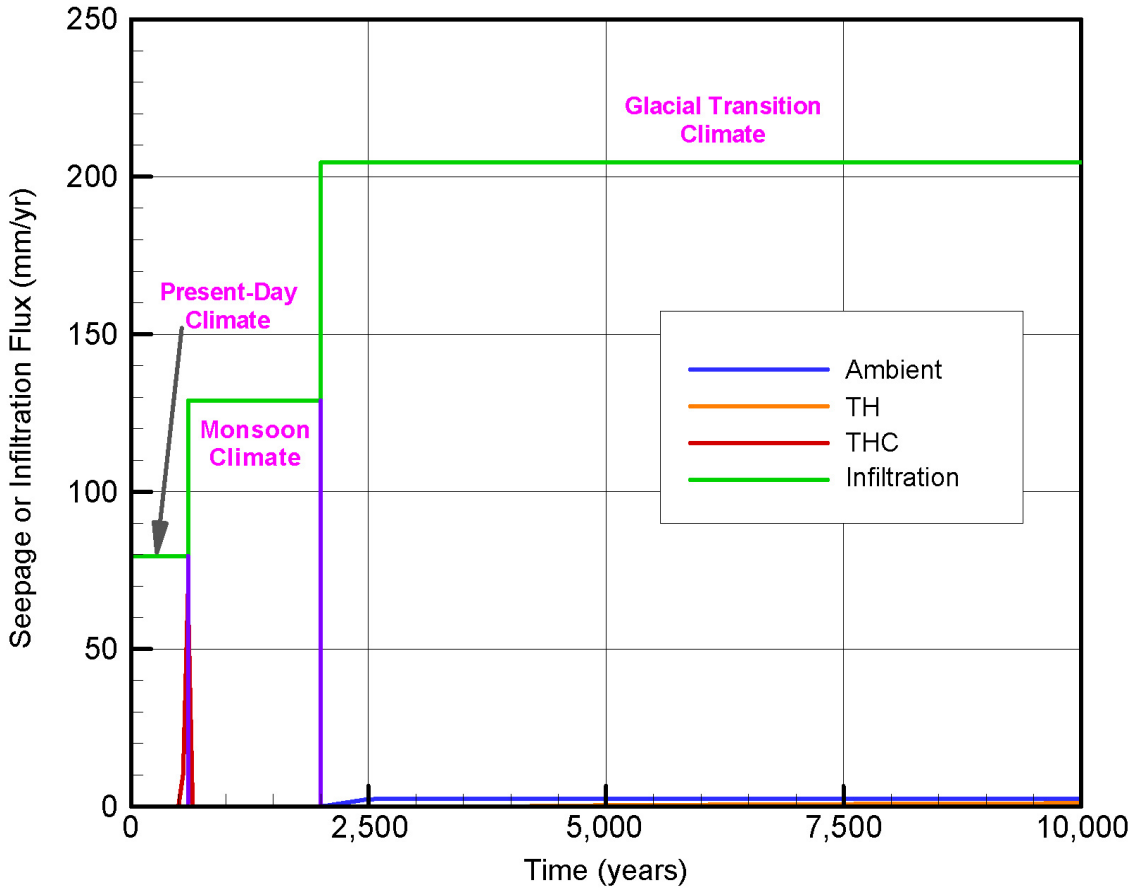

Source: Output DTNs: LB0705THCSENR2.004, LB0705THCSENR2.005, and LB0705THCSENR2.006.

NOTE: See Table 6.7-1 for explanation of simulation IDs. The vertical violet lines are used to distinguish the different climatic periods and they do not represent any seepage data.

Figure 6.7-2. Comparison of Seepage Fluxes from Ambient (Simulation ID: "scm_r2_10x_nlev_amb"), TH (Simulation ID: "scm_r2_10x_nlev_th."), and THC (Simulation ID: "scm_r2_10x_nlev_thc") Simulations with Realization #2 of the Heterogeneous Fracture Permeability Distribution

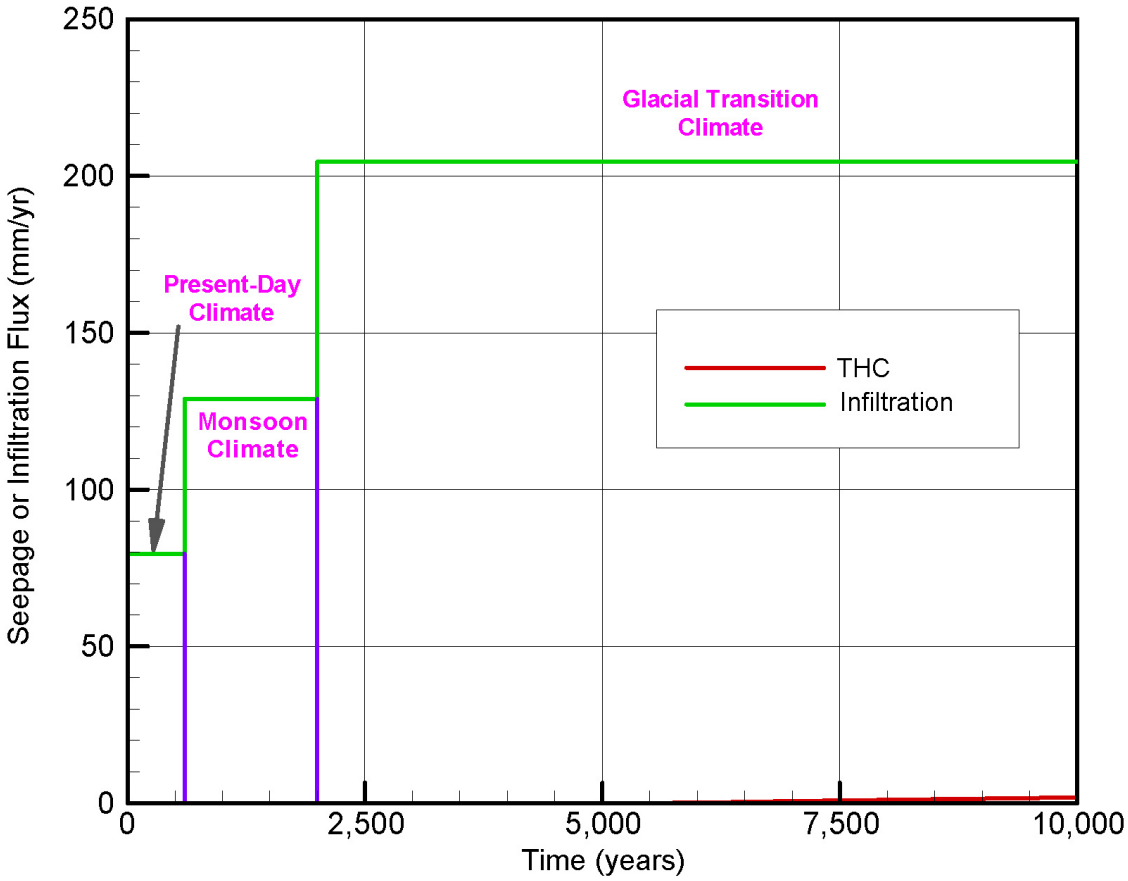

Source: Output DTNs: LB0705THCSENR3.004, LB0705THCSENR3.005, and LB0705THCSENR3.006.

NOTES: See Table 6.7-1 for explanation of simulation IDs. The vertical violet lines are used to distinguish the different climatic periods and they do not represent any seepage data.

Ambient (Simulation ID: "scm_r3_10x_nlev_amb") and TH (Simulation ID: "scm_r3_10x_nlev_th.") simulations do not predict seepage. Maximum predicted seepage from THC (Simulation ID: "scm_r3_10x_nlev_thc") simulations is less than 1.9 mm/yr.

Figure 6.7-3. Seepage Fluxes from THC (Simulation ID: "scm_r3_10x_nlev_thc") Simulations with Realization #3 of the Heterogeneous Fracture Permeability Distribution

From Figures 6.7-1 through 6.7-3, a few observations can be made.

- Local fracture heterogeneity plays a key role in determining whether seepage occurs. This is clear from the different transient patterns of seepage from the three realizations of the heterogeneous fracture permeability distribution. While simulations with Realization #1 of the heterogeneous fracture permeability distribution predict considerable long-term seepage (also a spike in seepage from THC simulation), simulations with the other two realizations of the fracture permeability distribution predict almost no seepage (except for a "spike" in seepage around 600 years from THC simulations with Realization #2 of the heterogeneous fracture permeability distribution). These results are summarized in Table 6.7-3.

Table 6.7-3. Seepage Percentage from Sensitivity Simulations with Homogeneous Fracture Capillarity (Leverett-Scaling Effects Not Included)

Serial No.	Simulation ID[a]	Permeability Realization[b]	Infiltration Flux[c]	Long-term Seepage Percentage	Remark
1.	scm_r1_10x_nlev_amb	#1	IMF10	37.50	Seepage begins after 600 years.
2.	scm_r1_10x_nlev_th	#1	IMF10	30.15	Seepage begins after 2,000 years.
3.	scm_r1_10x_nlev_thc	#1	IMF10	54.87	A minor spike of seepage happens between 600 and 650 years. Long-term seepage begins at 900 years. Seepage percent at the spike is 14.37.
4.	scm_r2_10x_nlev_amb	#2	IMF10	1.23	Seepage begins after 2,000 years.
5.	scm_r2_10x_nlev_th	#2	IMF10	0.52	Seepage begins after 3,500 years.
6.	scm_r2_10x_nlev_thc	#2	IMF10	0.00	A spike of seepage happens between 600 and 650 years. No long-term seepage afterwards. Seepage percent at the spike is 33.02.
7.	scm_r3_10x_nlev_amb	#3	IMF10	0.00	Seepage is not predicted.
8.	scm_r3_10x_nlev_th	#3	IMF10	0.00	Seepage is not predicted.
9.	scm_r3_10x_nlev_thc	#3	IMF10	0.90	Seepage begins after 5,000 years.

Source: Output DTNs: LB0705THCSENR1.004, LB0705THCSENR1.005, LB0705THCSENR1.006, LB0705THCSENR2.004, LB0705THCSENR2.005, LB0705THCSENR2.006, LB0705THCSENR3.004, LB0705THCSENR3.005, and LB0705THCSENR1.006.

[a] See Tables 6.7-1 and 6.7-2.
[b] See Section 6.4.10
[c] See Section 6.4.5. For IMF1, the infiltration fluxes are 7.96 mm/yr (0 to 600 years), 12.89 mm/yr (600 to 2,000 years), and 20.45 mm/yr (2,000 years and beyond). For IMF10, the infiltration fluxes are 79.6 mm/yr (0 to 600 years), 128.9 mm/yr (600 to 2,000 years), and 204.5 mm/yr (2,000 years and beyond).

NOTE: Maximum seepage percentage is calculated by dividing the actual seepage rate by the largest infiltration flux (i.e., infiltration flux beyond 2,000 years) for a given infiltration scenario. Thus, for IMF1, the denominator is 20.45 mm/yr. On the other hand, for IMF10, the denominator is 204.5 mm/yr.

The initial fracture capillary-strength parameter in all these simulations was 591 Pa. Consequently, these results should not be directly compared to even those base-case simulations (Section 6.6) where Leverett-scaling effects were ignored (those base-case simulations used an initial fracture capillary-strength parameter of 1,739 Pa). Using a smaller (by a factor of close to three) initial fracture capillary-strength parameter in these simulations ensured that situations favorable to seepage were created.

- Simulations with Realizations #1 and #2 show that there could be a spike in predicted seepage from THC simulations. Simulations with Realization #1 also predict that long-term THC seepage can be larger than ambient and TH seepage (not observed in any other simulation). While there may be differences in the magnitude of predicted seepage, these observations are similar to those reported in *THC Sensitivity Study of Repository Edge and Heterogeneous Permeability Effects* (BSC 2006 [DIRS 174104]) and in the

study by Mukhopadhyay et al. (2006 [DIRS 180822]). These predictions (of spike in seepage from THC simulations and THC seepage being larger than ambient seepage) have been explained in those earlier studies in terms of THC-induced permeability/porosity changes (because of mineral precipitation/dissolution) and resulting local flow channeling. Summarizing, when the corresponding change in fracture capillarity arising from changes in fracture permeability/porosity is not accounted for in the simulations (as in the sensitivity simulations in this subsection), the result is an overprediction of local flow-channeling and subsequently seepage in THC simulations. While the rock hydrological properties and the imposed infiltration fluxes are different between this report and the studies mentioned above (BSC 2006 [DIRS 174104]; Mukhopadhyay et al. 2006 [DIRS 180822]), prediction of a similar dynamic pattern of seepage adds confidence to our understanding of the underlying physical processes controlling seepage. In this instance, these results verify that not including Leverett-scaling effects can lead to overestimation of seepage in THC simulations compared to ambient or TH simulations. This also confirms that the THC-induced enhanced seepage (compared to ambient seepage), as reported in *THC Sensitivity Study of Repository Edge and Heterogeneous Permeability Effects* (BSC 2006 [DIRS 174104]) and in the study by Mukhopadhyay et al. (2006 [DIRS 180822]), happened because of non-inclusion of a key physical process (i.e., Leverett-scaling effects) in the conceptual model.

6.7.2 Heterogeneous Fracture Capillarity

In this section, patterns of ambient, TH, and THC seepage are analyzed when the host-rock fracture capillarity is heterogeneous. The analyses in Section 6.4.11.3 and the results presented in Table 6.4-8 show that, when Leverett-scaling effects are included in the conceptual model of seepage calibration, the resulting calibrated fracture capillary-strength parameter is larger than the calibrated fracture capillary-strength parameter obtained without considering Leverett-scaling effects. Table 6.4-8 shows that, when synthetic liquid release test data are generated using a fracture capillary-strength parameter of 591 Pa without Leverett-scaling effects, the 2-D calibration inclusive of Leverett-scaling effects resulted in a mean fracture capillary-strength parameter of 3,274 Pa (with a standard deviation of 713 Pa). Thus, for this illustrative calculation, a factor of about one-half order of magnitude is realized in transforming non-Leverett-scaling synthetic data to a Leverett-scaled, calibrated property. The other matter of concern is the transformation from 3-D to 2-D. The calibrated fracture capillary-strength parameter from the SCM (BSC 2004 [DIRS 171764]) was obtained using a 3-D calibration model. Limited sensitivity study has shown that, if synthetic liquid release test data were generated using a fracture capillary-strength parameter of 591 Pa, and without considering Leverett scaling, a 3-D calibration, which included Leverett scaling, would result in a fracture capillary-strength parameter of about 920 Pa (with a standard deviation of 50). This result also indicates that a 2-D to 3-D transformation has a more significant impact on the calibrated fracture capillary-strength parameter than the Leverett-scaling effects. The primary concern, therefore, is that there is some uncertainty as to which initial fracture capillary-strength parameter should be used in the predictive simulations, which include Leverett-scaling effects, i.e., predictive models which include heterogeneity in fracture capillarity in addition to heterogeneity in fracture permeability. This uncertainty did not exist in predictive models without Leverett-scaling effects, as, in a conservative approach (for seepage), the smallest

available fracture capillary-strength parameter from a 3-D calibration was used in a 2-D predictive model.

The base-case simulations in Section 6.6 are based on an initial fracture capillary-strength parameter of 1,739 Pa, which was obtained from *Calibrated Unsaturated Zone Properties* (SNL 2007 [DIRS 179545]). The selection of 1,739 Pa for the base-case simulations was justified, because that number is smaller than one standard deviation from the mean, and hence was considered conservative for seepage (the mean fracture capillary-strength parameter from the analyses in Section 6.4.11.3 is 3,274 Pa, and the standard deviation is 713 Pa; thus one standard deviation below the mean is 2,561 Pa, which is about 47% larger than 1,739 Pa). Also, since the modeling work in *Drift-Scale THC Seepage Models* (SNL 2007 [DIRS 177404]) is carried out with a Tptpll fracture capillary-strength parameter of 1,739 Pa, it is appropriate for the base-case simulations in this report, because such an approach permits a direct comparison between homogeneous THC models (SNL 2007 [DIRS 177404]) and the heterogeneous THC models in this sensitivity report (see discussion in Section 6.5).

However, since some uncertainty exists (see the two paragraphs above) with regard to the appropriate initial fracture capillary-strength parameter while considering both permeability and capillarity heterogeneity, additional sensitivity studies are performed in this section with the THC seepage model (SNL 2007 [DIRS 177404]). Moreover, from the base-case simulations in Section 6.6, it is not clear that the choice of 1,739 Pa is conservative enough for seepage. For example, base-case simulations with Realization #3 (see Table 6.6-1) of the heterogeneous fracture permeability distribution do not predict seepage at all, neither with the present-day mean infiltration fluxes (i.e., IMF1) nor with much-enhanced infiltration fluxes (i.e., IMF10). This implies that the imposed capillary-barrier was too strong for seepage for this realization of the permeability distribution. On the other hand, base-case simulations with Realization #2 (see Table 6.6-1) of the heterogeneous fracture permeability distribution predict that seepage may occur even with present-day mean infiltration, implying that the capillary-barrier effect was too weak for this realization of the permeability distribution . In summary, when capillarity heterogeneity is included in the predictive model, a range of the initial fracture capillary-strength parameter needs to be considered (in place of a single one). Such an observation is borne out of the local nature of the process, since fracture capillarity is now a strong function of local permeability heterogeneity. The analyses in Section 6.4.11.3 (by predicting a large standard deviation in the calibrated fracture capillary-strength parameter) also point to the local nature of the problem.

6.7.2.1 Iterative Ambient Simulations

From the discussion above, it is clear that, performing simulations with different initial fracture capillary-strength parameters, for different realizations of the fracture permeability distribution, is a necessity. How such simulations are accomplished is elaborated next. For a particular realization of the heterogeneous fracture permeability (such as Realizations #1 and #3) distribution, the base-case ambient simulation results (see Table 6.6-1) are used as the starting point. If seepage has not occurred for that realization with present-day mean infiltration fluxes (i.e., IMF1, see Section 6.4.5), the initial fracture capillary-strength parameter is reduced and the ambient simulation (without heat or chemistry) is repeated. If seepage still does not occur, the initial fracture capillary-strength parameter is reduced further and the ambient simulation

repeated with the new value for the fracture parameter. This process is repeated until a fracture capillary-strength parameter is reached for which seepage commences under ambient conditions. It is assumed at this point that the capillary-barrier effect has become too weak, and ambient, TH, and THC simulations are performed with the fracture capillary-strength parameter just above the minimum number in the iterative process. On the other hand, if seepage is found to have occurred in the ambient base-case simulation for a particular realization (such as Realization #2), the process is repeated in reverse (i.e., start with the base-case fracture capillary-strength parameter and continue to increase this parameter value until a condition of no ambient seepage is reached). The results from this iterative process for the three realizations of the fracture permeability distribution are provided in Table 6.7-4.

Table 6.7-4. Summary of Results from Iterative Ambient Simulations

Serial No.	Simulation Type	Heterogeneous Fracture Permeability Realization[a]	Infiltration Fluxes[b]	Leverett Scaling[c]	Fracture ($1/\alpha_0$) at Which Seepage Happens (Pa)	Fracture ($1/\alpha_0$) at Which Seepage Does Not Happen (Pa)	Output DTN
1.	Ambient	#1	IMF1	Yes	1,282	1,313	LB0705THCSENR1.006
2.	Ambient	#2	IMF1	Yes	1,739	2,000	LB0705THCSENR2.006
3.	Ambient	#3	IMF1	Yes	700	750	LB0705THCSENR3.006

[a] See Section 6.4.10.
[b] See Section 6.4.5.
[c] See Sections 6.3 and 6.4.11.

As seen from Table 6.7-4, these iterative ambient simulations produce a range of initial fracture capillary-strength parameter, depending upon the realization of the heterogeneous fracture permeability distribution. For example, ambient simulations with Realization #1 produced seepage when the initial fracture capillary-strength parameter was 1,282 Pa, but no seepage was observed when the same parameter is 1,313 Pa. The transformation from seepage to no seepage may have happened at any initial fracture capillary-strength parameter between 1,282 Pa and 1,313 Pa. However, a value of 1,313 Pa is acceptable as adequate for the purpose of this report, because the impact is expected to be small. The same applies for the other two realizations of the heterogeneous fracture permeability distribution. In the following, ambient, TH, and THC simulations will be performed with these values for the initial fracture capillary-strength parameters (and inclusive of Leverett-scaling effects).

6.7.2.2 Seepage Results

Seepage results (whether seepage occurs) from the sensitivity simulations in this section (Section 6.7.2) are summarized in Table 6.7-5. These results have been submitted to the TDMS; the output DTN for each of the 18 sensitivity simulations is also included in Table 6.7-5 (see the note below Table 6.7-5). The seepage results can be extracted from files "flow.out" in the output DTNs. Appendix D describes the procedures for how to extract the seepage results from the "flow.out" files.

Table 6.7-5. Summary of Seepage Results from Sensitivity Simulations with Heterogeneous Capillarity (Leverett-Scaling Effects Included)

Serial No.	Infiltration Flux[a]	Fracture ($1/\alpha$) Value (Pa)[b]	Permeability Heterogeneity[c]	Leverett Scaling[d]	Simulation Type[e]	Simulation ID	Seepage	Output DTN
1.	IMF1	1,313	Realization #1	Yes	THC	itr_r1_1x_lev_thc	No	LB0705THCSENR1.004
2.	IMF10	1,313	Realization #1	Yes	THC	itr_r1_10x_lev_thc	Yes	LB0705THCSENR1.004
3.	IMF1	1,313	Realization #1	Yes	TH	itr_r1_1x_lev_th	No	LB0705THCSENR1.005
4.	IMF10	1,313	Realization #1	Yes	TH	itr_r1_10x_lev_th	Yes	LB0705THCSENR1.005
5.	IMF1	1,313	Realization #1	Yes	Ambient	itr_r1_1x_lev_amb	No	LB0705THCSENR1.006
6.	IMF10	1,313	Realization #1	Yes	Ambient	itr_r1_10x_lev_amb	Yes	LB0705THCSENR1.006
7.	IMF1	2,000	Realization #2	Yes	THC	itr_r2_1x_nev_thc	No	LB0705THCSENR2.004
8.	IMF10	2,000	Realization #2	Yes	THC	itr_r2_10x_lev_thc	Yes	LB0705THCSENR2.004
9.	IMF1	2,000	Realization #2	Yes	TH	itr_r2_1x_lev_th	No	LB0705THCSENR2.005
10.	IMF10	2,000	Realization #2	Yes	TH	itr_r2_10x_lev_th	Yes	LB0705THCSENR2.005
11.	IMF1	2,000	Realization #2	Yes	Ambient	itr_r2_1x_lev_amb	No	LB0705THCSENR2.006
12.	IMF10	2,000	Realization #2	Yes	Ambient	itr_r2_10x_lev_amb	Yes	LB0705THCSENR2.006
13.	IMF1	750	Realization #3	Yes	THC	itr_r3_1x_nev_thc	No	LB0705THCSENR3.004
14.	IMF10	750	Realization #3	Yes	THC	itr_r3_10x_lev_thc	Yes	LB0705THCSENR3.004
15.	IMF1	750	Realization #3	Yes	TH	itr_r3_1x_nev_th	No	LB0705THCSENR3.005
16.	IMF10	750	Realization #3	Yes	TH	itr_r3_10x_lev_th	Yes	LB0705THCSENR3.005
17.	IMF1	750	Realization #3	Yes	Ambient	itr_r3_1x_lev_amb	No	LB0705THCSENR3.006
18.	IMF10	750	Realization #3	Yes	Ambient	itr_r3_10x_nev_amb	Yes	LB0705THCSENR3.006

[a] See Section 6.4.5 for definition of infiltration fluxes.
[b] See Sections 6.4.11 and 6.7.2.1 for choice of fracture capillary-strength parameters.
[c] See Section 6.4.10 for definition of heterogeneous fracture permeability fields.
[d] See Sections 6.3, 6.4.11.3, and 6.4.11.4.
[e] THC = simulations with emplacement drifts, heat and chemistry; TH = simulations with emplacement drifts and heat (no chemistry); Ambient = simulations with emplacement drifts (no heat or chemistry).

From Table 6.7-5, it can be seen that seepage is not predicted to occur for any of the three realizations of heterogeneous fracture permeability distribution, if IMF1 infiltration fluxes are imposed. This is true for THC simulations as well as ambient and TH simulations. In other words, for the IMF1 infiltration fluxes (7.96 mm/yr for 0 to 600 years, 12.45 mm/yr for 600 to 2,000 years, and 20.45 mm/yr for 2,000 years and beyond), the saturation buildup near the emplacement drift is not sufficient to overcome the capillary-barrier effect. This is expected because we have constrained the initial fracture capillary-strength parameter, such that seepage does not happen under ambient conditions with present-day mean infiltration fluxes (see Section 6.7.2.1 and Table 6.7-4). In addition, there is no evidence of seepage enhancement because of THC processes.

When IMF10 infiltration fluxes (79.6 mm/yr for 0 to 600 years, 128.9 mm/yr for 600 to 2,000 years, and 204.5 mm/yr for 2,000 years and beyond) are imposed on the THC seepage model (SNL 2007 [DIRS 177404]), seepage is predicted to occur. Figures 6.7-4, 6.7-5, and 6.7-6 show the seepage flux (in mm/yr) from Realizations #1, #2, and #3, respectively.

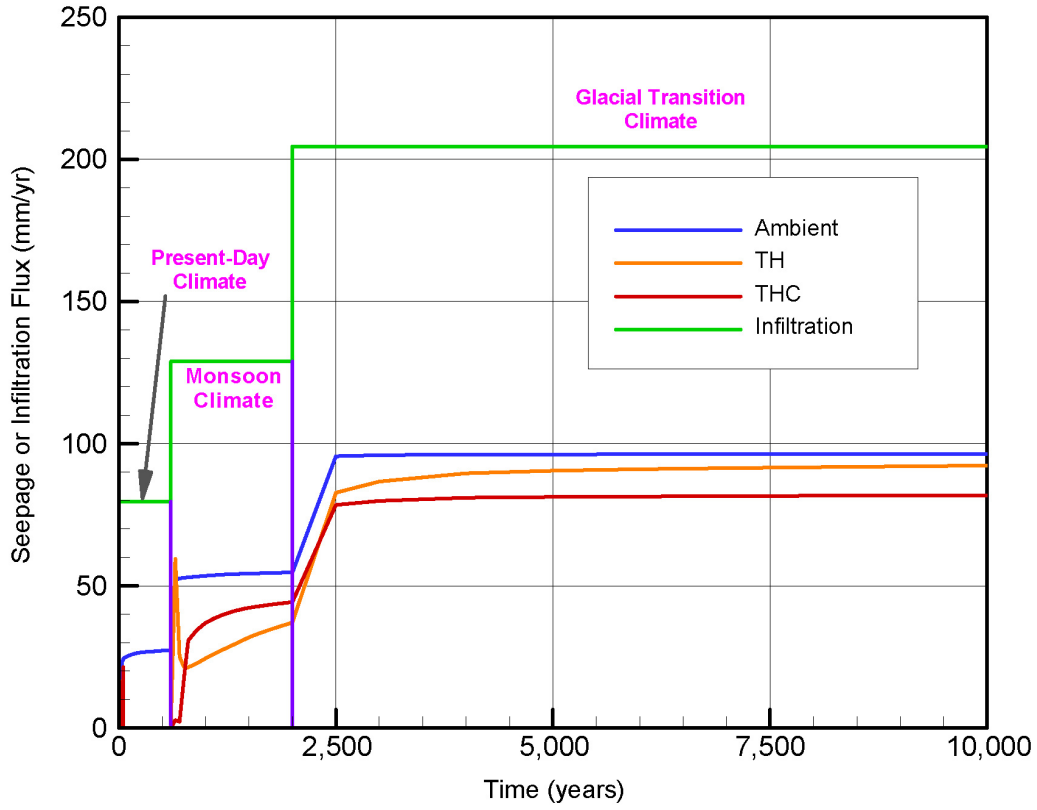

Source: Output DTNs: LB0705THCSENR1.004, LB0705THCSENR1.005, and LB0705THCSENR1.006.

NOTE: See Table 6.7-5 for explanation of simulation IDs. The vertical violet lines are used to distinguish the different climatic periods and they do not represent any seepage data.

Figure 6.7-4. Comparison of Seepage Fluxes from Ambient (Simulation ID: “itr_r1_10x_lev_amb”), TH (Simulation ID: “itr_r1_10x_lev_th.”), and THC (Simulation ID: “itr_r1_10x_lev_thc”) Simulations with Realization #1 of the Heterogeneous Fracture Permeability Distribution and Initial Fracture Capillary-strength Parameter of 1,313 Pa (see Section 6.7.2.1 and Table 6.7–4)

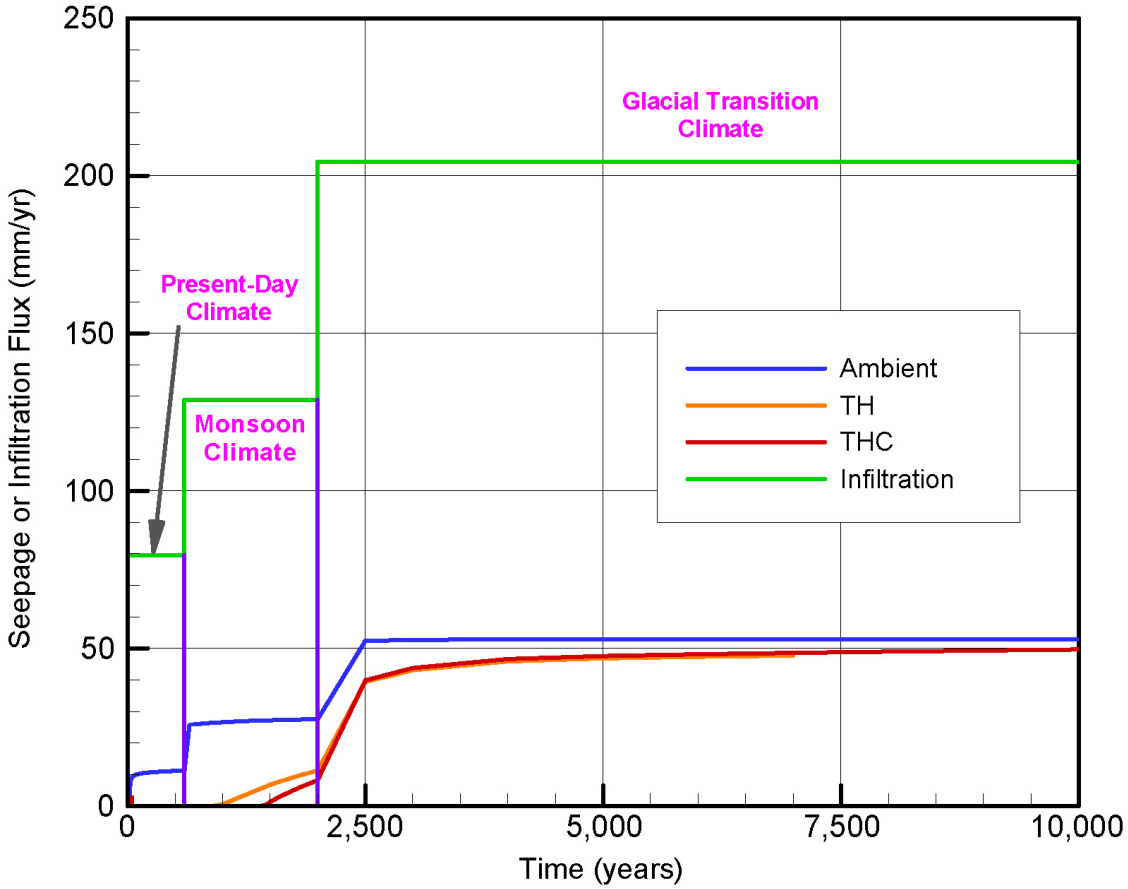

Source: Output DTNs: LB0705THCSENR2.004, LB0705THCSENR2.005, and LB0705THCSENR2.006.

NOTE: See Table 6.7-5 for explanation of simulation IDs. The vertical violet lines are used to distinguish the different climatic periods and they do not represent any seepage data.

Figure 6.7-5. Comparison of Seepage Fluxes from Ambient (Simulation ID: "tr_r2_10x_lev_amb"), TH (Simulation ID: "itr_r2_10x_lev_th."), and THC (Simulation ID: "itr_r2_10x_lev_thc") Simulations with Realization #2 of the Heterogeneous Fracture Permeability Distribution and Initial Fracture Capillary-strength Parameter of 2,000 Pa (see Section 6.7.2.1 and Table 6.7–4)

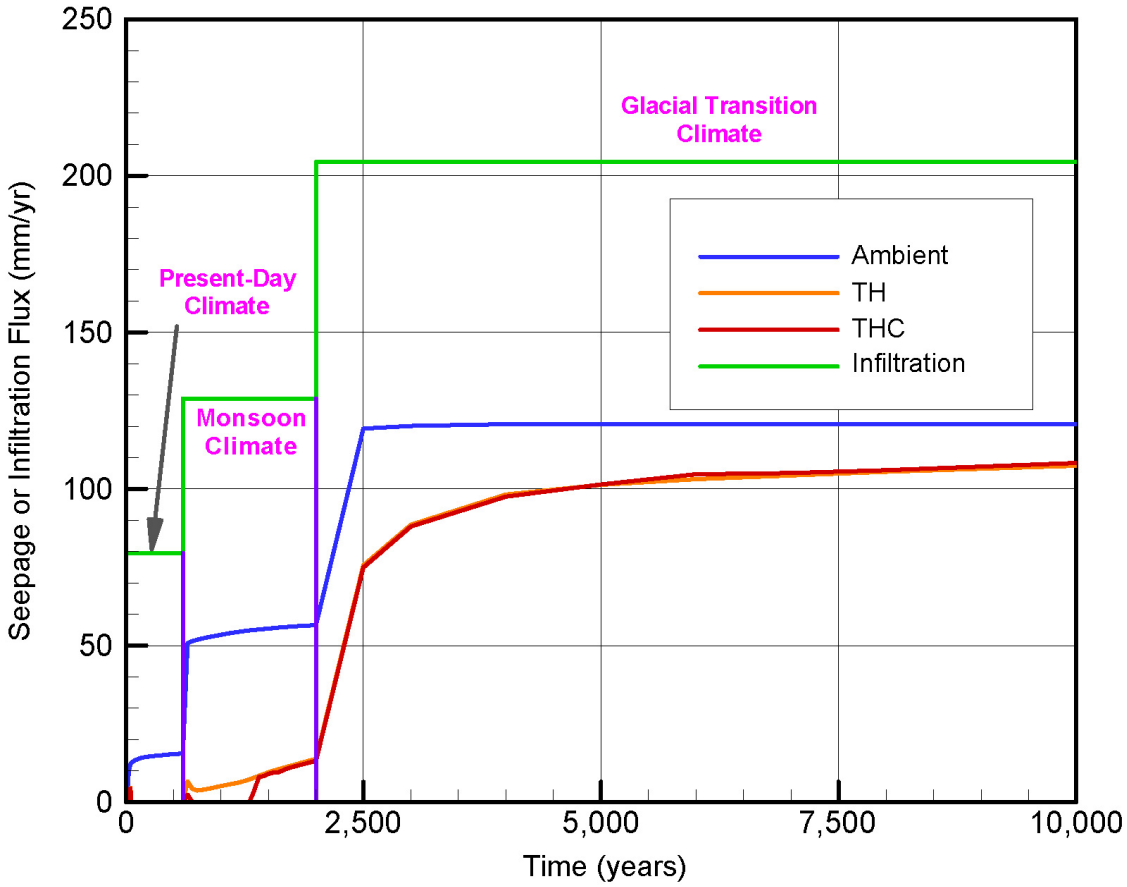

Source: Output DTNs: LB0705THCSENR3.004, LB0705THCSENR3.005, and LB0705THCSENR3.006.

NOTE: See Table 6.7-5 for explanation of simulation IDs. The vertical violet lines are used to distinguish the different climatic periods and they do not represent any seepage data.

Figure 6.7-6. Comparison of Seepage Fluxes from Ambient (Simulation ID: "itr_r3_10x_lev_amb"), TH (Simulation ID: "itr_r3_10x_lev_th."), and THC (Simulation ID: "itr_r3_10x_lev_thc") Simulations with Realization #3 of the Heterogeneous Fracture Permeability Distribution and Initial Fracture Capillary-strength Parameter of 750 Pa (see Section 6.7.2.1 and Table 6.7-4)

As anticipated, the dynamic pattern of seepage (in terms of the magnitude of seepage flux) is different from one realization of the heterogeneous fracture permeability distribution to another (because of the local nature of the underlying physical phenomenon). However, some broad observations can be made from these simulations:

- Long-term TH and THC seepage commence well after the time when ambient seepage is applied in TSPA (BSC 2004 [DIRS 169131]) after cooldown. This happens because of the presence of the vaporization barrier effects (Birkholzer et al. 2004 [DIRS 172262]; BSC 2005 [DIRS 172232]; BSC 2006 [DIRS 174104]; Mukhopadhyay et al. 2006 [DIRS 180822]) resulting from repository heating in TH and THC seepage simulations. The actual time at which long-term seepage commences is different from one realization to another, controlled mostly by changes in infiltration fluxes resulting from climate change and the speed with which the fractures rewet (in turn controlled by the TH and

THC processes, including the impact of the heterogeneity in fracture capillary-strength parameter) after the boiling period.

- Because the simulations were performed at the limit of the capillary-barrier effects (by selecting the minimum fracture capillary-strength parameter that will prevent ambient seepage under present-day mean infiltration fluxes and then increasing the infiltration fluxes by a factor of 10), ambient seepage begins at the start of the simulations. The same phenomenon is observed from TH and THC simulations. However, seepage stops in TH and THC simulations after ventilation is stopped (at 50 years) and boiling conditions occur in the rock. Long-term seepage in TH and THC simulations returns after the boiling period is over.

- It appears that THC seepage is similar (or marginally smaller) compared to TH seepage. This implies that mineral dissolution and precipitation in the THC simulations actually reduce seepage, which is qualitatively reasonable.

  Since heterogeneity in fracture capillarity was not accounted for in *THC Sensitivity Study of Repository Edge and Heterogeneous Permeability Effects* (BSC 2006 [DIRS 174104) or in the study by Mukhopadhyay et al. (2006 [DIRS 180822]), while accounting for fracture permeability heterogeneity, a conclusion contrary to the above was reached (as explained in Section 6.3, because of an overprediction of local flow channeling). This has been reproduced by the simulations in Section 6.7.1 of this report.

- The more important observation is that ambient seepage is greater than either TH or THC seepage, for conditions when ambient seepage is applied in TSPA after cooldown (BSC 2004 [DIRS 169131]), suggesting that seepage abstraction can still be based on ambient seepage rates, i.e., no modification in current seepage abstraction methodology is necessary because of THC processes.

- Based on the sensitivity simulations performed in this report, it may be concluded that Leverett-scaling effects influence the overall seepage rate. The seepage abstraction procedure (BSC 2004 [DIRS 169131]) does not include Leverett-scaling effects. However, the abstraction procedure (BSC 2004 [DIRS 169131) uses the fracture capillary-strength parameter from the SCM (BSC 2004 [DIRS 171764]), which also does not include Leverett-scaling effects, thereby providing a consistent basis for abstraction. However, as the discussion in Section 6.4.11.3 indicates, if the liquid-release test data in the SCM (BSC 2004 [DIRS 171764]) were to be recalibrated including Leverett scaling, a different (larger) fracture capillary-strength parameter value would be obtained. This newly calibrated fracture capillary-strength parameter should be used in seepage prediction, if the abstraction is ever to include Leverett-scaling effects. As a caution, using the SCM (BSC 2004 [DIRS 171764]) calibrated fracture capillary-strength parameter in an abstraction procedure that includes Leverett scaling will lead to inconsistent results.

The maximum seepage percentages from these sensitivity simulations are summarized in Table 6.7-6.

Table 6.7-6. Seepage Percentage from Sensitivity Simulations with Heterogeneous Fracture Permeability and Capillarity (Leverett-Scaling Effects Included)

Serial No.	Simulation ID[a]	Permeability Realization[b]	Infiltration Flux[c]	Long-Term Seepage Percentage
1.	itr_r1_10x_lev_amb	#1	IMF10	47.07
2.	itr_r1_10x_lev_th	#1	IMF10	45.12
3.	itr_r1_10x_lev_thc	#1	IMF10	40.01
4.	itr_r2_10x_lev_amb	#2	IMF10	25.88
5.	itr_r2_10x_lev_th	#2	IMF10	23.81
6.	itr_r2_10x_lev_thc	#2	IMF10	24.28
7.	itr_r3_10x_lev_amb	#3	IMF10	59.07
8.	itr_r3_10x_lev_th	#3	IMF10	52.52
9.	itr_r3_10x_lev_thc	#3	IMF10	52.96

Source: Output DTNs: LB0705THCSENR1.004, LB0705THCSENR1.005, LB0705THCSENR1.006, LB0705THCSENR2.004, LB0705THCSENR2.005, LB0705THCSENR2.006, LB0705THCSENR3.004, LB0705THCSENR3.005, and LB0705THCSENR1.006.

[a] See Tables 6.7-5.
[b] See Section 6.4.10
[c] See Section 6.4.5. For IMF1, the infiltration fluxes are 7.96 mm/yr (0 to 600 years), 12.89 mm/yr (600 to 2,000 years), and 20.45 mm/yr (2,000 years and beyond). For IMF10, the infiltration fluxes are 79.6 mm/yr (0 to 600 years), 128.9 mm/yr (600 to 2,000 years), and 204.5 mm/yr (2,000 years and beyond).

NOTE: Maximum seepage percentage is calculated by dividing the actual seepage rate by the largest infiltration flux (i.e., infiltration flux beyond 2,000 years) for a given infiltration scenario. Thus, for IMF10, the denominator is 204.5 mm/yr.

6.8 APPROXIMATIONS AND IDEALIZATIONS

Approximations and idealizations for the THC seepage model discussed in this sensitivity report are similar to those described in *Drift-Scale THC Seepage Model* (SNL 2007 [DIRS 177404], Sections 5 and 6.4.6). One specific idealization needs mentioning here. The initial fracture capillary-strength parameter obtained from the SCM (BSC 2004 [DIRS 171764]) has been used for the entire Tptpll hydrogeologic unit, though it may actually represent conditions prevailing in the vicinity of the emplacement drifts. Such an idealization is justified for the following reasons. First, the objective here is to perform sensitivity analyses that are conservative (i.e., favorable in this context) towards seepage. Using a smaller fracture capillary-strength parameter value for the entire Tptpll hydrogeologic unit is expected to produce conditions favorable for seepage. Second, a possible alternative was to use the fracture capillary-strength parameter value from the calibrated seepage testing data within a limited area near the drift and to apply that value from the drift-scale calibrated property set to the rest of the Tptpll. However, such an approach creates an unphysical capillary-barrier effect at the interface of those two zones (and introduces numerical difficulties as well). Thus, this option was not adopted in the simulations presented in this section. Further discussion on this issue can be found in *Drift-Scale Coupled Processes (DST and TH Seepage) Models* (BSC 2005 [DIRS 172232], Section 6.2.2.1.4).

6.9 ALTERNATIVE APPROACHES

Alternative approaches to investigate the THC seepage model sensitivity to heterogeneity and seepage would primarily consist of alternative representations of heterogeneity. The impact of heterogeneity on THC processes and seepage has been investigated with three realizations of the fracture permeability field. An alternative would be to use more realizations of the same heterogeneous fracture permeability distribution. Using more than three realizations would have allowed for a more statistically robust analysis. Nonetheless, the selected approach of using three realizations of the heterogeneous fracture permeability distribution provides useful insights regarding the interplay of fracture permeability and capillarity heterogeneities, feedback of TH and THC processes on hydrologic properties, and ultimately their impact on seepage (or its absence).

A full 3-D mesh may also be considered as an alternative approach. Again, using a 3-D model would have its limitations in utility, given the substantially longer simulation times. In addition, a 3-D model would not be directly comparable with the 2-D THC seepage model. For this model, ambient, TH, and THC simulations were performed in two dimensions. The use of 2-D models for simulating TH processes and seepage has been justified in *Drift-Scale Coupled Process (DST and TH Seepage) Models* (BSC 2005 [DIRS 172232], Section 6.2.1.2); the same justifications apply for the ambient, TH, and THC simulations presented here.

Compared to the THC seepage model, the numerical grid used in the SMPA (BSC 2004 [DIRS 167652]) is substantially more refined, but has considerably less spatial extent. The THC seepage model grid, though it is refined in the vicinity of the drift similar to the SMPA model, is coarser away from the drift (because of the larger spatial extent of this model from the ground surface to the water table). Such coarsening of the numerical grid away from the drift has necessitated the averaging of heterogeneous permeabilities in the gridblocks far away from the drift. This averaging is not expected to alter the outcome of the THC seepage model as far as seepage is concerned. However, an alternative model could be developed with a grid similar to the SMPA for the entire THC seepage model domain. Such an alternative approach would still not be consistent with the THC seepage model, and would also significantly increase the computational burden. For these reasons, the adopted modeling approach (Section 6.1.2.1) was deemed the most appropriate.

Lastly, one possible alternative approach could have been to use a different calibrated property set and the corresponding infiltration fluxes, i.e., one could have used one of the other three drift-scale calibrated property sets (the 10th percentile, 50th percentile, or 90th percentile property set) instead of the 30th percentile property set selected for the base-case simulations in this report. The selection of the 30th percentile property set (in preference to the other three drift-scale calibrated property sets) could be justified as follows.

- The 10th percentile property set corresponds to smaller infiltration fluxes compared to the 30th percentile property set. Since the objective is conservatism with respect to seepage, selecting larger infiltration fluxes and the corresponding property set is logical. If seepage did not occur with the infiltration fluxes corresponding to the 30th percentile property set, it was unlikely that seepage would occur with the smaller infiltration fluxes of the 10th percentile property set.

- Sensitivity studies were performed using ten times the infiltration fluxes given in the 30th percentile property set. These enhanced infiltration fluxes far exceed the mean infiltration fluxes corresponding to the 50th percentile and 90th percentile. Thus, through these sensitivity studies, the higher end of the infiltration fluxes have already been covered.

- This sensitivity report has demonstrated the role of the fracture capillary-strength parameter in determining seepage. The Tptpll fracture capillary-strength parameter in the 30th percentile property set is 1,739 Pa. On the other hand, the same parameter has a value of about 3,165 Pa in the 90th percentile property set. Consequently, even though the mean infiltration fluxes are larger in the 90th percentile property set (compared to the 30th percentile property set), the large Tptpll fracture capillary-strength parameter in that property set would have reduced the possibility of seepage. Selecting the 30th percentile property set is thus a conservative approach as far as seepage is concerned (the smaller Tptpll fracture capillary-strength parameter in the 30th percentile property set enhances the possibility of seepage).

- It has already been mentioned that using the 30th percentile property set is more conservative for seepage than using the 10th percentile property set. This is primarily because the infiltration fluxes in the 30th percentile property set are larger than those in the 10th percentile property set. It is also conservative because the Tptpll fracture capillary strength parameter of 1,739 Pa in the 30th percentile property set is smaller than that in the 10th percentile property set (approximately 3,165 Pa).

6.10 UNCERTAINTIES

Uncertainties in the THC seepage model and its results have been discussed in *Drift-Scale THC Seepage Model* (SNL 2007 [DIRS 177404], Sections 6.6 and 8.4). Those same uncertainties apply to the sensitivity analyses presented in this report. Since the primary focus of the sensitivity studies presented in this report is heterogeneity (both in fracture permeability and capillarity) and its impact on seepage owing to THC processes, some specific uncertainties related to seepage are discussed here.

The THC seepage model has been validated (SNL 2007 [DIRS 177404], Section 7) against measured data from the DST (BSC 2004 [DIRS 169900]), which is located in the Tptpmn unit at Yucca Mountain. Thus, validation of the THC seepage model does not include direct comparison with measured data from the Tptpll. However, the agreement of the model predictions with data from the Tptpmn provides confidence that the fundamental THC processes in the fractured rock are well captured by the model. Some uncertainty, however, remains about the rock properties of the Tptpll unit and the influence of lithophysal cavities.

A pertinent discussion about model uncertainties and model validation is found in *Drift-Scale Coupled Processes (DST and TH Seepage) Models* (BSC 2005 [DIRS 172232]). While the discussion in that report (BSC 2005 [DIRS 172232]) was specifically applicable for the TH seepage model, it is relevant for the THC model as well (at least as far as seepage is concerned). For the sake of convenience, a relevant part of that discussion as appropriate for a THC model is summarized here. No seepage of liquid water has been observed in the Heated Drift of the DST.

The DST results allow for a unique model validation with respect to the near-field THC conditions in the rock mass, but offer no seepage data (observed seepage rates) that can be used directly for thermal seepage validation purposes. Thus, validation of the seepage part of the THC seepage model is an indirect one. First, the better the overall THC behavior can be predicted by the DST THC simulations, the more confidence is gained for the seepage results obtained with the THC seepage model. In other words, the successful validation of the DST THC simulations adds confidence in the seepage part of the THC seepage model because the thermally perturbed water fluxes are accurately represented. Second, the modeling framework for the capillary-barrier treatment in the THC seepage model can already be considered validated, because the conceptual model is identical to the one validated and successfully applied in the ambient seepage studies. As described in *Seepage Calibration Model and Seepage Testing Data* (BSC 2004 [DIRS 171764], Section 7), the conceptual model developed in the SCM was tested by performing blind predictions of seepage rates for niche liquid-release tests that had not been used for model calibration and that were conducted in a different drift section. It was demonstrated that the measured ambient seepage data (seepage threshold and seepage rate) were accurately represented by the simulated results. Validation of the coupled THC processes (using the DST data) together with validation of the ambient seepage conceptual model (using liquid-release data) provides confidence in the seepage results of the THC seepage model. However, some uncertainty remains, since no direct test data on thermal seepage at extreme flux conditions are available.

For numerical models, the main sources of uncertainty are uncertainty in model input parameters and uncertainty in implemented process models. As discussed above, most uncertainties with respect to THC process models have been addressed through model validation, building confidence in the validity of the conceptual model for seepage. The uncertain and spatially variable model input parameters are rock properties and model boundary conditions. For example, the permeability decrease is a strong function of the permeability-porosity coupling relationship used in the model, which relies on parameters such as fracture spacing, surface area, and initial permeability. It is also a strong function of initial fracture porosity. Uncertainties in these properties will affect the response of the model, from almost no permeability decrease to complete plugging of fractures. To evaluate uncertainty, other permeability-porosity coupling relationships may be examined. However, the heterogeneity in fracture permeability input into the model is likely to encompass the uncertainty in other fracture properties, such that the results shown here can be regarded as encompassing these uncertainties.

Sensitivity to parameters relevant for seepage (such as heterogeneity in fracture permeability, the fracture $1/\alpha$ parameter, and infiltration fluxes) was explicitly studied with the THC seepage model. Some uncertainty exists because only three realizations of the heterogeneous fracture permeability field were used. Nonetheless, these three realizations provide useful insights regarding THC effects on flow and seepage. They also encompass uncertainties in other fracture properties such as initial porosity, spacing, and surface area.

One uncertainty was not addressed in the earlier revison of this report (BSC 2006 [DIRS 174104], Section 6.2.4). The heterogeneous fracture permeability field in that report was allowed to change dynamically, because of the processes of mineral precipitation and dissolution during each THC simulation. While fracture capillarity is known to vary with changes in permeability and porosity, simulations in the earlier revision of this report (BSC 2006

[DIRS 174104], Section 6.2.2.1.2) were conducted by holding the fracture capillary-strength parameter constant. This approach was consistent with previous seepage studies under ambient (BSC 2004 [DIRS 167652]; BSC 2004 [DIRS 171764]) or thermal simulations (Birkholzer et al. 2004 [DIRS 172262]; BSC 2005 [DIRS 172232]). The simulations in this report (see Section 6.7) demonstrate that excluding fracture capillarity heterogeneity while including permeability heterogeneity results in overprediction of local flow channeling (and seepage) in THC simulations (compared to ambient and TH simulations). To reduce this uncertainty, simulations are thus performed in this report by including heterogeneities in both fracture permeability and capillarity. To cover the range of possible initial fracture capillary-strength parameter values (since no direct experimental data are available in this instance), sensitivity studies are performed starting with initial fracture capillary-strength parameters that are themselves dependent on the specific realization of the fracture permeability distribution. Consequently, seepage results were obtained covering a large range of the initial fracture capillary-strength parameter values (750 to 2,000 Pa). These simulations definitely reduce uncertainty with regard to seepage prediction under THC conditions at Yucca Mountain. However, a small amount of uncertainty still remains because of the unavailabilty of direct seepage-related data under thermal conditions.

6.11 INTENDED USE OF OUTPUTS

Results of simulations presented above are intended to provide information on the THC seepage model sensitivity to heterogeneity in fracture permeability and capillarity of the host rock (Tptpll). Heterogeneity in host rock fracture permeability was introduced by using three realizations of a heterogeneous fracture permeability distribution. The heterogeneous fracture permeability distribution created for the ambient/TH/THC simulations presented in this report was generated with the same geostatistical inputs (Table 4.1-1) as those used for generating the fracture permeability distribution in the SMPA (BSC 2004 [DIRS 167652]).

The output from this sensitivity analysis is amount of seepage, if any, into the drifts, and the time when seepage happens. It should be remembered, however, that for full consistency with previous THC seepage model simulations, simulations discussed above were run with the same input data as used in *Drift-Scale THC Seepage Model* (SNL 2007 [DIRS 177404]), except for those data on which sensitivity analyses were performed, as described in Table 4.1-1. As mentioned in Section 1.1, the objective of these sensitivity studies is the reduction of risk associated with the THC seepage model. The sensitivity studies documented in this report provide additional information regarding the use of the THC seepage model. The products of this report may be used as direct inputs to TSPA or to any of the abstractions used by TSPA, even though they were not developed specifically for this use.

7. CONCLUSIONS

7.1 MAIN FINDINGS AND IMPLICATIONS FOR TSPA

Sensitivity studies were carried out to determine the impact of heterogeneity in fracture permeability and capillarity on the evolution of ambient/TH/THC processes in the near-field rock. These sensitivity studies were performed with the objective of determining whether the TH/THC changes in the host rock would influence the quantity and chemistry of seepage. The THC seepage model, based on the TOUGHREACT V3.1.1 reactive transport software (see Section 3.1 and Table 3-1), was used to perform these sensitivity studies. Heterogeneity in the fracture permeability of the Tptpll host rock unit in the THC seepage model was introduced by using a heterogeneous fracture permeability distribution, adopted from that used in the SMPA (BSC 2004 [DIRS 167652]) for the sake of consistency with the ambient seepage models. Heterogeneity in fracture capillarity of the host rock was considered through two processes: (1) considering the impact of fracture permeability heterogeneity on fracture capillarity through Leverett scaling relations (Section 6.3); and (2) using different initial fracture capillary-strength parameters for different realizations of the same fracture permeability distribution, covering a wide range of fracture capillary-strength parameters.

The fracture capillary-strength parameter of the host rock is a critical factor in determining whether seepage will occur. In the base-case simulations presented in this report, the fracture capillary-strength parameter was adopted from *Calibrated Unsaturated Zone Properties* (SNL 2007 [DIRS 179545]) (see Section 6.4.11.4 of the present report, which justifies this selection). Additional simulations were performed where the fracture capillary-strength parameter was either from the SCM (to demonstrate the impact on seepage of not including capillary heterogeneity while including permeability heterogeneity) or from iterative ambient simulations, which determined the minimum fracture capillary-strength parameter that would prevent ambient seepage. These iterative simulations were further supported by analyses of synthetic liquid-release test data (see Sections 6.4.11.3 and 6.4.11.4), which also demonstrated the impact of dimensionality (3-D vs. 2-D), scale (small-scale fractures near the emplacement tunnels vs. fracture continuum encompassing the entire host rock unit), and the calibration method employed (including or excluding Leverett-scaling effects in the calibration model) on the estimated fracture capillary-strength parameter. The analyses in Section 6.4.11.3 indicated that the calibrated (inclusive of Leverett scaling) effects have a large standard deviation, pointing to the local nature of the phenomenon (local permeability heterogeneity has a strong impact on the estimated fracture capillary-strength parameter). As a result, sensitivity studies (which included Leverett-scaling effects) were performed in this report covering a large range of initial fracture capillary-strength parameters.

Seepage into the drifts, of course, is also determined by the infiltration fluxes. In the sensitivity studies of this report, two sets of infiltration fluxes were used to demonstrate whether or not seepage occurs, and if it does occur, to predict its quantity and chemistry. The complete suite of simulations performed is listed in Tables 6.5-1 (steady-state simulations), 6.5-2 (base-case simulations), 6.7-1 (simulations with SCM fracture capillary-strength parameter and without Leverett-scaling effects), 6.7-4 (iterative ambient simulations), and 6.7-5 (simulations with heterogeneity in both fracture permeability and capillarity). For each of these parameter combinations (different realizations of the heterogeneous fracture permeability distribution,

different fracture capillary-strength parameters, and infiltration flux values), simulations were performed for ambient, TH-only, and full THC conditions. These were necessary to establish the enhancement in seepage (if any) that may occur because of THC changes in the rock (see below).

The base-case simulations (36 in total) are discussed in Sections 6.5 and 6.6. All of these base-case simulations have a fixed initial fracture capillary-strength parameter, while the other parameters were varied (three realizations of the fracture permeability distribution, two sets of infiltration fluxes, and inclusion/exclusion of Leverett-scaling effects). These base-case simulations demonstrate the impact of fracture permeability and capillarity heterogeneity on seepage. When fracture permeability heterogeneity is included in the conceptual model and capillarity is assumed homogeneous (i.e., Leverett scaling is not included), the selected fracture capillary-strength parameter (1,739 Pa) results in a large seepage threshold saturation (~0.8196), which does not allow seepage to occur with either the present-day mean or ten times the present-day mean infiltration flux. However, with inclusion of both permeability and capillarity heterogeneity in the conceptual model through Leverett scaling (see Section 6.3), local situations are created in which the seepage threshold saturations are considerably smaller (i.e., locations with considerably larger permeability than the mean fracture permeability). Such a local decrease in seepage threshold saturation makes seepage possible when capillarity heterogeneities are included in the model, particularly when larger infiltration fluxes are imposed. Note that, even though the base-case simulations all had the same initial fracture capillary-strength parameters, the capillary-barrier effects imposed in simulations that exclude Leverett scaling are not the same as in simulations that include Leverett scaling (see Section 6.4.11.3). Accordingly, care should be exercised in directly comparing seepage results from simulations excluding Leverett scaling to simulations including it (see discussion below as well). It is also observed that, when seepage occurs (because of larger infiltration fluxes), ambient seepage is always larger than TH or THC simulations. This is important because this implies that no modification is necessary in seepage abstraction procedures because of THC processes.

Seepage water chemistries from one of the base-case THC simulations (Simulation ID: "base_r2_10x_lev_thc"; see Table 6.5-2) were compared with the chemistry of water from a homogeneous THC simulation (SNL 2007 [DIRS 177404], Section 6.5.5.4) in Section 6.6.3. The results show that heterogeneity does not have any significant impact on the chemistry of seepage.

As indicated in the paragraph above, the base-case simulations have a fixed initial fracture capillary-strength parameter (for the Tptpll unit). The next set of sensitivity simulations was carried out by changing the initial fracture capillary-strength parameter. These sensitivity simulations assume a homogeneous capillarity (i.e., Leverett-scaling effects are not included). A uniform fracture capillary-strength parameter (591 Pa) obtained from the SCM (BSC 2004 [DIRS 171764]) is used in all these simulations. There were two primary objectives in performing these homogeneous-capillarity sensitivity simulations with SCM parameter: (1) to illustrate the impact of ignoring Leverett-scaling effects (which permitted a better understanding of the impact of capillarity heterogeneity) on seepage, and (2) to reevaluate earlier simulation results (BSC 2006 [DIRS 174104]; Mukhopadhyay et al. [DIRS 180822]), which were performed with incomplete consideration of capillarity heterogeneity.

Results from these sensitivity simulations with ten times the present-day mean infiltration fluxes (Section 6.7.1) show that local fracture heterogeneity play a key role in determining whether seepage occurs. Simulations with Realizations #1 and #2 show that there could be a spike in predicted seepage from THC simulations. Simulations with Realization #1 also predict that long-term THC seepage can be larger than ambient and TH seepage. While there may be differences in the magnitude of predicted seepage, these observations are similar to those reported in *THC Sensitivity Study of Repository Edge and Heterogeneous Permeability Effects* (BSC 2006 [DIRS 174104]) and in the study by Mukhopadhyay et al. (2006 [DIRS 180822]). These predictions (with the spike in seepage from THC simulations and THC seepage being larger than ambient seepage) were explained in those earlier studies in terms of THC-induced permeability/porosity changes (because of mineral precipitation/dissolution), and resulting local flow channeling. Summarizing, when the corresponding change in fracture capillarity arising from changes in fracture permeability/porosity is not accounted for in the simulations (as in the sensitivity simulations in Section 6.7.1), the result is an overprediction of local flow channeling and seepage (see Section 6.3). While the rock hydrological properties and the imposed infiltration fluxes are different between this report and those used in the reports cited above (BSC 2006 [DIRS 174104]; Mukhopadhyay et al. 2006 [DIRS 180822]), prediction of a similar dynamic pattern of seepage adds confidence to the current understanding of the underlying physical processes controlling seepage. In this instance, these results verify that not including Leverett-scaling effects can lead to overestimation of seepage in THC simulations, when compared to ambient or TH simulations. This also confirms that the THC-induced enhanced seepage (compared to ambient seepage) reported in the two earlier studies (BSC 2006 [DIRS 174104]; Mukhopadhyay et al. 2006 [DIRS 180822]) happened because of non-inclusion of a key physical process (i.e., Leverett-scaling effects) in the conceptual model.

The final set of sensitivity simulations involves heterogeneity in both fracture permeability and capillarity. They also involve use of different values of the initial fracture capillary-strength parameter for different realizations of the heterogeneous fracture permeability distribution. As a first step (Section 6.7.2.1), a number of ambient simulations are performed for each realization of the heterogeneous fracture permeability distribution. The objective is to estimate (within reasonable limits) the minimum fracture capillary-strength parameter that is required to prevent seepage under ambient conditions. In other words, the objective is to create situations in which the capillary-barrier effect is at its minimum (or close to it), and then perform ambient, TH, and THC simulations with these minimal capillary-barrier systems and larger infiltration fluxes. This combination (of capillary-barrier at its minimum and larger infiltration fluxes) represents conditions favorable for seepage. Results from these simulations can be found in Section 6.7.2.

As the simulations were performed with minimum values of the fracture capillary-strength parameter and increased infiltration (IMF10), ambient seepage began at the start of these simulations. The same phenomenon is observed from TH and THC simulations. However, seepage stops in TH and THC simulations after ventilation stops (at 50 years) and boiling conditions occur in the host rock. Long-term seepage in TH and THC simulations returns after the boiling period is over. It appears from these results that THC seepage is similar (or marginally smaller) compared to TH seepage. This implies that the processes of mineral precipitation in the THC simulations reduce seepage. Also, no “spike” in seepage results was observed in these simulations, contrary to the results reported in the earlier studies (BSC 2006

[DIRS 174104]; Mukhopadhyay et al. 2006 [DIRS 180822]), where heterogeneity in fracture capillarity was not accounted for.

The more important observation was that ambient seepage was larger than either TH or THC seepage. These findings partially address the concerns expressed in CR-7037. The results in this report suggest that the anomalous THC seepage predicted by *THC Sensitivity Study of Repository Edge and Heterogeneous Permeability Effects* (BSC 2006 [DIRS 174104]) was the result of not including an important physical process (Leverett scaling). The findings in this report also suggest that seepage abstraction methodology can be based on ambient seepage rates, and no change in the seepage abstraction procedure is necessary because of THC-related processes.

Based on the sensitivity simulations performed in this report, it is concluded that Leverett-scaling effects influence the overall seepage rate. The seepage abstraction procedure (BSC 2004 [DIRS 169131]) does not include Leverett-scaling effects. However, the abstraction procedure (BSC 2004 [DIRS 169131]) uses the fracture capillary-strength parameter from the SCM (BSC 2004 [DIRS 171764]), which also does not include Leverett-scaling effects, thereby providing a consistent basis for abstraction. As the discussion in Section 6.4.11.3 indicates, if the liquid-release test data from the SCM (BSC 2004 [DIRS 171764]) were to be calibrated including Leverett scaling, a different (likely larger) fracture capillary-strength parameter value would be obtained. This newly calibrated fracture capillary-strength parameter value should be used in seepage prediction, if the abstraction were to include Leverett-scaling effects. On the other hand, using the SCM (BSC 2004 [DIRS 171764]) calibrated fracture capillary-strength parameter in an abstraction procedure that includes Leverett scaling would lead to inconsistent results.

In summary, the main conclusions from this report are (1) if only heterogeneity in fracture permeability is considered without consideration of corresponding heterogeneity in fracture capillarity, seepage from THC simulations may be predicted that is larger than ambient seepage (because of an overprediction of local flow channeling effects), (2) when both fracture capillarity and permeability heterogeneity is included in the conceptual model, ambient seepage is expected to be larger than TH or THC, (3) abstraction of drift seepage may be based on ambient seepage and no change in abstraction procedure is necessary because of THC-induced processes, and (4) Leverett scaling plays an important role in controlling seepage. If seepage abstraction were to include Leverett-scaling effects, seepage testing data would have to be recalibrated.

7.2 UNCERTAINTIES AND RESTRICTIONS FOR SUBSEQUENT USE

Uncertainties related to sensitivity analyses presented in this report are discussed in Section 6.10. The intended use of outputs from this report has been discussed in Section 6.11. Uncertainties regarding model results and restrictions for use are the same as for the THC seepage model simulations (SNL 2007 [DIRS 177404]). The objective of this work is the reduction of risk associated with the abstraction of drift seepage (BSC 2004 [DIRS 169131]), which supports TSPA (Section 1.1). The sensitivity studies documented in this report also provide additional information regarding the use of the drift-scale THC seepage model. While the products of this report were not developed specifically for use as direct inputs to TSPA or to any of the abstractions used by TSPA, they may be used as such.

For full consistency with original THC seepage model simulations (SNL 2007 [DIRS 177404]), sensitivity analyses presented in this report were run with the same input data as used in *Drift-Scale THC Seepage Model* (SNL 2007 [DIRS 177404]), except for those parameters on which sensitivity analyses were performed. Additional sensitivity studies could further reduce uncertainty. For example, additional calculations (including recalibration to seepage testing data) could be used to estimate the initial fracture capillary strength parameter to be used in simulations that include Leverett-scaling effects from THC processes. Computing resources permitting, a limited number of 3-D THC sensitivity studies could also provide additional confidence. Notwithstanding these opportunities for further reduction of uncertainty, the primary conclusions of this report would not be expected to change significantly.

7.3 ASSOCIATED CRS

As stated in Section 4.2, the TWP (SNL 2007 [DIRS 179287], Sections 1.2.1 and 1.2.4) specifies that this analysis report address two CRs, CR-7037 and CR-7193. In the following, a summary is provided on how these CRs have been addressed in this report.

7.3.1 CR-7037

CR 7037 notes that information provided in Revision 00 of the THC sensitivity study (BSC 2006 [DIRS 174104]) shows that predicted seepage is enhanced by THC effects not considered in *Abstraction of Drift Seepage* (BSC 2004 [DIRS 169131]). Results available from this report show that the enhancement of seepage due to THC processes, as reported in *THC Sensitivity Study of Repository Edge and Heterogeneous Permeability Effects* (BSC 2006 [DIRS 174104]) and in the study by Mukhopadhyay et al. (2006 [DIRS 180822]), happened because certain physical processes were not included in the predictive models. More specifically, the overprediction of THC seepage in the earlier reports (BSC 2006 [DIRS 174104]; Mukhopadhyay et al. 2006 [DIRS 180822]) was a result of excluding fracture capillarity heterogeneity, while including heterogeneities in fracture permeability and dynamic changes in porosities in the predictive models. The following results from this report confirm the above finding.

1. Qualified and software TOUGHREACT V3.1.1 (see Section 3.1 and Table 3-1) has been used in performing the simulations in this report.

2. Though the values of infiltration fluxes and rock thermal, hydrological, and chemical properties used in this report are different from those used in *THC Sensitivity Study of Repository Edge and Heterogeneous Permeability Effects* (BSC 2006 [DIRS 174104]), the physical and chemical processes modeled in the simulations in Section 6.7.1 are the same as those in the earlier report (BSC 2006 [DIRS 174104]). The results (see Figures 6.7-1 through 6.7-3) in Section 6.7.1, derived from simulations, which exclude Leverett-scaling effects and use the SCM calibrated fracture capillary strength parameter value, are similar to those in the earlier report (BSC 2006 [DIRS 174104], Section 6.2.3.4 and Figure 6.2-11). Figures 6.7-1 through 6.7-3 thus confirm the findings of *THC Sensitivity Study of Repository Edge and Heterogeneous Permeability Effects* (BSC 2006 [DIRS 174104], Section 6.2.3.4 and Figure 6.2-11). In other words, when heterogeneity in fracture permeability is included in any predictive model while ignoring the

corresponding heterogeneity in fracture capillarity, THC seepage is expected to be larger than simulations with consistent treatment of permeability and capillarity.

In addition, the findings in *THC Sensitivity Study of Repository Edge and Heterogeneous Permeability Effects* (BSC 2006 [DIRS 174104]) were based on only one realization of the heterogeneous fracture permeability distribution. However, the results in the study by Mukhopadhyay et al. (2006 [DIRS 180822]) and this report (see Figures 6.7-1 through 6.7-3) are based on three different realizations of the heterogeneous fracture permeability distribution.

In performing the simulations in *THC Sensitivity Study of Repository Edge and Heterogeneous Permeability Effects* (BSC 2006 [DIRS 174104]), the software TOUGHREACT V3.0 was used. Since similar results are produced in this report using an updated TOUGHREACT code, the enhanced THC seepage in the earlier report (BSC 2006 [DIRS 174104) was not the result of any software error.

3. That non-inclusion of a key physical process (i.e., Leverett-scaling effects), and not any software error, was the root cause of the predicted enhanced THC seepage in *THC Sensitivity Study of Repository Edge and Heterogeneous Permeability Effects* (BSC 2006 [DIRS 174104], Figure 6.2-11) is evident from the simulation results in Section 6.7.2. In this section, simulations were performed where THC processes of mineral precipitation and dissolution were allowed to impact fracture porosity and permeability as well as fracture capillarity (through Leverett-scaling effects; see Equation 6.3-7). Figures 6.7-4 through 6.7-6 confirm that, when heterogeneities in both fracture permeability and capillarity are included in the predictive model, THC seepage is predicted to be smaller than ambient seepage. Not only that, Figures 6.7-4 through 6.7-6 confirm that in fact THC seepage can be marginally smaller than even TH seepage, which is reasonable qualitatively.

   The simulations in Section 6.7.2 were performed at the (minimum) limit of the capillary-barrier effects under ambient conditions (by employing initial fracture capillary-strength parameter values that will barely prevent seepage under ambient conditions). Thus, these simulations were conservative in nature as far as seepage is concerned. These conservative simulations confirm that Leverett scaling plays an important role in controlling seepage, particularly when THC processes are included. Since Leverett-scaling effects were not included in *THC Sensitivity Study of Repository Edge and Heterogeneous Permeability Effects* (BSC 2006 [DIRS 174104]), that report predicted a larger THC seepage than ambient seepage. That observation is not supported by those simulations (in the present report) where Leverett-scaling effects have been included.

4. The seepage results in Section 6.6.2 from the base-case simulations further confirm these observations, i.e., when Leverett-scaling effects are included in the predictive model accounting for fracture capillarity heterogeneities arising from the THC processes of mineral precipitation and dissolution, THC seepage is expected to be smaller than ambient seepage (see Section 6.6.2 and Figures 6.6-2 and 6.6-3).

5. The seepage abstraction (BSC 2004 [DIRS 169131]) does not include Leverett scaling. However, the abstraction is based on ambient seepage rates and the fracture capillary strength parameter values used in determining the seepage rates for abstraction is based on the SCM (BSC 2004 [DIRS 171764]), which also does not include Leverett scaling. Thus, seepage abstraction (BSC 2004 [DIRS 169131]) is based on a consistent approach.

   This report also observes that abstraction of drift seepage may be based on ambient seepage and no change in abstraction procedure is necessary because of THC-induced processes. This report also observes that Leverett scaling plays an important role in controlling seepage. If seepage abstraction were to include Leverett-scaling effects, seepage testing data would have to be recalibrated. A more complete set of findings from this report and their implications for TSPA are provided in Section 7.1.

6. The uncertainties associated with the results from this report are described in Section 6.10.

7.3.2 CR-7193

CR-7193 calls for a better integration of the THC seepage model with the SMPA (BSC 2004 [DIRS 167652]). This has been accomplished as described below.

1. Heterogeneity in fracture permeability is a key parameter in controlling seepage. The THC seepage model (SNL 2007 [DIRS 177404]) employs a homogeneous fracture permeability field, resulting in some concerns regarding the compatibility of the THC seepage model and the SMPA. In this report, the compatibility between the two models is enhanced by including a heterogeneous fracture permeability field in the THC seepage model.

2. The various realizations of the heterogeneous fracture permeability field used in the simulations of this report are derived from the same distribution as in the SMPA. This is described in greater detail in Section 6.4.10.

3. The SMPA has a regular grid with uniform element size and orientation. In the drift vicinity, the grid size designed for the THC seepage model in this report is 0.2 m in the radial direction, compared to 0.1 m for the SMPA (BSC 2004 [DIRS 167652], Section 6.3.1). The issue of grid-resolution effects was analyzed in a previous version of the SMPA report (CRWMS M&O 2000 [DIRS 153314], Section 6.7). It was concluded that the grid-size dependence is rather small, similar to or less than the variability from different realizations of the heterogeneous permeability field. Also note that the model grid size used in the drift vicinity is comparable to the 1-ft interval length of the air-injection tests conducted in the niches, assuring that the scale of measurement is consistent with the scale of heterogeneity described in the model. More discussion on this issue can be found in Section 6.4.10.

4. Fracture capillary strength parameter of the host rock is another key hydrological parameter controlling seepage. The simulations in Section 6.7.1 (with uniform fracture capillarity) have been carried out with the SCM calibrated initial fracture capillary strength parameter value of 591 Pa. The SMPA performs sensitivity

analyses with respect to this parameter, with the SCM value as the base-case for its simulations. The similarity in values used for host rock fracture capillary strength parameter enhances the integration of the SMPA and the THC seepage models. Sections 6.4.11.1 and 6.4.11.3 provide more discussion on this subject.

5. The simulations in SMPA are based on a 3-D conceptual model. The conceptual model underlying the SCM is also a 3-D model. In addition, neither the SMPA nor the SCM include Leverett-scaling effects in their conceptual models. In contrast, the THC seepage model is 2-D, and also Leverett-scaling effects are an important factor in THC simulations. To account for the uncertainties arising from using a 2-D model (instead of a 3-D model as in the SMPA and SCM) and including Leverett-scaling effects in the conceptual model, data from synthetic liquid-release tests were calibrated with and without Leverett-scaling effects both in 2-D and 3-D. The resultant fracture capillary-strength parameter values were used in determining an appropriate range for this parameter to be used in the THC simulations of this report. Section 6.4.11.3 provides more discussion about this. In addition, see Sections 6.6.2, 6.7.1, and 6.7.2 for seepage results over a large range of initial fracture capillary strength parameter value.

   Because the range of initial fracture capillary strength parameter values were determined by a consistent calibration model, it enhanced the compatibility of the SMPA and the THC seepage model.

7.4 PRODUCT OUTPUTS

LB0704THRMLPRP.001. Thermal Properties of UZ Model Layers: Data Summary. Submittal date: 04/10/2007.

LB0705THCSENHF.001. Input and Output Files for Generating Heterogeneous Fracture Permeability Field. Submittal date: 05/07/2007.

LB0705THCSENR1.001. Input and Output Files of Drift-Scale Steady-State and THC Simulation with Water HDPERM3 (w0) and Realization #1 of the Heterogeneous Fracture Permeability Distribution. Submittal date: 05/07/2007.

LB0705THCSENR1.002. Input and Output Files of Drift-Scale Steady-State and TH Simulation with Realization #1 of the Heterogeneous Fracture Permeability Distribution. Submittal date: 05/07/2007.

LB0705THCSENR1.003. Input and Output Files of drift-Scale Steady-State and Ambient Simulation with Realization #1 of the Heterogeneous Fracture Permeability Distribution. Submittal date: 05/07/2007.

LB0705THCSENR2.001. Input and Output Files of Drift-Scale Steady-State and THC Simulation with Water HDPERM3 (w0) and Realization #2 of the Heterogeneous Fracture Permeability Distribution. Submittal date: 05/07/2007.

LB0705THCSENR2.002. Input and Output Files of Drift-Scale Steady-State and TH Simulation with Realization #2 of the Heterogeneous Fracture Permeability Distribution. Submittal date: 05/07/2007.

LB0705THCSENR2.003. Input and Output Files of Drift-Scale Steady-State and Ambient Simulation with Realization #2 of the Heterogeneous Fracture Permeability Distribution. Submittal date: 05/07/2007.

LB0705THCSENR3.001. Input and Output Files of Drift-Scale Steady-State and THC Simulation with Water HDPERM3 (w0) and Realization #3 of the Heterogeneous Fracture Permeability Distribution. Submittal date: 05/07/2007.

LB0705THCSENR3.002. Input and Output Files of Drift-Scale Steady-State and TH Simulation with Realization #3 of the Heterogeneous Fracture Permeability Distribution. Submittal date: 05/07/2007.

LB0705THCSENR3.003. Input and Output Files of Drift-Scale Steady-State and Ambient Simulation with Realization #2 of the Heterogeneous Fracture Permeability Distribution. Submittal date: 05/07/2007.

LB0705THCSENR1.004. Input and Output Files of Drift-Scale Steady-State and THC Simulation with Water HDPERM3 (w0), and Realization #1 of the Heterogeneous Fracture Permeability Distribution for Sensitivity to Fracture Capillary-Strength Parameter. Submittal date: 05/21/2007.

LB0705THCSENR1.005. Input and Output Files of Drift-Scale Steady-State and TH Simulation with Realization #1 of the Heterogeneous Fracture Permeability Distribution for Sensitivity to Fracture Capillary-Strength Parameter. Submittal date: 05/21/2007.

LB0705THCSENR1.006. Input and Output Files of Drift-Scale Steady-State and Ambient Simulation with Realization #1 of the Heterogeneous Fracture Permeability Distribution for Sensitivity to Fracture Capillary-Strength Parameter. Submittal date: 05/21/2007.

LB0705THCSENR2.004. Input and Output Files of Drift-Scale Steady-State and THC Simulation with Water HDPERM3 (w0), and Realization #2 of the Heterogeneous Fracture Permeability Distribution for Sensitivity to Fracture Capillary-Strength Parameter. Submittal date: 05/21/2007.

LB0705THCSENR2.005. Input and Output Files of Drift-Scale Steady-State and TH Simulation with Realization #2 of the Heterogeneous Fracture Permeability Distribution for Sensitivity to Fracture Capillary-Strength Parameter. Submittal date: 05/21/2007.

LB0705THCSENR2.006. Input and Output Files of Drift-Scale Steady-State and Ambient Simulation with Realization #2 of the Heterogeneous Fracture Permeability Distribution. Submittal date: 05/21/2007.

LB0705THCSENR3.004. Input and Output Files of Drift-Scale Steady-State and THC Simulation with Water HDPERM3 (w0), and Realization #3 of the Heterogeneous Fracture Permeability Distribution for Sensitivity to Fracture Capillary-Strength Parameter. Submittal date: 05/30/2007.

LB0705THCSENR3.005. Input and Output Files of Drift-Scale Steady-State and TH Simulation with Realization #3 of the Heterogeneous Fracture Permeability Distribution for Sensitivity to Fracture Capillary-Strength Parameter. Submittal date: 05/21/2007.

LB0705THCSENR3.006. Input and Output Files of Drift-Scale Steady-State and Ambient Simulation with Realization #3 of the Heterogeneous Fracture Permeability Distribution for Sensitivity to Fracture Capillary-Strength Parameter. Submittal date: 05/21/2007.

LB0706THCSENPP.001. Supplemental Data Files for Postprocessing Procedures Described in Appendices D, E, and F of ANL-NBS-HS-000047 REV 01. Submittal date: 06/08/2007.

LB0706THCSENSC.001. Comparison of seepage water chemistry results from drift-scale THC simulations with and without fracture permeability heterogeneity for initial water HDPERM3 (w0). Submittal date: 06/08/2007.

LB0706THCSENFC.001. Estimation of capillary-strength parameter including Leverett scaling: simulation files. Submittal date: 06/08/2007.

8. INPUTS AND REFERENCES

8.1 DOCUMENTS CITED

103750 Altman, W.D.; Donnelly, J.P.; and Kennedy, J.E. 1988. *Qualification of Existing Data for High-Level Nuclear Waste Repositories: Generic Technical Position.* NUREG-1298. Washington, D.C.: U.S. Nuclear Regulatory Commission. TIC: 200652.

103597 Altman, W.D.; Donnelly, J.P.; and Kennedy, J.E. 1988. *Peer Review for High-Level Nuclear Waste Repositories: Generic Technical Position.* NUREG-1297. Washington, D.C.: U.S. Nuclear Regulatory Commission. TIC: 200651.

101379 Bear, J. 1988. *Dynamics of Fluids in Porous Media.* New York, New York: Dover Publications. TIC: 217568.

154608 Birkholzer, J.T. and Tsang, Y.W. 2000. "Modeling the Thermal-Hydrologic Processes in a Large-Scale Underground Heater Test in Partially Saturated Fractured Tuff." *Water Resources Research, 36,* (6), 1431-1447. Washington, D.C.: American Geophysical Union. TIC: 248278.

172262 Birkholzer, J.T.; Mukhopadhyay, S.; and Tsang, Y.W. 2004. "Modeling Seepage into Heated Waste Emplacement Tunnels in Unsaturated Fractured Rock." *Vadose Zone Journal, 3*. Madison, Wisconsin: Soil Science Society of America. TIC: 256702.

169131 BSC (Bechtel SAIC Company) 2004. *Abstraction of Drift Seepage.* MDL-NBS-HS-000019 REV 01. Las Vegas, Nevada: Bechtel SAIC Company. ACC: DOC.20041103.0003.

169855 BSC 2004. *Development of Numerical Grids for UZ Flow and Transport Modeling.* ANL-NBS-HS-000015 REV 02. Las Vegas, Nevada: Bechtel SAIC Company. ACC: DOC.20040901.0001.

168848 BSC (Bechtel SAIC Company) 2004. *Drift-Scale Coupled Processes (DST and THC Seepage) Models.* MDL-NBS-HS-000001 REV 02 Errata 002. Las Vegas, Nevada: Bechtel SAIC Company. ACC: DOC.20030804.0004; DOC.20040219.0002; DOC.20040405.0005.

164327 BSC 2004. *In-Drift Natural Convection and Condensation.* MDL-EBS-MD-000001 REV 00. Las Vegas, Nevada: Bechtel SAIC Company. ACC: DOC.20041025.0006; DOC.20050330.0001; DOC.20051122.0005.

169858 BSC 2004. *Post-Processing Analysis for THC Seepage.* ANL-NBS-HS-000045 REV 00. Las Vegas, Nevada: Bechtel SAIC Company. ACC: DOC.20040929.0002; DOC.20050606.0006.

171764 BSC 2004. *Seepage Calibration Model and Seepage Testing Data.* MDL-NBS-HS-000004 REV 03. Las Vegas, Nevada: Bechtel SAIC Company. ACC: DOC.20040922.0003; DOC.20051121.0012.

167652 BSC 2004. *Seepage Model for PA Including Drift Collapse.* MDL-NBS-HS-000002 REV 03. Las Vegas, Nevada: Bechtel SAIC Company. ACC: DOC.20040922.0008; DOC.20051205.0001.

169900 BSC 2004. *Thermal Testing Measurements Report.* TDR-MGR-HS-000002 REV 00. Las Vegas, Nevada: Bechtel SAIC Company. ACC: DOC.20040928.0005.

169862 BSC 2004. *Ventilation Model and Analysis Report.* ANL-EBS-MD-000030 REV 04. Las Vegas, Nevada: Bechtel SAIC Company. ACC: DOC.20041025.0002.

172232 BSC 2005. *Drift-Scale Coupled Processes (DST and TH Seepage) Models.* MDL-NBS-HS-000015 REV 02. Las Vegas, Nevada: Bechtel SAIC Company. ACC: DOC.20050114.0004; DOC.20051115.0002.

174101 BSC 2005. *Mountain-Scale Coupled Processes (TH/THC/THM) Models.* MDL-NBS-HS-000007 REV 03. Las Vegas, Nevada: Bechtel SAIC Company. ACC: DOC.20050825.0007.

175539 BSC 2005. *Q-List.* 000-30R-MGR0-00500-000-003. Las Vegas, Nevada: Bechtel SAIC Company. ACC: ENG.20050929.0008.

174104 BSC 2006. *THC Sensitivity Study of Repository Edge and Heterogeneous Permeability Effects.* ANL-NBS-HS-000047 REV 00. Las Vegas, Nevada: Bechtel SAIC Company. ACC: DOC.20060112.0001.

100617 Buscheck, T.A. and Nitao, J.J. 1993. "Repository-Heat-Driven Hydrothermal Flow at Yucca Mountain, Part I: Modeling and Analysis." *Nuclear Technology, 104,* (3), 418-448. La Grange Park, Illinois: American Nuclear Society. TIC: 224039.

160749 Buscheck, T.A.; Rosenberg, N.D.; Gansemer, J.; and Sun, Y. 2002. "Thermohydrologic Behavior at an Underground Nuclear Waste Repository." *Water Resources Research, 38,* (3), 10-1 through 10-19. Washington, D.C.: American Geophysical Union. TIC: 253566.

105210 Carlos, B.A.; Chipera, S.J.; Bish, D.L.; and Craven, S.J. 1993. "Fracture-Lining Manganese Oxide Minerals in Silicic Tuff, Yucca Mountain, Nevada, U.S.A." *Chemical Geology, 107,* 47-69. Amsterdam, The Netherlands: Elsevier. TIC: 208629.

153314 CRWMS M&O 2000. *Seepage Model for PA Including Drift Collapse.* MDL-NBS-HS-000002 REV 01. Las Vegas, Nevada: CRWMS M&O. ACC: MOL.20010221.0147.

151875 Finsterle, S. 2000. "Using the Continuum Approach to Model Unsaturated Flow in Fractured Rock." *Water Resources Research, 36,* (8), 2055-2066. Washington, D.C.: American Geophysical Union. TIC: 248769.

163214 Finsterle, S.; Ahlers, C.F.; Trautz, R.C.; and Cook, P.J. 2003. "Inverse and Predictive Modeling of Seepage into Underground Openings." *Journal of Contaminant Hydrology, 62-63,* 89-109. New York, New York: Elsevier. TIC: 254205.

127326 Francis, N.D. 1997. "The Base-Case Thermal Properties for TSPA-VA Modeling." Memorandum from N.D. Francis (SNL) to Distribution, April 16, 1997. ACC: MOL.19980518.0229.

181353 Grinstead, C.M. and Snell, J.L. 1997. I*ntroduction to Probability*. Second Revised Edition. 510pp. Providence, RI: American Mathematical Society. TIC: 259520.

100350 Hardin, E.L. 1998. *Near-Field/Altered-Zone Models Report.* UCRL-ID-129179 DR. Livermore, California: Lawrence Livermore National Laboratory. ACC: MOL.19980504.0577.

137562 Haukwa, C.B.; Wu, Y-S.; and Bodvarsson, G.S. 1999. "Thermal Loading Studies Using the Yucca Mountain Unsaturated Zone Model." *Journal of Contaminant Hydrology, 38,* (1-3), 217-255. New York, New York: Elsevier. TIC: 244160.

165165 Haukwa, C.B.; Wu, Y-S.; and Bodvarsson, G.S. 2003. "Modeling Thermal–Hydrological Response of the Unsaturated Zone at Yucca Mountain, Nevada, to Thermal Load at a Potential Repository." *Journal of Contaminant Hydrology, 62-63,* 529-552. New York, New York: Elsevier. TIC: 254205.

141523 Jackson, C.P.; Hoch, A.R.; and Todman, S. 2000. "Self-Consistency of a Heterogeneous Continuum Porous Medium Representation of a Fractured Medium." *Water Resources Research, 36,* (1), 189-202. Washington, D.C.: American Geophysical Union. TIC: 247466.

139133 Kneafsey, T.J. and Pruess, K. 1998. "Thermohydrological Laboratory Tests-Insights into Processes and Behavior." *High-Level Radioactive Waste Management, Proceedings of the Eighth International Conference, Las Vegas, Nevada, May 11-14, 1998.* Pages 261-263. La Grange Park, Illinois: American Nuclear Society. TIC: 237082.

117091 Lasaga, A.C. 1998. *Kinetic Theory in the Earth Sciences.* Princeton, New Jersey: Princeton University Press. TIC: 246279.

100588 Leverett, M.C. 1941. "Capillary Behavior in Porous Solids." *AIME Transactions, Petroleum Development and Technology, Tulsa Meeting, October 1940. 142,* 152-169. New York, New York: American Institute of Mining and Metallurgical Engineers. TIC: 240680.

163714 Li, G. and Tsang, C-F. 2003. "Seepage into Drifts with Mechanical Degradation." *Journal of Contaminant Hydrology, 62-63,* 157-172. New York, New York: Elsevier. TIC: 254205.

105729 Liu, H.H.; Doughty, C.; and Bodvarsson, G.S. 1998. "An Active Fracture Model for Unsaturated Flow and Transport in Fractured Rocks." *Water Resources Research, 34,* (10), 2633-2646. Washington, D.C.: American Geophysical Union. TIC: 243012.

160788 Mukhopadhyay, S. and Tsang, Y.W. 2002. "Understanding the Anomalous Temperature Data from the Large Block Test at Yucca Mountain, Nevada." *Water Resources Research, 38,* (10), 28-1 through 28-12. Washington, D.C.: American Geophysical Union. TIC: 253867.

160790 Mukhopadhyay, S. and Tsang, Y.W. 2003. "Uncertainties in Coupled Thermal–Hydrological Processes Associated with the Drift Scale Test at Yucca Mountain, Nevada." *Journal of Contaminant Hydrology, 62-63,* 595-612. New York, New York: Elsevier. TIC: 254205.

180822 Mukhopadhyay, S.; Sonnenthal, E.L.; and Spycher, N. 2006. "Modeling Coupled Thermal-Hydrological-Chemical Processes in the Unsaturated Fractured Rock of Yucca Mountain, Nevada: Heterogeneity and Seepage." *Physics and Chemistry of the Earth, 31,* 626-633. New York, New York: Elsevier. TIC: 259367.

163274 NRC (U.S. Nuclear Regulatory Commission) 2003. *Yucca Mountain Review Plan, Final Report.* NUREG-1804, Rev. 2. Washington, D.C.: U.S. Nuclear Regulatory Commission, Office of Nuclear Material Safety and Safeguards. TIC: 254568.

144773 Or, D. and Ghezzehei, T.A. 2000. "Dripping into Subterranean Cavities from Unsaturated Fractures under Evaporative Conditions." *Water Resources Research, 36,* (2), 381-393. Washington, D.C.: American Geophysical Union. TIC: 246982.

162576 Peterman, Z.E. and Cloke, P.L. 2002. "Geochemistry of Rock Units at the Potential Repository Level, Yucca Mountain, Nevada (includes Erratum)." *Applied Geochemistry, 17,* (6, 7), 683-698, 955-958. New York, New York: Pergamon. TIC: 252516; 252517; 254046.

105743 Philip, J.R.; Knight, J.H.; and Waechter, R.T. 1989. "Unsaturated Seepage and Subterranean Holes: Conspectus, and Exclusion Problem for Circular Cylindrical Cavities." *Water Resources Research, 25,* (1), 16-28. Washington, D.C.: American Geophysical Union. TIC: 239117.

144794 Pruess, K. 1997. "On Vaporizing Water Flow in Hot Sub-Vertical Rock Fractures." *Transport in Porous Media, 28,* (3), 335-372. Boston, Massachusetts: Kluwer Academic Publishers. TIC: 238922.

144801 Pruess, K.; Tsang, Y.W.; and Wang, J.S.Y. 1984. *Numerical Studies of Fluid and Heat Flow Near High-Level Nuclear Waste Packages Emplaced in Partially Saturated Fractured Tuff.* LBL-18552. Berkeley, California: Lawrence Berkeley Laboratory. TIC: 211033.

100819 Pruess, K.; Wang, J.S.Y.; and Tsang, Y.W. 1990. "On Thermohydrologic Conditions Near High-Level Nuclear Wastes Emplaced in Partially Saturated Fractured Tuff, 2. Effective Continuum Approximation." *Water Resources Research, 26,* (6), 1249-1261. Washington, D.C.: American Geophysical Union. TIC: 224854.

179545 SNL (Sandia National Laboratories) 2007. *Calibrated Unsaturated Zone Properties.* ANL-NBS-HS-000058 REV 00. Las Vegas, Nevada: Sandia National Laboratories. ACC: DOC.20070530.0013.

177404 SNL 2007. *Drift-Scale THC Seepage Model.* MDL-NBS-HS-000001 REV 05. Las Vegas, Nevada: Sandia National Laboratories.

177412 SNL 2007. *Engineered Barrier System: Physical and Chemical Environment.* ANL-EBS-MD-000033 REV 06. Las Vegas, Nevada: Sandia National Laboratories.

179287 SNL 2007. *Technical Work Plan for: Revision of Model Reports for Near-Field and In-Drift Water Chemistry.* TWP-MGR-PA-000038 REV 02. Las Vegas, Nevada: Sandia National Laboratories. ACC: DOC.20070110.0004.

179466 SNL 2007. *Total System Performance Assessment Data Input Package for Requirements Analysis for Subsurface Facilities.* TDR-TDIP-PA-000001 REV 00. Las Vegas, Nevada: Sandia National Laboratories.

176005 Sonnenthal E.; Ito, A.; Spycher, N.; Yui, M.; Apps, J.; Sugita, Y.; Conrad, M.; and Kawakami, S. 2005. "Approaches to Modeling Coupled Thermal, Hydrological, and Chemical Processes in the Drift Scale Heater Test at Yucca Mountain." *International Journal of Rock Mechanics and Mining Sciences, 42,* 698-719. New York, New York: Elsevier. TIC: 258018.

162121 Spycher, N.F.; Sonnenthal, E.L.; and Apps, J.A. 2003. "Fluid Flow and Reactive Transport Around Potential Nuclear Waste Emplacement Tunnels at Yucca Mountain, Nevada." *Journal of Contaminant Hydrology, 62-63,* 653-673. New York, New York: Elsevier. TIC: 254205.

101480 Steefel, C.I. and Lasaga, A.C. 1994. "A Coupled Model for Transport of Multiple Chemical Species and Kinetic Precipitation/Dissolution Reactions with Application to Reactive Flow in Single Phase Hydrothermal Systems." *American Journal of Science, 294,* (5), 529-592. New Haven, Connecticut: Yale University, Kline Geology Laboratory. TIC: 235372.

160335 Trautz, R.C. and Wang, J.S.Y. 2002. "Seepage into an Underground Opening Constructed in Unsaturated Fractured Rock Under Evaporative Conditions." *Water Resources Research, 38,* (10), 6-1 through 6-14. Washington, D.C.: American Geophysical Union. TIC: 253348.

137577 Tsang, Y.W. and Birkholzer, J.T. 1999. "Predictions and Observations of the Thermal-Hydrological Conditions in the Single Heater Test." *Journal of Contaminant Hydrology, 38,* (1-3), 385-425. New York, New York: Elsevier. TIC: 244160.

100610 van Genuchten, M.T. 1980. "A Closed-Form Equation for Predicting the Hydraulic Conductivity of Unsaturated Soils." *Soil Science Society of America Journal, 44,* (5), 892-898. Madison, Wisconsin: Soil Science Society of America. TIC: 217327.

157427 Vaniman, D.T.; Chipera, S.J.; Bish, D.L.; Carey, J.W.; and Levy, S.S. 2001. "Quantification of Unsaturated-Zone Alteration and Cation Exchange in Zeolitized Tuffs at Yucca Mountain, Nevada, USA." *Geochimica et Cosmochimica Acta, 65,* (20), 3409-3433. New York, New York: Elsevier. TIC: 251574.

106146 Wang, J.S.Y.; Trautz, R.C.; Cook, P.J.; Finsterle, S.; James, A.L.; and Birkholzer, J. 1999. "Field Tests and Model Analyses of Seepage into Drift." *Journal of Contaminant Hydrology, 38,* (1-3), 323-347. New York, New York: Elsevier. TIC: 244160.

180274 Wu, Y-S.; Mukhopadhyay, S.; Zhang, K.; and Bodvarsson, G.S. 2006. "A Mountain-Scale Thermal–Hydrologic Model for Simulating Fluid Flow and Heat Transfer in Unsaturated Fractured Rock." *Journal of Contaminant Hydrology, 86,* 128-159. New York, New York: Elsevier. TIC: 259285.

8.2 CODES, STANDARDS, REGULATIONS, AND PROCEDURES

173273 10 CFR 63. 2005 Energy: Disposal of High-Level Radioactive Wastes in a Geologic Repository at Yucca Mountain, Nevada. ACC: MOL.20050405.0118.

AP-16.1Q, Rev. 10, ICN 1. *Condition Reporting and Resolution*. Washington, D.C.: U.S. Department of Energy, Office of Civilian Radioactive Waste Management. ACC: DOC.20070302.0002.

IM-PRO-002, Rev. 0, ICN 0. *Control of the Electronic Management of Information*. Washington, D.C.: U.S. Department of Energy, Office of Civilian Radioactive Waste Management. ACC: DOC.20060927.0023.

IM-PRO-003, Rev. 2, ICN 0. *Software Management*. Washington, D.C.: U.S. Department of Energy, Office of Civilian Radioactive Waste Management. ACC: DOC.20070228.0002.

SCI-PRO-005, Rev. 4, ICN 0. *Scientific Analyses and Calculations*. Washington, D.C.: U.S. Department of Energy, Office of Civilian Radioactive Waste Management. ACC: DOC.20070718.001.

YMP-LBNL-QIP-SV.0, Rev. 2, Mod. 1. Management of YMP-LBNL Electronic Data. Berkeley, California: Lawrence Berkeley National Laboratory. ACC: MOL.20020717.0319.

8.3 SOURCE DATA, LISTED BY DATA TRACKING NUMBER

113495 LA9908JC831321.001. Mineralogic Model "MM3.0" Version 3.0. Submittal date: 08/16/1999.

146447 LA9912SL831151.001. Fracture Mineralogy of Drill Core ESF-HD-TEMP-2. Submittal date: 01/04/2000.

146449 LA9912SL831151.002. Percent Coverage by Fracture-Coating Minerals in Core ESF-HD-TEMP-2. Submittal date: 01/05/2000.

159525 LB0205REVUZPRP.001. Fracture Properties for UZ Model Layers Developed from Field Data. Submittal date: 05/14/2002.

161243 LB0208UZDSCPMI.002. Drift-Scale Calibrated Property Sets: Mean Infiltration Data Summary. Submittal date: 08/26/2002.

162273 LB0302SCMREV02.002. Seepage-Related Model Parameters K and 1/A: Data Summary. Submittal date: 02/28/2003.

173235 LB0304SMDCREV2.001. Seepage Modeling for Performance Assessment, Including Drift Collapse: Input/Output Files. Submittal date: 04/11/2003.

173280 LB0407AMRU0120.001. Supporting Calculations and Analysis for Seepage Abstraction and Summary of Abstraction Results. Submittal date: 07/29/2004.

179180 LB0610UZDSCP30.001. Drift-Scale Calibrated Property Set for the 30-Percentile Infiltration Map. Submittal date: 11/02/2006.

179286 LB0701UZMTHCAL.001. Input and Output of 3-D UZ Ambient Thermal Model for Present-Day Climate of 10th-, 30th-, 50th- and 90th-Percentile Infiltration Maps. Submittal date: 01/22/2007. TBV-7851

180853 LB0704DSSSTFLW.002. 1-D and 2-D Drift-Scale Steady-State Flow Field Simulations. Submittal date: 04/23/2007.

181217 LB0705DSTHC001.001. Drift-Scale THC Simulation Results with Water HDPERM3 (w0). Submittal date: 05/02/2007.

180854 LB0705DSTHC001.002. Input and Output Files of Drift-Scale THC Simulations with Water HDPERM3 (W0). Submittal date: 05/02/2007.

104055 LB997141233129.001. Calibrated Base-case Infiltration 1-D Parameter Set for the UZ Flow and Transport Model, FY99. Submittal date: 07/21/1999.

150930 MO0005PORWATER.000. Perm-Sample Pore Water Data. Submittal date: 05/04/2000.

170541 MO0406MWDAC8VD.001. Analytical-LA-COARSE-800M Ventilation with the Delta Method Analysis. Submittal date: 06/04/2004.

181613 MO0706SPAFEPLA.001. FY 2007 LA FEP List and Screening. Submittal date: 06/20/2007.

180552 MO0612MEANTHER.000. Mean Thermal Conductivity of Yucca Mountain Repository Units. Submittal date: 04/27/2007.

162401 SN0303T0503102.008. Revised Thermal Conductivity of the Non-Repository Layers of Yucca Mountain. Submittal date: 03/19/2003.

164196 SN0307T0510902.003. Updated Heat Capacity of Yucca Mountain Stratigraphic Units. Submittal date: 07/15/2003.

8.4 SOFTWARE CODES

152822 AddBorehole VV1.0. 2000. SUN w/Unix OS. 10373-1.0-00.

152823 AddBound VV1.0. 2000. SUN w/Unix OS. 10357-1.0-00.

175950 avgperm.f V. 1.0. 2000. SUN, DEC, SUN OS 5.5.1, Os1f V4.0. STN: 10378-1.0-00.

181352 CUTCHEM V2.0. 2007. PC, Windows XP/32bit. 10898-2.0-00.

152816 CutDrift VV1.0. 2000. SUN w/Unix OS. 10375-1.0-00.

175981 GSLIB V. 1.0SISIMV1.204. 2000. SUN, SUN O.S. 5.5.1.
STN: 10397-1.0SISIMV1.204-00.

160106 iTOUGH2 V. 5.0. 2002. SunOS 5.5.1, OSF1 V5.1, RedHat V7.2 and V7.3.
STN: 10003-5.0-00.

152824 MoveMesh V. 1.0. 2000. SUN O.S. 5.5.1. STN: 10358-1.0-00.

152826 Perm2Mesh VV1.0. 2000. SUN w/Unix OS. 10359-1.0-00.

180937 TOUGHREACT V3.1.1. 2007. Alpha System OSF1.V5.1. 10396-3.1.1-00.

APPENDIX A.1

INPUT AND OUTPUT FILES FOR GENERATING HETEROGENEOUS FRACTURE PERMEABILITY IN DTN: LB0705THCSENHF.001

INTENTIONALLY LEFT BLANK

Generic Input and Output File Names

Three heterogeneous fracture permeability fields were generated: These are given in the folders **\realization#1**, **\realization#2**, and **\realization#3**. Also, for the sensitivity studies, starting points ("INCON" files) with and without Leverett-scaling effects are needed. These are given in the folders **\leveret.dir** and **\no_leverett.dir**.

The heterogeneous fracture permeability distribution was generated in two steps. First, log permeability modifiers were calculated using GSLIB V1.0 module SISIM V1.204 (see Section 3.1 and Table 3-1). The input and output files for these calculations can be found in the folder **\xsisim.dir**. In the second step, the log permeability modifiers obtained in the first step are mapped onto the THC seepage model numerical mesh. This second step was accomplished using avgperm.f V1.0 (see Table 3-1). The input and output files can be found in the folder **\avgperm.dir**. The contents of each of these folders are further explained below.

1. Folder **\xsisim.dir**

Input File

a. perm.par: This file contains the permeability distribution information obtained from DTN: LB0304SMDCREV2.001 [DIRS 173235]. The file "perm.par" is used by GSLIB V1.0 module SISIM V1.204 (see Section 3.1 and Table 3-1).

Output File

a. perm.dat: This file provides the log permeability modifiers at 0.2 m spacing in both the horizontal and vertical directions. This file is used in the next step (see below) to generate the heterogeneous fracture permeability distribution.

README

A "README" file has been provided to assist users with these procedures.

2. Folder **\avgperm.dir**

Input Files

a. fract*a.dat, where * can be 1, 2, or 3: This file is a copy of the "perm.dat" file discussed above, except the total number of data points (389,500) is added at the top.

b. MESH: This is the numerical mesh on which the fracture permeabilities are mapped. This mesh is obtained from DTN: LB0704DSSSTFLW.002 [DIRS 180853] (file: "MESH" in folder **\2dflow_81m**).

c. INCON_start: This file contains some arbitrary initial condition values (pressure, gas saturation or temperature, and saturation pressure) for each element in the numerical mesh. It also has the homogeneous permeability and porosity for each element of the mesh.

d. inp_avgperm_real*, where * can be 1, 2, or 3: This file contains a list of input files (including those listed in items a through c above) expected by avgperm.f V1.0 (see Table 3-1).

Output Files

a. incon_real*, where * can be 1, 2, or 3: This file is used as the initial condition (INCON) file for the steady-state (preheating) simulations.

README

A "README" file has been provided to assist users with these procedures.

Organization of Data Files

The organization of data files in this DTN is summarized Figure A.1-1 below.

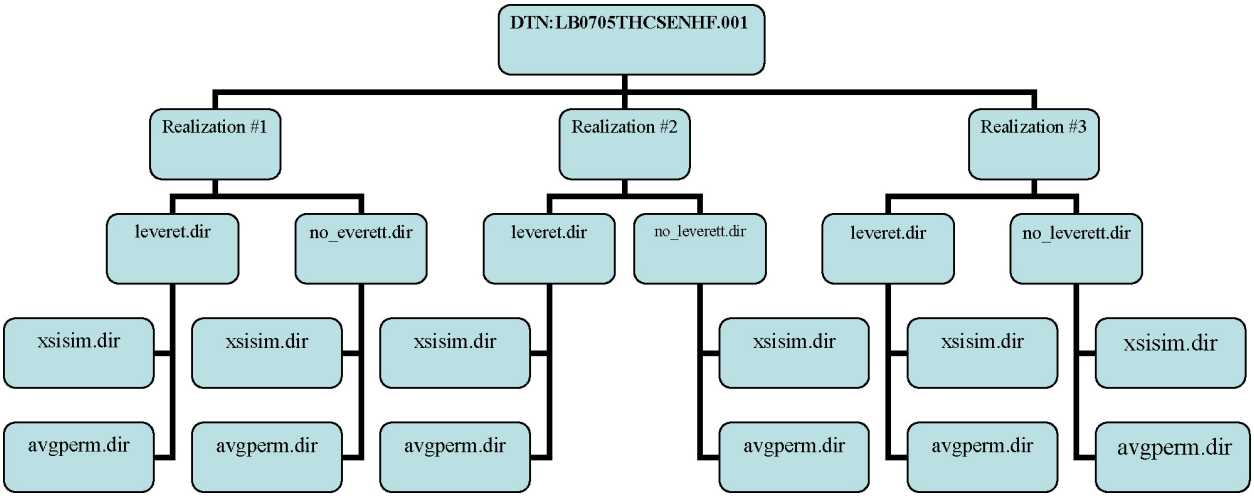

Figure A.1-1. Organization of Folders in DTN: LB0705THCSENHF.001

APPENDIX A.2

LIST OF INPUT AND OUTPUT FILES SUBMITTED TO TDMS FOR STEADY-STATE AND THC SIMULATIONS IN DTNS: LB0705THCSENR1.001, LB0705THCSENR2.001, LB0705THCSENR3.001, LB0705THCSENR1.004, LB0705THCSENR2.004, AND LB0705THCSENR3.004

INTENTIONALLY LEFT BLANK

The structure of input and output file names for steady-state and THC simulations is explained with respect to the simulations with Realization #1 of the heterogeneous fracture permeability fields. These data were submitted to the TDMS as Output DTN: LB0705THCSENR1.001. THC simulation data with other realizations of the fracture permeability field and with different fracture capillary-strength parameters have also been submitted (such as Output DTNs: LB0705THCSENR2.001, LB0705THCSENR3.001, LB0705THCSENR1.004, LB0705THCSENR2.004, and LB0705THCSENR3.004). These DTNs have similar input/output file structures.

Generic Input and Output File Names in DTN: LB0705THCSENR1.001

To carry out the THC simulations, the initial hydrological conditions need to be obtained by running the model over a long time without application of heat, chemistry, or the emplacement drift until steady-state conditions are reached. These simulations are termed the steady-state simulations, and will henceforth be called **STEADY** simulations. The simulations that account for heat, chemistry, and emplacement drift will be termed **THC** simulations.

The generic input and output file names for the STEADY simulations are given in Table A.2-1.

Table A.2-1. Generic Input and Output File Names for STEADY Simulations

flow.inp	Rock thermal and hydrologic properties, run flags, and other specifications (input)
flow.out	Thermal and hydrologic results (gas/liquid saturation, T, P, air mass fraction, etc.) (output)
GENER	Infiltration rates (input)
INCON	Initial thermal and hydrologic conditions (T, P, liquid saturation, etc.) – this can be arbitrary (input)
MESH	Input numerical mesh without the emplacement drifts (input)
SAVE	Thermal and hydrologic conditions (T, P, liquid saturation, etc.) at the end of the steady-state run (output)
run.t2react	Script file for running the steady-state simulations
sub*.sh	Script file for submitting batch jobs to the computing cluster

Compared to the STEADY simulations, many more input files are needed for the THC simulations and many more output files are produced by the simulations. The generic names of input and output files for the THC simulations are given in Table A.2-2.

Table A.2-2. Generic Input and Output File Names for THC Simulations

flow.inp	Rock thermal and hydrologic properties, run flags, and other specifications (input)
flow.out	Thermal and hydrologic results (gas/liquid saturation, T, P, air mass fraction, etc.) (output)
GENER	Infiltration rates, heat load, and effective thermal conductivity (input)

Table A.2-2. Generic Input and Output File Names for THC Simulations (Continued)

INCON	Initial thermal and hydrologic conditions (T, P, liquid saturation, etc.) (input)
MESH	Input numerical mesh (input)
SAVE	Thermal and hydrologic conditions (T, P, liquid saturation, etc.) to use for restarting a run (output, same format as INCON file)
chemical.inp	Water chemistry, mineralogy, and CO_2 partial pressure data (input)
chemical.out	Echo of data read in chemical.inp
solute.inp	Run flags and other data relating to reactive transport (input)
solute.out	Echo of data read in solute.inp
thc_ymp1.1.dat	Thermodynamic database (input). Note: The solid KNO_3 in this file is actually $NaNO_3$
tec_conc.dat	Calculated concentrations of aqueous species (moles/liter) at each grid node (two records for each node—first record for fractures and second record for matrix) (output)
tec_min.dat	Calculated volume fraction change for minerals at each grid node (two records for each node—first record for fractures and second record for matrix) (output)
tec_gas.dat	Calculated CO_2 volume fraction at each grid node (two records for each node—first record for fractures and second record for matrix) (output)
time.dat	Chemical data at selected grid nodes (output)
chdump.out	Chemical speciation of initial water (output) and nodes with convergence problems
inchem	Chemistry data at all grid nodes to use for restarting a run (input)
savechem	Chemistry data at all grid nodes to use for restarting a run (output, same format as inchem file)
iter.dat	Iteration information (output)
runlog.out	Miscellaneous run-time information. Note: Mass balances may not be printed out correctly in this file for runs that have been restarted (i.e., starting at times different than zero)
mbalance.out	Mass balance information for chemical species. Note: Mass balances may not be accurate for runs that have been restarted (i.e., starting at times different than zero). Also, mass balances do not reflect mass loss by transport into large boundary gridblocks
GASOBS.DAT	Optional tabular flow output for individual grid
rctn_rate.out	Calculated reaction rates of kinetics-controlled minerals at each grid node (two records for each node—first record for fractures and second record for matrix) (output)
min_SI.out	Calculated saturation index for minerals at each grid node (two records for each node—first record for fractures and second record for matrix) (output)
run.t2react	Script file for running the simulations
sub*.sh	Script file for submitting jobs to the computing cluster

Organization of File Folders

The organization of file folders in this DTN is shown in the organization chart below (Figure A.2-1). In the following, the logic behind the organization of the file folders is explained.

1. STEADY Simulations

The STEADY simulations were performed for two scenarios:

a. Leverett scaling (i.e., capillarity changes because of differences in permeability) is included – these simulations are included in folder **leverett**.

b. Leverett scaling (i.e., capillarity changes because of differences in permeability) is *not* included – these simulations are included in folder **no_leverett**.

2. THC Simulations

At the first level, THC simulations are performed with two sets of infiltration fluxes:

i. The infiltration fluxes are 7.96, 12.89, and 20.45 mm/yr, respectively, between 0 to 600, 600 to 2,000, and beyond 2,000 years (the source of these infiltration flux data is DTN: LB0705DSTHC001.002 [DIRS 180854]; also see Section 4.1.4 and Table 4.1-5 of SNL 2007 [DIRS 177404]) – these simulations are included in folder **focus_1**. These are also the *base-case* simulations.

ii. The infiltration fluxes are ten times the fluxes in (i) above in each time period, i.e., the infiltration fluxes are 79.6 (0 to 600 years), 128.9 (600 to 2,000 years), and 204.5 mm/yr (beyond 2,000 years). These simulations are included in folder **focus_10**.

Subsequently, The simulations were performed for either with Leverett scaling (folder: **leverett**) or without Leverett scaling (folder: **no_leverett**).

Furthermore, simulations were performed with a fracture capillary-strength parameter of 0.5750×10^{-3} Pa^{-1}. The source of this fracture capillary-strength parameter (for the host rock "Tptpll" or "tsw35") is DTN: LB0705DSTHC001.002 [DIRS 180854], file "flow.inp," which corresponds to the 30th percentile parameter set. Hence the subfolder names of **alpha_fy07_30pc**.

In each of these subfolders, the actual THC simulations were performed in four temporal stages:

A. Simulations between 0 and 50 years: folder **thc_0_50**
B. Simulations between 50 and 600 years: folder **thc_50_600**
C. Simulations between 600 and 2,000 years: folder **thc_600_2000**
D. Simulations between 2,000 and 10,000 years: folder **thc_2000_10000**.

If a particular simulation for a particular time period could not be completed for numerical reasons, it was restarted in a subfolder **restart** within the folder for that time period (Note that

restarting was necessary for the following situation: If an element had a gas saturation of 1.000 (at the time the "numerical problem" happened) and water tries to get in, the simulation slowed down to unacceptable levels on rare occasions. The gas saturation was then manually changed from 1.0000 to 0.999999999… for that element, and the simulation was restarted.) Since these were rare occurrences (i.e., the restart of the simulations), they have not been included in the organization chart (Figure A.2-1) below.

NOTE: The "SAVE" and "savechem" files from **thc_0_50** are used as "INCON" and "inchem" files in **thc_50_600**. The "SAVE" and "savechem" files from **thc_50_600** are used as "INCON" and "inchem" files in **thc_600_2000**. Similarly, the "SAVE" and "savechem" files from **thc_600_2000** are used as "INCON" and "inchem" files in **thc_2000_10000**.

NOTE: The simulation corresponding to "focus_10/leveret" in DTN: LB0705THCSENR1.001 could not be completed (see Table 6.6-1). Hence the input/output files for that particular simulation were not submitted to the TDMS. This was an exception as the "focus_10/leveret" THC simulations in all other DTNs (LB0705THCSENR2.001, LB0705THCSENR3.001, LB0705THCSENR1.004, LB0705THCSENR2.004, and LB0705THCSENR3.004) were completed.

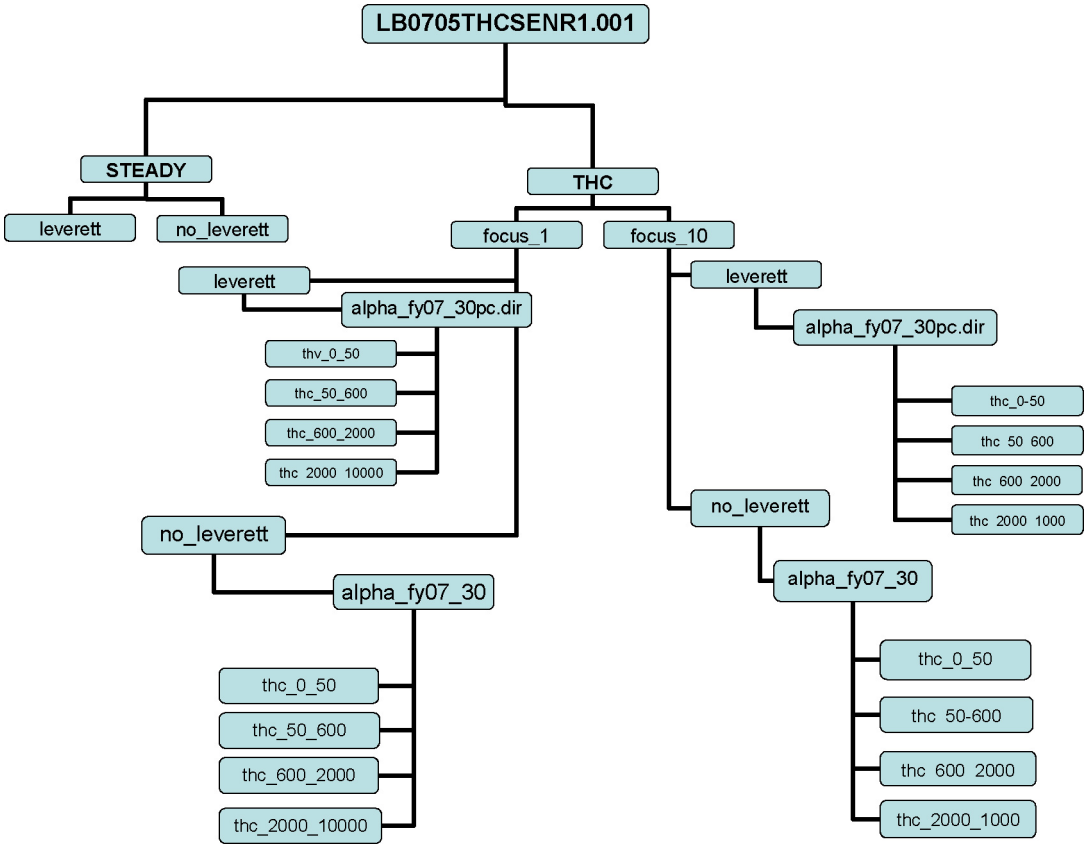

Figure A.2-1. Organization Chart of Folders Containing STEADY and THC Simulation Input and Output Files

APPENDIX A.3

LIST OF INPUT AND OUTPUT FILES SUBMITTED TO TDMS FOR STEADY-STATE AND TH SIMULATIONS IN DTNS: LB0705THCSENR1.002, LB0705THCSENR2.002, LB0705THCSENR3.002, LB0705THCSENR1.005, LB0705THCSENR2.005, AND LB0705THCSENR3.005

INTENTIONALLY LEFT BLANK

The structure of input and output file names for steady-state and TH simulations are explained with respect to the simulations with Realization #1 of the heterogeneous fracture permeability field. These data were submitted to the TDMS as Output DTN: LB0705THCSENR1.002. TH simulation data with other realizations of the fracture permeability field and with different fracture capillary-strength parameters have also been submitted (such as Output DTNs: LB0705THCSENR2.002, LB0705THCSENR3.002, LB0705THCSENR1.005, LB0705THCSENR2.005, and LB0705THCSENR3.005). These DTNs have similar input/output file structures.

Generic Contents of LB0705THCSENR1.002

To carry out the TH simulations, the initial hydrological conditions need to be obtained by running the model over a long time without application of heat, chemistry, or the emplacement drift till steady-state conditions are reached. These simulations are termed the steady-state simulations, and will henceforth be called **STEADY** simulations. The simulations which account for heat and emplacement drifts (but no chemistry) will be termed **TH** simulations.

The generic input and output file names for the STEADY simulations are given in Table A.3-1.

Table A.3-1. Generic Input and Output File Names for STEADY Simulations

flow.inp	Rock thermal and hydrologic properties, run flags, and other specifications (input)
flow.out	Thermal and hydrologic results (gas/liquid saturation, T, P, air mass fraction, etc.) (output)
GENER	Infiltration rates (input)
INCON	Initial thermal and hydrologic conditions (T, P, liquid saturation, etc.) – this can be arbitrary (input)
MESH	Input numerical mesh without the emplacement drifts (input)
SAVE	Thermal and hydrologic conditions (T, P, liquid saturation, etc.) at the end of the steady-state run (output)
run.t2react	Script file for running the steady-state simulations
sub*.sh	Script file for submitting batch jobs to the computing cluster

The generic names of input and output files for the TH simulations are given in Table A.3-2.

Table A.3-2. Generic Input and Output File Names for TH Simulations

flow.inp	Rock thermal and hydrologic properties, run flags, and other specifications (input)
flow.out	Thermal and hydrologic results (gas/liquid saturation, T, P, air mass fraction, etc.) (output)
GENER	Infiltration rates, heat load, and effective thermal conductivity (input)
INCON	Initial thermal and hydrologic conditions (T, P, liquid saturation, etc.) (input)
MESH	Input numerical mesh (input)
SAVE	Thermal and hydrologic conditions (T, P, liquid saturation, etc.) to use for restarting a run (output, same format as INCON file) (output)
GASOBS.DAT	Optional tabular flow output for individual grid (output)
run.t2react	Script file for running the simulations
sub*.sh	Script file for submitting jobs to the computing cluster

Organization of File Folders

The organization of file folders in this DTN is shown in the organization chart below (Figure A.3-1). The following explains the logic behind the organization of the file folders.

1. STEADY Simulations

The STEADY simulations were performed for two scenarios:

a. Leverett scaling (i.e., capillarity changes because of differences in permeability) is included – these simulations are included in folder **leverett**.

b. Leverett scaling (i.e., capillarity changes because of differences in permeability) is *not* included – these simulations are included in folder **no_leverett**.

2. TH Simulations

At the first level, TH simulations are performed with two sets of infiltration fluxes:

i. The infiltration fluxes are 7.96, 12.89, and 20.45 mm/yr, respectively, between 0 to 600, 600 to 2,000, and beyond 2,000 years (the source of these infiltration flux data is DTN: LB0705DSTHC001.002 [DIRS 180854]; also see Section 4.1.4 and Table 4.1-5 of SNL 2007 [DIRS 177404]) – these simulations are included in folder **focus_1**. These are also the *base-case* simulations.

ii. The infiltration fluxes are ten times the fluxes in (i) above in each time period, i.e., the infiltration fluxes are 79.6 (0 to 600 years), 128.9 (600 to 2,000 years), and 204.5 mm/yr (beyond 2,000 years). These simulations are included in folder **focus_10**.

Subsequently, the simulations were performed for either with Leverett scaling (folder: **leverett**) or without Leverett scaling (folder: **no_leverett**).

Furthermore, simulations were performed with a fracture capillary-strength parameter of 0.5750×10^{-3} Pa^{-1}. The source of this fracture capillary-strength parameter (for the host rock "Tptpll" or "tsw35") is DTN: LB0705DSTHC001.002 [DIRS 180854], file: "flow.inp," which corresponds to the 30th percentile parameter set. Hence the subfolder names of **alpha_fy07_30pc**.

In each of these subfolders, the actual TH simulations were performed in four temporal stages:

A. Simulations between 0 and 50 years: folder **th_0_50**
B. Simulations between 50 and 600 years: folder **th_50_600**
C. Simulations between 600 and 2,000 years: folder **th_600_2000**
D. Simulations between 2,000 and 10,000 years: folder **th_2000_10000**.

If a particular simulation for a particular time period could not be completed for numerical reasons, it was restarted in a subfolder **restart** within the folder for that time period (Note that restarting was necessary the following situation: If an element had a gas saturation of 1.000 (at the time the "numerical problem" happened) and water tries to get in, the simulation slowed down to unacceptable levels on rare occasions. The gas saturation was then manually changed from 1.0000 to 0.999999999… for that element, and the simulation was restarted.) Since these were rare occurrences (i.e., restart of the simulations), they have not been included in the organization chart (Figure A.3-1) below.

NOTE: The "SAVE" files from **th_0_50** are used as "INCON" files in **th_50_600**. The "SAVE" files from **th_50_600** are used as "INCON" files in **th_600_2000**. Similarly, the "SAVE" files from **th_600_2000** are used as "INCON" files in **th_2000_10000**.

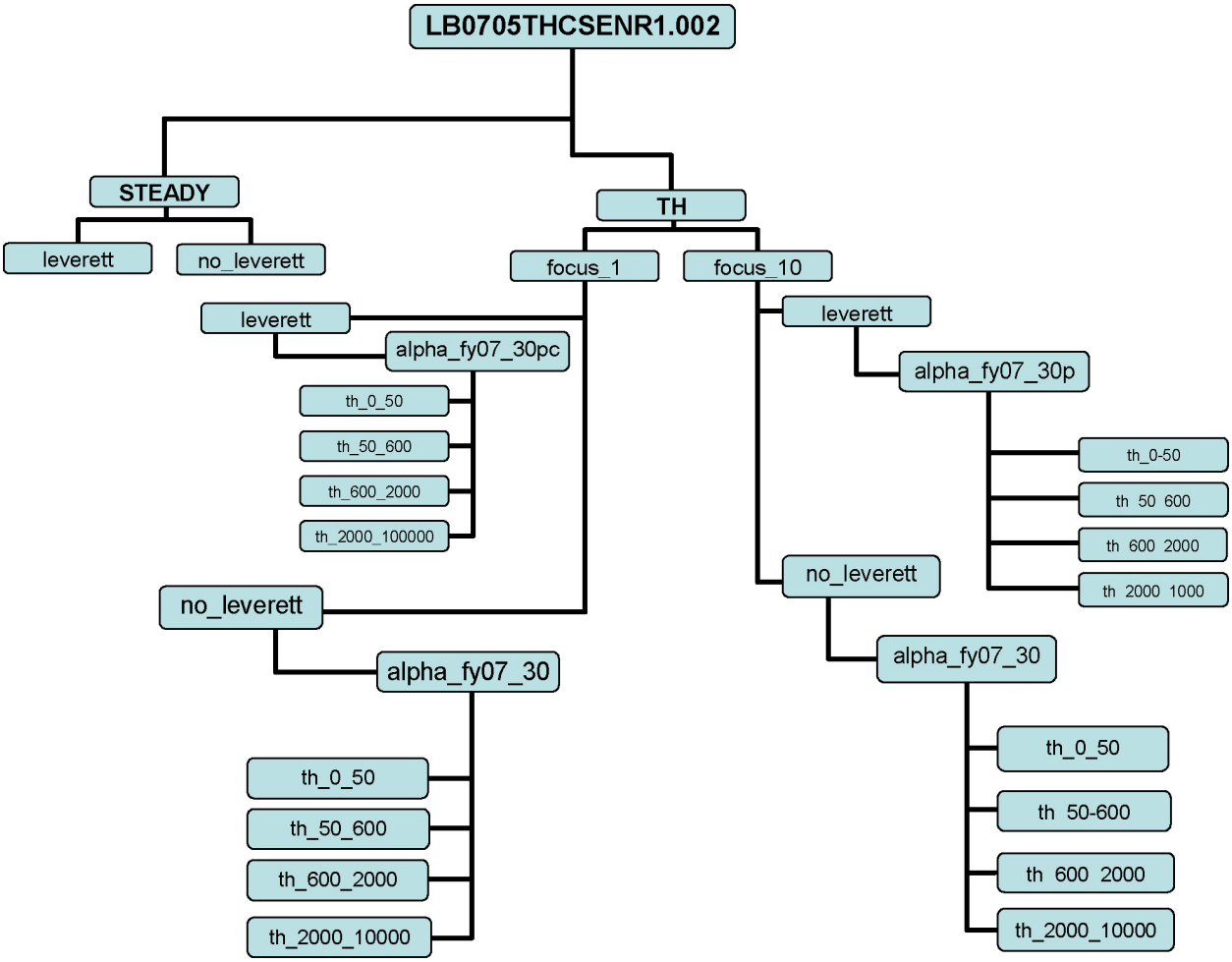

Figure A.3-1. Organization Chart of Folders Containing STEADY and TH Simulation Input and Output Files

APPENDIX A.4

LIST OF INPUT AND OUTPUT FILES SUBMITTED TO TDMS FOR STEADY-STATE AND AMBIENT SIMULATIONS IN DTNS: LB0705THCSENR1.003, LB0705THCSENR2.003, LB0705THCSENR3.003, LB0705THCSENR1.006, LB0705THCSENR2.006, AND LB0705THCSENR3.006

INTENTIONALLY LEFT BLANK

The structure of input and output file names for steady-state and ambient simulations are explained with respect to the simulations with Realization #1 of the heterogeneous fracture permeability field. These data were submitted to the TDMS as Output DTN: LB0705THCSENR1.003. Ambient simulation data with other realizations of the fracture permeability field and with different fracture capillary-strength parameters have also been submitted (such as Output DTNs: LB0705THCSENR2.003, LB0705THCSENR3.003, LB0705THCSENR1.006, LB0705THCSENR2.006, and LB0705THCSENR3.006). These DTNs have similar input/output file structures.

Generic Contents of DTN: LB0705THCSENR1.003

To carry out the ambient simulations, the initial hydrological conditions need to be obtained by running the model over a long time without application heat, chemistry, or the emplacement drift till steady-state conditions are reached. These simulations are termed the steady-state simulations, and will henceforth be called **STEADY** simulations. The simulations do not account for heat or chemistry but include an emplacement drift will be termed **AMBIENT** simulations.

The generic input and output file names for the STEADY simulations are given in Table A.4-1.

Table A.4-1. Generic Input and Output File Names for STEADY Simulations

flow.inp	Rock thermal and hydrologic properties, run flags, and other specifications (input)
flow.out	Thermal and hydrologic results (gas/liquid saturation, T, P, air mass fraction, etc.) (output)
GENER	Infiltration rates (input)
INCON	Initial thermal and hydrologic conditions (T, P, liquid saturation, etc.) – this can be arbitrary (input)
MESH	Input numerical mesh without the emplacement drifts (input)
SAVE	Thermal and hydrologic conditions (T, P, liquid saturation, etc.) at the end of the steady-state run (output)
run.t2react	Script file for running the steady-state simulations
sub*.sh	Script file for submitting batch jobs to the computing cluster

The generic names of input and output files for the AMBIENT simulations are given in Table A.4-2.

Table A.4-2. Generic Input and Output File Names for AMBIENT Simulations

flow.inp	Rock thermal and hydrologic properties, run flags, and other specifications (input)
flow.out	Thermal and hydrologic results (gas/liquid saturation, T, P, air mass fraction, etc.) (output)
GENER	Infiltration rates, heat load, and effective thermal conductivity (input)
INCON	Initial thermal and hydrologic conditions (T, P, liquid saturation, etc.) (input)
MESH	Input numerical mesh (input)
SAVE	Thermal and hydrologic conditions (T, P, liquid saturation, etc.) to use for restarting a run (output, same format as INCON file) (output)
GASOBS.DAT	Optional tabular flow output for individual grid (output)
run.t2react	Script file for running the ambient simulations
sub*.sh	Script file for submitting jobs to the computing cluster

Organization of File Folders

The organization of file folders in this DTN is shown in the organization chart below (Figure A.4-1). The following explains the logic behind the organization of the file folders.

1. STEADY Simulations

The STEADY simulations were performed for two scenarios:

a. Leverett scaling (i.e., capillarity changes because of differences in permeability) is included – these simulations are included in folder **leverett**.

b. Leverett scaling (i.e., capillarity changes because of differences in permeability) is *not* included – these simulations are included in folder **no_leverett**.

2. AMBIENT Simulations

At the first level, AMBIENT simulations are performed with two sets of infiltration fluxes:

i. The infiltration fluxes are 7.96, 12.89, and 20.45 mm/yr, respectively, between 0 to 600, 600 to 2,000, and beyond 2,000 years (the source of these infiltration flux data is DTN: LB0705DSTHC001.002 [DIRS 180854]; also see Section 4.1.4 and Table 4.1-5 of SNL 2007 [DIRS 177404) – these simulations are included in folder **focus_1**. These are also the *base-case* simulations.

ii. The infiltration fluxes are ten times the fluxes in (i) above in each time period, i.e., the infiltration fluxes are 79.6 (0 to 600 years), 128.9 (600 to 2,000 years), and 204.5 mm/yr (beyond 2,000 years). These simulations are included in folder **focus_10**.

Subsequently, the simulations were performed for either with Leverett scaling (folder: **leverett**) or without Leverett scaling (folder: **no_leverett**).

Furthermore, simulations were performed with a fracture capillary-strength parameter of 0.5750×10^{-3} Pa^{-1}. The source of this fracture capillary-strength parameter (for the host rock "Tptpll" or "tsw35") is DTN: LB0705DSTHC001.002 [DIRS 180854], file: "flow.inp," which corresponds to the 30th percentile parameter set. Hence the subfolder names of **alpha_fy07_30pc**.

In each of these subfolders, the actual AMBIENT simulations were performed in four temporal stages:

A. Simulations between 0 and 50 years: folder **amb_0_50**
B. Simulations between 50 and 600 years: folder **amb_50_600**
C. Simulations between 600 and 2,000 years: folder **amb_600_2000**
D. Simulations between 2,000 and 10,000 years: folder **amb_2000_10000**.

If a particular simulation for a particular time period could not be completed for numerical reasons, it was restarted in a subfolder **restart** within the folder for that time period (Note that restarting was necessary for this situation: If an element had a gas saturation of 1.000 (at the time the "numerical problem" happened) and water tries to get in, the simulation slowed down to unacceptable levels on rare occasions. The gas saturation was then manually changed from 1.0000 to 0.999999999… for that element, and the simulation was restarted.) Since these were rare occurrences (i.e., restart of the simulations), they have not been included in the organization chart (Figure A.4-1) below.

NOTE: The "SAVE" files from **amb_0_50** are used as "INCON" files in **amb_50_600**. The "SAVE" files from **amb_50_600** are used as "INCON" files in **amb_600_2000**. Similarly, the "SAVE" files from **amb_600_2000** are used as "INCON" files in **amb_2000_10000**.

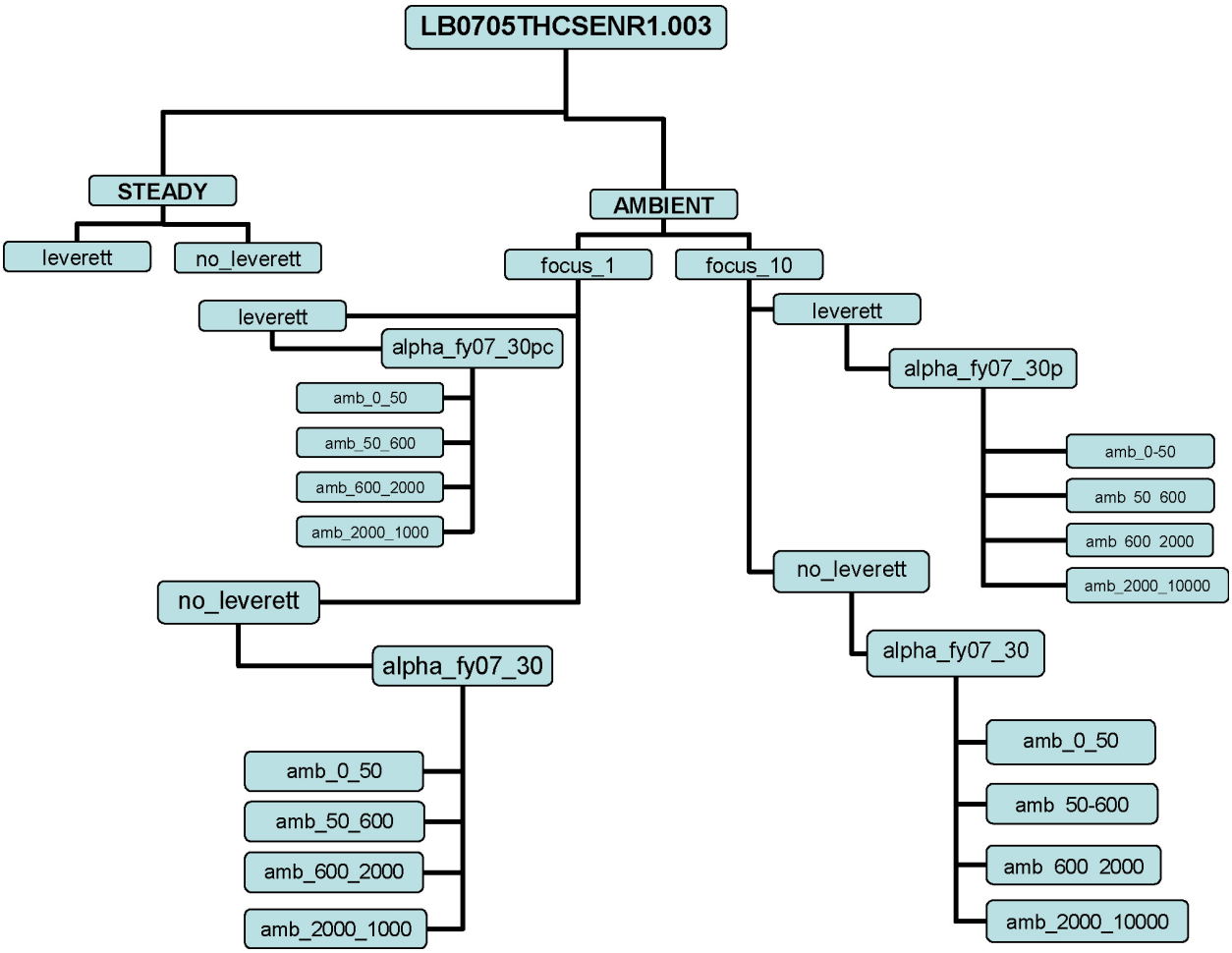

Figure A.4-1. Organization Chart of Folders Containing STEADY and AMBIENT Simulation Input and Output Files

APPENDIX B

DERIVATION OF THERMAL PROPERTIES FOR UZ MODEL LAYERS IN DTN: LB0704THRMLPRP.001

INTENTIONALLY LEFT BLANK

Thermal properties include rock grain density, dry and wet rock thermal conductivities, rock grain specific heat capacity, and matrix porosity. These properties are basic inputs into model studies involving heat flow.

The thermal properties are a compilation of matrix porosity in DTN: LB0208UZDSCPMI.002 [DIRS 161243], dry and wet thermal conductivities of the repository stratigraphic units in DTN: MO0612MEANTHER.000 [DIRS 180552], dry and wet thermal conductivities of the nonrepository stratigraphic units in DTN: SN0303T0503102.008 [DIRS 162401], and grain densities and grain specific heat capacities in DTN: SN0307T0510902.003 [DIRS 164196]. While those source DTNs provide the thermal properties for different stratigraphic units of the mountain, thermal properties are needed for the different model layers of the THC model grid. A comparison of GFM model layers and UZ model layers can be found in *Development of Numerical Grids for UZ Flow and Transport Modeling* (BSC 2004 [DIRS 169855], Table 6-5).

In most cases, a UZ model layer directly corresponds to a unique lithostratigraphic unit. In such instances, the thermal properties are adopted directly from their corresponding stratigraphic unit without alteration. On the other hand, when a UZ model layer is composed of two or more adjacent lithostratigraphic units, the averaging technique of Francis (1997 [DIRS 127326], pp. 5 to 7) is used for estimating the properties, while assuming an equal thickness for all the relevant units. The conceptual model underlying this technique is that heat flow is one-dimensional and in a direction normal to interfaces between the units under consideration. This is appropriate considering that heat flow in the ambient system and in the disturbed system (during repository heating) at Yucca Mountain is predominantly vertical (because the horizontal dimensions of the repository horizon are much larger than the vertical dimension). The corresponding equivalent thermal conductivity ($\lambda_{wet\ or\ dry,\ eq}$), grain density ($\rho_{g,eq}$), and heat capacity ($C_{p,eq}$) are calculated using the following equations, derived from those of Francis (1997 [DIRS 127326], pp. 5 to 7), assigning a uniform thickness for different geologic units within each model layer containing more than one geologic unit:

$$\lambda_{k,eq} = \frac{n\prod_{i=1}^{n}\lambda_{k,i}}{\sum_{j=1}^{n}\left(\prod_{i=1,i\neq j}^{n}\lambda_i\right)} \quad \text{(k = wet or dry)} \qquad \text{(Eq. B-1)}$$

$$\rho_{g,eq} = \frac{\sum_{i=1}^{n}\rho_{g,i}}{n} \qquad \text{(Eq. B-2)}$$

$$C_{p,eq} = \frac{\sum_{i=1}^{n}C_{p,i}\rho_{g,i}}{n\rho_{g,eq}} \qquad \text{(Eq. B-3)}$$

where n is the total number of the involved lithostratigraphic units, and $\lambda_{g,I}$, $\rho_{g,i}$, and $C_{p,i}$ are heat conductivity, grain density, and heat capacity, respectively, for a lithostratigraphic unit i. Note that the use of an equal thickness for all the relevant units within a model layer is adequate here

because differences among thermal properties for these units (within a model layer) are not significant. Additionally, resultant matrix porosities are the simple arithmetic mean of the porosities for the constituent stratigraphic units. The calculated thermal properties for the UZ model layers are given in Table B-1.

The data reported in Table B-1 have been compiled and submitted to the TDMS under Output DTN: LB0704THRMLPRP.001. The spreadsheet *LB0704THRMLPRP.001.xls* in that DTN can be used to understand/verify the calculations.

Table B-1. Thermal Properties for UZ Model Layers

Model Layer	Porosity (−)	Grain Density (kg/m^3)	Grain Specific Heat Capacity (J/kg-K)	Dry Thermal Conductivity (W/m-K)	Wet Thermal Conductivity (W/m-K)
tcw11	0.241	2510	930	1.3000	1.8100
tcw12	0.088	2510	930	1.3000	1.8100
tcw13	0.200	2430	950	0.5724	0.9092
ptn21	0.387	2320	960	0.4900	1.0600
ptn22	0.428	2320	960	0.4900	1.0600
ptn23	0.233	2320	960	0.4900	1.0600
ptn24	0.413	2320	960	0.4900	1.0600
ptn25	0.498	2320	960	0.4900	1.0600
ptn26	0.490	2320	960	0.4900	1.0600
tsw31	0.054	2505	940	0.8998	1.1057
tsw32	0.157	2540	930	1.3000	1.8100
tsw33	0.155	2520	930	1.2200	1.7800
tsw34	0.111	2520	930	1.3900	2.0600
tsw35	0.131	2540	930	1.2400	1.8700
tsw36	0.103	2540	930	1.4400	2.1100
tsw37	0.103	2540	930	1.4400	2.1100
tsw38	0.043	2380	980	0.6880	0.7960
tsw39v	0.229	2320	960	0.4900	1.0600
tsw39z	0.275	2280	1020	0.4900	1.0600
ch1Mv	0.331	2270	960	0.4900	1.0600
ch1Mz	0.285	2250	1120	0.4900	1.0600
ch2Mv	0.346	2240	960	0.5950	1.2600
ch3Mv	0.346	2240	960	0.5950	1.2600
ch4Mv	0.346	2240	960	0.5950	1.2600
ch5Mv	0.346	2240	970	0.5950	1.2600

Table B-1. Thermal Properties for UZ Model Layers (Continued)

Model Layer	Porosity (−)	Grain Density (kg/m^3)	Grain Specific Heat Capacity (J/kg-K)	Dry Thermal Conductivity (W/m-K)	Wet Thermal Conductivity (W/m-K)
ch2Mz	0.322	2280	1110	0.5950	1.2600
ch3Mz	0.322	2280	1100	0.5950	1.2600
ch4Mz	0.322	2280	1100	0.5950	1.2600
ch5Mz	0.322	2280	1100	0.5950	1.2600
ch6Mv	0.331	2350	970	0.5950	1.2600
ch6Mz	0.271	2370	1030	0.5950	1.2600
pp4Mz	0.321	2350	1040	0.5690	1.1300
pp3Md	0.318	2550	930	0.5690	1.1300
pp2Md	0.221	2550	930	0.7405	1.3347
pp1Mz	0.297	2390	1100	0.5959	1.1493
bf3Md	0.175	2560	930	0.7877	1.3434
bf2Mz	0.234	2350	1050	0.6112	1.1584
tr3Md	0.175	2390	940	0.6408	1.2337
tr2Mz	0.234	2390	940	0.5350	1.1000

Source: DTNs: LB0208UZDSCPMI.002 [DIRS 161243], MO0612MEANTHER.000 [DIRS 180552], SN0303T0503102.008 [DIRS 162401], and SN0307T0510902.003 [DIRS 164196].

INTENTIONALLY LEFT BLANK

APPENDIX C

PROCEDURES TO GENERATE A HETEROGENEOUS FRACTURE PERMEABILITY FIELD IN DTN: LB0705THCSENHF.001

INTENTIONALLY LEFT BLANK

Three realizations of a heterogeneous fracture permeability field were generated in this report. The discussion below provides information about how one realization of the heterogeneous fracture permeability field was generated. The other two realizations can be generated following the same procedures, except for changing the random seed number in file "perm.dat" (see below).

Software Used to Generate the Data:

- GSLIB V1.0SISIM V1.204 (see Section 3.1 and Table 3-1)
- avgperm.f V1.0 (see Table 3-1).

Table 3-1 provides more information about the software and the computing platform/operating system on which the software was used.

Procedures

The heterogeneous fracture permeability distribution was generated in two steps. First, log permeability modifiers were calculated using GSLIB V1.0 module SISIM V1.204. In the second step, the log permeability modifiers obtained in the first step were mapped onto the THC seepage model mesh, using avgperm.f V1.0. In the following, step-wise instructions are given for generating the fracture permeability distributions using these two software.

1. Download the file "perm.par" (located in folder *\20_k-realizations*) from DTN: LB0304SMDCREV2.001 [DIRS 173235]. Make the following changes:

   i. Change the dimesionality of the system from 3-D to 2-D (*x* and *y* only)

   ii. Set the model domain to 0 to 41 m in *x* direction and −190.0 m to +190 m in *y* direction

   iii. Set the spatial step size to 0.2 m in both *x* and *y* directions. Thus, there will be 205 (=41/0.2) steps in *x* direction and 1,900 (=380/0.2) steps in *y* direction, giving a total number of 389,500 (=205 × 1,900) rectangular gridblocks covering the model domain. The choice of the model domain was restricted by the requirement of a maximum 400,000 gridblocks by avgperm.f V1.0 (see Table 3-1 for more details.

   iv. Change the seed number to generate random numbers. The seed number is arbitrary.

2. Then execute GSLIB V1.0SISIM V1.204 (the executable is xsisim) on a SUN computing system running on a SUN O.S. 5.5.1 operating system (see Table 3-1).

3. The output file from (2) is "perm.dat." Copy this file as "fract*a.dat," where "*" can be "1," "2," or "3" depending upon the realization number of the permeability field being generated.

4. Add the number 389,500 at the top of the files "fract*a.dat."

5. Download the file "MESH" (located in folder *\2dflow_81m*) from DTN: LB0704DSSSTFLW.002 [DIRS 180853]. Check whether the MESH file has the elements F1388 to F1408. If these elements are present, remove them with a text editor.

6. Add the total number of gridblocks (2,887) and connections (7,447) at the top of the file "MESH."

7. Provide an "INCON_start" file. Add the total number of gridblocks (2,887) at the top of the "INCON_start" file. The porosity and permeabilities in "INCON_start" are taken from DTN: LB0705DSTHC001.002 [DIRS 180854] (folder: *\thc7_81_w0_*, file: "flow.inp"). The physical conditions (pressure, gas saturation/temperature, and saturation pressure) in "INCON_start" are arbitrary.

8. On a Dec Alpha System operating on OSF1 V4.0 (see Table 3-1), execute the following:

   >> ./run_avgperm

   A copy of the file "run_avgperm" is included below.

9. The output file is "incon_real*," where "*" can be "1," "2," or "3" depending on the realization number of the permeability field.

10. With a text editor, add the elements F1388 to F1408 (and some arbitrary initial conditions for them). These elements do not participate in any calculations (they are absent in the connection list). They are retained because of convenience of plotting.

11. This "incon_real*" is used as the starting point for the steady-state simulations.

Example File "run_avgperm"

```
/usersraid2/SCM/Installed-Routines.dir/avgperm.f_V1.0/avgperm_dec < inp_avgperm_rel1
```

Example File "inp_avgperm_rel1"

```
'fract1a.dat'
'mesh_u110_rev2'
'INCON_start'
'real1'
'F'
'd'
```

*NOTE: The above file is an example, used in generating **Realization #1** of the heterogeneous fracture permeability distribution. Change the name of the input/output files for the other realizations.*

APPENDIX D

PROCEDURES TO CALCULATE SEEPAGE FLUX FROM "FLOW.OUT" FILES

INTENTIONALLY LEFT BLANK

Seepage fluxes are extracted from the "flow.out" files resulting from ambient, TH, or THC simulations. The procedures involved in extracting the seepage flux data are explained in this appendix. As an example, the "flow.out" files are taken from DTN: LB0705THCSENR1.001 (directory: */THC/focus_1/leveret/alpha_fy07_30pc.dir*; there are four "flow.out" files in four subdirectories: *thc_0_50*, *thc_50_600*, *thc_600_2000*, and *thc_2000_10000*). These files are copied into the respective directories of DTN: LB0706THCSENPP.001 (in directory *Appendix_D*). The procedures are equally applicable to other "flow.out" files from other ambient, TH, or THC simulations.

1. There are 12 connections in the first quadrant (between 0^o and 90^o, 0^o being the horizontal axis and 90^o representing the vertical axis) between the emplacement drift and the fracture gridblocks outside, as verified from file "MESH" in DTN: LB0705THCSENR1.001. These connections are shown in Table D-1, and are also provided in the example file "drift_top_ele" (DTN: LB0706THCSENPP.001, directory: *Appendix_D\thc_0_50*).

Table D-1. Drift-Fracture Connections in the First Quadrant

Serial No.	Drift Element	Fracture Gridblock	Radial Location of Fracture Gridblock Center (°)
1.	dr357	F 44	3.75
2.	dr359	F 51	11.25
3.	dr361	F 58	18.75
4.	dr363	F 65	26.25
5.	dr365	F 72	33.75
6.	dr367	F 79	41.25
7.	dr369	F 86	48.75
8.	dr371	F 93	56.25
9.	dr373	F 100	63.75
10.	dr375	F 107	71.25
11.	dr377	F 114	78.75
12.	dr379	F 121	86.25

2. A script file named "extract_drift_fluxes_from_top" is provided in DTN: LB0706THCSENPP.001 (directory: *Appendix_D\thc_0_50*). Always have this file located in the simulation run corresponding to 0 to 50 years.

3. Execute the script file by typing:

   >> *chmod +x extract_drift_fluxes_from_top* (this step is needed only for first time use).

   >> *./extract_drift_fluxes_from_top*

4. The standard operations (consisting of Unix utility functions such as "grep," "awk," "cp," "mv," and "paste") in (3) above extract the times at which printouts are available, and the

liquid fluxes (in kg/s) in the connections of Table D-1. The output file is named "flux_vs_time.dat" (DTN: LB0706THCSENPP.001, directory: *\Appendix_D\thc_0_50*)

5. Transfer the file "flux_vs_time.dat" to a PC and open it with Excel. Add a header line as shown in the example Excel worksheet *flux_vs_time.xls* (see Output DTN: LB0706THCSENPP.001, directory: *\Appendix_D\thc_0_50*).

6. The first column in *flux_vs_time.xls* is time in seconds (from file "flux_vs_time.dat"), the second column was inserted to convert time in seconds to time in years by dividing a factor of 86,400 × 365.24 (86,400 is the number of seconds in a day and 365.24 is the average number of days in a year).

7. The infiltration column is inserted next. The infiltration fluxes can be found in Section 4.1.4 and Table 4.1-5 of *Drift-Scale THC Seepage Model* (SNL 2007 [DIRS 177404]).

8. The various "dr%%%*F&&&&" columns are obtained from "flux_vs_time.dat," where the "dr%%%" and "F&&&&" represent the various drift and fracture elements, respectively, in file "drift_top_ele" (see DTN: LB0706THCSENPP.001, directory: *\Appendix_D\thc_0_50*).

9. In between these columns, columns are added with titles "Seepage Flux in D," "Seepage Flux in E," etc., to decide whether seepage occurs or not. If the number in the column immediately to its left is positive, seepage occurs, and the flux value is written in this column. If not, a flux of "0" is written in this column. See Item 10 below for further details.

10. Per TOUGHREACT V3.1.1 convention, if a flux is positive then flow is coming from the second element into the first element. On the other hand, if flux is negative then flow is directed from the first element into the second element. Since the drift elements are lined up as the "first" element, for seepage to occur (liquid water entering the drift), "positive" fluxes must be looked for.

11. Then, all the seepage fluxes (SF), if any, are added up in Column AB (see DTN: LB0706THCSENPP.001, directory: *\Appendix_D\thc_0_50*), and converted to mm/yr (from kg/s) by doing the following conversion in Column AC (see DTN: LB0706THCSENPP.001, directory: *\Appendix_D\thc_0_50*)

$$SF(mm/year) = SF(kg/\sec) \times \frac{365.24 \times 86400}{1 \times 10^{-3} \times 2.75 \times 997.5}$$

12. In this particular example, there was no seepage (see Column AC).

13. The factor listed in Column AD (see DTN: LB0706THCSENPP.001, directory: */Appendix_D/thc_0_50*) is the factor on the right hand side of the equation in Item 11 above.

Example File "**drift_top_ele**"

```
dr357 F  44
dr359 F  51
dr361 F  58
dr363 F  65
dr365 F  72
dr367 F  79
dr369 F  86
dr371 F   93
dr373 F 100
dr375 F 107
dr377 F 114
dr379 F 121
```

Example Script File "extract_drift_fluxes_from_top**"**

```
#! /bin/sh

grep -A1 'TOTAL TIME' ../thc_0_50.dir/flow.out | grep '0.' | awk '{print $1}' > dummy_times

cp dummy_times flow_times

grep -A1 'TOTAL TIME' ../thc_50_600.dir/flow.out | grep '0.' | awk '{print $1}' > dummy_times

cat dummy_times >> flow_times

grep -A1 'TOTAL TIME' ../thc_600_2000.dir/flow.out | grep '0.' | awk '{print $1}' > dummy_times

cat dummy_times >> flow_times

grep -A1 'TOTAL TIME' ../thc_2000_10000.dir/flow.out | grep '0.' | awk '{print $1}' >
dummy_times

cat dummy_times >> flow_times

mv flow_times flow_times_full.dat

grep -f drift_top_ele  ../thc_0_50.dir/flow.out | awk '{ print substr($0,4,7), substr($0,11,5),
substr($0,87,13)}' > dummy_fluxes

cp dummy_fluxes fluxes

grep -f drift_top_ele  ../thc_50_600.dir/flow.out | awk '{ print substr($0,4,7), substr($0,11,5),
substr($0,87,13)}' > dummy_fluxes

cat dummy_fluxes >> fluxes

grep -f drift_top_ele  ../thc_600_2000.dir/flow.out | awk '{ print substr($0,4,7), substr($0,11,5),
substr($0,87,13)}' > dummy_fluxes
```

```
cat dummy_fluxes >> fluxes

grep -f drift_top_ele  ../thc_2000_10000.dir/flow.out | awk '{ print substr($0,4,7), substr($0,11,5), substr($0,87,13)}' > dummy_fluxes

cat dummy_fluxes >> fluxes

mv fluxes dr_fluxes_full.dat

rm dummy_times dummy_fluxes

grep 'dr357' dr_fluxes_full.dat | awk '{print substr($0,15,27)}'> flux_f44

grep 'dr359' dr_fluxes_full.dat | awk '{print substr($0,15,27)}'> flux_f51

grep 'dr361' dr_fluxes_full.dat | awk '{print substr($0,15,27)}'> flux_f58

grep 'dr363' dr_fluxes_full.dat | awk '{print substr($0,15,27)}'> flux_f65

grep 'dr365' dr_fluxes_full.dat | awk '{print substr($0,15,27)}'> flux_f72

grep 'dr367' dr_fluxes_full.dat | awk '{print substr($0,15,27)}'> flux_f79

grep 'dr369' dr_fluxes_full.dat | awk '{print substr($0,15,27)}'> flux_f86

grep 'dr371' dr_fluxes_full.dat | awk '{print substr($0,15,27)}'> flux_f93

grep 'dr373' dr_fluxes_full.dat | awk '{print substr($0,15,27)}'> flux_f100

grep 'dr375' dr_fluxes_full.dat | awk '{print substr($0,15,27)}'> flux_f107

grep 'dr377' dr_fluxes_full.dat | awk '{print substr($0,15,27)}'> flux_f114

grep 'dr379' dr_fluxes_full.dat | awk '{print substr($0,15,27)}'> flux_f121

paste flow_times_full.dat flux_f44 flux_f51 flux_f58 flux_f65 flux_f72 flux_f79 flux_f86 flux_f93 flux_f100 flux_f107 flux_f114 flux_f121 > flux_vs_time.dat

rm flux_f*
```

APPENDIX E

IMPACT OF CHANGING THE CONVERGENCE CRITERION FROM 1.0×10^{-5} TO 1.0×10^{-4} ON FINAL STEADY-STATE CONDITIONS

INTENTIONALLY LEFT BLANK

Whether ambient, TH, or THC, before the commencement of the actual simulation runs (simulations including an emplacement drift), simulations were carried out without application of heat and excluding an emplacement drift to achieve steady-state conditions for each of the three realizations of the heterogeneous fracture permeability distribution, with and without Leverett-scaling effects. There were thus six steady-state simulations in total. The input and output files for these steady-state simulations can be found in the folder *\STEADY* of DTNs: LB0705THCSENR1.001 (for Realization #1), LB0705THCSENR2.001 (for Realization #2), and LB0705THCSENR3.001 (for Realization #3); look into folder *\leverett* for steady-state simulations inclusive of Leverett-scaling effects and folder *\no_leverett* for simulations without Leverett-scaling effects.

In Section 4.1.1.2, it has been pointed out that these steady-state simulations were performed with a convergence criterion of 1.0×10^{-4}. On the other hand, the steady-state simulations in *Drift-Scale THC Seepage Model* (SNL 2007 [DIRS 177404]) were performed with a convergence criterion of 1.0×10^{-5}. In Section 4.1.1.2, it was also mentioned that increasing the convergence criterion was not expected to impact the final steady-state condition achieved through TOUGHREACT simulation. In this appendix, the validity of that statement is verified, i.e., whether increasing the convergence criterion from 1.0×10^{-5} to 1.0×10^{-4} would have a significant impact on the steady-state conditions).

To accomplish this confirmation, an additional steady-state simulation was carried out with Realization #1 of the heterogeneous fracture permeability distribution, which also included Leverett-scaling effects. In other words, this additional steady-state simulation is similar to the steady-state simulation "base_r1_lev_std" mentioned in Table 6.5-1. The convergence criterion (in file "flow.inp") was changed from 1.0×10^{-4} to 1.0×10^{-5}. Also, a slightly different initial condition was chosen for this additional simulation. (Remember that the initial condition at the start of a steady-state run can be arbitrary.)

The input and output files for this additional steady-state simulation have been submitted in Output DTN: LB0706THCSENPP.001 (folder: *\Appendix_E\steady_tol_1e-5*). The input and output files for the steady-state simulation "base_r1_lev_std" (with convergence limit of 1.0×10^{-4}) have been submitted in Output DTN: LB0705THCSENR1.001 (folder: *\STEADY\leveret*). However, for the sake of convenience, the important input ("flow.inp," "GENER," "INCON," and "MESH") and output ("flow.out" and "SAVE") files from that simulation are reproduced in Output DTN: LB0706THCSENPP.001 (folder: *\Appendix_E\steady_tol_1e-4*).

If the input files from the two simulations are compared, the following can be observed:

- The "MESH" files are identical.
- The "GENER" files are identical.
- The only difference between files "flow.inp" is the convergence criterion. The result of comparison of the two "flow.inp" files is provided in file "diff_flow.inp" of the folder *\comparison*.

- The initial conditions (in files "INCON") are slightly different; however, the permeabilities and porosities are the same.

After the simulations were run for an identical time (5×10^6 years), files "SAVE" from the two simulations are compared. The result of such a comparison is provided in file "diff_save" of folder *comparison*. From file "diff_save," it can be easily seen that the steady-state conditions produced with a convergence criterion of 1.0×10^{-5} are quite similar to those produced with a convergence criterion of 1.0×10^{-4}. While this exercise can be repeated for the other five steady-state simulations with similar expected results, it can be concluded that changing the convergence criterion from 1.0×10^{-5} (as in SNL 2007 [DIRS 177404]) to 1.0×10^{-4} (as in this report) did not influence the end results of the steady-state simulations in any significant way.

APPENDIX F

PROCEDURES TO OBTAIN TEMPERATURE CONTOUR PLOTS FROM "FLOW.OUT" FILES

INTENTIONALLY LEFT BLANK

Temperature contour plots can be extracted from "flow.out" files. For example, consider the "flow.out" file in the directory path *\THC\focus_1\leveret\alpha_fy07_30pc.dir\thc_50_600* in Output DTN: LB0705THCSENR1.001. This "flow.out" file contains flow simulation data between 50 and 600 years. This particular THC simulation corresponds to IMF1 infiltration fluxes and a fracture capillary-strength parameter of 0.5750×10^{-3} Pa^{-1} with Realization #1 of the heterogeneous fracture permeability distribution. The simulation is inclusive of Leverett-scaling effects. This simulation run has been identified as "base_r1_1x_lev_thc" in Table 6.5-2 (see Section 6.5).

To carry out the steps outlined below, the user obtains the files "flow.out" and "MESH" from Output DTN: LB0705THCSENR1.001 (directory: */THC/focus_1/leveret/alpha_fy07_30pc.dir /thc_50_600*). Thus, the source DTN is LB0705THCSENR1.001.

If the user is interested in analyzing the temperature data at 100 years ($= 0.31557 \times 10^{10}$ seconds), search, with a text editor for the keyword "TOTAL TIME" in file "flow.out," and select the output corresponding to total time 0.31557×10^{10}. Then, select the output information between "F 2" and "wp001," and, with the help of a text editor save this to a file, for example "flow.out_100y." Next, perform the following operations on a Unix operating system.

>> grep –v 'M' flow.out_100y > flow.out_100y_Fdr

>> grep –v 'M' MESH > MESH_Fdr_ele

The first command extracts the state variables (pressure, temperature, etc.) for the fracture and drift elements. Open the file "MESH_Fdr_ele" with a text editor and remove the portion below keyword "CONNE" (remove the keyword "CONNE" as well). Resave this file as "MESH_Fdr_ele."

Open the file "flow.out_100y_Fdr" with Excel. Use the "fixed width" option to parse the data file into 12 columns (from column A to column L) while opening the file with Excel. Note that the delimited columns in the Excel worksheet must be consistent with that in the original "flow.out" file (see user information document for TOUGHREACT V3.1.1). Delete the first two columns (containing the name and serial number of an element) and the blank rows. Now insert two blank columns at the left. Open also the file "MESH_Fdr_ele" with Excel. Use the "fixed width" option to parse the data file into 7 columns (from column A to column G) while opening the file with Excel. Note that the delimited columns in the Excel worksheet must be consistent with that in the original "MESH" file (see user information document for TOUGHREACT V3.1.1). Then copy the fifth (Column "E" containing the *x* coordinates) and seventh (Column "G" containing the *z* coordinates) columns from this file and paste them onto the two leftmost blank columns in "flow.out_100y_Fdr." Save this file as *Contour_R1F1L_100y_Fdr.txt* with the ".txt (Tab Delimited)" option in Excel. This is the file that is used for plotting the temperature contours (temperatures are given in the fourth column).

Next, load the file *Contour_R1F1L_100y_Fdr.txt* in TECPLOT. Select the "2D" button in TECPLOT. Then, select "data/triangulate." Next, select the "Contour" plot option and generate the contour plot with "V4" (the fourth column) as the contour variable (temperature).

Files "MESH," "MESH_Fdr_ele," "flow.out," "flow.out_100y," "flow.out_100y_Fdr," have been provided in Output DTN: LB0706THCSENPP.001 (directory: *\Appendix_F*). The example *Contour_R1F1L_100y_Fdr.txt* file can be found in the same location. A "README" file has also been included for convenience.

APPENDIX G

TOUGHREACT V3.1.1 AND CUTCHEM V 2.0 EXECUTABLES INSTALL INFORMATION

INTENTIONALLY LEFT BLANK

G.1 TOUGHREACT V3.1.1 INSTALLATION ON LBNL MACHINE WORKHORSE (CAOS LINUX)

G.1.1 Installation on Workhorse for Preliminary Modeling Prior to Qualification of TOUGHREACT V3.1.1.

Directory and file listings for TOUGHREACT V3.1.1 executables and installation tests on Lawrence Berkeley National Laboratory (LBNL) machine workhorse:

```
/home/ymp/tr3.1.1_X
total 20
drwxr-xr-x   2 jwong users 4096 Nov 15 23:08 executables
drwxr-xr-x   8 jwong users 4096 Dec  8 09:38 install_tests
drwxr-xr-x   2 jwong users 4096 Nov 15 22:39 source
drwxr-xr-x  25 jwong users 4096 Nov 15 22:43 test_problems_dec
drwxr-xr-x  25 jwong users 4096 Nov 15 22:37 test_problems_lin

/home/ymp/tr3.1.1_X/executables
total 8344
-r-xr-xr-x  1 jwong users 1267120 Nov 15 23:08 tr3.1.1e3_40k_dec
-r-xr--r--  1 jwong users 1571881 Nov 15 23:08 tr3.1.1e3_40k_lin
-r-xr-xr-x  1 jwong users 1277184 Nov 15 23:08 tr3.1.1e4_40k_dec
-r-xr--r--  1 jwong users 1583453 Nov 15 23:08 tr3.1.1e4_40k_lin
-r-xr-xr-x  1 jwong users 1256656 Nov 15 23:08 tr3.1.1e9_40k_dec
-r-xr--r--  1 jwong users 1556024 Nov 15 23:08 tr3.1.1e9_40k_lin

/home/ymp/tr3.1.1_X/install_tests
total 12
drwxr-xr-x  2 jwong users 4096 Nov 15 22:35 eos3
drwxr-xr-x  2 jwong users 4096 Nov 15 22:35 eos4
drwxr-xr-x  2 jwong users 4096 Nov 15 22:35 eos9

/home/ymp/tr3.1.1_X/install_tests/eos3
total 896
-r-xr--r--  1 jwong users 172953 Nov 15 22:35 GASOBS.DAT
-r-xr--r--  1 jwong users     91 Nov 15 22:35 GENER
-r-xr--r--  1 jwong users    149 Nov 15 22:35 INCON
-r-xr--r--  1 jwong users      0 Nov 15 22:35 LINEQ
-r-xr--r--  1 jwong users   9228 Nov 15 22:35 MESH
-r-xr--r--  1 jwong users   7518 Nov 15 22:35 SAVE
-r-xr--r--  1 jwong users      0 Nov 15 22:35 TABLE
-r-xr--r--  1 jwong users   6640 Nov 15 22:35 VERS
-r-xr--r--  1 jwong users   7049 Nov 15 22:35 chdump.out
-r-xr--r--  1 jwong users   5517 Nov 15 22:35 chemical.inp
-r-xr--r--  1 jwong users  14625 Nov 15 22:35 chemical.out
-r-xr--r--  1 jwong users   9711 Nov 15 22:35 flow.inp
-r-xr--r--  1 jwong users 228245 Nov 15 22:35 flow.out
```

```
-r-xr--r--  1 jwong users  12001 Nov 15 22:35 iter.dat
-r-xr--r--  1 jwong users  15528 Nov 15 22:35 mbalance.out
-r-xr--r--  1 jwong users  31174 Nov 15 22:35 min_SI.out
-r-xr--r--  1 jwong users  15277 Nov 15 22:35 runlog.out
-r-xr--r--  1 jwong users  62613 Nov 15 22:35 savechem
-r-xr--r--  1 jwong users   1646 Nov 15 22:35 solute.inp
-r-xr--r--  1 jwong users   6209 Nov 15 22:35 solute.out
-r-xr--r--  1 jwong users  33914 Nov 15 22:35 tec_conc.dat
-r-xr--r--  1 jwong users  14089 Nov 15 22:35 tec_gas.dat
-r-xr--r--  1 jwong users  48093 Nov 15 22:35 tec_min.dat
-r-xr--r--  1 jwong users  88384 Nov 15 22:35 ther_dummy.dat
-r-xr--r--  1 jwong users  60384 Nov 15 22:35 time.dat

/home/ymp/tr3.1.1_X/install_tests/eos4
total 896
-r-xr--r--  1 jwong users 172557 Nov 15 22:35 GASOBS.DAT
-r-xr--r--  1 jwong users     91 Nov 15 22:35 GENER
-r-xr--r--  1 jwong users    149 Nov 15 22:35 INCON
-r-xr--r--  1 jwong users      0 Nov 15 22:35 LINEQ
-r-xr--r--  1 jwong users   9228 Nov 15 22:35 MESH
-r-xr--r--  1 jwong users   7518 Nov 15 22:35 SAVE
-r-xr--r--  1 jwong users      0 Nov 15 22:35 TABLE
-r-xr--r--  1 jwong users   7047 Nov 15 22:35 VERS
-r-xr--r--  1 jwong users   7049 Nov 15 22:35 chdump.out
-r-xr--r--  1 jwong users   5517 Nov 15 22:35 chemical.inp
-r-xr--r--  1 jwong users  14625 Nov 15 22:35 chemical.out
-r-xr--r--  1 jwong users   9711 Nov 15 22:35 flow.inp
-r-xr--r--  1 jwong users 227315 Nov 15 22:35 flow.out
-r-xr--r--  1 jwong users  12001 Nov 15 22:35 iter.dat
-r-xr--r--  1 jwong users  15528 Nov 15 22:35 mbalance.out
-r-xr--r--  1 jwong users  31174 Nov 15 22:35 min_SI.out
-r-xr--r--  1 jwong users  15277 Nov 15 22:35 runlog.out
-r-xr--r--  1 jwong users  62613 Nov 15 22:35 savechem
-r-xr--r--  1 jwong users   1646 Nov 15 22:35 solute.inp
-r-xr--r--  1 jwong users   6209 Nov 15 22:35 solute.out
-r-xr--r--  1 jwong users  33914 Nov 15 22:35 tec_conc.dat
-r-xr--r--  1 jwong users  14089 Nov 15 22:35 tec_gas.dat
-r-xr--r--  1 jwong users  48093 Nov 15 22:35 tec_min.dat
-r-xr--r--  1 jwong users  88384 Nov 15 22:35 ther_dummy.dat
-r-xr--r--  1 jwong users  60384 Nov 15 22:35 time.dat

/home/ymp/tr3.1.1_X/install_tests/eos9
total 200
-r-xr--r--  1 jwong users 29403 Nov 15 22:35 GASOBS.DAT
-r-xr--r--  1 jwong users    91 Nov 15 22:35 GENER
-r-xr--r--  1 jwong users  7383 Nov 15 22:35 INCON
-r-xr--r--  1 jwong users     0 Nov 15 22:35 LINEQ
```

```
-r-xr--r--  1 jwong users 13967 Nov 15 22:35 MESH
-r-xr--r--  1 jwong users  7491 Nov 15 22:35 SAVE
-r-xr--r--  1 jwong users     0 Nov 15 22:35 TABLE
-r-xr--r--  1 jwong users  3791 Nov 15 22:35 VERS
-r-xr--r--  1 jwong users 41322 Nov 15 22:35 flow.inp
-r-xr--r--  1 jwong users 79596 Nov 15 22:35 flow.out

/home/ymp/tr3.1.1_X/source
total 1312
-r-xr--r--  1 jwong users   3081 Nov 15 22:34 T2_40K
-r-xr--r--  1 jwong users   1839 Nov 15 22:34 chempar23_q311.inc
-r-xr--r--  1 jwong users   3412 Nov 15 22:34 common23.inc
-r-xr--r--  1 jwong users  46113 Nov 15 22:34 eos3.f
-r-xr--r--  1 jwong users  60724 Nov 15 22:34 eos4.f
-r-xr--r--  1 jwong users  32044 Nov 15 22:34 eos9.f
-r-xr--r--  1 jwong users 204231 Nov 15 22:34 geochem.f
-r-xr--r--  1 jwong users  97464 Nov 15 22:34 inichm.f
-r-xr--r--  1 jwong users   1550 Nov 15 22:34 ma28abc.f
-r-xr--r--  1 jwong users   1716 Nov 15 22:34 makefile_eos3q311_dec
-r-xr--r--  1 jwong users   1894 Nov 15 22:34 makefile_eos3q311_linux
-r-xr--r--  1 jwong users   1716 Nov 15 22:34 makefile_eos4q311_dec
-r-xr--r--  1 jwong users   1894 Nov 15 22:34 makefile_eos4q311_linux
-r-xr--r--  1 jwong users   1716 Nov 15 22:34 makefile_eos9q311_dec
-r-xr--r--  1 jwong users   1894 Nov 15 22:34 makefile_eos9q311_linux
-r-xr--r--  1 jwong users  41911 Nov 15 22:34 meshm.f
-r-xr--r--  1 jwong users 141763 Nov 15 22:34 multi.f
-r-xr--r--  1 jwong users  33584 Nov 15 22:34 newton.f
-r-xr--r--  1 jwong users    507 Nov 15 22:34 perm23.inc
-r-xr--r--  1 jwong users  17941 Nov 15 22:34 rctprop.f
-r-xr--r--  1 jwong users  20523 Nov 15 22:34 readsolu.f
-r-xr--r--  1 jwong users    827 Nov 15 22:34 second_dec.f
-r-xr--r--  1 jwong users  73085 Nov 15 22:34 t2cg22.f
-r-xr--r--  1 jwong users 165569 Nov 15 22:34 t2f.f
-r-xr--r--  1 jwong users  73236 Nov 15 22:34 t2solv.f
-r-xr--r--  1 jwong users 225993 Nov 15 22:34 treact.f
```

G.1.2 Installation on Workhorse Using Qualified TOUGHREACT V 3.1.1 Media from Software Configuration Management

```
/home/jleem/tr3.1.1_X
total 20
drwxr-xr-x   2 jleem users 4096 2006-11-15 23:08:36.000000000 -0800 executables
drwxr-xr-x   5 jleem users 4096 2006-11-15 22:35:30.000000000 -0800 install_tests
drwxr-xr-x   2 jleem users 4096 2006-11-15 22:39:37.000000000 -0800 source
drwxr-xr-x  25 jleem users 4096 2006-11-15 22:43:01.000000000 -0800 test_problems_dec
drwxr-xr-x  25 jleem users 4096 2006-11-15 22:37:33.000000000 -0800 test_problems_lin
```

```
/home/jleem/tr3.1.1_X/executables
total 8344
-r-xr-xr-x  1 jleem users 1267120 2006-11-15 23:08:07.000000000 -0800 tr3.1.1e3_40k_dec
-r-xr--r--  1 jleem users 1571881 2006-11-15 23:08:07.000000000 -0800 tr3.1.1e3_40k_lin
-r-xr-xr-x  1 jleem users 1277184 2006-11-15 23:08:07.000000000 -0800 tr3.1.1e4_40k_dec
-r-xr--r--  1 jleem users 1583453 2006-11-15 23:08:06.000000000 -0800 tr3.1.1e4_40k_lin
-r-xr-xr-x  1 jleem users 1256656 2006-11-15 23:08:06.000000000 -0800 tr3.1.1e9_40k_dec
-r-xr--r--  1 jleem users 1556024 2006-11-15 23:08:06.000000000 -0800 tr3.1.1e9_40k_lin

/home/jleem/tr3.1.1_X/install_tests
total 12
drwxr-xr-x  2 jleem users 4096 2006-11-15 22:35:30.000000000 -0800 eos3
drwxr-xr-x  2 jleem users 4096 2006-11-15 22:35:30.000000000 -0800 eos4
drwxr-xr-x  2 jleem users 4096 2006-11-15 22:35:30.000000000 -0800 eos9

/home/jleem/tr3.1.1_X/install_tests/eos3
total 896
-r-xr--r--  1 jleem users 172953 2006-11-15 22:35:30.000000000 -0800 GASOBS.DAT
-r-xr--r--  1 jleem users     91 2006-11-15 22:35:30.000000000 -0800 GENER
-r-xr--r--  1 jleem users    149 2006-11-15 22:35:30.000000000 -0800 INCON
-r-xr--r--  1 jleem users      0 2006-11-15 22:35:30.000000000 -0800 LINEQ
-r-xr--r--  1 jleem users   9228 2006-11-15 22:35:30.000000000 -0800 MESH
-r-xr--r--  1 jleem users   7518 2006-11-15 22:35:30.000000000 -0800 SAVE
-r-xr--r--  1 jleem users      0 2006-11-15 22:35:30.000000000 -0800 TABLE
-r-xr--r--  1 jleem users   6640 2006-11-15 22:35:30.000000000 -0800 VERS
-r-xr--r--  1 jleem users   7049 2006-11-15 22:35:29.000000000 -0800 chdump.out
-r-xr--r--  1 jleem users   5517 2006-11-15 22:35:29.000000000 -0800 chemical.inp
-r-xr--r--  1 jleem users  14625 2006-11-15 22:35:29.000000000 -0800 chemical.out
-r-xr--r--  1 jleem users   9711 2006-11-15 22:35:30.000000000 -0800 flow.inp
-r-xr--r--  1 jleem users 228245 2006-11-15 22:35:30.000000000 -0800 flow.out
-r-xr--r--  1 jleem users  12001 2006-11-15 22:35:30.000000000 -0800 iter.dat
-r-xr--r--  1 jleem users  15528 2006-11-15 22:35:30.000000000 -0800 mbalance.out
-r-xr--r--  1 jleem users  31174 2006-11-15 22:35:30.000000000 -0800 min_SI.out
-r-xr--r--  1 jleem users  15277 2006-11-15 22:35:30.000000000 -0800 runlog.out
-r-xr--r--  1 jleem users  62613 2006-11-15 22:35:30.000000000 -0800 savechem
-r-xr--r--  1 jleem users   1646 2006-11-15 22:35:30.000000000 -0800 solute.inp
-r-xr--r--  1 jleem users   6209 2006-11-15 22:35:30.000000000 -0800 solute.out
-r-xr--r--  1 jleem users  33914 2006-11-15 22:35:30.000000000 -0800 tec_conc.dat
-r-xr--r--  1 jleem users  14089 2006-11-15 22:35:30.000000000 -0800 tec_gas.dat
-r-xr--r--  1 jleem users  48093 2006-11-15 22:35:30.000000000 -0800 tec_min.dat
-r-xr--r--  1 jleem users  88384 2006-11-15 22:35:29.000000000 -0800 ther_dummy.dat
-r-xr--r--  1 jleem users  60384 2006-11-15 22:35:30.000000000 -0800 time.dat

/home/jleem/tr3.1.1_X/install_tests/eos4
total 896
-r-xr--r--  1 jleem users 172557 2006-11-15 22:35:30.000000000 -0800 GASOBS.DAT
-r-xr--r--  1 jleem users     91 2006-11-15 22:35:30.000000000 -0800 GENER
```

```
-r-xr--r--  1 jleem users    149 2006-11-15 22:35:30.000000000 -0800 INCON
-r-xr--r--  1 jleem users      0 2006-11-15 22:35:30.000000000 -0800 LINEQ
-r-xr--r--  1 jleem users   9228 2006-11-15 22:35:30.000000000 -0800 MESH
-r-xr--r--  1 jleem users   7518 2006-11-15 22:35:30.000000000 -0800 SAVE
-r-xr--r--  1 jleem users      0 2006-11-15 22:35:30.000000000 -0800 TABLE
-r-xr--r--  1 jleem users   7047 2006-11-15 22:35:30.000000000 -0800 VERS
-r-xr--r--  1 jleem users   7049 2006-11-15 22:35:30.000000000 -0800 chdump.out
-r-xr--r--  1 jleem users   5517 2006-11-15 22:35:30.000000000 -0800 chemical.inp
-r-xr--r--  1 jleem users  14625 2006-11-15 22:35:30.000000000 -0800 chemical.out
-r-xr--r--  1 jleem users   9711 2006-11-15 22:35:30.000000000 -0800 flow.inp
-r-xr--r--  1 jleem users 227315 2006-11-15 22:35:30.000000000 -0800 flow.out
-r-xr--r--  1 jleem users  12001 2006-11-15 22:35:30.000000000 -0800 iter.dat
-r-xr--r--  1 jleem users  15528 2006-11-15 22:35:30.000000000 -0800 mbalance.out
-r-xr--r--  1 jleem users  31174 2006-11-15 22:35:30.000000000 -0800 min_SI.out
-r-xr--r--  1 jleem users  15277 2006-11-15 22:35:30.000000000 -0800 runlog.out
-r-xr--r--  1 jleem users  62613 2006-11-15 22:35:30.000000000 -0800 savechem
-r-xr--r--  1 jleem users   1646 2006-11-15 22:35:30.000000000 -0800 solute.inp
-r-xr--r--  1 jleem users   6209 2006-11-15 22:35:30.000000000 -0800 solute.out
-r-xr--r--  1 jleem users  33914 2006-11-15 22:35:30.000000000 -0800 tec_conc.dat
-r-xr--r--  1 jleem users  14089 2006-11-15 22:35:30.000000000 -0800 tec_gas.dat
-r-xr--r--  1 jleem users  48093 2006-11-15 22:35:30.000000000 -0800 tec_min.dat
-r-xr--r--  1 jleem users  88384 2006-11-15 22:35:30.000000000 -0800 ther_dummy.dat
-r-xr--r--  1 jleem users  60384 2006-11-15 22:35:30.000000000 -0800 time.dat

/home/jleem/tr3.1.1_X/install_tests/eos9
total 200
-r-xr--r--  1 jleem users 29403 2006-11-15 22:35:30.000000000 -0800 GASOBS.DAT
-r-xr--r--  1 jleem users    91 2006-11-15 22:35:30.000000000 -0800 GENER
-r-xr--r--  1 jleem users  7383 2006-11-15 22:35:30.000000000 -0800 INCON
-r-xr--r--  1 jleem users     0 2006-11-15 22:35:30.000000000 -0800 LINEQ
-r-xr--r--  1 jleem users 13967 2006-11-15 22:35:30.000000000 -0800 MESH
-r-xr--r--  1 jleem users  7491 2006-11-15 22:35:30.000000000 -0800 SAVE
-r-xr--r--  1 jleem users     0 2006-11-15 22:35:30.000000000 -0800 TABLE
-r-xr--r--  1 jleem users  3791 2006-11-15 22:35:30.000000000 -0800 VERS
-r-xr--r--  1 jleem users 41322 2006-11-15 22:35:30.000000000 -0800 flow.inp
-r-xr--r--  1 jleem users 79596 2006-11-15 22:35:30.000000000 -0800 flow.out

/home/jleem/tr3.1.1_X/source
total 1312
-r-xr--r--  1 jleem users   3081 2006-11-15 22:34:50.000000000 -0800 T2_40K
-r-xr--r--  1 jleem users   1839 2006-11-15 22:34:50.000000000 -0800 chempar23_q311.inc
-r-xr--r--  1 jleem users   3412 2006-11-15 22:34:50.000000000 -0800 common23.inc
-r-xr--r--  1 jleem users  46113 2006-11-15 22:34:50.000000000 -0800 eos3.f
-r-xr--r--  1 jleem users  60724 2006-11-15 22:34:50.000000000 -0800 eos4.f
-r-xr--r--  1 jleem users  32044 2006-11-15 22:34:50.000000000 -0800 eos9.f
-r-xr--r--  1 jleem users 204231 2006-11-15 22:34:50.000000000 -0800 geochem.f
-r-xr--r--  1 jleem users  97464 2006-11-15 22:34:50.000000000 -0800 inichm.f
```

-r-xr--r-- 1 jleem users 1550 2006-11-15 22:34:50.000000000 -0800 ma28abc.f
-r-xr--r-- 1 jleem users 1716 2006-11-15 22:34:50.000000000 -0800 makefile_eos3q311_dec
-r-xr--r-- 1 jleem users 1894 2006-11-15 22:34:50.000000000 -0800 makefile_eos3q311_linux
-r-xr--r-- 1 jleem users 1716 2006-11-15 22:34:50.000000000 -0800 makefile_eos4q311_dec
-r-xr--r-- 1 jleem users 1894 2006-11-15 22:34:50.000000000 -0800 makefile_eos4q311_linux
-r-xr--r-- 1 jleem users 1716 2006-11-15 22:34:50.000000000 -0800 makefile_eos9q311_dec
-r-xr--r-- 1 jleem users 1894 2006-11-15 22:34:50.000000000 -0800 makefile_eos9q311_linux
-r-xr--r-- 1 jleem users 41911 2006-11-15 22:34:50.000000000 -0800 meshm.f
-r-xr--r-- 1 jleem users 141763 2006-11-15 22:34:50.000000000 -0800 multi.f
-r-xr--r-- 1 jleem users 33584 2006-11-15 22:34:50.000000000 -0800 newton.f
-r-xr--r-- 1 jleem users 507 2006-11-15 22:34:50.000000000 -0800 perm23.inc
-r-xr--r-- 1 jleem users 17941 2006-11-15 22:34:50.000000000 -0800 rctprop.f
-r-xr--r-- 1 jleem users 20523 2006-11-15 22:34:50.000000000 -0800 readsolu.f
-r-xr--r-- 1 jleem users 827 2006-11-15 22:34:50.000000000 -0800 second_dec.f
-r-xr--r-- 1 jleem users 73085 2006-11-15 22:34:50.000000000 -0800 t2cg22.f
-r-xr--r-- 1 jleem users 165569 2006-11-15 22:34:50.000000000 -0800 t2f.f
-r-xr--r-- 1 jleem users 73236 2006-11-15 22:34:50.000000000 -0800 t2solv.f
-r-xr--r-- 1 jleem users 225993 2006-11-15 22:34:50.000000000 -0800 treact.f

G.2 TOUGHREACT V3.1.1 INSTALLATION ON LBNL MACHINE WORKHORSE2 (CAOS LINUX)

G.2.1 Installation on Workhorse2 for Preliminary Modeling Prior to Qualification of TOUGHREACT V3.1.1

/home/ymp/tr3.1.1_X
total 20
drwxr-xr-x 2 jwong users 4096 Nov 15 23:08 executables
drwxr-xr-x 8 jwong users 4096 Dec 8 09:38 install_tests
drwxr-xr-x 2 jwong users 4096 Nov 15 22:39 source
drwxr-xr-x 25 jwong users 4096 Nov 15 22:43 test_problems_dec
drwxr-xr-x 25 jwong users 4096 Nov 15 22:37 test_problems_lin

/home/ymp/tr3.1.1_X/executables
total 8344
-r-xr-xr-x 1 jwong users 1267120 Nov 15 23:08 tr3.1.1e3_40k_dec
-r-xr--r-- 1 jwong users 1571881 Nov 15 23:08 tr3.1.1e3_40k_lin
-r-xr-xr-x 1 jwong users 1277184 Nov 15 23:08 tr3.1.1e4_40k_dec
-r-xr--r-- 1 jwong users 1583453 Nov 15 23:08 tr3.1.1e4_40k_lin
-r-xr-xr-x 1 jwong users 1256656 Nov 15 23:08 tr3.1.1e9_40k_dec
-r-xr--r-- 1 jwong users 1556024 Nov 15 23:08 tr3.1.1e9_40k_lin

/home/ymp/tr3.1.1_X/install_tests
total 12
drwxr-xr-x 2 jwong users 4096 Nov 15 22:35 eos3
drwxr-xr-x 2 jwong users 4096 Nov 15 22:35 eos4
drwxr-xr-x 2 jwong users 4096 Nov 15 22:35 eos9

```
/home/ymp/tr3.1.1_X/install_tests/eos3
total 896
-r-xr--r--  1 jwong users 172953 Nov 15 22:35 GASOBS.DAT
-r-xr--r--  1 jwong users     91 Nov 15 22:35 GENER
-r-xr--r--  1 jwong users    149 Nov 15 22:35 INCON
-r-xr--r--  1 jwong users      0 Nov 15 22:35 LINEQ
-r-xr--r--  1 jwong users   9228 Nov 15 22:35 MESH
-r-xr--r--  1 jwong users   7518 Nov 15 22:35 SAVE
-r-xr--r--  1 jwong users      0 Nov 15 22:35 TABLE
-r-xr--r--  1 jwong users   6640 Nov 15 22:35 VERS
-r-xr--r--  1 jwong users   7049 Nov 15 22:35 chdump.out
-r-xr--r--  1 jwong users   5517 Nov 15 22:35 chemical.inp
-r-xr--r--  1 jwong users  14625 Nov 15 22:35 chemical.out
-r-xr--r--  1 jwong users   9711 Nov 15 22:35 flow.inp
-r-xr--r--  1 jwong users 228245 Nov 15 22:35 flow.out
-r-xr--r--  1 jwong users  12001 Nov 15 22:35 iter.dat
-r-xr--r--  1 jwong users  15528 Nov 15 22:35 mbalance.out
-r-xr--r--  1 jwong users  31174 Nov 15 22:35 min_SI.out
-r-xr--r--  1 jwong users  15277 Nov 15 22:35 runlog.out
-r-xr--r--  1 jwong users  62613 Nov 15 22:35 savechem
-r-xr--r--  1 jwong users   1646 Nov 15 22:35 solute.inp
-r-xr--r--  1 jwong users   6209 Nov 15 22:35 solute.out
-r-xr--r--  1 jwong users  33914 Nov 15 22:35 tec_conc.dat
-r-xr--r--  1 jwong users  14089 Nov 15 22:35 tec_gas.dat
-r-xr--r--  1 jwong users  48093 Nov 15 22:35 tec_min.dat
-r-xr--r--  1 jwong users  88384 Nov 15 22:35 ther_dummy.dat
-r-xr--r--  1 jwong users  60384 Nov 15 22:35 time.dat

/home/ymp/tr3.1.1_X/install_tests/eos4
total 896
-r-xr--r--  1 jwong users 172557 Nov 15 22:35 GASOBS.DAT
-r-xr--r--  1 jwong users     91 Nov 15 22:35 GENER
-r-xr--r--  1 jwong users    149 Nov 15 22:35 INCON
-r-xr--r--  1 jwong users      0 Nov 15 22:35 LINEQ
-r-xr--r--  1 jwong users   9228 Nov 15 22:35 MESH
-r-xr--r--  1 jwong users   7518 Nov 15 22:35 SAVE
-r-xr--r--  1 jwong users      0 Nov 15 22:35 TABLE
-r-xr--r--  1 jwong users   7047 Nov 15 22:35 VERS
-r-xr--r--  1 jwong users   7049 Nov 15 22:35 chdump.out
-r-xr--r--  1 jwong users   5517 Nov 15 22:35 chemical.inp
-r-xr--r--  1 jwong users  14625 Nov 15 22:35 chemical.out
-r-xr--r--  1 jwong users   9711 Nov 15 22:35 flow.inp
-r-xr--r--  1 jwong users 227315 Nov 15 22:35 flow.out
-r-xr--r--  1 jwong users  12001 Nov 15 22:35 iter.dat
-r-xr--r--  1 jwong users  15528 Nov 15 22:35 mbalance.out
-r-xr--r--  1 jwong users  31174 Nov 15 22:35 min_SI.out
-r-xr--r--  1 jwong users  15277 Nov 15 22:35 runlog.out
```

```
-r-xr--r--  1 jwong users  62613 Nov 15 22:35 savechem
-r-xr--r--  1 jwong users   1646 Nov 15 22:35 solute.inp
-r-xr--r--  1 jwong users   6209 Nov 15 22:35 solute.out
-r-xr--r--  1 jwong users  33914 Nov 15 22:35 tec_conc.dat
-r-xr--r--  1 jwong users  14089 Nov 15 22:35 tec_gas.dat
-r-xr--r--  1 jwong users  48093 Nov 15 22:35 tec_min.dat
-r-xr--r--  1 jwong users  88384 Nov 15 22:35 ther_dummy.dat
-r-xr--r--  1 jwong users  60384 Nov 15 22:35 time.dat

/home/ymp/tr3.1.1_X/install_tests/eos9
total 200
-r-xr--r--  1 jwong users 29403 Nov 15 22:35 GASOBS.DAT
-r-xr--r--  1 jwong users    91 Nov 15 22:35 GENER
-r-xr--r--  1 jwong users  7383 Nov 15 22:35 INCON
-r-xr--r--  1 jwong users     0 Nov 15 22:35 LINEQ
-r-xr--r--  1 jwong users 13967 Nov 15 22:35 MESH
-r-xr--r--  1 jwong users  7491 Nov 15 22:35 SAVE
-r-xr--r--  1 jwong users     0 Nov 15 22:35 TABLE
-r-xr--r--  1 jwong users  3791 Nov 15 22:35 VERS
-r-xr--r--  1 jwong users 41322 Nov 15 22:35 flow.inp
-r-xr--r--  1 jwong users 79596 Nov 15 22:35 flow.out

/home/ymp/tr3.1.1_X/source
total 1312
-r-xr--r--  1 jwong users   3081 Nov 15 22:34 T2_40K
-r-xr--r--  1 jwong users   1839 Nov 15 22:34 chempar23_q311.inc
-r-xr--r--  1 jwong users   3412 Nov 15 22:34 common23.inc
-r-xr--r--  1 jwong users  46113 Nov 15 22:34 eos3.f
-r-xr--r--  1 jwong users  60724 Nov 15 22:34 eos4.f
-r-xr--r--  1 jwong users  32044 Nov 15 22:34 eos9.f
-r-xr--r--  1 jwong users 204231 Nov 15 22:34 geochem.f
-r-xr--r--  1 jwong users  97464 Nov 15 22:34 inichm.f
-r-xr--r--  1 jwong users   1550 Nov 15 22:34 ma28abc.f
-r-xr--r--  1 jwong users   1716 Nov 15 22:34 makefile_eos3q311_dec
-r-xr--r--  1 jwong users   1894 Nov 15 22:34 makefile_eos3q311_linux
-r-xr--r--  1 jwong users   1716 Nov 15 22:34 makefile_eos4q311_dec
-r-xr--r--  1 jwong users   1894 Nov 15 22:34 makefile_eos4q311_linux
-r-xr--r--  1 jwong users   1716 Nov 15 22:34 makefile_eos9q311_dec
-r-xr--r--  1 jwong users   1894 Nov 15 22:34 makefile_eos9q311_linux
-r-xr--r--  1 jwong users  41911 Nov 15 22:34 meshm.f
-r-xr--r--  1 jwong users 141763 Nov 15 22:34 multi.f
-r-xr--r--  1 jwong users  33584 Nov 15 22:34 newton.f
-r-xr--r--  1 jwong users    507 Nov 15 22:34 perm23.inc
-r-xr--r--  1 jwong users  17941 Nov 15 22:34 rctprop.f
-r-xr--r--  1 jwong users  20523 Nov 15 22:34 readsolu.f
-r-xr--r--  1 jwong users    827 Nov 15 22:34 second_dec.f
-r-xr--r--  1 jwong users  73085 Nov 15 22:34 t2cg22.f
```

```
-r-xr--r--  1 jwong users 165569 Nov 15 22:34 t2f.f
-r-xr--r--  1 jwong users  73236 Nov 15 22:34 t2solv.f
-r-xr--r--  1 jwong users 225993 Nov 15 22:34 treact.f
```

G.2.2 Installation on Workhorse 2 Using Qualified TOUGHREACT V3.1.1 Media from Software Configuration Management

```
/home/jleem/tr3.1.1_X
total 20
drwxr-xr-x   2 jleem users 4096 2006-11-15 23:08:36.000000000 -0800 executables
drwxr-xr-x   5 jleem users 4096 2006-11-15 22:35:30.000000000 -0800 install_tests
drwxr-xr-x   2 jleem users 4096 2006-11-15 22:39:37.000000000 -0800 source
drwxr-xr-x  25 jleem users 4096 2006-11-15 22:43:01.000000000 -0800 test_problems_dec
drwxr-xr-x  25 jleem users 4096 2006-11-15 22:37:33.000000000 -0800 test_problems_lin

/home/jleem/tr3.1.1_X/executables
total 8344
-r-xr-xr-x  1 jleem users 1267120 2006-11-15 23:08:07.000000000 -0800 tr3.1.1e3_40k_dec
-r-xr--r--  1 jleem users 1571881 2006-11-15 23:08:07.000000000 -0800 tr3.1.1e3_40k_lin
-r-xr-xr-x  1 jleem users 1277184 2006-11-15 23:08:07.000000000 -0800 tr3.1.1e4_40k_dec
-r-xr--r--  1 jleem users 1583453 2006-11-15 23:08:06.000000000 -0800 tr3.1.1e4_40k_lin
-r-xr-xr-x  1 jleem users 1256656 2006-11-15 23:08:06.000000000 -0800 tr3.1.1e9_40k_dec
-r-xr--r--  1 jleem users 1556024 2006-11-15 23:08:06.000000000 -0800 tr3.1.1e9_40k_lin

/home/jleem/tr3.1.1_X/install_tests
total 12
drwxr-xr-x  2 jleem users 4096 2006-11-15 22:35:30.000000000 -0800 eos3
drwxr-xr-x  2 jleem users 4096 2006-11-15 22:35:30.000000000 -0800 eos4
drwxr-xr-x  2 jleem users 4096 2006-11-15 22:35:30.000000000 -0800 eos9

/home/jleem/tr3.1.1_X/install_tests/eos3
total 896
-r-xr--r--  1 jleem users 172953 2006-11-15 22:35:30.000000000 -0800 GASOBS.DAT
-r-xr--r--  1 jleem users     91 2006-11-15 22:35:30.000000000 -0800 GENER
-r-xr--r--  1 jleem users    149 2006-11-15 22:35:30.000000000 -0800 INCON
-r-xr--r--  1 jleem users      0 2006-11-15 22:35:30.000000000 -0800 LINEQ
-r-xr--r--  1 jleem users   9228 2006-11-15 22:35:30.000000000 -0800 MESH
-r-xr--r--  1 jleem users   7518 2006-11-15 22:35:30.000000000 -0800 SAVE
-r-xr--r--  1 jleem users      0 2006-11-15 22:35:30.000000000 -0800 TABLE
-r-xr--r--  1 jleem users   6640 2006-11-15 22:35:30.000000000 -0800 VERS
-r-xr--r--  1 jleem users   7049 2006-11-15 22:35:29.000000000 -0800 chdump.out
-r-xr--r--  1 jleem users   5517 2006-11-15 22:35:29.000000000 -0800 chemical.inp
-r-xr--r--  1 jleem users  14625 2006-11-15 22:35:29.000000000 -0800 chemical.out
-r-xr--r--  1 jleem users   9711 2006-11-15 22:35:30.000000000 -0800 flow.inp
-r-xr--r--  1 jleem users 228245 2006-11-15 22:35:30.000000000 -0800 flow.out
-r-xr--r--  1 jleem users  12001 2006-11-15 22:35:30.000000000 -0800 iter.dat
-r-xr--r--  1 jleem users  15528 2006-11-15 22:35:30.000000000 -0800 mbalance.out
```

```
-r-xr--r--  1 jleem users  31174 2006-11-15 22:35:30.000000000 -0800 min_SI.out
-r-xr--r--  1 jleem users  15277 2006-11-15 22:35:30.000000000 -0800 runlog.out
-r-xr--r--  1 jleem users  62613 2006-11-15 22:35:30.000000000 -0800 savechem
-r-xr--r--  1 jleem users   1646 2006-11-15 22:35:30.000000000 -0800 solute.inp
-r-xr--r--  1 jleem users   6209 2006-11-15 22:35:30.000000000 -0800 solute.out
-r-xr--r--  1 jleem users  33914 2006-11-15 22:35:30.000000000 -0800 tec_conc.dat
-r-xr--r--  1 jleem users  14089 2006-11-15 22:35:30.000000000 -0800 tec_gas.dat
-r-xr--r--  1 jleem users  48093 2006-11-15 22:35:30.000000000 -0800 tec_min.dat
-r-xr--r--  1 jleem users  88384 2006-11-15 22:35:29.000000000 -0800 ther_dummy.dat
-r-xr--r--  1 jleem users  60384 2006-11-15 22:35:30.000000000 -0800 time.dat

/home/jleem/tr3.1.1_X/install_tests/eos4
total 896
-r-xr--r--  1 jleem users 172557 2006-11-15 22:35:30.000000000 -0800 GASOBS.DAT
-r-xr--r--  1 jleem users     91 2006-11-15 22:35:30.000000000 -0800 GENER
-r-xr--r--  1 jleem users    149 2006-11-15 22:35:30.000000000 -0800 INCON
-r-xr--r--  1 jleem users      0 2006-11-15 22:35:30.000000000 -0800 LINEQ
-r-xr--r--  1 jleem users   9228 2006-11-15 22:35:30.000000000 -0800 MESH
-r-xr--r--  1 jleem users   7518 2006-11-15 22:35:30.000000000 -0800 SAVE
-r-xr--r--  1 jleem users      0 2006-11-15 22:35:30.000000000 -0800 TABLE
-r-xr--r--  1 jleem users   7047 2006-11-15 22:35:30.000000000 -0800 VERS
-r-xr--r--  1 jleem users   7049 2006-11-15 22:35:30.000000000 -0800 chdump.out
-r-xr--r--  1 jleem users   5517 2006-11-15 22:35:30.000000000 -0800 chemical.inp
-r-xr--r--  1 jleem users  14625 2006-11-15 22:35:30.000000000 -0800 chemical.out
-r-xr--r--  1 jleem users   9711 2006-11-15 22:35:30.000000000 -0800 flow.inp
-r-xr--r--  1 jleem users 227315 2006-11-15 22:35:30.000000000 -0800 flow.out
-r-xr--r--  1 jleem users  12001 2006-11-15 22:35:30.000000000 -0800 iter.dat
-r-xr--r--  1 jleem users  15528 2006-11-15 22:35:30.000000000 -0800 mbalance.out
-r-xr--r--  1 jleem users  31174 2006-11-15 22:35:30.000000000 -0800 min_SI.out
-r-xr--r--  1 jleem users  15277 2006-11-15 22:35:30.000000000 -0800 runlog.out
-r-xr--r--  1 jleem users  62613 2006-11-15 22:35:30.000000000 -0800 savechem
-r-xr--r--  1 jleem users   1646 2006-11-15 22:35:30.000000000 -0800 solute.inp
-r-xr--r--  1 jleem users   6209 2006-11-15 22:35:30.000000000 -0800 solute.out
-r-xr--r--  1 jleem users  33914 2006-11-15 22:35:30.000000000 -0800 tec_conc.dat
-r-xr--r--  1 jleem users  14089 2006-11-15 22:35:30.000000000 -0800 tec_gas.dat
-r-xr--r--  1 jleem users  48093 2006-11-15 22:35:30.000000000 -0800 tec_min.dat
-r-xr--r--  1 jleem users  88384 2006-11-15 22:35:30.000000000 -0800 ther_dummy.dat
-r-xr--r--  1 jleem users  60384 2006-11-15 22:35:30.000000000 -0800 time.dat

/home/jleem/tr3.1.1_X/install_tests/eos9
total 200
-r-xr--r--  1 jleem users 29403 2006-11-15 22:35:30.000000000 -0800 GASOBS.DAT
-r-xr--r--  1 jleem users    91 2006-11-15 22:35:30.000000000 -0800 GENER
-r-xr--r--  1 jleem users  7383 2006-11-15 22:35:30.000000000 -0800 INCON
-r-xr--r--  1 jleem users     0 2006-11-15 22:35:30.000000000 -0800 LINEQ
-r-xr--r--  1 jleem users 13967 2006-11-15 22:35:30.000000000 -0800 MESH
-r-xr--r--  1 jleem users  7491 2006-11-15 22:35:30.000000000 -0800 SAVE
```

```
-r-xr--r--  1 jleem users     0 2006-11-15 22:35:30.000000000 -0800 TABLE
-r-xr--r--  1 jleem users  3791 2006-11-15 22:35:30.000000000 -0800 VERS
-r-xr--r--  1 jleem users 41322 2006-11-15 22:35:30.000000000 -0800 flow.inp
-r-xr--r--  1 jleem users 79596 2006-11-15 22:35:30.000000000 -0800 flow.out

/home/jleem/tr3.1.1_X/source
total 1312
-r-xr--r--  1 jleem users   3081 2006-11-15 22:34:50.000000000 -0800 T2_40K
-r-xr--r--  1 jleem users   1839 2006-11-15 22:34:50.000000000 -0800 chempar23_q311.inc
-r-xr--r--  1 jleem users   3412 2006-11-15 22:34:50.000000000 -0800 common23.inc
-r-xr--r--  1 jleem users  46113 2006-11-15 22:34:50.000000000 -0800 eos3.f
-r-xr--r--  1 jleem users  60724 2006-11-15 22:34:50.000000000 -0800 eos4.f
-r-xr--r--  1 jleem users  32044 2006-11-15 22:34:50.000000000 -0800 eos9.f
-r-xr--r--  1 jleem users 204231 2006-11-15 22:34:50.000000000 -0800 geochem.f
-r-xr--r--  1 jleem users  97464 2006-11-15 22:34:50.000000000 -0800 inichm.f
-r-xr--r--  1 jleem users   1550 2006-11-15 22:34:50.000000000 -0800 ma28abc.f
-r-xr--r--  1 jleem users   1716 2006-11-15 22:34:50.000000000 -0800 makefile_eos3q311_dec
-r-xr--r--  1 jleem users   1894 2006-11-15 22:34:50.000000000 -0800 makefile_eos3q311_linux
-r-xr--r--  1 jleem users   1716 2006-11-15 22:34:50.000000000 -0800 makefile_eos4q311_dec
-r-xr--r--  1 jleem users   1894 2006-11-15 22:34:50.000000000 -0800 makefile_eos4q311_linux
-r-xr--r--  1 jleem users   1716 2006-11-15 22:34:50.000000000 -0800 makefile_eos9q311_dec
-r-xr--r--  1 jleem users   1894 2006-11-15 22:34:50.000000000 -0800 makefile_eos9q311_linux
-r-xr--r--  1 jleem users  41911 2006-11-15 22:34:50.000000000 -0800 meshm.f
-r-xr--r--  1 jleem users 141763 2006-11-15 22:34:50.000000000 -0800 multi.f
-r-xr--r--  1 jleem users  33584 2006-11-15 22:34:50.000000000 -0800 newton.f
-r-xr--r--  1 jleem users    507 2006-11-15 22:34:50.000000000 -0800 perm23.inc
-r-xr--r--  1 jleem users  17941 2006-11-15 22:34:50.000000000 -0800 rctprop.f
-r-xr--r--  1 jleem users  20523 2006-11-15 22:34:50.000000000 -0800 readsolu.f
-r-xr--r--  1 jleem users    827 2006-11-15 22:34:50.000000000 -0800 second_dec.f
-r-xr--r--  1 jleem users  73085 2006-11-15 22:34:50.000000000 -0800 t2cg22.f
-r-xr--r--  1 jleem users 165569 2006-11-15 22:34:50.000000000 -0800 t2f.f
-r-xr--r--  1 jleem users  73236 2006-11-15 22:34:50.000000000 -0800 t2solv.f
-r-xr--r--  1 jleem users 225993 2006-11-15 22:34:50.000000000 -0800 treact.f
```

G.3.1 CUTCHEM V2.0 Installation on PC

G.3.1.1 Folders and Files of Installation (prior to qualification of CUTCHEM V2.0) on LBNL PC DOE #6574913 with Windows XP

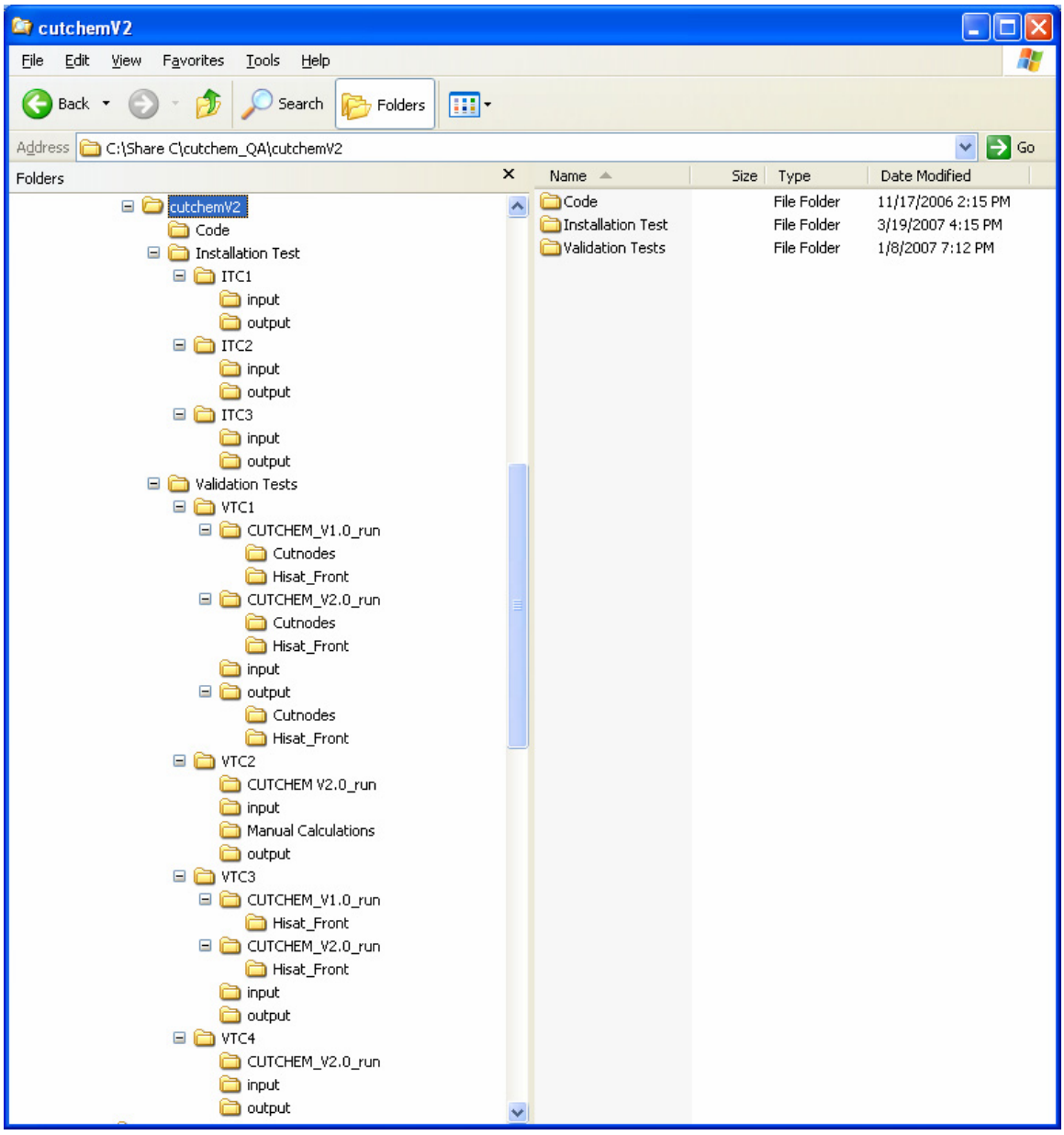

Figure G-1. Folders of CUTCHEM on the LBNL PC DOE # 6574913

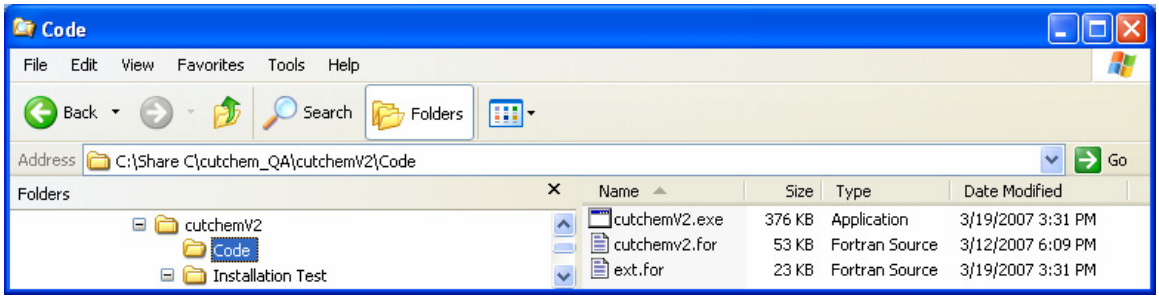

NOTE: The source codes (i.e., cutchemv2.for and ext.for) were removed in the qualified version of CUTCHEM.

Figure G-2. List of Source Files and the Executable File in Subfolder *\Code*

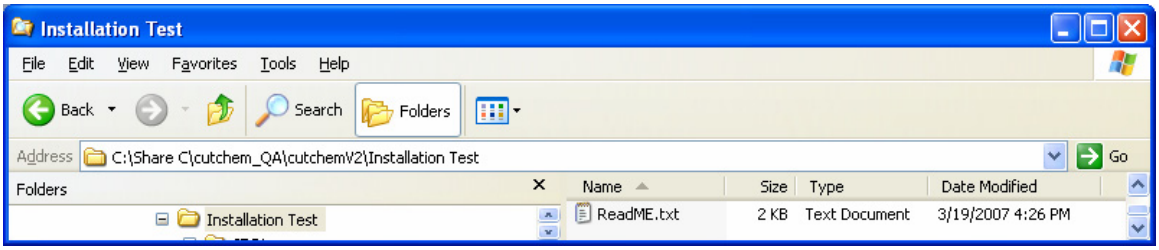

Figure G-3. List of the ReadMe File of CUTCHEM V2.0 Installation Tests

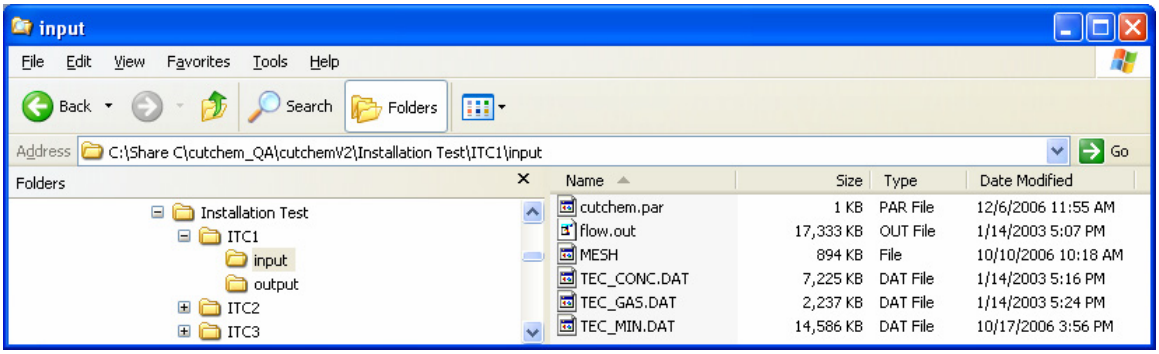

Figure G-4. List of Files in Subfolder *\Installation Test\ITC1\input*

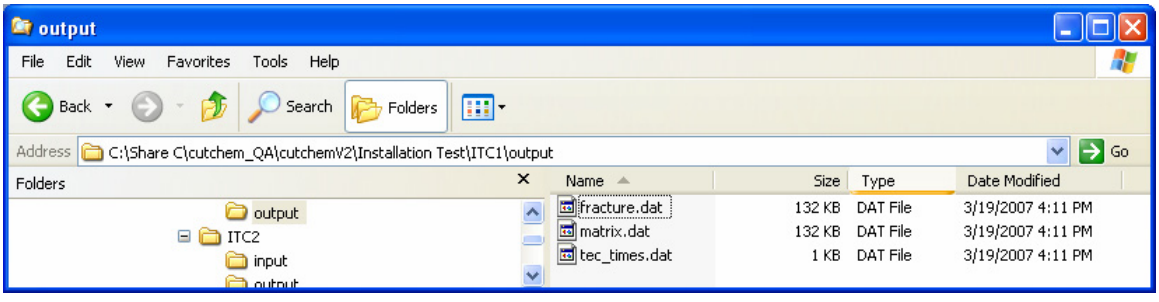

Figure G-5. List of Files in Subfolder *\Installation Test\ITC1\output*

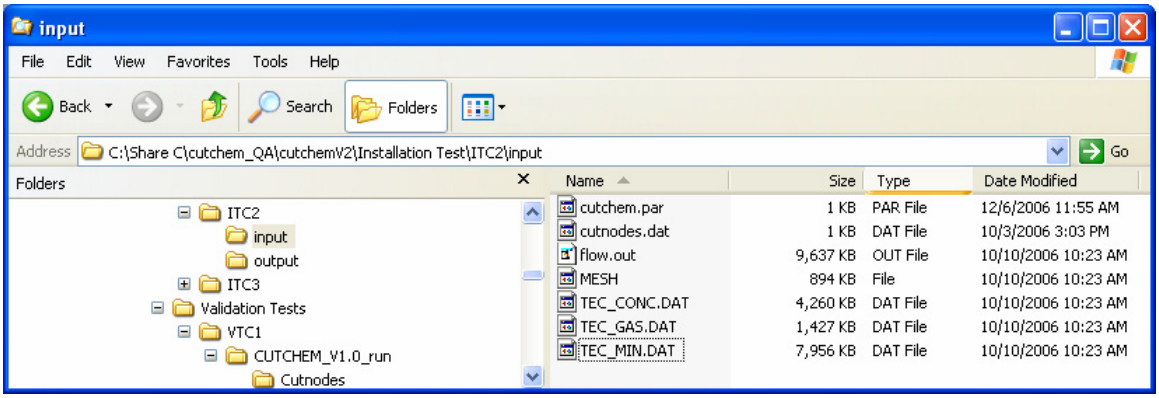

Figure G-6. List of Files in Subfolder *\Installation Test\ITC2\input*

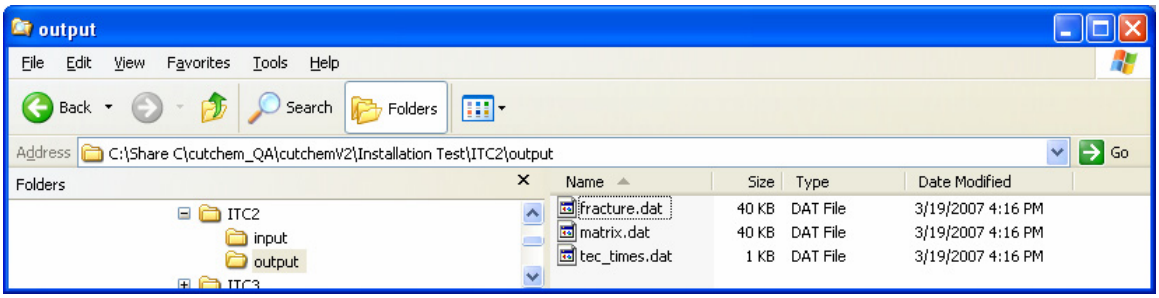

Figure G-7. List of Files in Subfolder *\Installation Test\ITC2\output*

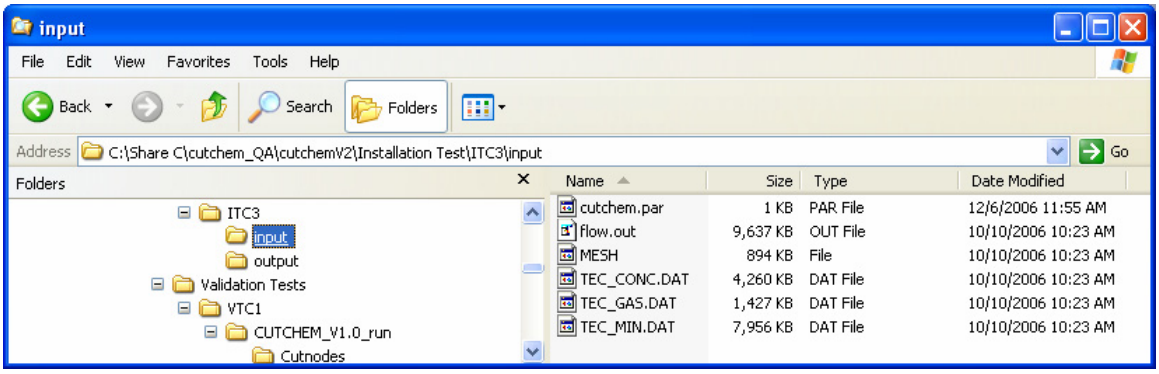

Figure G-8. List of Files in Subfolder *\Installation Test\ITC3\input*

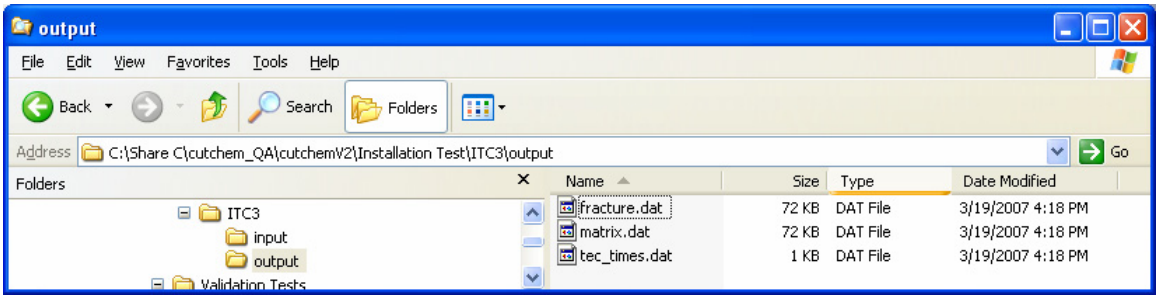

Figure G-9. List of Files in Subfolder *\Installation Test\ITC3\output*

G.3.2 Folders and Files of Installation from the Qualified CUTCHEM V2 Media from Software Configuration Management on SNL PC S885719 with Windows XP

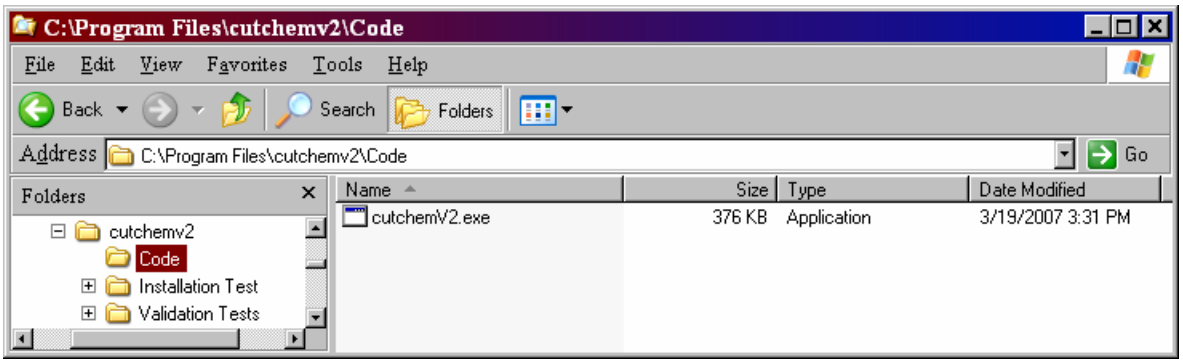

Figure G-10. List of Source Files and the Executable File in Subfolder *\Code*

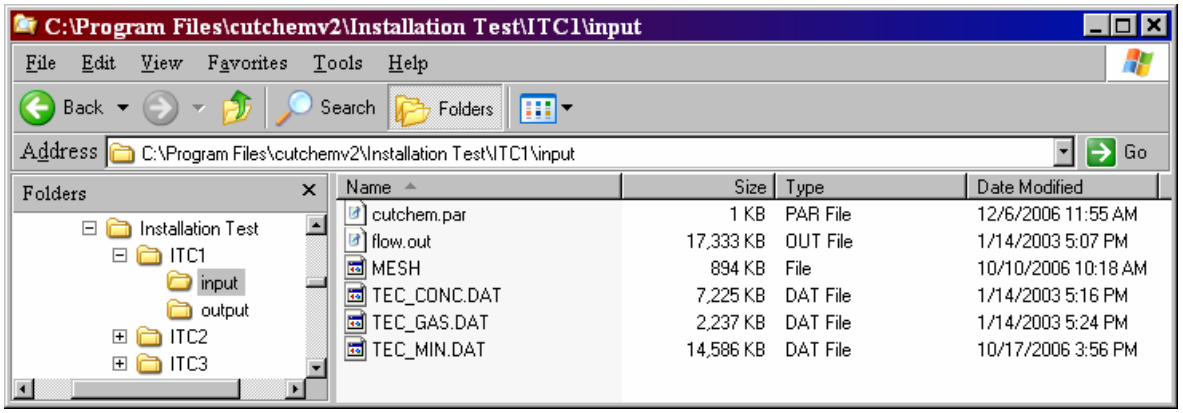

Figure G-11. List of Files in Subfolder *\Installation Test\ITC1\input*

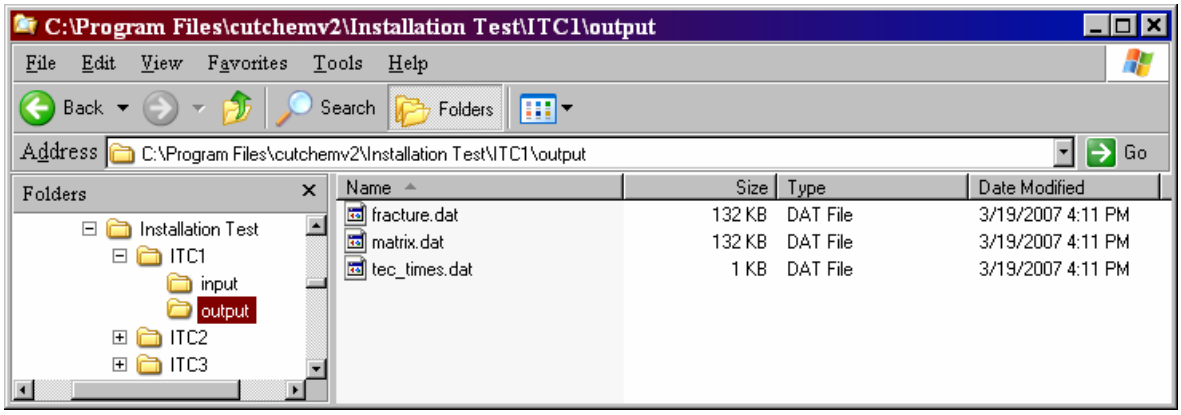

Figure G-12. List of Files in Subfolder *\Installation Test\ITC1\output*

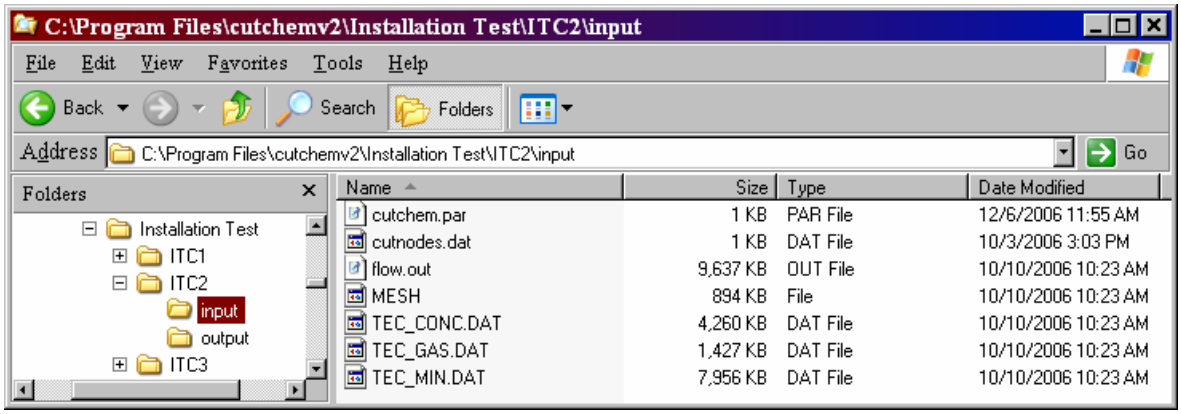

Figure G-13. List of Files in Subfolder *\Installation Test\ITC2\input*

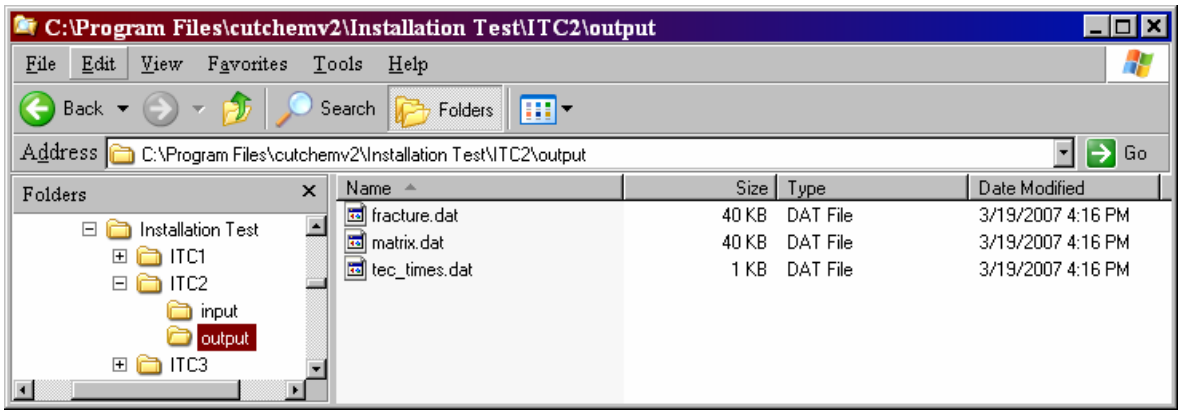

Figure G-14. List of Files in Subfolder *\Installation Test\ITC2\output*

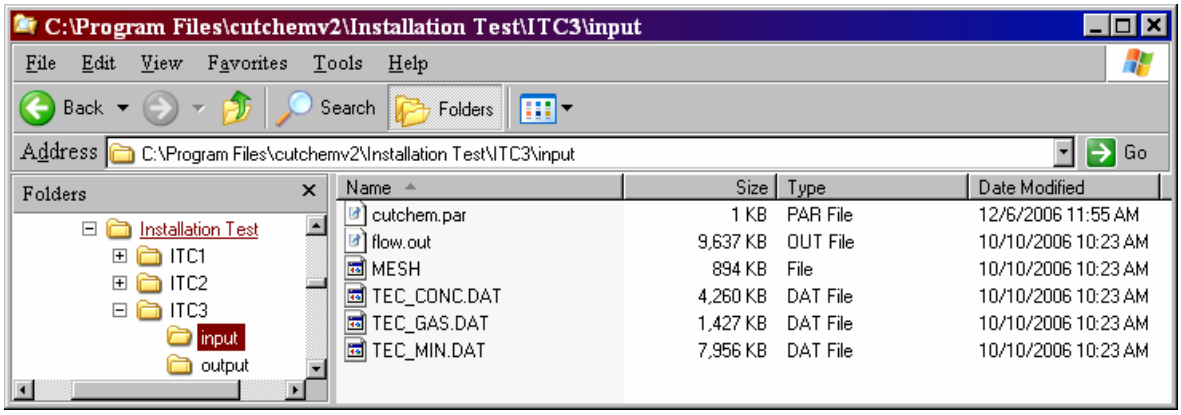

Figure G-15. List of Files in Subfolder *\Installation Test\ITC3\input*

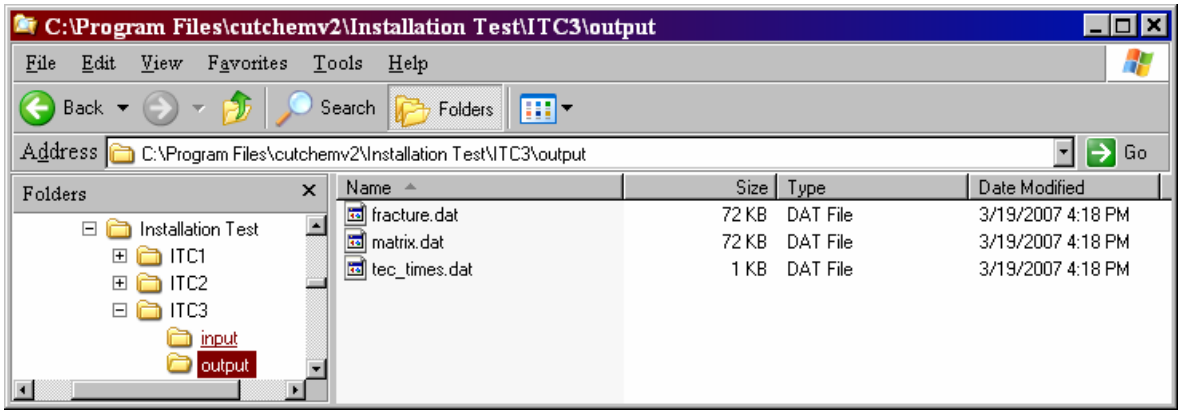

Figure G-16. List of Files in Subfolder *\Installation Test\ITC3\output*

INTENTIONALLY LEFT BLANK